INVESTIGATIONS ON ARSENITE INDUCED PREMATURE SENESCENCE IN HUMAN VASCULAR ENDOTHELIAL CELLS

Thesis submitted for the degree of

Doctor of Philosophy

at the University of Leicester

By

Qudsia Malik MSc, BSc (Hons)

Department of Cardiovascular Sciences

University of Leicester

2013

Dedication

This PhD thesis is lovingly dedicated to Mummy, Farida Malik, and Papa, Mohammed Umar Malik, for their unconditional love and support throughout my life.

Abstract

Chronic exposure of humans to arsenic contaminated drinking water promotes the development of atherosclerosis and is a problem in many countries worldwide. The pathogenic mechanisms are ill-defined, although arsenite-induced endothelial dysfunction has been hypothesised. Ageing is a major risk factor for atherosclerosis and aged (senescent) endothelial cells have been observed in human and experimental atherosclerosis, including in people with arsenicosis. Senescence is a cellular state of irreversible growth arrest, the accumulation of such cells could contribute to the development of age-related diseases. The aim of this thesis was to determine whether arsenite induced premature senescence in human vascular endothelial cells *in vitro* and whether the mechanisms involved reactive oxygen species-mediated cellular damage. Since mitochondria are a major source of cellular oxidants, studies to determine whether mitochondria were the primary targets for arsenic toxicity were carried out.

At sub-cytotoxic concentrations, using a cell culture model, arsenite caused stress-induced premature senescence in HUVECs which was quantitatively similar to induction of senescence by low levels of serial peroxide. Microarray-based transcriptomics revealed that antioxidant responses, including Nrf2-oxidative stress response pathway and metallothioneins, were upregulated in HUVECs treated with sub-cytotoxic arsenite concentrations supporting arsenite-induced oxidative stress as a possible mechanism. This was accompanied by an increase in nuclear DNA damage observed using the Comet assay. Although no statistically significant effects on mitochondrial biogenesis or mtDNA damage were seen using qPCR, analysis by extracellular flux analyzer revealed a decline in mitochondrial function, specifically the mitochondrial reserve capacity. These findings cast serious doubt that mitochondria are the primary targets of arsenite in endothelial cells, with the oxidative stress occurring through cytoplasmic sources and leading to cellular damage. This forms a possible mechanism for the observed premature senescence in endothelial cells due to arsenite which is linked with the process of atherosclerosis in humans.

Acknowledgements

First and foremost I would like to express my deepest gratitude to Dr Karl Herbert for his faultless supervision and guidance. I am very grateful for all his contributions and efforts during my doctorate study and for always being approachable and encouraging, especially through the stressful times. I am thankful to Professor Andy Smith for his continuous advice and support and to the Medical Research Council for providing funding for this PhD.

I would like to acknowledge all members of the cardiovascular department at the University of Leicester who supported and helped me during my research. A special thank you to William Dott for not only being a helpful colleague but also a good friend, making the time spent in the lab/office enjoyable with his quirky comments and sense of humour. I would also like to thank Dr Nicolas Sylvius and the research groups of Dr Kalvin Cain and Dr Mark Evans for their help/collaboration.

Conducting a PhD has been a challenging experience, I am very fortunate to have had a strong support system to help me get through it. My sisters, Anisa Malik, Aisha Yunus, Uzma Malik and Arusa Malik, have been my inspirations in life and I am forever indebted to them for supporting me through my every endeavour. I am very grateful to my best friend and husband, Safeer Mughal, for being my 'rock', always knowing what to say to lift my spirits and giving me the confidence to overcome every hurdle. I am also thankful to my brother in laws, Yunus Vhora, Sa'id Din and Nomaan Sheikh, and my parents in law, Shakeel and Shala Mughal, for their help, advice and encouraging words.

I would like to take this opportunity to express my heartfelt gratitude to my parents, Farida and Mohammad Umar Malik, for all their love, prayers and reassurance. They have always believed in me and helped me believe in myself, if it wasn't for the immense support they provided me throughout my life, especially these past few years, none of my accomplishments would be possible. I dedicate this thesis to them.

Most importantly, I sincerely thank God for providing me with this opportunity, for looking over me at all times and blessing me with all my achievements. Alhamdulillah.

Contents

CHAPTER EIGHT: General Discussion and Future Work

APPENDICES

Index of Tables

Index of Figures

List of Abbreviations

ρ	Mitochondrial DNA deficient/rho
AA	Antimycin A
ADP	Adenosine diphosphate
AFU	Arbitrary fluorescence unit
Amplex red	10-acetyl-3,7-dihydroxyphenoxazine
ANGPT2	Angiopoietin 2
ANOVA	One-way analysis of variance
AP	Activator protein
AQPs	Aquaglyceroporins
ATM	Ataxia telangiectasia mutated
ATP	Adenosine triphosphate
As^{3+}	Arsenite
BCL2	B-cell leukemia/lymphoma 2
BFD	Blackfoot disease
BH_4	Tetrahydrobiopterin
bp	Base pairs
BSA	Bovine serum albumin
$CaCl_2$	Calcium chloride
CAD	Coronary artery disease
CCK8	Cell counting kit 8
CCL15	Chemokine ligand 14
CCL15	Chemokine ligand 15

CDKN1A	Cyclin-dependent kinase inhibitor 1A
cDNA	Copy DNA
CHK	Checkpoint kinases
CM-H_2DCFDA	5,6-chloromethyl- 2',7'-dichlorohydrofluorescein diacetate
CO_2	Carbon dioxide
COX	Cytochrome c oxidase
cRNA	Copy RNA
Ct	Cycle threshold
CVD	Cardiovascular disease
Cyt c	Cytochrome c
DCF	(fluorescent) 2', 7'-dichlorofluorescein
DCFH	(non-fluorescent) 2'-7'-dichlorofluorescin
DCFH-DA	Dichlorodihydrofluorescin diacetate
DDIT3	DNA damage-inducible transcript 3
DDR	DNA damage response
DHE	Dihydroethidium
DHE-HPLC	Dihydroethidium-High performance liquid chromatography
dH_2O	Distilled water
DMEM	Dulbecco's modified Eagle's medium (Sigma-Aldrich D5546)
DMNQ	2,3-dimethoxy-1,4-napthoquinone
DMSO	Dimethyl sulfoxide
DNA	Deoxyribonucleic acid
dNTP	Deoxyribonucleotide triphosphates
DOX	Doxorubicin
DPBS	Dulbecco’s phosphate buffer solution
DSB	Double-strand break
DTT	Dithiothreitol

EA.hy 926	Fusion of human umbilical vein endothelial cells with the permanent human cell line A549 derived from a human lung carcinoma
EDTA	Ethylenediaminetetraacetic acid
eNOS	Endothelial nitric oxide synthase
ER	Endoplasmic reticulum
ETC	Electron transport chain
$FADH_2$	Flavin adenine dinucleotide
FBS	Fetal bovine serum
FC	Fold change
FCCP	Carbonyl cyanide 4-(trifluoromethoxy)phenylhydrazone.
FDR	False discovery rate
FITC	Fluorescein isothiocyanate
β-gal	β-galactosidase
GPCR	G-protein coupled receptors
GSH	Glutathione
γ-H2A.X	Phosphorylated histone H2A.X
HBSS	Hank's balanced salt solution
H9C2	Cell line derived from rat cardiac myoblasts
H_2DCF-DA	2',7'-dichlorodihydrofluorescein diacetate
HepG2 cells	Human hepatocellular liver carcinoma cells
HGPS	Hutchinson-Gilford progeria syndrome
HIF1A	Hypoxia-inducible factor-1α
H_2O	Water
H_2O_2	Hydrogen peroxide
hOGG1	human 8-hydroxyguanine DNA-glycosylase
HSPA5	Heat shock 70kDa protein 5
HUVECs	Human umbilical vein endothelial cells

IARC	International Agency of Research on Cancer
IGF-1	Insulin-like growth factor-1
IMDM	Iscove's modified Dulbecco's medium
IL8	Interleukin 8
IPA	Ingenuity pathway analysis
KCl	Potassium Chloride
KH_2PO_4	Potassium phosphate
LDL	Low-density lipoproteins
LMP	Low melting point
LPA	Lysophosphatidic acid
LPAR1	Lysophosphatidic acid receptor 1
LPAR2	Lysophosphatidic acid receptor 2
MAPK	Mitogen activated protein kinase
MEN	Menadione
$MgCl_2$	Magnesium chloride
MitoSOX™	MitoSOX™ red mitochondrial superoxide indiucator
mRNA	micro RNA
mtDNA	Mitochondrial DNA
MTs	Metallothioneins
MT1G	Metalothionein 1G
MT1H	Metalothionein 1H
MT1X	Metalothionein 1X
mTOR	Mammalian target of rapamycin
MTT	3-(4,5-dimethylthiazol-2-yl)-2,5-diphenyltetrazolium bromide
NaCl	Sodium Chloride
NADH	Nicotinamide adenine dinucleotide oxidase
NADPH	Nicotinamide adenine dinucleotide phosphate-oxidase

Na_2HPO_4	Disodium hydrogen phosphate
nDNA	Nuclear DNA
NER	Nucleotide excision repair
NF-$_K$B	Nuclear factor kappa B
NO	Nitric oxide
NOS	Nitric oxide synthase
NQO1	NAD(P)H dehydrogenase, quinine 1
NRF2	Nuclear factor erythroid 2-related factor 2
NTP	Nucleoside triphosphate
O_2	Oxygen
OC	Oxygen consumption
OCR	Oxygen consumption rate
8-oxo-dG	8-hydroxy-2-deoxyguanosine
P21	Another name for CDKN1A
PBS	Phosphate buffer solution
PC	Principal component
PCA	Principal component analysis
PCR	Polymerase chain reaction
PI	Propidium iodide
PS	Phosphatidylserine
PVD	Peripheral vascular disease
qPCR	Quantitative real-time polymerase chain reaction
RGS4	Regulator of G-protein signalling 4
RNA	Ribonucleic acid
RNase	Ribonuclease
RNS	Reactive nitrogen species
ROS	Reactive oxygen species

RPLPO	Large ribosomal protein
SA-β-Gal	Senescence associated β-galactosidase
SEM	Standard error of mean
SIPS	Stress-induced premature senescence
SOD	Superoxide dismutase
SOD1	Superoxide dismutase 1
SOD2	Superoxide dismutase 2
SS	Staurosporin
STASIS	Stress or aberrant signalling induced senescence
SVEC4-10	Mouse vascular endothelial derived cell line
t-BHP	tert-Butyl hydrogen peroxide
TE	Tris-EDTA
TMRM	Tetramethylrhodamine methyl ester
TNF	Tumour necrosis factor
TPP	Triphenylphosphonium
UP	Ultra pure
UPR	Unfolded protein response
UROtsa cells	Urothelium cell line
VSMCs	Vascular smooth muscle cells
WHO	World health organisation
WS	Werner's syndrome
WST-8	2-(2-methoxy-4-nitrophenyl)-3-(4-nitrophenyl)-5-(2,4-disulfophenyl)-2H-tetrazolium, monosodium salt
XF analyzer	Extracellular flux analyser
XF24	Extracellular flux 24 well cell culture microplates
X-gal	5-bromo-4-chloro-3-indolyl-beta-D-galacto-pyranoside

CHAPTER ONE

Introduction

1: Introduction

1.1 Arsenic

1.1.1 Arsenic in the environment

Arsenic is a naturally occurring toxic chemical known as a metalloid due to its metal and non-metal like properties, present as the twentieth most abundant element in the earth's crust. It occurs in its native element form as well as a constituent to over 200 minerals and has been found to be present at varying concentrations in air, rocks, soil, water and food (Luong *et al*., 2007). Arsenic exists in both organic and inorganic forms in several oxidation states, with the inorganic forms trivalent arsenite and pentavalent arsenate being the most prevalent and thus the species to which humans are commonly exposed (Garelick *et al*., 2008) (Table 1.1).

The exposure of humans to arsenic can occur through many means due to its large distribution in the environment e.g. through the air as arsine, food which contains both organic and inorganic arsenic and through dgrrinking water which generally consists of the inorganic forms (Abernathy *et al*., 2003). The form of arsenic exposure to humans that is associated with the most adverse health effects is the consumption of contaminated drinking water (Abernathy *et al*., 2003), which has increased due to the development of water wells in the ground enabling arsenic to leech out from rocks. In many countries, such as Bangladesh, Taiwan and India, arsenic from drinking water has become a major health hazard due to its toxic effects.

NAME	STRUCTURE
Inorganic	
Arsenate	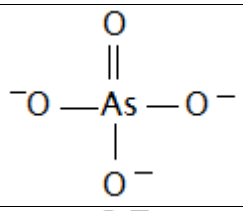
Arsenite	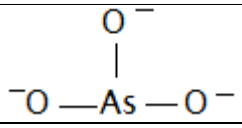
Organic	
Monomethylarsonic acid	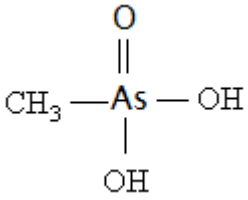
Dimethylarsinic acid	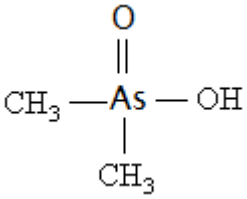
Trimethylarsine oxide	

Table 1.1 Naturally occurring arsenic species in both their organic and inorganic forms. (Adapted from WHO, 2001)

1.1.2 Arsenic metabolism

Of the two biologically relevant inorganic arsenic species, trivalent arsenite is more toxic than pentavalent arsenate, exerting its toxicity through the formation of strong bonds with functional groups on proteins, i.e. thiolates of cysteine residues with inhibition of the protein function (Bhattacharjee *et al*., 2009). Arsenite is taken up in the body through aquaglyceroporins (AQPs); AQP channels enable the transport of water, glycerol and other small molecules (Bhattacharjee *et al*., 2009), whereas arsenate mimics inorganic phosphate and therefore is taken up by phosphate transporters (Wysocki and Tamas, 2010).

On entering the body arsenate is reduced to arsenite. Arsenite then undergoes oxidative methylation and reduction steps by the enzymes arsenic methyltransferase and methylarsonic acid reductase in the presence of glutathione and S-adenosyl methionine to give the products monomethylarsenic (MMA) and dimethylarsenic (DMA) (Kedderis *et al*., 2006) (Figure 1.1). The methylation of inorganic arsenic helps the excretion process of this toxicant as MMA and DMA are more easily removed from the body in urine (WHO, 2001).

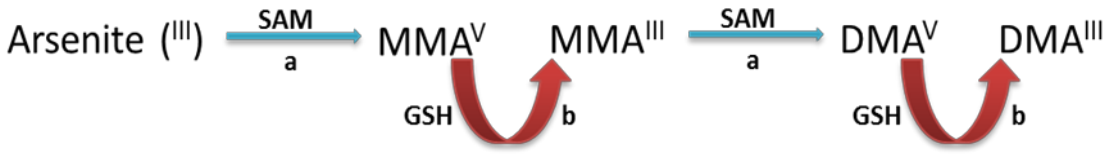

Figure 1.1 Metabolism of inorganic arsenic relies on oxidative methylation steps; represented by the blue arrows involving the methyltransferase Cyt19 (a) and cofactor S- adenosylmethionine (SAM), and reduction steps; represented by the red arrows, involving glutathione S- transferase omega 1-1 (b) and glutathione (GSH). (Adapted from Kedderis *et al*., 2006).

1.2. Health effects of Arsenic

The epidemiological effects of chronic arsenic exposure in humans, mainly through the consumption of arsenic contaminated drinking water, predominantly consisting of the inorganic arsenite and arsenate forms, have been manifested and researched globally (Figure 1.2).

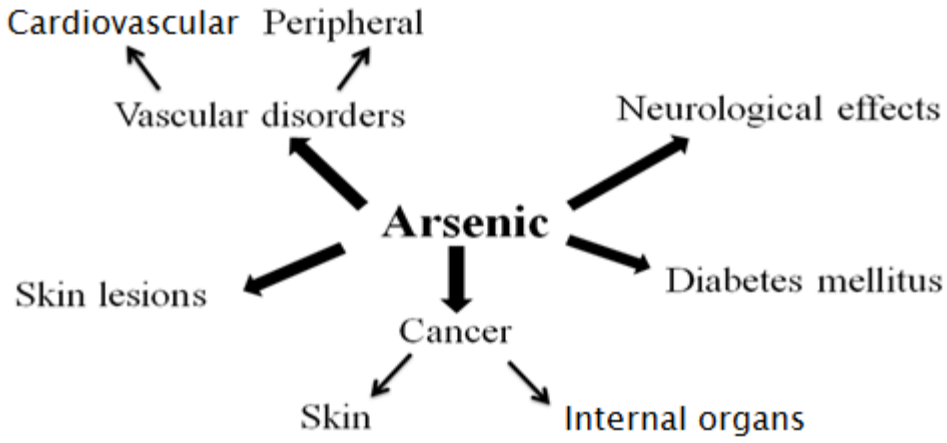

Figure 1.2 The health effects of chronic arsenic exposure on the human body. (Adapted from Smith *et al*., 2000)

1.2.1. Cancer

Arsenic has been classified as a group 1 carcinogen by the International Agency for Research on Cancer (IARC, 2012), suggesting arsenic to be the most carcinogenic environmental compound to humans, with incidents of arsenic induced cancer being manifested globally. The first study which identified the relationship between arsenic contaminated drinking water and cancer in humans was through the study of a population in Taiwan in which individuals developed skin cancer. The study found 10% of men chronically exposed to arsenic; approximately 500 µg/L found in their drinking

water, developed skin cancer by 60 years of age (Tseng *et al*., 1968). The occurrence of skin cancer however is found to be relatively low in comparison to the incidents of internal cancers observed in arsenicism (Smith *et al*., 2000).

Internal cancers have been found to give the highest mortality amongst the health effects of chronic arsenicism. In certain regions of Taiwan, where the arsenic concentration in water is as high as 800 μg/L, high incidents of bladder and lung cancer were observed (Chen *et al*., 1988; Smith *et al*., 1992; Bates *et al*., 1992). Lung cancer was also observed in 66% of the autopsies carried out on 163 male wine growers in Chile. These individuals had chronic arsenic poisoning due to the consumption of 'haustrunk'; a wine substitute made up of grapes of high arsenic content. As well as lung cancer, 5 of these males also suffered from liver cancer (Luchtrath, 1983). Liver cancer was also seen in 1 in 16 arsenic-induced cancer patients in Chile that consumed water containing arsenic at concentrations varying between 200- 2000 μg/L (Zaldivar *et al*., 1981).

Similarly in Bangladesh, high incidences of cancers have been noted in response to consumption of arsenic contaminated water. Chen and Ahsan (2004) calculated at least a 2-fold increase in the lifetime mortality risk of lung, bladder or liver cancer in response to arsenic consumption than the background lifetime mortality risk of these cancers in a Bangladeshi population. Furthermore, the excess cancer risk with lifetime exposure to arsenic contaminated drinking water that exceeds the WHO guidelines of <10 μg/L was determined at approximately 1 in 300 individuals, which poses a risk up to 300 times higher than other known carcinogens found in drinking water at

concentrations compliant with the U.S. regulations for drinking water (Smith *et al*., 2002).

1.2.2 Vascular disorders

Through the analyses of many of the arsenic exposed regions of the world such as the arseniasis endemic areas in Taiwan and Bangladesh, arsenic has been found to cause vascular disease through atherosclerosis (Tseng *et al*., 1996; Chen *et al*., 2006). Atherosclerosis is the thickening of the arterial walls due to the accumulation of fatty deposits which form plaques (Figure 1.3). Atherosclerosis has been found to be the primary cause of many cardiovascular and peripheral vascular disorders (PVD) (Wang *et al*., 2002).

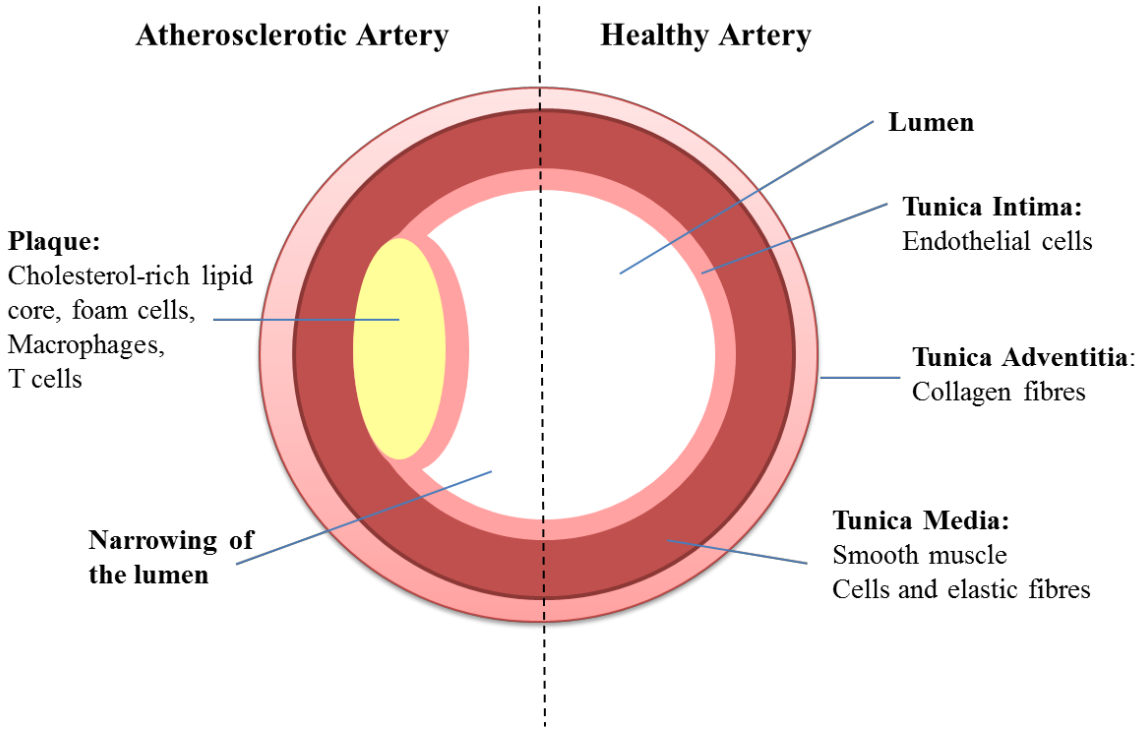

Figure 1.3 The comparison between a healthy artery against an atherosclerotic artery which displays the build-up of plaque and the narrowing of the lumen, restricting blood flow.

1.2.2.1 Peripheral vascular disease

The PVD called Blackfoot disease (BFD) is a characteristic to arsenicism, which is seen as endemic in Taiwan through the consumption of inorganic arsenic in water. The name of this disease is given due to the gangrene like symptoms that appear in the lower extremities of patients due to arterial occlusion (Tseng, 2002). Studies carried in the arsenic exposed regions of Taiwan have shown a concentration response relationship between the consumption of arsenic contaminated artesian well water and the prevalence of BFD. The cumulative arsenic exposure of ≥20,000 μg/L-years through contaminated water gave a prevalence rate of up to 19.8% for the development of PVD compared to 4.4% in a control group not exposed to arsenic contaminated water (Tseng, 2002).

This association between arsenic and BFD is supported by the display of other symptoms that have been associated with arsenic exposure, i.e. skin lesions and skin cancer (Tseng *et al*., 1968), as well as the decline in the number of BFD cases that have occurred in these 'BFD-hyperendemic regions' of Taiwan after the implementation of clean tap water (Tseng *et al*., 1996).

Atherosclerosis is the main pathological change that occurs to give rise to BFD. In a study of 52 limbs taken from BFD patients, 70% displayed features of atherosclerosis. Thrombus formation was also seen with a decrease in the number and size of newly formed blood vessels and changes in the vessel walls (Tseng *et al*., 2003).

1.2.2.2 Cardiovascular diseases

Cardiovascular disease (CVD) may not be as prevalent an effect of arsenic exposure to humans as cancer, however many global epidemiological studies have reported cases of CVD in arsenicism, particularly in arsenic rich areas such as Taiwan.

A relationship between long term arsenic exposure and the risk of developing carotid atherosclerosis was established in Taiwan by Wang *et al* (2002). Observations of intima media thickness and/or the presence of plaques in arteries were carried out using ultrasonography in individuals who had not yet developed heart disease. The study revealed arsenic exposure to lead to carotid atherosclerosis development and progression, giving rise to general atherosclerosis over time before the development of clinical events including myocardial infarctions (Wang *et al*., 2002). A concentration-dependent link was also established between arsenic exposure and hypertension in Taiwan, where long-term consumption of arsenic contaminated drinking water gave a 1.5 fold increase in the incidence of hypertension compared to non-exposed individuals (Chen *et al*., 1995).

Epidemiological studies carried out in Chile also found a direct relationship between the exposure to arsenic and CVD; autopsies of 10 infants and young adults ranging from the age of 1-18 years found intimal thickening in the arterial walls in 9 of the individuals. Furthermore, 2 of them displayed signs of myocardial infarction prior to death. Moreover, comparing adults <40 years in arsenic exposed and non-exposed areas of Chile showed a significant increase in the incidence of myocardial infarctions compared to the non-arsenic exposed population (Zaldivar, 1980).

1.3 Cardiovascular disease

CVD is one of the leading causes of death worldwide. The onset of CVD is usually as a result of vascular dysfunction due to factors such as high blood pressure, thrombosis and the development of atherosclerosis (Bosson, 2008), with atherosclerosis known to be the most common underlying cause for CVD.

1.3.1 Atherosclerosis

Atherosclerosis is an immune-inflammatory disease of the arteries that results in the narrowing of the arterial lumen due to the build-up of plaque (Figure 1.3). Atherosclerosis is initiated as a result of increased cholesterol and low-density lipoprotein (LDL) concentrations and developed further involving endothelial cells, smooth muscle cells and leukocytes (Falk, 2006), with the formation of plaques in the intima of blood vessels (Figure 1.3). In the formation of plaques, LDLs are sequestered within the intima, where they are oxidised by reactive oxygen species (ROS) produced by endothelial cells (Packard and Libby, 2008). Oxidised LDLs induce an inflammatory/ immune response and are taken up by macrophages by endocytosis, becoming lipid-rich foam cells (Siegel-Axel *et al*., 2008). Lipid-rich macrophages secrete pro-inflammatory cytokines, some of which cause recruitment of T lymphocytes (Packard and Libby, 2008). Disruption of the plaque leads to thrombus formation which results in the occurrence of fatal cardiovascular complications i.e. transient ischemic attack and stroke (Yuan *et al*., 2002).

Atherosclerosis is thought to occur as an immune/inflammatory response to lipid mediated endothelial cell damage (Siegel-Axel *et al*., 2008). The involvement of endothelial dysfunction in the early stages of atherosclerosis results in its use as an

indicator of early stage atherosclerosis (Davignon and Ganz, 2004). Since endothelial cells have anti-inflammatory and antithrombotic properties (Landmesser *et al*., 2004), the dysfunction of endothelial cells can be seen as an early and important factor in the pathogenesis of atherosclerosis

1.3.2 Mechanism of arsenic induced cardiovascular disease

The endothelium is a vital component of all blood vessels. It forms a metabolically active layer of cells with anti-coagulant and anti-thrombotic properties enabling laminar blood flow. The vascular endothelium also regulates the release of certain mediators e.g. nitric oxide (NO), angiotensin II, cytokines and prostanoids. Therefore, the endothelium can be seen to play a role in allowing the cardiovascular system to fulfil its functions (Balakumar and Kaur, 2009). Endothelial dysfunction has been found to be involved in the pathogenesis of arsenic-induced cardiovascular disease including atherosclerosis (Davignon and Ganz, 2004), hypertension (Savoia and Schiffrin, 2007) and heart failure (Desjardins and Balligand, 2006). Endothelial dysfunction is the imbalance that occurs between endothelial-mediated vasodilation and vasoconstriction. This can be as a result of many factors including a lack NO, inactivation or uncoupling of endothelial nitric oxide synthase (eNOS), increased reactive oxygen species (ROS) and reactive nitrogen species (RNS) generation and a decrease in the antioxidant defence mechanisms (Balakumar and Kaur, 2009; Cai and Harrison, 2000). The proposed effects of arsenic on these factors are shown in figure 1.4.

Arsenic contributes towards atherosclerosis through the enhancement of adhesion factors. Exposure of endothelial cells to arsenic up-regulated the tumour necrosis factor (TNF)-α mediated vascular cell adhesion molecule-1 protein expression (Tsou *et al*.,

2005). The increased expression of adhesion molecules by TNF-α is through the activator protein (AP)-1 and NF-$_K$B transcription factor signalling pathways, the activities of which are also seen to be enhanced by arsenite in endothelial cells (Barchowsky *et al*., 1996; Tsou *et al*., 2004).

Short-term exposure of endothelial cells to a relatively low concentration of arsenic, <650 μg/L, for up to 4 hours, resulted in an increase in ROS (Barchowsy *et al*., 1996), which correlates with an increased expression of NADPH oxidase (Smith *et al*., 2000) by arsenic exposure. Furthermore, an increase in glutathione (GSH) activity is seen in endothelial cells treated with low arsenite concentrations; <1,300 μg/L, (Tsou *et al*., 2003). With the antioxidant function of GSH, this increase implicates an increase in ROS and thus supports an increase in ROS as a possible mechanism of arsenite induced endothelial dysfunction.

An increase in ROS through arsenic exposure could result in the lack of nitric oxide NO bioavailability. NO is known as the endothelium derived relaxation factor as it is responsible for the dilation of blood vessels (Ignarro *et al*., 1987). However, ROS rapidly react with and therefore diminishes NO (see section 1.5.1), possibly contributing towards the development of atherosclerosis. Arsenic can also bring about this effect by targeting eNOS, the enzyme responsible for NO production in the endothelium (Figure 1.6). Arsenic concentration-dependently inhibits eNOS in endothelial cells by reacting with the vicinal thiol groups, resulting in a dysfunction of blood vessel relaxation and thus promoting cardiovascular complications (Lee *et al*., 2003; Kumagai and Pi, 2004).

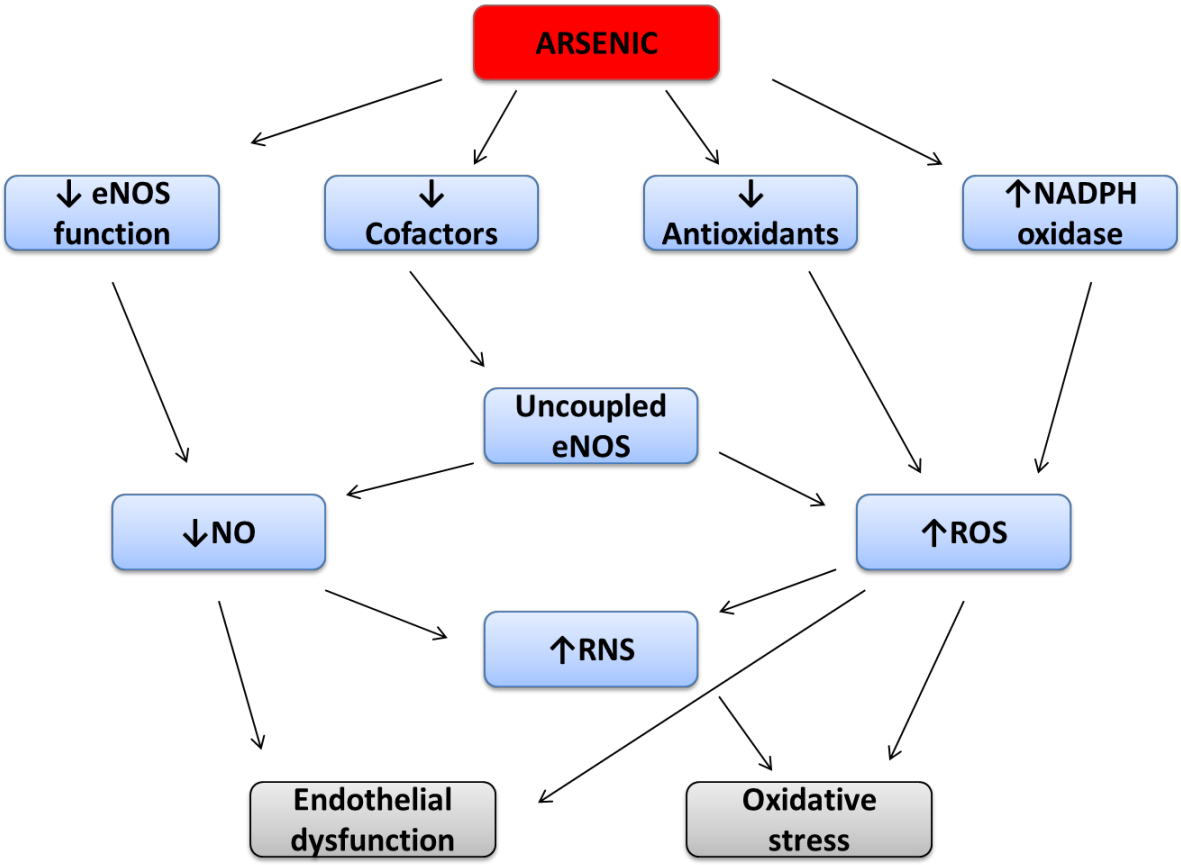

Figure 1.4 Mechanisms by which arsenic may bring about its effects in endothelial cells giving rise to endothelial dysfunction through the increase in oxidative stress. (Adapted from Kumagai and Pi, 2004)

1.4 Cardiovascular ageing

1.4.1 Cardiovascular disease, ageing and senescence

Epidemiological studies have revealed age to be a significant risk factor in the development of CVD, with incidences of diseases such as hypertension, coronary heart disease, congestive heart failure and stroke significantly increasing with age (Najjar *et al*., 2005). Growing evidence supports the involvement of cellular senescence in the process of human ageing (Faragher and Kipling, 1998). Cellular senescence is the phrase used to describe cells that undergo irreversible cell cycle arrest, displaying changes in their cellular physiology, morphology and gene expression. These changes contribute towards ageing of tissues and have the potential of giving rise to age-related diseases (Faragher and Kipling, 1998).

There are many factors that have been suggested to be involved in the onset of cellular senescence in endothelial cells including oxidants and antioxidants (Furumoto *et al*., 1998; Kurz *et al*., 2004), increased blood glucose concentrations (Yokoi *et al*., 2006), NO (Vasa *et al*., 2000), angiotensin II (Imanishi *et al*., 2005; Schleicher *et al*., 2008), inflammatory molecules (Breitschopf *et al*., 2001) and mitochondria (Schleicher *et al*., 2008). These are hypothesised to act by affecting the activity of telomerase; the enzyme responsible for adding the telomeric repeat sequences to the ends of eukaryotic chromosomes and/or to act by influencing the intracellular oxidative stress levels (reviewed in (Erusalimsky, 2009) (Figure 1.5).

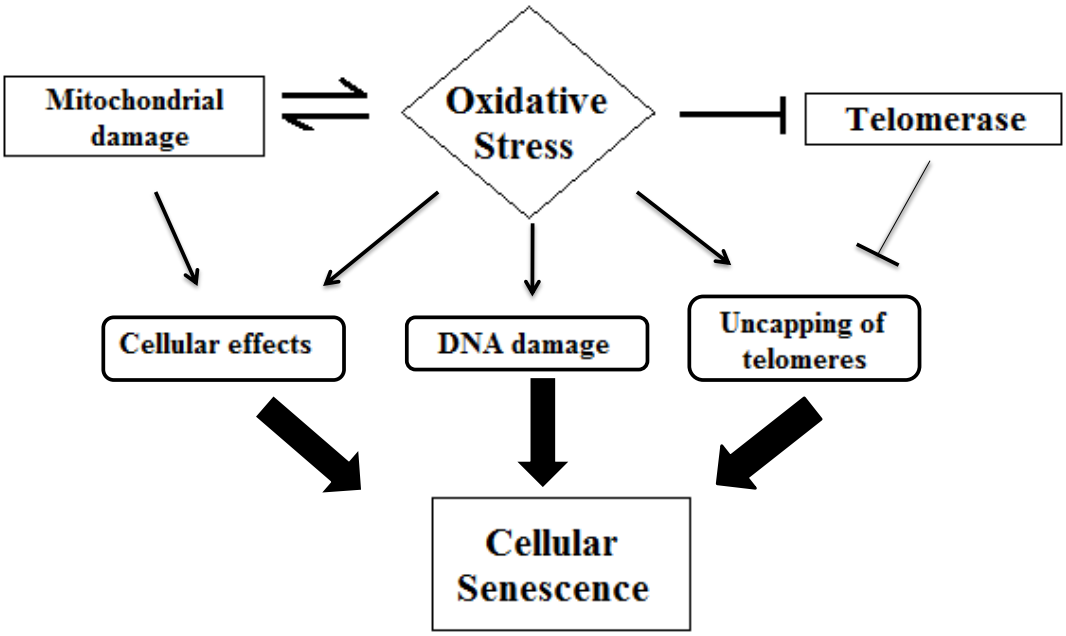

Figure 1.5 Factors that contribute to the induction of cellular senescence in endothelial cells (Adapted from Erusalimsky, 2009).

1.4.2 Cellular senescence

1.4.2.1 Replicative senescence

As senescent cells display shortened telomeres, telomeric length has become a good marker for the identification of cellular senescence *in vivo*. Telomeres are structures that form a 'cap' at the end of chromosomes. They are an array of DNA repeat sequences; TTAGGG, that along with 6 proteins form the telomere-shelterin complex. This complex has the function of protecting the ends of the chromosomes from damage and degradation during the cycles of DNA replication (de Lange, 2005; Oeseburg *et al*., 2010). However, this does not render cells immortal. With every cycle of replication, the length of the telomeres shortens until a critical length is reached where cells can no longer undergo replication and become dysfunctional. The cell then enters the state of senescence.

This form of 'replicative senescence' was first proposed by Hayflick and colleagues, where they observed the inability of human cells to infinitely proliferate *in vitro* despite optimum culture conditions for cellular growth (Hayflick and Moorhead, 1961; Hayflick, 1965). Despite the exact mechanism by which cells enter the senescence state not being completely clear, replicative senescence has shown the involvement of the cellular DNA damage response (DDR) triggered by the dysfunctional telomeres. The dysfunctional telomeres are thus recognised as double-strand breaks which are flagged up by the DNA damage checkpoint ceasing the cell cycle progression (d'Adda di Fagagna *et al*., 2003).

1.4.2.2 Stress-induced premature senescence

Stress-induced premature senescence (SIPS) is the term used to describe the onset of senescence independent of telomeric mechanisms, also known as stress or aberrant signalling induced senescence (STASIS). SIPS occurs due to cells being under a variety of stresses, which can results in the inhibition of genes involved in cellular proliferation and the activation of genes involved in growth inhibition (Chang *et al*., 2002). Oxidative stress is an effective inducer of premature senescence as seen through the exposure of cells to hydrogen peroxide (Chen *et al*., 1998) and t-BHP (Dumont *et al*., 2001), most probably through oxidative DNA damage (Chen *et al*., 1995) which would lead to cell cycle arrest. Other factors that bring about SIPS include non-oxidative DNA damage (Robles and Adami, 1998) and inadequate cell culture conditions (Ramirez *et al*., 2001).

Comparing the two main forms of senescence; replicative senescence and SIPS, although occurring through different mechanisms, they share many common properties.

Both senescence cell types display senescence-associated morphological changes e.g. flattened and enlarged appearance. The initiation of senescence involves the recognition of DNA damage, which leads to the activation of the cell-cycle checkpoints and induction of irreversible cell cycle arrest through the p53 and $p16^{INK4A}$-RB pathways (Wright *et al*., 1996; Kuilman *et al*., 2010). The involvement of these tumour-suppressor pathways can be used as biomarkers of senescence as senescent cells show an increased activity of p53, induction of $p16^{INK4A}$ and the accumulation of RB, the accumulation of proteins p^{21CIP1} and $p^{15INK4B}$ have also been seen in senescent cells (Kuilman *et al*., 2010). The senescence associated secretory phenotype (SASP) is also common between t both cell forms, in which the senescent cells undergo transcriptional changes resulting in the secretion of many factors such as cytokines and chemokines (Kuilman *et al*., 2010).

However, whereas in replicative senescence cells that are programmed to undergo a number of replication cycles before senescence is achieved, SIPS is not programmed to occur in such a way. Furthermore, the presence of telomerase can prevent replicative senescence through the constant renewal of the telomeres (Wright *et al*., 1996), whereas such a phenomenon is not possible for SIPS.

1.4.3 Cellular senescence in cardiovascular diseases

Observing plaques that are formed in cases of atherosclerosis has revealed insightful information into the replicative ability of vascular cells. Vascular smooth muscle cells (VSMCs) in plaques display an earlier onset of senescence (Ross *et al*., 1984; Bennett *et al*., 1995), a slower proliferative ability (Ross *et al*., 1984; Bennett *et al*., 1995; Mosse *et al*., 1985) and higher incidence of apoptosis (Bennett *et al*., 1995) when compared to

the smooth muscle cells taken from healthy blood vessels . These observations were found to be the result of changes in the activity of cell signalling molecules e.g. p53 and $p105^{RB}$, in the plaque smooth muscle cells (Bennett *et al*., 1998). Vascular endothelial cells located on the surface of plaques also displayed morphological features of senescence i.e. flattened and enlarged appearance, indicating that endothelial cells also undergo early senescence in atherosclerosis (Burrig, 1991).

As endothelial cells get older, the production of NO decreases (Sato *et al*., 1993), in line with diminished expression of eNOS (Matsushita *et al*., 2001). These changes disrupt the vasodilatory ability of blood vessels, providing a possible mechanism for the pathogenesis of CVD in ageing. Along with the decrease in NO, an up regulation of pro-inflammatory cytokines and adhesion molecules seen in senescent endothelial cells makes them more prone to interaction with monocytes, thus enhancing atherogenesis (Maier *et al*., 1993).

The endothelium is generally considered to have a low cell turnover, however at regions where the blood flow is perturbed i.e. branching points, the endothelial cells have been found to undergo an increased number of replicative cycles (Caplan and Schwartz, 1973). Such sites in the vasculature are prone to atherosclerosis, where endothelial cell senescence has been found to occur by an accelerated shortening of telomeres, in comparison to the general age-related telomeric shortening (Aviv *et al*., 2001, Chang and Harley, 1995). The increased shortening of telomeres in cases of vascular disease is supported by a study looking into coronary artery disease which also found that endothelial cells from the diseased artery had shorter telomeres than endothelial cells in

healthy arteries (Ogami *et al*., 2004). Thus, replicative senescence occurs at sites prone to atherogenesis, suggesting a direct link between cellular ageing and CVD.

1.4.3.1 Telomeres and CVD

Age is one of the biggest risk factors for CVD development, along with genetic and environmental factors, contributing to an individual's susceptibility to CVD development. Telomeres have been recently found to play an important role in the onset of CVD through their importance in determining 'biological age' which can be used to partly explain why the susceptibility to CVD and the age of onset differs in individuals (Samani and van der Harst, 2008).

As described above (Section 1.4.3), shortening of telomeres may contribute to the onset of CVD through senescence of endothelial cells in atherosclerosis (Aviv *et al*., 2001, Chang and Harley, 1995). Further support for the role of shortened telomeres in human CVDs has been established in cases of atherosclerosis (Samani *et al*., 2001), premature myocardial infarction (Brouilette *et al*., 2003) and chronic heart failure (van her Harst *et al*., 2007). Additionally, coronary artery disease (CAD) has also been associated with shortening of telomeres. Studying the telomeric lengths in leukocytes of middle-aged individuals with hypercholestrolaemia identified the presence of shortened telomere length prior to CAD development when compared to those of healthy non-hypercholestrolaemic middle-aged individuals, proving telomere shortening as a cause rather than effect of CAD (Brouilette *et al*., 2007).

1.4.4 Premature ageing and cardiovascular disease

Studying certain human genetic disorders such as Werner's syndrome (WS) and Hutchinson-Gilford progeria syndrome (HGPS), which gives individuals the phenotype of premature ageing, has proven insightful when studying the effects of ageing on CVD (Capell *et al*., 2007). Individuals with HGPS have been found to develop cardiovascular complications during childhood resulting in myocardial infarction or stroke by the age of 13 (DeBusk, 1972). Both WS and HGPS display cell cycle abnormalities which result in the onset of premature cellular senescence and ageing with the development of premature atherosclerosis (Capell *et al*., 2007).

WS occurs as a result of a mutation in the *WRN* gene giving rise to a truncated form of the WRN protein (Huang *et al*., 2006). This protein is a tumour suppressor and also plays a role in DNA repair, recombination and replication (Huang *et al*., 2006). One of its functions involves the repair and maintenance of telomeres, therefore mutations in WRN result in a limited replicative capacity of cells and therefore a higher rate of senescence. This is seen in cell culture experiments when comparing normal human fibroblasts with those of WS patients which showed up to a 6-fold increase in the loss of proliferating cells in the WS fibroblasts (Kill *et al*., 1994). Study of both HGPS and WS therefore support the concept of senescence being a contributor of ageing, in turn leading to the onset of CVD.

1.5 Oxidative stress

Oxidative stress is brought about by the overproduction or accumulation of ROS, i.e. through the increased ROS generation from the mitochondria and/ or as a result of overstimulation of ROS generating enzymes i.e. NAD(P)H oxidase, xanthine oxidase, lipoxygenases and NOS, or through the depletion of antioxidants. Therefore oxidative stress can be defined as an imbalance between ROS and antioxidants.

1.5.1 Reactive oxygen species

The generation of ROS in cells is a by-product of normal cellular metabolism, however, excessive production of ROS leads to oxidative stress. In endothelial cells, oxidative stress results in the lack of NO bioavailability through the rapid reaction of ROS with NO or the uncoupling of eNOS. In endothelial cells, the synthesis of NO is catalysed by eNOS in the presence of many cofactors (Figure 1.6), of which tetrahydrobiopterin (BH_4) has been found to be the most important as the absence of BH_4 results in significant decrease of NO synthesis through eNOS uncoupling (Kumagai and Pi, 2004).

The uncoupling of eNOS is the term used to describe the effects on NO and ROS generation in the absence of cofactors; BH_4 (Kumagai and Pi, 2004). In normal circumstances, eNOS is able to produce abundant amounts of NO with a low level of ROS, namely superoxide, generation. However, in abnormal circumstances e.g. lack of BH_4 or of L-arginine (Figure 1.6), there is an increased generation of superoxide and a reduced amount of NO synthesised (Heinzel *et al*., 1992; Pi *et al*., 2003).

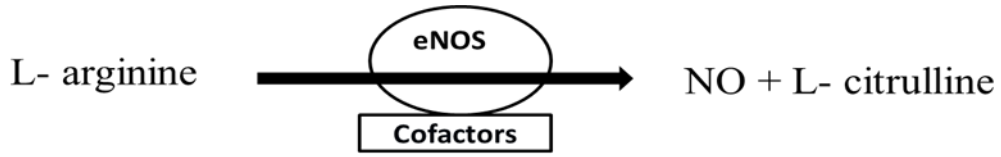

Figure 1.6 The synthesis of NO involves the substrates L-arginine, NADPH, H^+ and O_2, in which L-arginine is converted by eNOS into L-citrulline and NO along with the generation of $NADP^+$. This reaction occurs in the presence of many cofactors e.g. BH_4, calcium, calmodulin, flavin mononucleotide and flavin adenine nucleotide, which are required for the activation of eNOS (Kumagai and Pi, 2004).

The reaction between NO and superoxide gives rise to peroxynitrite; a RNS (Table 1.2) (Kumagai and Pi, 2004). Peroxynitrite is a strong oxidising agent and can influence gene expression, interfere with cell signalling pathways and bring about cellular and tissue damage (Uppu *et al*., 2007). In endothelial cells, ROS and RNS, i.e. peroxynitrite, are both produced from highly controlled enzymes, and have both beneficial and harmful effects on the cell (Valko *et al*., 2006). In normal circumstances when present at low levels, they have been found to have roles in cellular responses and signalling pathways (Sundaresan *et al*., 1995; Shirasu *et al*., 1996), however excessive levels can result in damage to cellular biomolecules including DNA, proteins and lipids. ROS are especially considered to have a 'two-faced' character as low levels are involved in protecting the cell against ROS mediated oxidative stress and maintaining the cellular redox balance (Storz *et al*., 1990; Schreck *et al*., 1991), whereas high levels induce oxidative damage.

The superoxide anion radical is the primary ROS species, which is formed by many enzymes such as eNOS, NAD(P)H oxidase and xanthine oxidase in endothelial cells (Barchowsky *et al*., 1999), by the addition of an electron to molecular oxygen (Miller *et al*., 1990). It is believed that in most non-phagocytic cells, superoxide is mainly produced in the mitochondria, through the reaction between electrons which leak from

the electron transport chain (ETC) and molecular oxygen (Murphy 2009). Superoxide is considered as the primary ROS in many cell types as it undergoes disproportionation to give rise to hydrogen peroxide by the enzyme superoxide dismutase (SOD). Hydroxyl radicals are also produced by the iron catalysed Haber-Weiss reaction, in which superoxide reacts with hydrogen peroxide giving rise to the very reactive hydroxyl radical (Kumagai and Pi, 2004, Valko *et al*., 2007, Liochev and Fridovich, 2002).

1.5.2 Antioxidants

Under normal circumstances, cells are protected from the effects of ROS and RNS due to the presence of antioxidants. Antioxidants provide protection against damage through the removal of free radicals and are present in both enzymatic and non-enzymatic forms (Table 1.2) (Valko *et al*., 2006). SOD is an example of a very efficient enzymatic antioxidant; it is responsible for the dismutation of superoxide to give a less reactive product; hydrogen peroxide, and molecular oxygen (McCord and Fridovich, 1969). Catalase is another enzymatic antioxidant which has a very high turn-over rate in comparison to other enzymes. It acts on hydrogen peroxide and has the ability of catalysing the conversion of approximately 6,000,000 hydrogen peroxide molecules to water and molecular oxygen per minute (Chance *et al*., 1979; Mates *et al*., 1999).

Examples of non-enzymatic antioxidants include ascorbic acid (vitamin C) (Mates *et al*., 1999) and α-tocopherol (vitamin E) which work in partnership in aqueous conditions to convert α-tocopherol radicals found in lipoproteins and membranes, back into α-tocopherol (Kojo, 2004). Vitamin E is also vital for its chain-breaking antioxidant role in preventing free radical reactions occurring in the membranes of cells during the process of lipid peroxidation (Devasagayam *et al*., 2004).

Reactive species		**Antioxidants**	
Reactive oxygen species		*Enzymatic antioxidants*	
Superoxide	Produced by the mitochondria, involved in producing other reactive oxygen species e.g. Hydrogen peroxide	Superoxide dismutase	Catalyses the dismutation of superoxide to give hydrogen peroxide and molecular oxygen, 3 isoforms in humans
Hydroxyl radical	Highly reactive, generated in conditions of high iron concentration	Catalase	Efficiently reacts with hydrogen peroxide to give molecular oxygen and water
Hydrogen peroxide	Formed in the body through many reactions, has potential of producing hydroxyl radicals	Glutathione peroxidise	Contains selenium, catalyses the reduction of hydroperoxides and degrades hydrogen peroxide, essential for cell antioxidant protection
Peroxyl radical	formed as a result of oxidative damage from cellular components e.g. DNA, proteins, lipids		
Organic hydroperoxide	Generates reactive species by reacting with metal ions	Peroxiredoxins	Have peroxidase activity, reduce and detoxify hydrogen peroxide and hydroperoxides
Singlet oxygen	formed during chemical and photochemical reactions, highly reactive	Thioredoxin	Disulfide reductase, keeps proteins in a reduced state. Is reduced by thioredoxin reductase
Reactive nitrogen species		*Non-enzymatic antioxidants*	
Nitric oxide	Many functions in the body i.e. vasodilator, reacts with superoxide to generate peroxynitrite	Vitamin E	Prevents the occurrence of free radical reactions by intercepting ROS and free radicals at the membrane
Peroxynitrite	highly reactive, oxidising agent	Vitamin C	Part of cellular defence mechanism, works in conjunction with vitamin E
Peroxynitrous acid	protonated form of peroxynitrite	Thiol antioxidants	Disulphide redox buffer, quenches free radicals, acts as substrate for redox reactions

Table 1.2 Examples of some antioxidants and reactive oxygen and nitrogen species. (Holmgren, 1985; Hofmann *et al*., 2002; Wood *et al*., 2003; Devasagayam *et al*., 2004; Valko *et al*., 2006)

1.5.3 Reactive oxygen species and cardiovascular ageing: potential role of arsenic?

Age is a major risk factor for the development of CVD. One theory which provides insight into the mechanism by which natural ageing occurs is the free radical theory proposed by Harman (1956). This suggests that the free radicals generated in cells during cellular metabolism, specifically reactive oxygen species (ROS) have deleterious side effects on cellular components i.e. bringing about oxidative damage to DNA, proteins and lipids, which accumulate over time and contribute to the ageing process (Harman, 1956). This theory is supported by a study investigating whether the extent of oxidative damage of these three cellular components correlates with ageing by examining muscle biopsy specimens taken from individuals between the ages of 25 and 93 years. An age-dependent increase in 8-oxo-dG; a marker for oxidative DNA damage, malondialdehyde; a marker for lipid peroxidation, and protein carbonyl groups; a marker for protein oxidation, were observed (Mecocci *et al*., 1999). After a few years, Harman recognised mitochondria as the main sources of intracellular ROS and modified his ageing theory to hypothesise mitochondria as the main culprit in ageing, forming the 'mitochondrial free radical theory of ageing' (MFRTA) (Harman, 1972).

Despite being the current most popular theory of ageing, the MFRTA does face some controversy. Studies focussing on the over-expression of antioxidants in animal models to combat the damaging effects of free radicals have not always shown significant increases in maximum life span, which can be seen as evidence against the MFRTA (Sanz and Stefanatos, 2008). Furthermore, studying mice mutant for polymerase gamma (Polγ), mitochondrial specific DNA polymerase, have also shown discrepancies between the effects on ageing. Trifunovic (2004) observed the appearance of age-related phenotypes in knock-in mice that express a proof-reading deficient version of

Polγ, suggesting accelerated ageing, whereas Vermulst *et al* (2007) found no signs of premature ageing in mice carrying a mutant form of Polγ, despite having 500-times the increased DNA mutation burden than wild-type mice.

ROS are important for the normal function of cells due to their involvement in many cellular processes such as signal transduction (Mittal and Murard, 1977), immunity (Roth and Droge, 1987), regulating the expression of oxidative-stress response genes (Storz *et al*., 1990; Schreck *et al*., 1991) and apoptosis (Buttke and Sandstrom, 1994). The concept of ROS also having deleterious effects was supported by the discovery of antioxidant enzymes such as superoxide dismutase which serve the function of ROS detoxification (McCord and Fridovich, 1969). Such deleterious effects of ROS have been seen to affect the cardiovascular system in an age-related manner, e.g. oxidative stress is found to reduce cell viability and play a role in myocardial atrophy by inducing cell death (Bhatnagar, 1994). Furthermore, through the oxidation of lipids and the expression of ROS-sensitive inflammatory genes, ROS are proposed to be involved in initiating the atherosclerotic processes (Kondo *et al*., 2009).

The increase in oxidative stress in aged hearts can be explained by the increase in ROS generation from the mitochondria over time (Muscari *et al*., 1996). ROS from either the mitochondria or from the intra/extra-cellular sources results in damage to the mitochondria and in this way initiates cellular degeneration contributing to the process of ageing. This can therefore be seen to be one of the underlying concepts of the free radical theory of ageing (Cadenas and Davies, 2000).

One of the ways in which arsenic has been proposed to bring about its toxic effects to the cardiovascular system is through the stimulation of ROS generating enzymes i.e. NADPH oxidase, as seen in vascular endothelial cells (Smith *et al*., 2001), thus inducing oxidative stress (Balakumar and Kaur, 2009). Following the free radical theory of ageing, arsenic exposure can be seen to have the potential to contribute to the process of cardiovascular ageing.

1.5.4 Arsenic induced reactive oxygen species generation in endothelial cells

Arsenic has been hypothesised to bring about its toxicity through the induction of oxidative stress in cells. This hypothesis is supported by the research carried out on the effects of arsenite on endothelial cells.

The involvement of ROS in the cytotoxicity exhibited by arsenic was displayed through the acute exposure of porcine aortic endothelial cells to 650 μg/L arsenite. A significant increase in oxygen consumption was noted over a period of 20 minutes exposure due to the increased formation of superoxide by NADPH oxidase as well as an increase in the generation of hydrogen peroxide measured using the homovanillic acid assay (Barchowsky *et al*., 1999). The association of arsenite with superoxide generation in porcine aortic endothelial cells was also supported by Smith *et al* (2001). A two-fold increase in the activity of NADPH oxidase seen after 1 hour exposure to 650 μg/L arsenite, measured using the superoxide-dependent lucigenin chemiluminescence method (Griendling *et al*., 1994; Smith *et al*., 2001), thus suggesting an increase in the amount of superoxide generated (Smith *et al*., 2001).

Arsenic has been found to induce oxidative stress by ROS generation in vascular endothelial cells at sub-cytotoxic concentrations ≤650 µg/L. This is through ROS-induced activation of regulatory enzymes and initiation of cellular pathways. An example of this is seen by observing the activity of NF-κB, a transcription factor that is activated by cellular stress such as oxidative stress (Schreck *et al*., 1991) and has been found to be activated by the exposure to ≤650 µg/L sodium arsenite and blocked by antioxidants in vascular endothelial cells (Barchowsky *et al*., 1996). Thus sub-cytotoxic levels of arsenic may contribute to vascular diseases by activating oxidant- dependant signalling pathways in endothelial cells.

More recently, work carried out on human umbilical vein endothelial cells (HUVECs) has shown an increase in ROS in response to arsenite. Sun *et al* (2009) used the dihydroethidium (DHE) superoxide specific fluorescent-dye with fluorescent microscopy to measure the generation of superoxide after 2 hours exposure to 0.2, 1 and 650 µg/L arsenite, with a concentration-dependent increase detected. In a subsequent study, flow cytometry was used with dichlorodihydrofluorescin diacetate (DCFH-DA), a fluorescent dye that potentially and controversially detects general ROS. In HUVECs treated over an 8 hour period with 650 and 6,500 µg/L arsenite an increase in ROS after 4 hours exposure was observed (Lii *et al*., 2011). However, using the same method of ROS detection, Shi *et al* (2010) showed that treating HUVECs for a longer time-point; 24 hours, results in a significant decrease in ROS generation for 650 and 1,300 µg/L arsenite, whereas treatment with 2,600- 5,200 µg/L results in a significant increase in ROS detected.

1.5.5 Arsenic induced DNA damage

Arsenic has been found to induce genotoxicity. The mutagenic effects of arsenic on DNA have been found to occur in a concentration-dependent manner, with arsenic mainly bringing about multi-locus deleterious mutations (Hei and Filipic, 2004). Using the A_L human hamster hybrid cells (Puck *et al*., 1971) the mutagenic property of arsenic was observed. Arsenic treatment resulted in the induction of large deleterious mutations and chromosome aberrations, which are found to be as a result of ROS generation, with hydroxyl radicals specifically implicated in the mutagenicity (Hei *et al*., 1998).
To confirm the role of ROS in mutation induction, the A_L cells were exposed to dimethyl sulfoxide (DMSO), an oxygen radical scavenger, after treating the cells with sodium arsenite concentrations varying from 0-3,000 μg/L for 24 hours. The mutagenic effects of arsenic were significantly reduced in comparison to cells without the addition of DMSO (Hei *et al*., 1998). This is supported by another study which showed the addition of antioxidants to cultured human lymphocytes reduced the onset of chromosome aberrations and sister chromatid exchange events that occur in response to arsenic. This further suggests the involvement of ROS in arsenic mutagenicity (Nordenson and Beckman, 1991).

There are many biomarkers that can be used to detect the onset of arsenic induced oxidative damage in human studies, i.e. 8-oxo-dG, a product of guanine oxidation. 8-oxo-dG can be easily detected in individuals as it is excreted in urine after being excised as part of its repair process (Wong *et al*., 2005). An investigation was carried out on individuals in Cambodia chronically exposed to varying concentrations of arsenic through contaminated drinking water, from ≤1-886 μg/L. Those subjects with higher levels of arsenic in their urine also had higher levels of 8-oxo-dG in comparison to those

with lower levels of arsenic in their urine (Kubota *et al*., 2006). This provides evidence for the ability of arsenic to induce DNA damage through the generation of ROS, as well as supporting the concentration-dependent nature of this oxidative DNA damage.

1.6 Mitochondria

1.6.1 Mitochondrial respiration, mitochondria ROS and ageing

Mitochondria are the 'power-houses' of cells; being the main source of adenosine triphosphate (ATP) production through oxidative phosphorylation. They are divided into 4 compartments; matrix, inner membrane, intermembrane space and outer membrane (Huang and Manton, 2004). The production of ATP occurs through oxidative phosphorylation coupled to ETC in the inner membrane, involving a series of 5 complexes (Figure 1.7). The ETC involves the first 4 complexes; NADH dehydrogenase (I), succinate dehydrogenase (II), Q-cytochrome c oxidoreductase (III) and cytochrome c oxidase (COX) (IV). NADH and $FADH_2$, generated through previous stages of respiration; glycolysis and Krebs cycle (Figure 1.7), are oxidised to give rise to free electrons that are transferred between these complexes. This transfer of electrons gives rise to a proton gradient which fuels the process of oxidative phophorylation. Oxidative phosphorylation occurs within the matrix involving the last complex (V); ATP synthase. The proton gradient generated catalyses the phosphorylation of ADP and generates ATP (Boekema and Braun, 2007).

The mitochondrial process of ATP formation results in the generation of ROS due to the leaky nature of the electron transport chain. Mitochondria take up approximately 90% of oxygen consumed by the cell (Huang and Manton, 2004), therefore electrons that

'leak' out of the chain are able to react with molecular oxygen, reducing it to form superoxide (Khansari *et al*., 2009) (Figure 1.7). Mitochondrial DNA (mtDNA), multiple copies of 16.5 kb double-stranded circular structures, is prone to oxidative damage. Thus, increases in mitochondrial ROS results in mtDNA damage (Yakes and Van Houten, 1997).

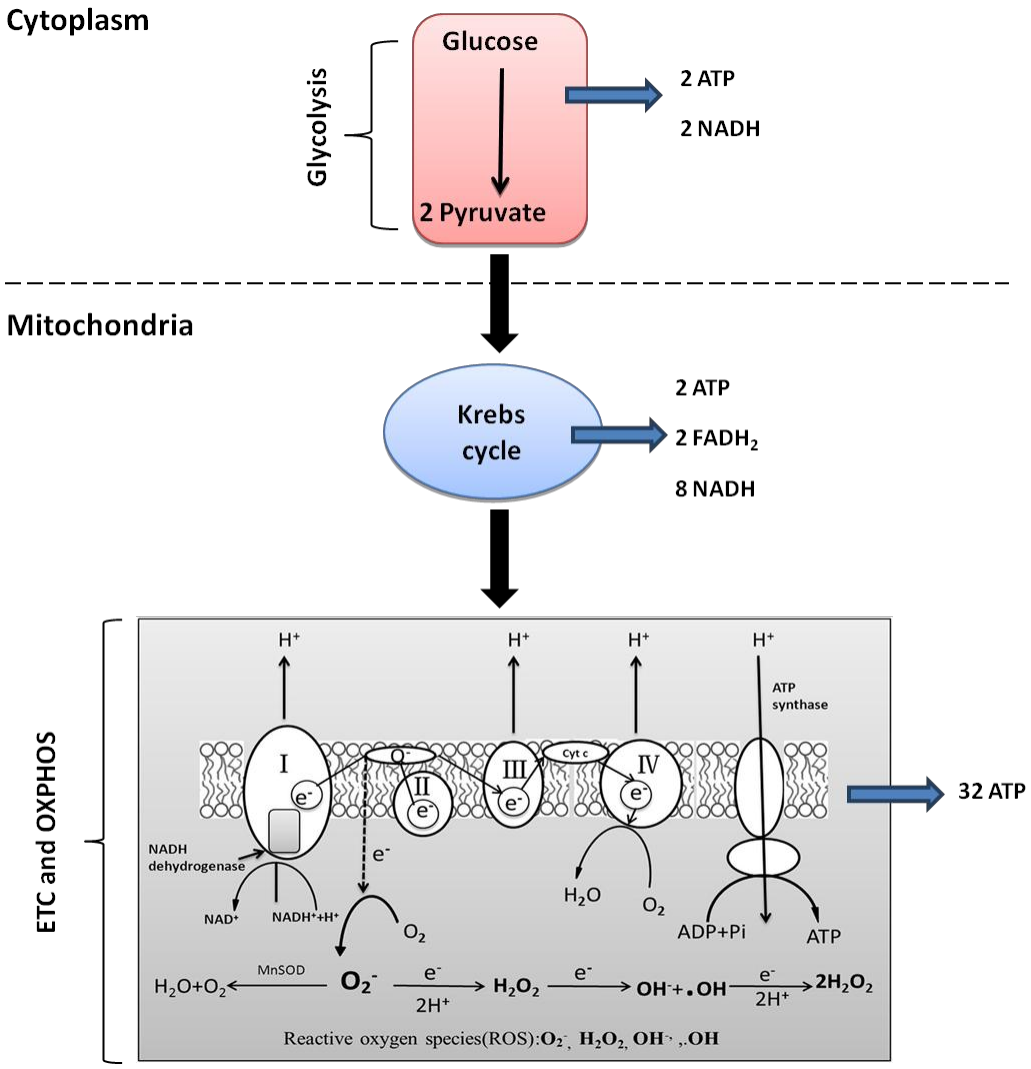

Figure 1.7 An overview of the process of cellular respiration in mammalian cells, highlighting the generation of ROS from the electron transport chain (ETC) in the mitochondria during ATP production. Most cellular ATP comes through the mitochondrial oxidative phosphorylation (OXPHOS) process coupled to the ETC, which involves a series of five complexes, with OXPHOS occurring at the final complex, ATP synthase. (Adapted from Zhuo *et al*., 2012)

The role of mitochondria in cells however goes beyond that of cellular energy conservation; they also play an important part in cellular development, metabolism, cell cycle control and apoptosis (McBride *et al*., 2006). Damage to mitochondria is thus detrimental to the cell. The accumulation of oxidative stress induced damage i.e. oxidative damage to mitochondrial biomolecules including DNA, is seen to be one of the underlying mechanisms involved in the process of ageing, contributing towards the 'free radical theory of ageing' (Harman, 1956) . Increased mitochondrial oxidative stress can contribute to cellular ageing through many routes; increased shortening of telomeres; accelerating the process of apoptosis through the release of apoptotic factors i.e. cytochrome c and apoptosis-inducing factor and inducing mitochondrial dysfunction. Mitochondrial dysfunction has critical consequences for the cell as mitochondria provide cellular protection against stress and damage. Furthermore, mitochondrial dysfunction results in a substantial decrease in ATP available for the cell to carry out the necessary processes required for survival (reviewed in Huang and Manton, 2004).

1.6.2 Arsenic induced mitochondrial DNA damage

Mitochondria are considered the primary targets for arsenic induced oxidative damage as they are the main source for ROS generation. The mitochondrial components are highly susceptible to damage by arsenic; oxidation of protein structures, damage to mtDNA and lipid peroxidation-which could in turn be the mechanism by which membrane impermeable ROS, e.g. superoxide, leak out of the mitochondria and into the cytoplasm causing further cellular damage (Liu *et al*., 2005).

In order to display its genotoxic effects, arsenic would therefore appear to be dependent on normal functioning of mitochondria. This was demonstrated by a study carried out on A_L cells. The exposure of normal A_L cells to sodium arsenite induced mutagenesis, however mtDNA deficient (ρ) A_L cells with diminished mitochondrial membrane potentials displayed reduced or no mutations above the background level. Furthermore, arsenite-induced nuclear DNA mutation also disappeared in ρ A_L cells, suggesting the presence of mtDNA and therefore functional mitochondria to be important for the genotoxic effects of arsenite (Liu *et al*., 2005).

Damage to mtDNA was further observed again using A_L cells. Cells were treated with 1,000 μg/L of sodium arsenite for 60 days and the effects on mitochondrial oxidative function were observed by assessing the activity of COX. In comparison to untreated cells, the arsenite treated cells displayed 45% less COX activity; as 3 of the 13 subunits of COX are encoded in mtDNA, this could be due to the genotoxic effects of arsenic on mtDNA (Partridge *et al*., 2007).

Arsenic has been known to be a chromosomal mutagen and induces deleterious mutations (Liu *et al*., 2005). On analysis, arsenic was found to induce large heteroplasmic deletions in mtDNA of A_L cells after chronic, 30 days, and acute, 24 hours, exposure to low levels of 250, 500 and 1,000 μg/L. Furthermore, treatment at these low concentrations of arsenite for 60 days resulted in a 65% reduction in the copy number of mtDNA in comparison to that of untreated cells (Partridge *et al*., 2007).

CHAPTER TWO

Hypothesis and Aims

2: Hypothesis and Aims

Arsenic exposure has been implicated in the onset of CVD, with particular emphasis on atherosclerosis. Studies into the pathophysiology of arsenic-induced CVD suggest an impact of arsenic on cardiovascular ageing, with an induction of oxidative stress being the main mechanism by which arsenic can be hypothesised to bring about premature ageing. Research into the *in vitro* effects of arsenic have shown an increased production of ROS, in accordance with the mitochondrial free-radical theory of ageing, along with effects on the mitochondria, indicating mitochondrial mediated ROS generation.

The aim of this thesis is to gain an understanding into the mechanisms by which arsenite induces changes within endothelial cells that result in the initiation of atherosclerosis. It can be hypothesised that arsenite exerts its toxicity on endothelial cells through oxidative stress-induced premature senescence, as a result of increased mitochondrial ROS generation, leading to oxidative intracellular damage.

The experimental aims of this project are to:

- Establish whether sub-cytotoxic concentrations of arsenite induce premature senescence in human endothelial cells
- Measure intracellular ROS generation in response to arsenite, and to investigate the source of ROS
- Investigate the impact of arsenite on mitochondrial function in HUVECs
- Identify the effects of arsenite on the *in vitro* gene expression profile of HUVECs

CHAPTER THREE

Materials and Methods

3. Materials and Methods

3.1 Cell culture

3.1.1 Materials

Human umbilical vein endothelial cells (HUVECs) were purchased from Invitrogen (C0035C). EA.hy926 cells are a fusion of HUVECs with the permanent human cell line A549 derived from a human lung carcinoma (Edgell *et al*., 1983) and were obtained from ATCC® (CRL-2922). Human hepatocellular liver carcinoma (HepG2) cells were purchased from abcam® (ab14659).

Tables 3.1, 3.2 and 3.3 show the composition of the cell culture growth media for HUVECs, EA.hy 926 cells and HepG2 cells. Table 3.4 shows the composition of the mixtures used to cryopreserve HUVECs, EA.926 cells and HepG2 cells.

Cell culture media	Quantity (ml)
HUVECs	
Medium 200 (Invitrogen M200500)	485
Low Serum Growth Supplement (Invitrogen S00310).	10
Penicillin/ streptomycin mix (Lonza, 1U/µg)	5
EA.hy 926 cells	
Dulbecco's Modified Eagle's Medium (Sigma-Aldrich D5546)	445
Foetal calf serum (Lonza, lot no: 7SB0014)	50
Penicillin/ streptomycin mix (Lonza, 1U/µg)	5

Table 3.1 The components required to make up the complete media for culturing HUVECs and EA.hy 926 cells.

COMPONENT	QUANTITY
High glucose DMEM	442.5 ml
Hepes buffer solution 1 M (Sigma-Aldrich, 83264)	2.5 ml, final concentration 5 mM
FBS	50 ml
Penicillin/streptomycin	5 ml

Table 3.2 Composition of high glucose HepG2 growth media.

COMPONENT	QUANTITY
DMEM, no glucose	430.5ml
Galactose (Sigma-Aldrich G6404)	5ml, final concentration 10mM
Hepes buffer solution 1 M (Sigma-Aldrich, 83264)	2.5ml, final concentration 5mM
L-Glutamine solution 200 mM (Sigma-Alrich G7513)	2ml, final concentration 6mM
Sodium pyruvate solution100 mM (Sigma-Aldrich, S8636)	5ml, final concentration 1mM
FBS	50ml`
1	5ml

Table 3.3 Composition of galactose containing media for HepG2 cell culture.

Trypsin/EDTA (Lonza, 10X concentration; 5 g/L trypsin, 2 g/L EDTA) was used at a trypsin concentration of 0.25% in Dulbecco's PBS (DPBS). All plastic culture flasks and plates used for growing HUVECs were coated with gelatin (Sigma-Aldrich 2% solution Type B from Bovine skin) as a 1% solution in DPBS, 0.05 mol/L sodium arsenite was purchased from Fluka Analytical Sigma-Aldrich.

Component	Volume (ml)
HUVECs	
Dimethyl sulfoxide (Sigma-Aldrich)	4
1M Hepes buffer (Whittakar®)	0.8
Media 199 (PAA) (complete)	15.2
EA.hy 926 and HepG2 cells	
Dimethyl sulfoxide (Sigma-Aldrich)	1
Foetal calf serum (Lonza, lot no: 7SB0014)	5
Dulbecco's Modified Eagle's Medium (Sigma-Aldrich D5546)	4

Table 3.4 The components required to make up the freeze mix for storing HUVECs and EA.hy 926 cells at -80°C and subsequently in liquid nitrogen.

3.1.2 Cell culture methods

3.1.2.1 Resuscitation of frozen cells

A frozen cryotube of cells was taken from liquid nitrogen storage and placed immediately into in a container. The cryotube was placed in a 37°C water bath for 1-2 minutes to enable the cells to fully thaw. Immediately upon thawing, the cells were pipetted into a sterile centrifuge tube and re-suspended in 10 ml of culture media, in a class II biosafety cabinet. The cells were centrifuged at 180 g for 5 minutes, the supernatant was discarded and the cell pellet was re-suspended in 1 ml culture media. The cells were added to T75 cm^3 flask (gelatin coated flask for HUVECs) (see section 3.1.2.2) which was topped up with 9 ml of culture media and placed into a 37°C, 5% CO_2 incubator.

3.1.2.2 Sub-culturing/passaging cells

For HUVECs, a 1% gelatin solution was pre- heated at 37° for approximately 15 minutes, along with culture media, Dulbecco's Phosphate buffered saline (DPBS) and 0.25% trypsin/ EDTA. All flasks were coated with gelatin by adding 2 ml of 1% gelatin per T75cm^3 flask and the flasks tilted back and forth to ensure coverage of the bottom surface. Flasks were put back into the incubator and after 5-10 minutes the excess

gelatin was aspirated. These gelatin-coated flasks were kept in the 37°C, 5% CO_2 incubator till required.

Cell flasks near confluent (80-100%) were taken from the incubator and within the class II biosafety cabinet, the media was aspirated and the cells were washed briefly with 5-6 ml of DPBS. Trypsin/ EDTA (2 ml) were added to the flask and left for 3-4 minutes in the incubator until cells had detached from the surface; this was monitored by checking under the microscope. The side of the flask was tapped gently to ensure complete detachment of cell from the surface. Culture media (6 ml) was added to the flask and the cell suspension was centrifuged at 180 g for 5 minutes. The supernatant was discarded and the cell pellet was re-suspended in 3 ml of culture media. For a typical 1:3 split ratio, 1 ml of the cell suspension was pipetted into 3 flasks (gelatin coated flasks for HUVECs) and topped up with 9 ml of culture media. The flasks were then incubated 37°C, 5% CO_2 to allow cell attachment and growth.

Cells grown in T25 cm^3 flasks were passaged and grown in the same way, with the total volume of the flask made up to 4 ml of culturing media. Therefore, smaller volumes of other reagents were also used; i.e. 1 ml 1% gelatine for HUVEC culture, 1 ml trypsin/EDTA and 2 ml DPBS.

3.1.2.3 Changing cell media

Media in the flasks was changed regularly, every 2 days until the cells were ready to be passaged. Media was aspirated and discarded from the flasks; 5 ml of DPBS (pre-warmed to room temperature) was used to wash over the cells and immediately

aspirated. Culturing media (10 ml pre-warmed to room temperature) was added to the flasks which were incubated at 37°C with 5% CO_2.

3.1.2.4 Cell counting using a haemocytometer

The haemocytometer was first cleaned thoroughly using 70% ethanol and affixed with a cover slip, 10 µl of a 1 ml cell suspension was then pippetted at the edge of the cover slip to enable the cell suspension to flow under the cover slip. Cells were counted in 4X 1 mm^2 square regions of a haemocytometer, the average of which was calculated and multiplied by the conversion factor of 10^4 (the volume of the 1 mm^2 square is equivalent to 10^4 ml) to give the number of cells in 1 ml.

3.1.2.5 Treating cells with arsenite

For treatment of cells with sodium arsenite, the appropriate concentrations were made-up fresh each time by diluting sodium arsenite from the stock using DPBS under sterile conditions.

3.2 Measuring cell viability

3.2.1 Materials

Sodium arsenite was used to treat HUVECs. Cell viability was determined using the trypan blue exclusion assay (Sigma-Aldrich T8154) and the colorimetric assay, 'Cell Counting Kit (CCK) 8' (Sigma-Aldrich 96992). The trypan blue solution (0.4% $^{w}/_{v}$) contains 0.81% sodium chloride, 0.06% potassium phosphate and bromophenol blue, the cells were counted using a haemocytometer under microscopy The CCK8 reagent contains the tetrazolium salt 2-(2-methoxy-4-nitrophenyl)-3-(4-nitrophenyl)-5-(2,4-

disulfophenyl)-2H-tetrazolium, monosodium salt which is acted upon by dehydrogenases present in viable cells to form a yellow formazan product. The intensity of the formazon dye produced was measured using a plate reader at $A_{450\ nm}$.

3.2.2 Method

3.2.2.1 Trypan blue exclusion assay

Cells grown in T25 cm^3 flasks were treated with differing concentrations of sodium arsenite for 24 hours after reaching a confluence of ~90%. 2 mls of 2X trypsin-EDTA was added to the flasks and kept in the 37°C, 5% CO_2 incubator for 3-4minutes, then tapped gently on the side to completely free the cells from the gelatin-coated surface, this was assessed by examining the flasks under the miscroscope. In a class II biosafety cabinet, the cells suspensions was aspirated from the flasks into centrifuge tubes and centrifuged at 1000 rpm for 5 minutes. The supernantant was discarded carefully without touching the cell pellet which was then resuspended in 250 µl culturing media. 20 µl of the cell suspension was mixed with 20µl of the trypan blue dye solution, 10µl of which was applied to the haemocytometer and used to count the cells under the microscope (See section 3.1.2.4). In this instance, the 10 µl of cell suspension was mixed with 10 µl of trypan blue dye and then applied to the haemocytometer, therefore after calculating the average of the number of cells in the 4X 1 mm^2 squares, the number was divided by 2, taking into account the dilution factor for the trypan blue solution used. Dead cells appear blue under the microscope due to the ability of the trypan blue dye to penetrate their cell membranes.

3.2.2.2 Cell Counting Kit 8 (CCK8)

The wells required in a 96 well plate for the assay were coated with 10 µl of 1% gelatin and incubated at 37°C, 5% CO_2 for 10 minutes and then the excess gelatin was pipetted out. The media in a confluent cell flask (~90%) was aspirated and the cells were detached from the surface of the flask using trypsin/EDTA (see section 3.1.2.2) and centrifuged at 180 g for 5 minutes. After discarding the supernantant, the cell pellet was re-suspended in 1ml complete media of which 10 µl were used to count the cells using the haemocytometer (see section 3.1.2.4).

Using the cell count, a dilution of the cell suspension was made so that there were 5000 cells/100 µl. Thus, 100 µl were directly added to each well to give 5000 cells/well in the 96 well plate, with 5 wells prepared for each concentration of arsenite. The cells were left overnight in the incubator and treated with appropriate concentrations of sodium arsenite the following day and incubated for 24 hours at 37°C, 5% CO_2. Ten µl of the CCK-8 reagent was directly added to each well, the plate incubated at 37°C, 5% CO_2 and absorbance recordings were taken every hour for 4 hours using a plate reader at $A_{450\ nm}$.

3.3 Measuring ROS levels

3.3.1The Amplex red assay

The Amplex red assay enables the measurement of hydrogen peroxide produced from cells. Experiments were carried out on HUVECs.

3.3.1.1 Materials

Component	Quantity
Ampliflu red (5mg, Sigma-Aldrich)	1 mg
Dimethyl sulfoxide (Sigma-Aldrich)	389 µl
Peroxidase type II from Horse Radish (188U/mg, Sigma-Alrdrich)	0.00005 g
Hydrogen peroxide (Sigma-Aldrich, 30% $^{w}/_{w}$ solution)	As required
Hanks buffered salt solution (GIBCO™, with $CaCl_2$ and $MgCl_2$)	As required
Menadione (Sigma-Aldrich)	50 mM

Table 3.5 The components required for the Amplex red assay used to detect the production of hydroge peroxide from HUVECs. Measured using a Cytoflour Plate reader at excitation 530 nm and emission 580 nm.

3.3.1.2 Methods

H_2O_2 concentration	1mM H_2O_2 solution (µl)	HBSS (µl)
1 mM H_2O_2 solution = 5 µl H_2O_2 stock (9.8 M) + 49 ml HBSS		
0	-	20/well
15	10	656
30	20	646
60	40	626
120	80	586

Table 3.6 The dilutions required to make the H_2O_2 standard curve used in the Amplex red assay. The dilutions were made using Hanks buffered salt solution (HBSS).

A 96 well plate was prepared with 5000 cells/ well and left overnight to adhere in a 37°C, 5% CO_2 incubator, the cells were treated with sodium arsenite concentrations in a class II biosafety cabinet and left in the incubator for 24 hours. An hour before the amplex red assay was carried out; 50 µM menadione was prepared and added to untreated cells as a positive control (Menadione preparation; 0.00172 g menadione was dissolved in 10 mls HBSS to give 1mM menadione solution, 5 µl of the 1 mM menadione solution was added to each of the wells containing 100 µl of media giving a 50 µM menadione exposure to the cells).

After an hour of menadione treatment, and 24 hour of sodium arsenite treatment, media in all the wells was discarded, each cell was washed with HBSS once and 20 µl of HBSS was added per well. The H_2O_2 dilutions prepared (Table 3.6) were added in cell free wells, in triplicates, and 100 µl of the Amplex red assay reaction mixture was added to all the wells. Amplex red assay reaction mixture preparation; 0.00005 g horse radish peroxidase was dissolved in 1 ml HBSS (10 U/ml) just before it was required, 100 µl of this was added to 50 µl of 10 mM ampliflu stock and 9850 µl HBSS, the mixture was then heated at 37°C for 10 minutes in the dark. The fluorescence readings for the 96 well plate were taken every 30 minutes for up to 1.5-2 hours using a Cytoflour plate reader at excitation 530nm and the emission 580 nm wavelength.

3.3.2 Assessment of levels of ROS with fluorescent based flow cytometry

3.3.2.1 Materials

Experiments were carried out on HUVECs and EA.hy 926 cells.

COMPONENT	Final Concentration/QUANTITY
Mitosox™Red (Invitrogen, M36008)	5 µM
Dihydroethidium (Invitrogen, C6827)	2.5 µM
CM-H_2DCFDA (Invitrogen, C6827)	10 µM
Iscove's modified Dulbecco's medium (IMDM), no phenol red (Invitrogen, 21056-023)	As required for assay
Dimethyl sulfoxide (DMSO) (Sigma-Aldrich, 472301)	As required for assay

Table 3.7 The fluorescent dyes and additional components required to measure ROS.

Table 3.7 identifies all the fluorescent staining dyes used to investigate ROS generation. The analysis was carried out by flow cytometry using the DakoCytomation CyAn ADP Flow Cytometer.

3.3.2.2 Methods

Assessment of levels of ROS in HUVECs and EA.hy 926 cells was performed using several ROS-reporter dyes and flow cytometry. For each cell type, cells were seeded in 6 well plates (gelatin-coated wells for HUVECs) and harvested when they reached approximately 70% confluence.

3.3.2.2.1 Estimation of superoxide with flow cytometry in EA.hy 926 cells

Superoxide was estimated using the ROS reporter's dihydroethidium (DHE) and MitoSOX™ Red. When EA.hy 926 cells reached 70% confluence, the cells were washed with PBS, 500 µl of 0.25% trypsin/EDTA was added to each well and incubated for 5 minutes at 37°C and 5% CO_2. Culture media (3 ml) was added to neutralise the

trypsin/EDTA and the cell suspension was centrifuged at 180 g for 5 minutes. The cell pellet was re-suspended in 1ml of culture media and incubated with either MitoSOX™ Red (stock made up in DMSO at 5 mM) at a final concentration of 5 µM or with 2.5 µM DHE for 30 minutes at 37°C and 5% CO_2. The cells were then centrifuged at 180 g for 5 minutes; the pellet was washed with PBS and centrifuged at 180 g for 5 minutes. The cell pellet was re-suspended in PBS with 1% FBS and transferred to 12X 75 mm FACS tubes (BD Biosciences 352235) the cells were then treated with arsenite and a positive control and incubated at 37°C and 5% CO_2 for a specific treatment period. The cells were then analysed using flow cytometry, MitoSOX™ Red and DHE were both excited at 488 nm and data collected at emission wavelength 575/25 nm.

3.3.2.2.2 Assessment of superoxide with flow cytometry in HUVECs

At 70% confluence, HUVECs were treated with different arsenite concentrations and a positive control in 2 ml media and incubated at 37°C and 5% CO_2. Thirty minutes before the treatment time was complete, to each well either MitoSOX™ Red (stock made up in DMSO at 5 mM) at final concentration of 5 µM or DHE at final concentration of 2.5 µM was added with incubation for 30 minutes at 37°C and 5% CO_2. The cells were then washed with PBS, 500 µl of 0.25% trypsin/EDTA was added to each well and incubated for 5 minutes at 37°C and 5% CO_2. Culture media (3 ml) was added to neutralise the trypsin/EDTA and the cell suspension was centrifuged at 180 g for 5 minutes. The cell pellet was re-suspended in 1ml PBS and transferred to FACS tubes for flow cytometric analysis. MitoSOX™ Red and DHE were both excited at 488 nm and data collected at emission wavelength 575/25 nm.

3.3.2.2.3 Measuring general ROS production

At 70% confluence, cells were treated with arsenite and a positive control and incubated at 37°C and 5% CO_2. Once the treatment period was complete, cells were washed with PBS and 500 µl of 0.25% trypsin/EDTA was added to each well and incubated for 5 minutes at 37°C and 5% CO_2. Culture media (3 ml) was added to each well to neutralise the trypsin/EDTA and the cell suspension was centrifuged at 180 g for 5 minutes. The cells were re-suspended in 10 µM CM-H_2DCFDA in 1 ml IMDM and incubated in FACS tubes for 30 minutes at 37°C and 5% CO_2. They were then analysed by flow cytometry. CM-H_2DCFDA was excited by laser light at 488 nm and the data collected at 530/40 nm emission wavelength.

3.4 Measuring apoptosis in EA.hy926 cells

3.4.1 Materials

Apoptosis and necrosis were determined using the Annexin V-FITC Apoptosis Detection Kit (abcam®, ab14085) in EA.hy926 cells. This kit enables the simultaneous staining of cells with Annexin V and PI therefore allowing the measure of both apoptosis and necreosis respectively. The analysis was carried out using the DakoCytomation CyAn ADP Flow Cytometer.

3.4.2 Methods

When EA.hy 926 cells reached 70% confluence, they were treated with arsenite and the positive control compounds in 6 well plates and left to incubate at 37°C and 5% CO_2. After the treatment period, the cells were washed briefly with PBS and 500 µl of 0.25% trypsin/EDTA were added to each well with incubation for 5 minutes at 37°C and 5%

CO_2. Culture media (3 ml) was added to each well to neutralise the trypsin/EDTA and the cell suspension was centrifuged at 180 g for 5 minutes. The resultant cell pellet was washed in PBS and centrifuged at 180 g for 5 minutes. This wash step was repeated and the pellet was re-suspended in 500 µl Annexin V Binding Buffer with 5 µl Annexin V-FITC and 5 µl Propidium iodide (PI) and incubated at room temperature in the dark for 15 minutes before flow cytometric analysis. Annexin V and PI were both excited by laser light at 488 nm and the fluorescence emission was collected at 530/40 nm and 575/25 nm emission wavelength respectively.

3.5 Measuring the Protein levels

Measuring the levels of proteins using the Bradford assay with HUVECs seeded in a in a 96 well plate.

3.5.1 Materials

COMPONENT	QUANTITY/AMOUNT
Bovine serum Albumin (Sigma-Aldrich)	1 mg/ml
Protein assay dye reagent (Bio Rad)	2 ml
Ultrapure water	As required for assay
CellLytic™ Cell lysis buffer (Sigma-Aldrich)	As required for assay

Table 3.8 The components required for the Bradford assay, measurements taken using a plate reader at $A_{595\ nm}$.

3.5.2 Methods

BSA mg/ml	BSA 1mg/ml stock solution (µl)	CellLytic buffer (µl)
BSA 1 mg/ml stock solution = 0.01 g BSA + 10 ml ultra pure water		
0.5	50	50
0.4	40	60
0.3	30	70
0.2	20	80
0.1	10	90
0.0	0	100

Table 3.9 Bovine serum albumin (BSA) dilutions were prepared in order to deduce a protein standard curve for the Bradford assay. The dilutions were prepared and kept on ice.

To measure the amount of proteins present in HUVECs grown at 5000 cells/well in a 96 well plate (media within the wells was discarded and 20 µl CellLytic reagent was added to each well, the plate was kept on a plate shaker for 20 minutes at room temperature to allow cell lysis to occur. The cell lysis samples were diluted 1:5 with CellLytic buffer and briefly vortexed at low speed, 10 µl/well of each of the samples and the BSA dilutions (Table 3.9) were pippetted in triplicates into a new 96 well plate. The diluted protein assay dye reagent was prepared (2 ml protein assay dye reagent with 8 ml ultra pure water) and 200 µl were added to each of the wells carefully avoiding bubbles forming. The plate was left for 5-15 minutes at room temperature before absorbance readings were taken using a plate reader at 595 nm.

3.6 Measuring ATP levels

The effects of arsenite on ATP production was determined using a highly sensitive bioluminescence assay based on the presence of firefly luciferase and D-luciferin. ATP reacts with D-luciferin in the presence of luciferase producing light (emission maximum approximately 560 nm at pH 7.8) which can be detected by a luminometer.

HepG2 cells were grown in media containing either high glucose (25 mM) or containing galactose (10 mM). The ATP determination kit (Invitrogen A22066) was employed to measure the levels of ATP.

3.6.1 Materials

COMPONENT	QUANTITY
dH_2O	8.9 ml
20X Reaction Buffer	500 ml
0.1 M DTT	100 ml
10 mM D-luciferin	500 ml
Firefly luciferase	2.5 µl

Table 3.10 Components used to make the standard reaction solution for the detection of ATP using the ATP determination kit.

3.6.2 Methods

The culture media for the cells grown in 96 well plates was discarded and each well was washed twice with 100 µls PBS. The standard reaction solution was then made up (Table 3.10) and 100 µl were added to each well. The plate was then placed on a plate shaker for 30 seconds and analysed on the NOVOstar multifunctional microplate reader using luminescence.

3.7 Measuring mitochondrial biogenesis

The extracellular flux analyzer (XF analyzer)/ Seahorse assay (Seahorse BioScience) is able to measure mitochondrial function and biogenesis effectively. It does this by very sensitively measuring the real time cellular oxygen consumption rate (respiration) and the extracellular acidification rate/ proton release (glycolysis) in response to known mitochondrial targeted compounds. Measurements are taken regularly every few seconds by sensor probes that sit 200 microns above the cell monolayer during the

sequential addition of the compounds. After each set of measurements, the probes are lifted to enable the micro-media to disperse and restore the cell values back to baseline before the addition of the next drug. Thus, a mitochondrial response profile is formed for both respiration and glycolysis. The comparison of the respiration and glycolytic profiles in un-treated HUVECs and HUVECs pre-treatment with arsenite concentrations was carried out.

3.7.1 Materials

Experiments were carried out on HUVECs.

Drug port	Compound	Concentration (µM)	Volume (µl)
A	Oligomycin A (Sigma-Aldrich, 75351)	5	75
B	FCCP* (Sigma-Aldrich, C2920)	4	83
C	Antimycin A (Sigma-Aldrich, A8674)	10	90
D	Assay specific media	-	75

Table 3.11 The table identifies the mitochondrial targeted compounds used in this study by addition to the drug ports on the assay calibration plates (Seahorse, Bioscience). Drug port D was left compound free and just assay specific media was added. *carbonyl cyanide 4-(trifluoromethoxy)phenylhydrazone.

The components used to make the assay specific media (Table 3.12) were dissolved in distilled water, set at pH 7.4 and made up to 1 litre. The media was then filter sterilised.

COMPONENT	QUANTITY
Dulbecco's Modified Eagle's Medium (Sigma-Aldrich, D5030)	8.3 g/L
Glutamax 200 mM (100X), (Gibco, 35050-061)	10 ml
Sodium Pyruvate 100 mM (Sigma-Aldrich S8636)	10 ml
D-(+)-Glucose (Sigma-Aldrich G8270)	2 g
Sodium Chloride (Sigma-Aldrich S3014)	1.85 g
Phenol Red sodium salt (Sigma-Aldrich P5530)	15 mg

Table 3.12 The components required to make up the assay specific media for the Seahorse/ extracellular flux analyser.

3.7.2 Methods

The assay cartridge sensor plate (Seahorse Bioscience) was left to calibrate in XF Calibration Solution (Seahorse Bioscience) over night at 37°C in a CO_2-free incubator.

HUVECs were grown in gelatin-coated 24 well assay microplates (Seahorse Biosciences) until they reached approximately 90% confluence. They were then treated with 0, 10, 100 and 1000 µg/L arsenite in a total of 1 ml HUVEC growth media with 5 well repeats per arsenite concentration and incubated for a specific treatment time at 37°C and 5% CO_2. After the treatment period was complete, 900 µl media per well was discarded and 900 µl of the assay specific media (Table 3.12) was added to each well, 900 µl was discarded again and 900 µl of fresh assay specific media was re-added per well, this wash step was repeated 3 times in total. Assay specific media (575 µl) was lastly added to the remaining 100 µl media per well and left to incubate at 37°C in a CO_2-free incubator.

The assay cartridge sensor plate drug injection ports were loaded up with the corresponding compounds (Figure 3.1) (Table 3.11) and inserted into the XF24

Analyzer (Seahorse Bioscience) to calibrate. Once the calibration was complete, the HUVEC treatment plate was loaded into the XF24 Analyzer, where the sequential injection of mitochondrial compounds and their individual cellular responses was measured.

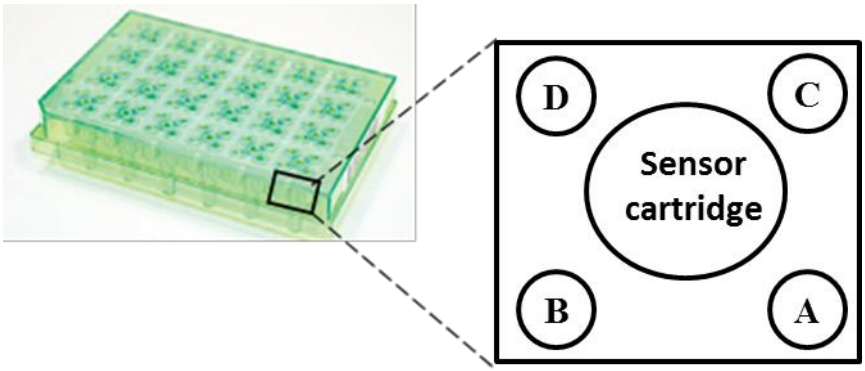

Figure 3.1 The diagram illustrates an assay calibration plate (Seahorse Bioscience), showing the layout of the sensor cartridge surrounded by 4 drug injection ports that is used to sequentially inject mitochondrial targeted compounds; in this study the compounds used were; (A) Oligomycin, (B) carbonyl cyanide 4-(trifluoromethoxy)phenylhydrazone (FCCP), and (C) Antimycin A.

3.8 Measuring mitochondrial DNA content and damage using qPCR

3.8.1 Materials

DNA extraction of HUVECs was carried out using the QIAamp® DNA blood mini kit (QIAGEN) following the manufacturer's instructions. DNA was quantified using a nanodrop ND-8000 8-sample spectrophotometer (Labtech international).

The primers used to measure mitochondrial DNA content, shown in table 3.13 include the amplification of the nDNA region consisting of the reference *RPLPO* gene and the

amplification of the entire mitochondrial genome. The primers used to measure mitochondrial DNA damage have been designed to amplify the D-Loop region of the mitochondrial genome (Table 3.14).

Accession no:	Primer name	Sequence	Length (bp)
NM_001002	36B4d (sense)	5'CCCATTCTATCATCAACGGGTACAA3'	1229
	36B4u (antisense)	5'CAGCAAGTGGDAAGGTGTAATCC3'	
J01415	mt14260 (sense)	5'CCCCACAAACCCCATTACTAAACCCA3'	16569
	mt14841 (antisense)	5'TTCATCATGCGGAGATGTTGGATGG3'	

Table 3.13 Primers used to measure mitochondrial DNA content, amplifying the mitochondrial genome and a reference nuclear sequence.

Primer name	Sequence	Length (bp)
AS1.F (sense)	CCCTAACACCAGCCTAACCA	55
AS1.R (antisense)	AAAGTGCATACCGCCAAAAG	
AL4.F (sense)	CTGTTCTTTCATGGGGAAGC	972
AS1.R (antisense)	AAAGTGCATACCGCCAAAAG	

Table 3.14 Primers used to measure DNA damage the at the D-loop region of the mitochondrial region (Rothfuss *et al*., 2010).

The quantitative real-time PCR (qPCR) reactions were made up using the Sensimix™ SYBR Kit (Bioline), water for molecular biology work (DNase and RNase free)

(Sigma-Aldrich), primers were purchased from Invitrogen (HPLC purified) and Tris-EDTA (TE) buffer (pH 7.4) (Sigma-Aldrich) was used for DNA dilutions. qPCR reactions were made up in ABI compatible frosted and semi-skirted, thin wall 96X 0.2 ml high profile PCR plates (GENEFLOW, P3-0292). The reactions were carried out in the ABI Prism 7900HT Sequence Detection System.

3.8.2 Methods

3.8.2.1 DNA extraction

HUVECs were grown to approximately 70% confluence in T75 cm^3 flasks and then treated with arsenite for 24 hours. Following the QIAamp® DNA blood mini kit protocol, DNA was extracted from arsenite treated HUVECs. Cells grown in a flask were trypsinised off the surface and transferred to a centrifuge tube. Cells were pelleted by centrifuging at 180 g for 5 minutes, the supernatant was discarded and the pellets were re-suspended with 200 µl of DPBS with the addition of 20 µl protease and 200 µl Buffer AL. The mixture was vortexed for 15 seconds and the lysate was incubated at 56°C for 10 minutes before centrifuging briefly and transferring into a QIAamp spin column (with collecting tubes to centrifuge for 11,000 g for 1 minute. The column was then placed in clean collecting tubes, 500 µl Buffer AW1 was added and centrifuged at 11,000 g for 1 minute. The column was discarded and replaced with a clean one to centrifuge again ensuring the entire wash buffer was removed. The column was then placed into a sterile 1.5 ml eppendorf tube, 55 µl of Buffer AE was added to the column and left for 5 minutes at room temperature, before centrifuging at 11,000 g for 1 minute to elute the DNA.

3.8.2.2 Quantitative Real-Time PCR

Quantification of the amplified target sequences was carried out using the SYBR green fluorescent dye, a constituent of the Sensimix™ SYBR Kit used to make the qPCRs. SYBR green binds to double-stranded DNA and fluoresces, thus is widely used as a measuring tool for the real-time amplification of DNA sequences in qPCR. The ABI Prism 7900HT sequence detection system is able to detect this fluorescent signal and produces an amplification plot representing the increase in fluorescence, i.e. the amplified target DNA sequence, over the course of the qPCR cycles. The amplified product is measured in terms of the threshold cycle (Ct) value; the number of replication cycles required in order for the fluorescent signal to exceed the threshold i.e. background level. The Ct value is inversely proportional to the amount of target DNA in the reaction, thus the lower the Ct value, the higher the amount of DNA.

The reactions were made up in sterile conditions, ensuring no source of DNA contamination. Each reaction was made up to a final concentration of 25 µl with 1X SensiMix™ SYBR kit, 0.1 µM sense primer, 0.1 µM antisense primer, distilled water and DNA at the appropriate concentration.

The reference DNA to make standard curves was extracted from untreated HUVECs. For measuring mtDNA content, a reference DNA standard curve using the nDNA primers; 36B4d and 36B4u, was made up with TE buffer (pH 7.4) for a 2-fold dilution of DNA concentrations ranging from 3.125 to 50 ng. The DNA from the experimental samples was diluted down to 3 ng/µl and 15 ng was used for each reaction. The reference DNA standard curve for the mtDNA primers; mt14620 and mt14841, was

made up ranging from 62.5 to 1000 pg by a 2-fold serial dilution using TE buffer (pH 7.4), the experimental DNA samples were diluted down to 50 pg/µl and 250 ng used per reaction. For measuring mtDNA damage, both primer sets AS1.F, AS1.R and AL4.F, AS1.R were used. The reference DNA standard curves were made up with TE buffer (pH 7.4) for a 2-fold dilution of DNA concentrations ranging from 62.5-1000 pg, DNA from the experimental samples was diluted down to 50 pg/µl and 250 pg was used in each reaction.

The thermal profile for the qPCR was as follows; 95°C for 10 minutes, 40 cycles of 95°C for 30 seconds, 60°C for 60 seconds and 72°C for 60 seconds. The data was analysed for both measuring the mtDNA content and mtDNA damage following the relative standard curve method (Pfaffl, 2001).

3.9 Measuring nuclear DNA Damage using the Comet assay

3.9.1 Materials

The materials required to carry out the alkaline comet assay are listed below.

Component	Concentration
Trizma®hydrochloride (pH 8) (Sigma-Aldrich T5941)	10 mM
EDTA (pH 8) (Sigma-Aldrich E6758)	1 mM

Table 3.15 The components used to make Tris-EDTA (TE) buffer

Component	Concentration
Sodium Chloride (Sigma-Aldrich S7653)	2.5 M
EDTA (Sigma-Aldrich E6758)	100 mM
Trizma® base (Sigma-Aldrich T1503)	10 mM
Sodium hydroxide (Sigma-Aldrich S5881)	200 mM
Adjusted to pH 10	
Triton-X100 (Sigma-Aldrich X100)	1%

Table 3.16 Components used to make up lysis buffer, triton-X100 added up to 30 minutes just before use.

Component	Concentration
Sodium hydroxide (Sigma-Aldrich S5881)	300 mM
EDTA (Sigma-Aldrich E6758)	1 mM

Table 3.17 Components required to make electrophoresis buffer. The buffer was made fresh each time in distilled water and adjusted to pH 13.

The neutralisation buffer was made up with 400 mM Trizma® base (Sigma-Aldrich T1503) at pH 7.5. 0.6% low melting point (LMP) agarose (Invitrogen 16520050) was made in PBS and 1.2% LMP agarose was made in distilled water.

3.8.2 Methods

The measure of nuclear DNA damage was carried out using the single cell alkaline gel electrophoresis technique (alkaline comet assay) as described below (Figure 3.2).

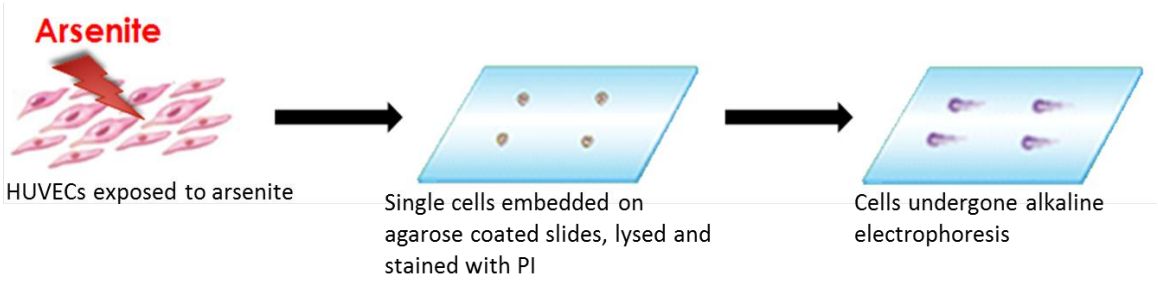

Figure 3.2 Overview of the alkaline comet assay.

Before starting the procedure, microscope slides were coated with 1.2% LMP agarose and left to set at 56°C for at least one hour before use. HUVECs were grown in gelatin-coated T25 cm^3 flasks until they reached 70% confluence, they were treated with arsenite concentrations for 24 hours in a 37°C and 5% CO_2 incubator. Cells were then removed from the flask using 0.25% Trypsin/ EDTA and centrifuged at 180 g for 5 minutes to form a cell pellet. The supernatant was completely removed and discarded and the cells were re-suspended in 1 ml fresh media. A 300 µl aliquot of the cell suspension was transferred into a sterile eppendorf and centrifuged at 5418 g for 1 minute.

In dark conditions (to minimise adventitious DNA damage due to photosensitivity reactions), the supernatant was discarded and the pellet was re-suspended in 900 µl of 0.6% LMP agarose, 60 µl of this cell suspension (approximately 20,000 cells/ slide) was placed on top of a 1.2% LMP agarose coated slide, covered with a cover slip and left on ice for 15 minutes. LMP agarose (60µl of 0.6%) was pipetted on top of the cell layer, covered with a cover slip and left on ice for another 15 minutes. The cells were then lysed by placing then in a Wilson jar filled with cold (~4°C) lysis buffer; the slides were left in there over night at 4°C, protected from the light.

The slides were washed three times in TE buffer for 5 minutes. The cells were then denatured by placing them in a comet assay specific electrophoresis tank containing chilled electrophoresis buffer for 30 minutes before carrying out electrophoresis for 20 minutes at 20 V and 200 mA at 4°C and light protected conditions. The slides were then washed three times in neutralisation buffer and twice in 100% ethanol, 5 minutes per wash. The slides were left to air dry. To stain the cells, slides were re-hydrated with distilled water and exposed to 2.5 μg/ml PI for 20 minutes, washed with distilled water again for 30 minutes and allowed to dry. The comets were analysed at 50 cells per slide with 2 slides per treatment condition per experiment. The comets were detected using a fluorescence microscope (Axioskop; Carl Zeiss,) with an excitation filter of 515-535 nm and a 590 nm barrier emission filter. The Comet Assay IV analysis software, version 4.2 (Perceptive instruments) was used to score the comets and the percentage tail length was recorded.

3.10 Microarray based Transcriptional Profiling

3.10.1 Materials

The extraction of total RNA from HUVECs was carried out using the miRNeasy Mini Kit (Qiagen 217004), chloroform (Sigma-Aldrich 472476) and isopropanol (2-propanol, Sigma-Aldrich I9516). The nucleic acid content of the extracted samples was determined using the nanodrop ND-8000 8-sample spectrophotometer (Labtech international) following the manufacturer's instructions and using the elution buffer from the miRNeasy Mini Kit as the sample blank. The qualities of the extractions were

observed using the Agilent 2100 bioanalyzer with the Agilent RNA 6000 Nano Kit, following the manufacturer's instructions.

The RNA amplification and cRNA conversion with Biotin labelling was carried out using the Illumina® TotalPrep RNA Amplification Kit (AMIL1791) and the microarray beadchip hybridisation was carried out using the HumanHT-12 v4 Expression BeadChip Kit (Illumina® BD-103-0204), BeadChip Hyb Chamber (Illumina® 210948), BeadChip Hyb Chamber inserts (Illumina® 222682), BeadChip Hyb Chamber gaskets (Illumina® 210930) and BeadChip wash rack (Illumina® 200037). The beadchip was analysed using the Illumina® Beadarray Scanner Bench Top™.

3.10.2 Methods

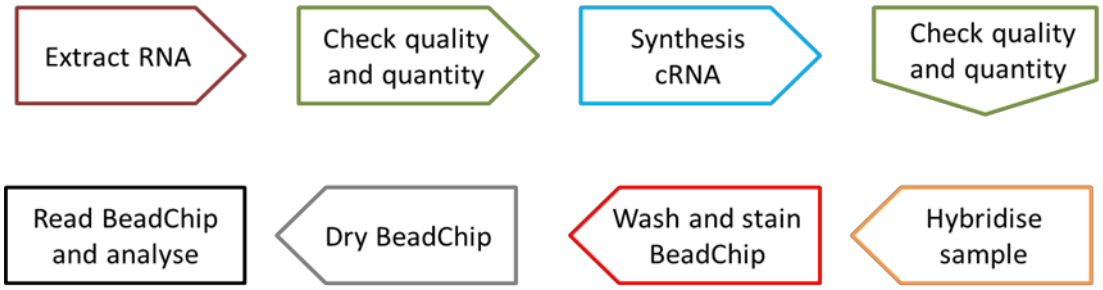

Figure 3.3 An overview of the whole-genome gene expression direct hybridisation methodology involved in transcriptional profiling.

3.10.2.1 Total RNA extraction

HUVECs were grown in gelatin coated T75 cm^3 flasks until they reached 70% confluency. They were then either treated with 1000 µg/L arsenite or left as untreated controls. After 24 hours they were detached from the flasks using 0.25% Trypsin/EDTA and washed in PBS.

The supernatant was discarded and 700 µl of QIAzol Lysis Reagent was added to each sample, transferred to a 2 ml flat bottom sample tube and homogenised. The homogenate was left at room temperature for 5 minutes, 140 µl chloroform was added to each tube before the samples were vortexed vigorously for 15 seconds and left at room temperature for 3 minutes. They were then centrifuged for 15 minutes at 12,000 g. The resultant samples were split into three phases; upper aqueous phase containing RNA, interphase containing DNA and an organic phase containing protein. The upper aqueous phase was carefully transferred into a sterile eppendorf where 1.5 volumes of 100% ethanol were added and mixed by pipetting. A 700 µl aliquot of the sample was then transferred into an RNeasy® Mini column in a collecting tube and centrifuged at 8,000 g for 2 minutes. The flow through was discarded and the remaining sample was added to the column and again centrifuged.

DNA digestion was then carried out. Isopropanol (45 ml) was added to the Buffer RWT and 350 µl of this was added to the Mini Spin column followed by centrifugation for 2 minutes at 8,000 g DNase I stock solution (10 µl) was added to 70 µl of Buffer RDD and gently inverted to mix. This was then added directly onto the membrane of the Mini Spin column and left at room temperature for 15 minutes. Buffer RWT with isopropanol (350 µl) was added into the Mini Spin column and centrifuged for 2 minutes at 8,000 g.

The flow through from the column was discarded and 500 µl of Buffer RPE was added into the Mini Spin column, left for 5 minutes at room temperature and then centrifuged for 2 minutes at 8,000 g. The flow through was discarded and this step was repeated. The collecting tube was replaced with a new one and the column was centrifuged for

8,000 g for 5 minutes to eliminate any retained buffer. The Mini Spin column was transferred into a new sterile eppendorf and 50 µl of RNase-free water was added directly onto the Mini Spin column membrane, the lid was closed and the column was centrifuged for 2 minutes at 8,000 g. The flow through which contained the eluted RNA was reapplied to the column membrane and centrifuged for another 2 minutes at 8,000 g. The sample was stored at -80°C until required.

3.10.2.2 RNA amplification and cRNA preparation

The extracted samples were prepared to give 500 ng RNA in 11 µl using nuclease-free water in a sterile RNase-free 0.5 ml microcentrifuge tube. The Reverse Transcription Master Mix was prepared (Table 3.18), mixed by gentle vortexing, briefly centrifuged and placed on ice. Master mix (9 µl) was mixed into the RNA samples by pipetting, then briefly centrifuged and incubated for 2 hours at 42°C. The samples were briefly centrifuged (~4000 g) and placed immediately on ice. A Second Strand Master Mix (Table 3.19) was prepared in a nuclease-free tube, mixed by gentle vortexing, briefly centrifuged before 80 µl was added to each sample and mixed by pipetting. The samples were then incubated for 2 hours at 16°C.

After the incubation, 250 µl of cDNA Binding Buffer was immediately added to each sample, mixed well by pipetting and all the sample was transferred onto a cDNA Filter cartridge to centrifuge at 10,000 g. The flow through was discarded and 500 µl Wash Buffer was applied. The columns were centrifuged for 1 minute at 10,000 g and the flow through was discarded and the centrifugation step was repeated to elute all the

wash buffer. The cDNA Filter Cartridge was transferred into a cDNA Elution Tube. Pre-heated (55°C) nuclease-free water (20 µl) was applied to the filter and left at room temperature for 2 minutes before centrifugation for 1 minute at 10,000 g. The cDNA was stored overnight at -20°C.

Component	Volume (µl)
T7 Oligo(dT) Primer	1
10X First Strand Buffer	2
dNTP Mix	4
RNase Inhibitor	1
ArrayScript	1

Table 3.18 Reverse Transcription Master Mix for a single RNA sample.

Component	Volume (µl)
Nuclease-Free Water	63
10X Second Strand Buffer	10
dNTP Mix	4
DNA Polymerase	2
RNase H	1

Table 3.19 Second Strand Master Mix for a single reaction.

An IVT Master Mix (Table 3.20) comprising of Biotin-NTPs was prepared, mixed by gentle vortexing and briefly centrifuged before adding 7.5 µl into each cDNA sample and incubating at 37°C over night. cRNA Binding Buffer (350 µl) was added to each cRNA sample and mixed gently by pipetting and the sample was immediately

transferred onto the centre of a cRNA Filter Cartridge. The samples were centrifuged for 1 minute at 10,000 g, the flow through was discarded, 650 µl Wash Buffer was added to each cartridge and centrifuged for 1 minute at 10,000g. The centrifugation was repeated once the flow through was discarded to ensure removal of the entire wash buffer. Pre-heated (55°C) nuclease-free water (200 µl) was added to each filter and the samples were incubated for 10 minutes at 55°C. The resultant Biotin labelled cRNA was eluted by centrifugation for 1.5 minutes at 10,000 g. The quantity and quality of the cRNA was assessed using the nanodrop ND-8000 8-sample spectrophotometer and the Agilent 2100 bioanalyzer respectively, following the manufacturer's instructions.

Component	Volume (µl)
T7 10X Reaction Mix	2.5
T7 Enzyme Mix	2.5
Biotin-NTP Mix	2.5

Table 3.20 Components of the IVT Master Mix for a single sample.

3.10.2.3 Beadchip Hybridisation

The cRNA samples were prepared using RNase-free water to yield 750 ng cRNA in 5 µl. Samples were mixed gently by pipetting and left at room temperature for 10 minutes, meanwhile the HYB and HCB tubes were incubated for 10 minutes (or more) at 58°C to allow any salts that had precipitated to dissolve. The tubes were left to cool at room temperature and mixed thoroughly before use. HYB (10 µl) was added to each sample and heated at 65°C for 5 minutes. Meanwhile, the Illumina Hyb Chamber gasket was placed into the BeadChip Hyb Chamber, 200 µl of HCB was added into the humidifying

buffer reservoirs (only for the ones located at the BeadChip loading position). The BeadChip was gently lowered into position on the Hyb Chamber using tweezers, ensuring the barcode was aligned accurately.

The samples were briefly vortexed, centrifuged to collect the sample and allowed to cool at room temperature. They were then immediately loaded onto the BeadChip sample ports; 15 µl per sample. The Hyb Chamber lid was sealed and the chamber was incubated over night at 58°C whilst gently rocking. High-Temp Wash buffer (1X) was prepared by mixing the 50 ml 10X stock with 450 ml RNase-free water and left over night at 55°C.

Block E1 buffer was warmed at room temperature, Block E1 buffer was prepared with streptavidin-Cy3; 2 µl of 1 mg/ml stock streptavidin Cy3 into 2 ml Block E1 buffer (kept protected from the light until used). Wash E1BC solution was made up by mixing 6 ml E1BC buffer into 2 L RNase-free water and 1 L was poured into a sterile RNase-free container. After the incubation period, wearing powder-free gloves the Hyb Chamber was dissembled, the BeadChip was carefully transferred (face upwards) into the bottom of the container and the cover seal was removed from the BeadChip. The BeadChip then transferred in a slide rack and washed in E1BC solution briefly, then incubated in High-Temp Wash buffer for 10 minutes, washed in E1BC solution for 5 minutes whilst on a shaker at high speed, transferred into 100% ethanol and placed on a shaker for 10 minutes. The BeadChip was then washed in clean E1BC solution for 2 minutes on a shaker, immersed in Block E1 buffer face up and rocked for 10 minutes. Next the BeadChip was transferred to Block E1 buffer with stretavidin face up and

placed on a rocker for 10 minutes, and lastly, washed in clean E1BC solution on shaker for 5 minutes in a slide rack.

The BeadChip was then placed and balanced in a plate-holder centrifuge for 275 g for 4 minutes to dry the chip; the chip was then scanned using the Illumina® Beadarray Scanner Bench Top™. Once the chip was scanned, the quality control checks of the data analysis were carried out using GenomeStudio Software (Illumina®). The ArrayTrack™ was used to perform normalisation on the raw data and apply, to eliminate systematic variation; this was done using the quantile normalisation method (Bolstad *et al*., 2003). The raw data was then subjected to two filters to refine and generate a significant gene list for further analysis, the filters applied were false discover rate (FDR)= 0.05 and fold change (FC) cut off of >1.5, and then analysed using principal component analysis. The significant gene list was then uploaded to the Ingenuity Pathway Analysis (INGENUITY®) to carry out gene expression changes and pathway analysis.

3.11 Induction of SIPS

At 60% confluence, HUVECs grown in 6-well plates were treated incubated with 650 and 1300 µg/L arsenite and 50 µM tert-butyl hydrogen peroxide (tBHP) (Sigma – Aldrich 458139) for 1 hour at 37°C and 5% CO_2, the treatment media was then aspirated, from the wells and the cells were washed in1 ml DPBS and replaced with 2 ml HUVEC culture media (Table 3.1), this treatment was repeated for 3 consecutive

days. After the third treatment, the plates were allowed to recover for 48 hours with fresh culture media at 37°C and 5% CO_2.

3.12 Senescence associated β-galactosidase (SA-β-Gal) staining

3.12.1 Materials

The reagents and materials used to detect senescence in HUVECs include the Senescent Cells Histochemical Staining Kit purchased from Sigma-Aldrich (CS0030) (Table 3.21), glycerol from Sigma-Aldrich (G5516), parafilm purchased from GMBH & Co, Germany and laboratory standard ultra pure (UP) H_2O was used for all dilutions.

Reagent	Components
10X Fixation buffer	Solution containing 20% formaldehyde, 2% glutaraldehyde, 70.4 mM $Na2HPO_4$, 14.7 mM KH_2PO_4, 1.37 M NaCl, and 26.8 mM KCl
10X PBS	-
Reagent B	400 mM Potassium ferricyanide
Reagent C	400 nM Potassium ferrocyanide
10X Staining solution	-
40 mg/ml X-gal solution	-

Table 3.21 The components of the senescence cells histochemical staining kit.

3.12.2 Methods

After inducing SIPS (section 3.11), the HUVECs were trypsinised, counted using a haemocytometer and re-seeded in gelatine coated 6-well plates at a seeding density of $5x10^4$ and allowed to adhere for 24 hours at 37°C and 5% CO_2. The culture media was aspirated and the wells were washed twice with 1 ml 1X PBS per well, 1.5 ml of 1X fixation buffer was added to each well and left to incubate at room temperature for 6-7 minutes while the staining mixture was prepared (Table 3.22). The wells were washed 3

times with 1ml 1X PBS before adding 1 ml staining mixture per well, the plates were then sealed with parafilm to prevent the wells drying out and the plates were incubated at 37°C without CO_2 for 24 hours. Since senescent cells specifically stain at pH 6, it is important for cells to not be in a CO_2-rich environment to avoid pH alterations of the solution.

The blue stained, senescent, cells were visualised using a Nikon inverted trinocular phase contrast light microscope, with images taken at ×100 magnification, quantification of the blue stained cells was done manually from 5 distinct fields of view from each well. After the wells were analysed, the staining solution was removed and 1 ml of 70% glycerol was added to each well, allowing long-term storage of the plates at 4°C.

CHAPTER FOUR

Effects of Arsenite on Cell Viability, Senescence and ROS

Chapter 4: Effects of arsenite on cell viability, senescence and ROS

4.1 Introduction

4.1.1 Investigating the underlying mechanisms of arsenite cytotoxicity

Arsenic is a known human toxicant, the exposure to which results in the development of a wide spectrum of diseases, including cardiovascular disease (see chapter 1). Since epidemiological studies carried out on the health effects of arsenic investigate individuals chronically exposed to arsenic, it is difficult to mimic these exposure conditions *in vitro*. Therefore investigations conducted in this thesis, determining the underlying mechanisms by which arsenite impacts endothelial cells, will focus on using sub-cytotoxic arsenite concentrations. The importance of using sub-cytotoxic concentrations is highlighted when investigating the initial intracellular effects of arsenic e.g. determining changes in levels of cellular ROS.

Shi *et al* (2010) carried out such an investigation, looking at the effects of arsenite on ROS generation in HUVECs. Arsenite induced a concentration dependent increase in ROS levels after 24 hour treatment at concentrations of ≥650 μg/L. However, they also found a significant concentration-dependent increase in the extent of apoptosis in the cell population treated for 24 hour with arsenite concentrations of ≥650 μg/L. Based on this study, it is apparent that the correlation of increased ROS with apoptosis induction makes it hard to distinguish whether the onset of apoptosis was a consequence of increased cellular ROS or vice-versa. Thus, the use of sub-cytotoxic arsenite

concentrations, where arsenite treatment is not inducing significant cell death, appears to be essential when investigating the mechanisms behind arsenite-induced toxicity.

4.1.2 Arsenic and cellular senescence

The relationship between arsenic and cellular senescence has not been researched extensively, however the few studies conducted have shown arsenic to induce premature senescence in a number of cell types i.e. Syrian hamster embryo cells (Liao *et al*., 2001), human mesenchymal stem cells (Cheng *et al*., 2011) and rat aortic vascular smooth muscle cells (Martin-Pardillos *et al*., 2013). The mechanism by which arsenic induces senescence is yet to be fully understood, however oxidative stress seems to be a strong candidate for the onset of stress-induced premature senescence (SIPS).

As described in section 1.4.2.2, oxidative stress has been associated with cellular senescence. The exposure of human diploid fibroblasts to H_2O_2 has shown the induction of SIPS (Frippiat *et al*., 2001), with H_2O_2 resulting in the acceleration of telomere attrition as a result of single-strand breaks within telomeres (von Zglinicki *et al*., 2000). Oxidative DNA damage has also been associated with replicative senescence. The oxidative DNA damage marker, 8-oxo-dG, increased by 30% in senescent human diploid fibroblast cells compared with non-senescent cells (Chen *et al*., 1995), indicating replicative senescence occurs as a result of DNA damage accumulation. Furthermore, reducing the oxygen tension of human diploid fibroblasts by decreasing the atmospheric O_2 concentration to 3% resulted in an increase in the population doublings required to reach the senescent phenotype (Chen *et al*., 1995). Thus,

oxidative stress can be seen as a possible mechanism by which arsenite mediates cellular senescence in endothelial cells although this has not been well studied.

4.2 Aims

This chapter is focussed on establishing whether, at sub-cytotoxic concentrations, arsenite causes SIPS in HUVECs and whether arsenite induces acute oxidative stress in HUVECs and EA.hy 926 cells as the primary response.

4.3 Investigative methodology

4.3.1 Determining Cell viability

The trypan blue assay was employed to assess the cytotoxicity of arsenite in HUVECs. The use of this assay to measure cell viability is reliant on the intact cell membrane of viable cells, preventing the penetration of the trypan blue dye (Strober, 2001). Thus, dead cells are distinguished from living cells as they appear blue under microscopy. Along with the trypan blue exclusion assay, the cell counting kit 8 (CCK8) was used to validate the results generated. The CCK8 assay relies on the reduction of the colourless 2-(2-methoxy-4-nitrophenyl)-3-(4-nitrophenyl)-5-(2,4-disulfophenyl)-2H-tetrazolium, monosodium salt (WST-8), to an orange/yellow coloured formazan dye in the presence of dehydrogenase activity. Thus, the amount of dye produced is a reflection of the number of viable cells in a cell population due to their ability to express dehydrogenases.

4.3.2 Detecting H_2O_2 generation

Measurement of H_2O_2 production in response to arsenite treatment was carried out using the Amplex red assay (Figure 4.1) for cells seeded in 96-well plates (see section 3.3.1). The Amplex red assay consists of the enzyme peroxidase which reduces H_2O_2 to water with the conversion of Amplex red to resorufin; a red fluorescent molecule. H_2O_2 produced within the cell diffuses out into the culture media and can be detected by the Amplex reagents. The Amplex red assay is applied to the cell culture and incubated for 1.5 hours at 37ºC to allow the production and diffusion of cellular H_2O_2 and subsequenct reaction with the assay reagents before taking the fluorescence readings. Therefore the fluorescence detected is a direct representation of the amount of H_2O_2 generated by cells. To ensure the readings generated were a representaton of arsenite-induced H_2O_2 and not compromised by cell death, the Bradford assay was applied to the wells after applying the Amplex red assay.

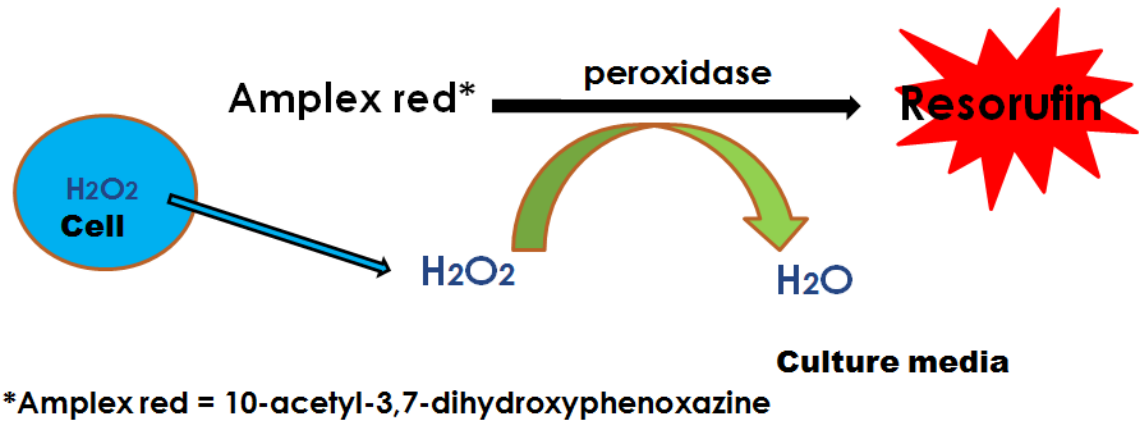

Figure 4.1 Basis of the Amplex Red assay for peroxide. Hydrogen peroxide is able to diffuse out of cells and into the culture media where it is reduced by the enzyme peroxidase to water. This reduction occurs via the conversion of Amplex red, which acts as an electron donor for the reduction reaction, to form the red fluorescent molecule resorufin.

The Bradford assay (Bradford, 1976) is a colorimetric assay based on the binding of the Coomassie Brilliant Blue G-250 dye, predominantly present in acidic conditions in its red cationic form with an absorbance maximum at 470 nm, which binds proteins and is converted to its blue unprotonated form measured at $A_{595\ nm}$ (Compton and Jones, 1985; Jones *et al*., 1989). Thus, this assay will measure the amount of proteins present in each well after the treatment with arsenite, and indicate the amount of cells lost due to the arsenite cytotoxcity.

4.3.3 Measuring ROS and cell death using flow cytometry

Measurements for both ROS generation and cell death i.e. apoptosis and necrosis in arsenite treated HUVECs were carried out using flow cytometry. Flow cytomtery is a laser based technique that enables the multi-parameter analysis of individual cells. The crucial aspect of flow cytometry is the point of intersection or the 'interrogation point', where each individual cell is hit by the laser beam, resulting in a 'scatter' of light wavelengths from the cell. The laser beam will also excite fluorescent molecules found within or attached to the cell, sending out an emission wavelength. The scatter and fluorescent wavelengths are recorded by detectors within the flow cytometer and interpreted by specialist flow cytometry software to give information regarding many of the cellular characteristics (Givan, 2004; Ibrahim and van den Engh, 2007).

Intracellular ROS were measured using flow cytometry with several fluorescent dyes. 5,6-chloromethyl- 2',7'-dichlorohydrofluorescein diacetate (CM-H_2DCFDA) is the popular and widely used dye to indicate the levels of intracellular ROS, and was initially used. CM-H_2DCFDA, a chloromethyl derivative of H_2DCF-DA which provides

more retention in living cells through its reactivity with glutathione and other intracellular thiols, is a non-fluorescent cell permeable probe that is hydrolysed by intracellular esterases and then proposed to undergo oxidation by ROS to give the fluorescent molecule, DCF (Rosenkranz *et al*., 1992; Tampo *et al*., 2003).

The generation of intracellular superoxide also was measured using both DHE, as well as MitoSOX™ which specifically measures mitochondrial superoxide production. DHE is suggested to undergo oxidation by intracellular superoxide to form 2-hydroxyethidium (2-OH-Et), which binds to DNA and fluoresces (Zielonka and Kalyanaraman, 2010). MitoSOX™ is made up of DHE but with a triphenylphosphonium (TPP) group attached by a hexyl carbon chain. TPP groups are cations which have properties that enable them to diffuse through phospholipid bilayers. Since mitochondria are the most negatively charged organelle in the cell, due to the transfer of hydrogen ions from the matrix to the inter membrane space of the mitochondria during the ETC, the TPP cations pass through the mitochondrial phospholipid bilayers and reside within the matrix (Ross *et al*., 2005).

Cell death was also measured using flow cytometry through the simultaneous staining of cells with FITC-labelled annexin V and propidium iodide (PI), enabling the differentiation between the apoptotic and necrotic populations within the sample. Annexin V belongs to a family of proteins that bind to phospholipids, with annexin V preferentially binding to phosphatidylserine (PS), usually found on the internally facing cellular membrane of viable cells. During early apoptosis, PS is translocated to the external surface of the cell, enabling the binding of annexin V and thus detection of early apoptosis through the fluorophore FITC (Vermes *et al*., 1995). Unlike early

apoptotic cells which still maintain an intact cellular membrane, necrotic cells are damaged cells with damaged membranes. PI is able to diffuse into necrotic cells and binds to DNA with a resultant increase in fluorescent signal, but is unable to penetrate the cellular membrane of viable cells. Therefore, PI is used to detect necrotic cells as it can enter cells with damaged membranes and bind to the DNA (Ormerod *et al*., 1993).

4.3.4 Detecting stress-induced cellular senescence

SA-β-gal is an established biomarker of cellular senescence. The detection of SA-β-gal at pH 6 has been found to be exclusively associated with cellular senescence, as measured in senescent human cells (Dimri *et al*., 1995). SA-β-gal localises to lysosomes within the cell (Lee *et al*., 2006), and the increase is because ageing cells have been found to accumulate lysosomal mass (Suzuki *et al*., 1995; Kurz *et al*., 2000). This forms a good marker to use for cellular ageing. Thus, the histochemical detection of SA-β-gal is used as a reliable method of determining senescence in both *in vivo* and *in vitro* investigations.

4.4 Results

4.4.1 Determining cell viability in response to arsenite treatment

To determine the concentrations at which arsenite displayed its cytotoxic effects, HUVECs were exposed to a 10-fold increasing arsenite concentration range of 1-1000 μg/L, for 24 hours. Subjecting the cells to the trypan blue exclusion assay gave a measure of cell viability. Arsenite exhibited a concentration-dependent increase in the

percentage of non-viable cells from the total cell population with statistical significance in the percentage of cell death seen for cells treated with concentrations of 1000 µg/L (10.6%, $p<0.05$) and 10,000 µg/L (26.2%, $p<0.001$) (Figure 4.2). Based on the trypan blue exclusion assay data, arsenite is cytotoxic at concentrations ≥1000 µg/L.

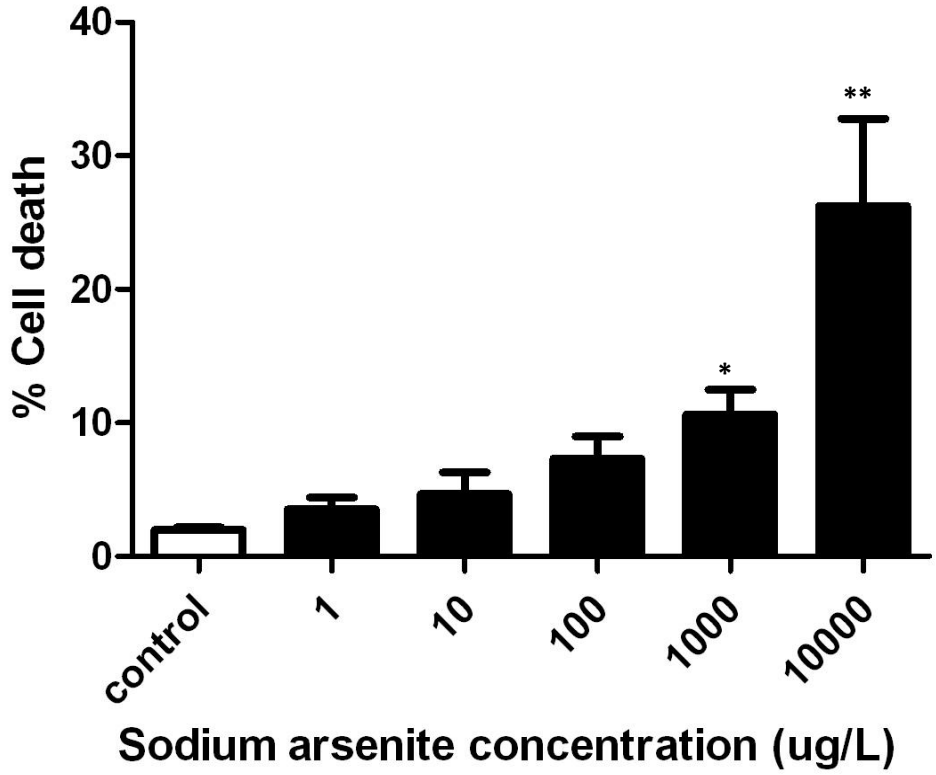

Figure 4.2 Percentage cell death induced by 24 hours arsenite treatment assessed using the trypan blue exclusion assay. Values represent mean of n=4 +SEM. The data were analysed with one-way ANOVA using the Dunnett post-test (* $p<0.05$, ** $p<0.01$ compared to untreated control cells).

The CCK8 colorimetric assay was also used to determine the concentration at which arsenite displayed cytotoxicity. Absorbance measurements were taken at a time-point during 1-4 hours incubation of cells with the CCK8 assay, following the manufacturer's instructions. To ensure optimum absorbance readings were generated from the cells exposed to the CCK8 assay, a seeding density gradient for HUVECs was set up in a 96

well plate (Figure 4.3). Overnight seeding of cells at 5000 cells/well gave the optimum absorbance readings after 4 hour exposure to the CCK8 reagent, where the absorbance readings were not too high, allowing for potential increases as well as decreases in absorbance during the subsequent experiments.

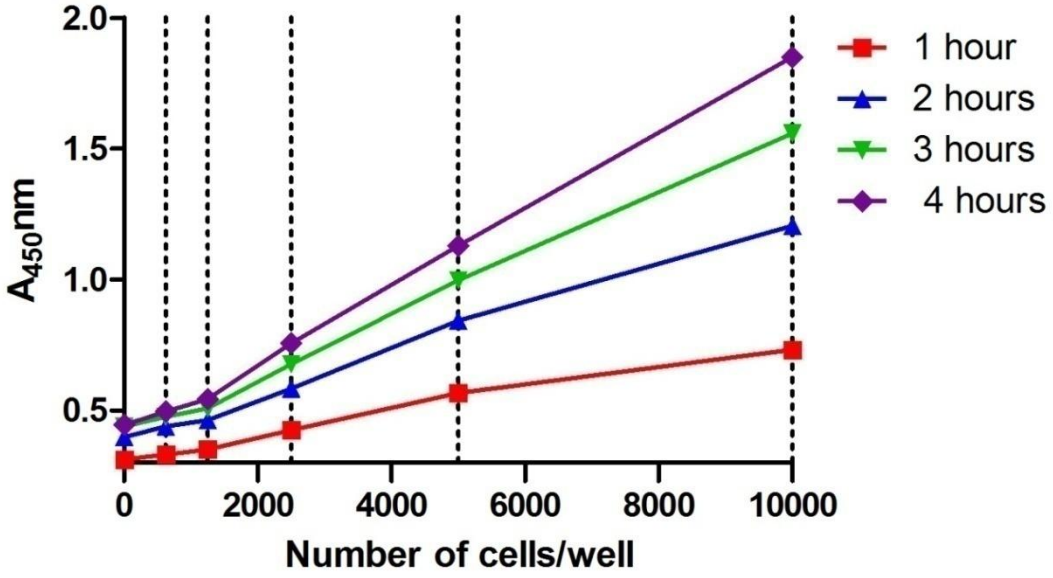

Figure 4.3 Optimisation of CCK8 assay. Cells, 625 to 10,000 per well were seeded into a 96 well plate to deduce the optimum seeding density for 24 hours, recording the absorbance values at 450nm using a plate reader after 1, 2, 3 and 4 hours of adding the CCK8 assay reagent. The values represent the mean ±SEM of n=5.

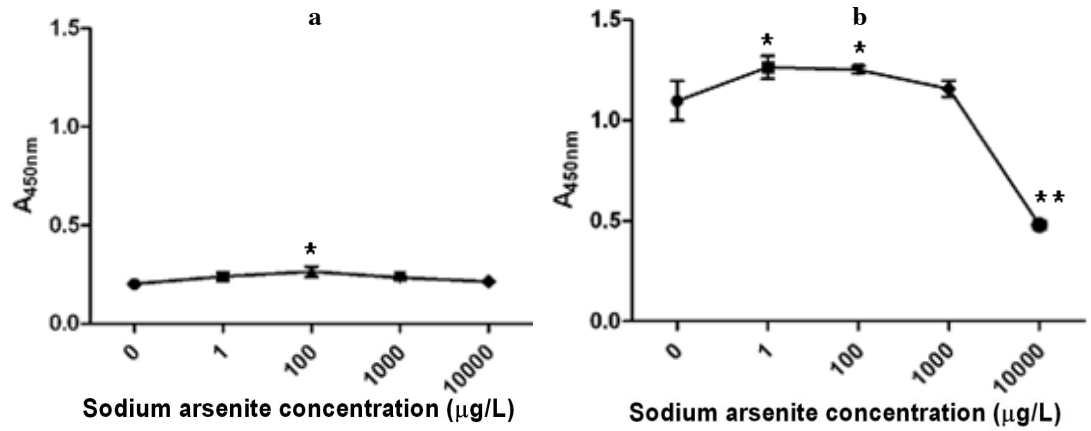

Figure 4.4 The viability of HUVEC after 24 hour treatment with arsenite concentrations between 1-10,000 μg/L. Absorbance readings at 450nm were taken using a plate reader after (a) 0 hours and (b) 4 hours of applying the CCK8 assay. Values represent means ±SEM of n= 5. The data were analysed using one-way ANOVA with Dunnett post-test, using the untreated cells as the control (* $p<0.05$, ** $p<0.01$ compared to the untreated control cells).

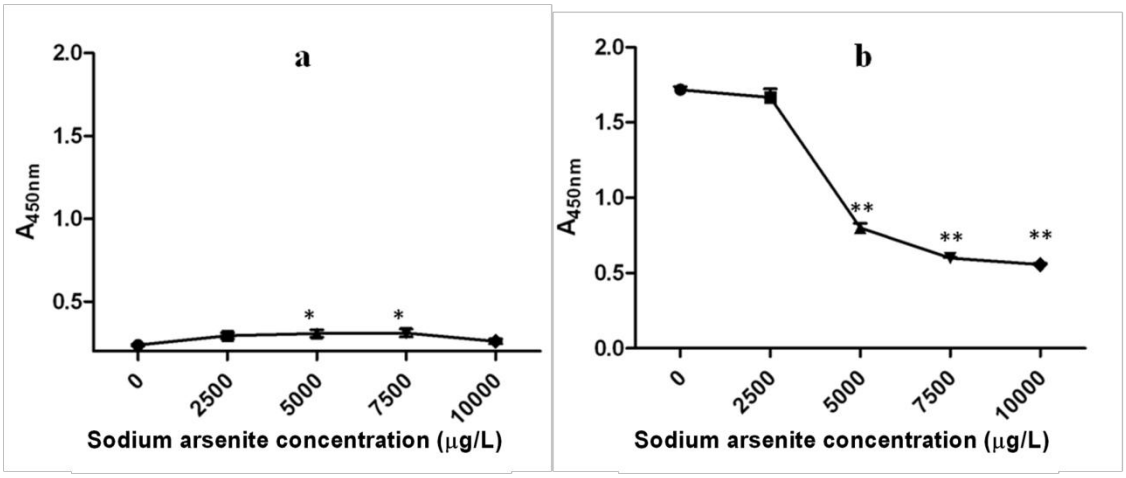

Figure 4.5 The viability of HUVEC after 24 hour treatment with increasing arsenite concentrations between 2,500-10,000 μg/L. Absorbance readings at 450nm were taken using a plate reader after (a) 0 hours and (b) 4 hours of applying the CCK8 assay. Values represent means ±SEM of n= 5. The data were analysed using one-way ANOVA with Dunnett post-test, using the untreated cells as the control (*$p<0.05$, ** $p<0.01$ compared to the untreated control cells).

This optimised CCK8 assay was used to investigate the effect of arsenite on HUVEC cell viability. HUVECs were treated for 24 hours at an arsenite concentration range between 1-10,000 μg/L. The cytotoxic effect of arsenite became apparent at the arsenite

concentration of 10,000 μg/L, where a significant decrease in cell viability was observed compared to the untreated cells ($p<0.01$).

To further investigate the precise concentration at which the cytotoxicity of arsenite was exhibited on HUVECs, the concentration range of arsenite was refined to concentrations between 2,500 and 10,000 μg/L (Figure 4.5). After 4 hours incubation with the CCK8 assay, cells treated with arsenite concentrations of 5000, 7500 and 10,000 μg/L displayed a significant concentration-dependent increase in cytotoxicity ($p<0.01$), interpreted as decreased cell viability. Therefore, concentrations below 2,500 μg/L can be seen to be sub-cytotoxic for 24 hours treatment of HUVECs.

To determine the sub-cytotoxic concentrations of arsenite to use for investigations involving more chronic arsenite treatment, HUVECs were treated for 5 days with an arsenite concentration range of 1,000 to 5,000 μg/L. All of the arsenite concentrations displayed cytotoxicity by 2 hours of incubation with CCK8 assay reagent (Figure 4.6). With significant cell death induced at all these concentrations ($p<0.001$), the arsenite concentration range tested for cytotoxicity was reduced to 1-1,000 μg/L. HUVECs exposed to these arsenite concentrations daily for 5 days showed significant concentration-dependent cell death at concentrations ≥ 200 μg/L after 3 hours CCK8 incubation (Figure 4.7). Further refinement of the arsenite concentration range between 0.1 and 200 μg/L also showed significant cell death at 200 μg/L arsenite after 5 days treatment ($p<0.01$), for absorbance readings taken after 3 hour incubation with the CCK8 assay (Figure 4.8). Therefore, the sub-cytotoxic concentrations established for

experiments involving 5 day arsenite exposure with HUVECs appears to be below 200 μg/L.

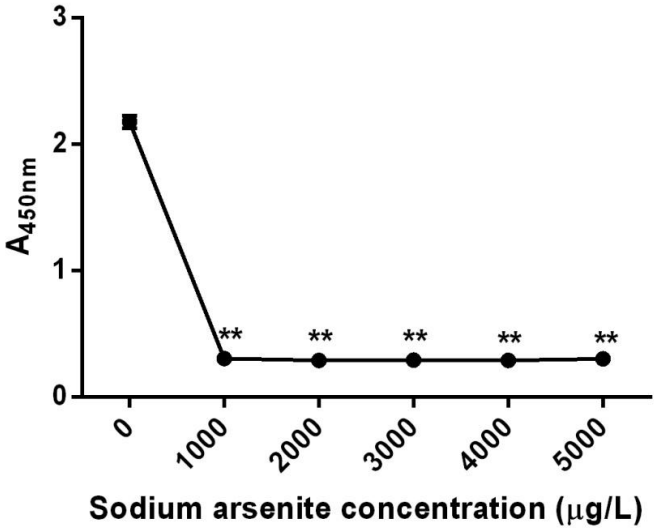

Figure 4.6 The viability of cells treated with arsenite for 5 days (I). Absorbance readings at 450nm were taken using a plate reader 2 hours after the CCK8 assay was applied. The values represent mean ±SEM of n= 5. The data were analysed using one-way ANOVA with Dunnett post-test, using the untreated cells as the control. (*** $p<0.001$ compared to the untreated control; 0 μg/L)

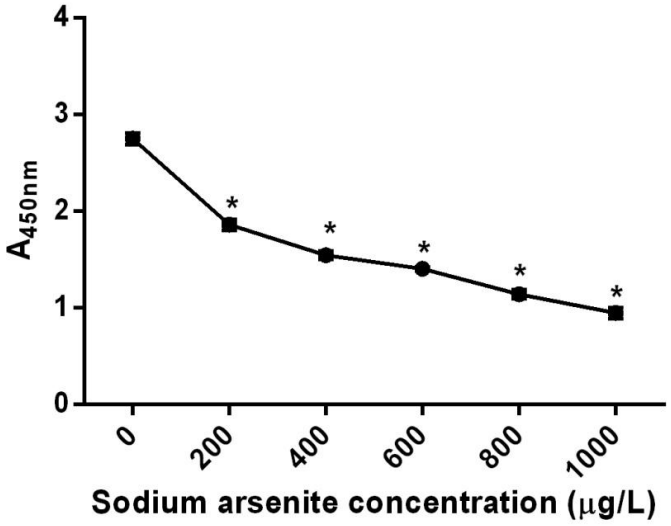

Figure 4.7 Effect of 5 day arsenite exposure on HUVEC viability (II). The viability of cells was determined by measuring the absorbance at 450 nm after 3 hours of applying the CCK8 using a plate reader. The values represent mean ±SEM of n= 5. The data were analysed using one-way ANOVA with Dunnett post-test, using the untreated cells as the control. (** $p<0.01$ compared to control; 0 mg/L)

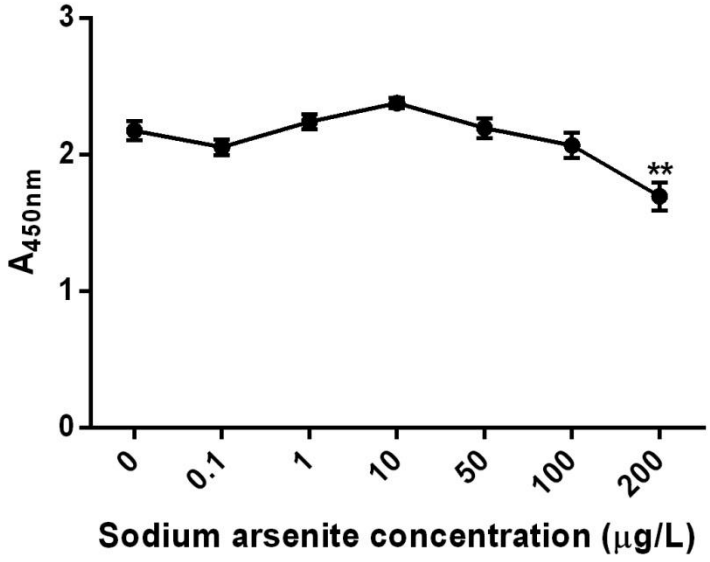

Figure 4.8 Effect of 5 day arsenite exposure on HUVEC viability (III). The viability of HUVEC treated for 5 days with arsenite was determined using the CCK8, the absorbance at 450 nm was measured after 3 hours CCK8 incubation using a plate reader. The values represent mean ±SEM of n= 5. The data were analysed using one-way ANOVA with Dunnett post-test, using the untreated cells as the control (** $p<0.01$ compared to control; 0μg/L).

4.4.2 Induction of stress-induced premature senescence (SIPS) by arsenite

In this thesis, investigations into whether arsenite induced senescence were carried out by using the senescence-associated β-galactosidase (SA-β-gal) staining assay alone. The induction of SIPS was investigated by subjecting HUVECs to 1 hour treatment consistently for 3 consecutive days at the sub-cytotoxic arsenite concentrations of 650 and 1,300 μg/L and using 50 μM tert-butyl hydrogen peroxide (t-BHP) as a positive control for SIPS. The occurrence of SIPS was assessed through the positive blue staining of cellular cytoplasm for SA-β-gal. Approximately 20% of the control, untreated HUVECs displayed blue staining in the cells when assessed under microscopy, in comparison to arsenite treated cells which had significantly increased number of staining for SA-β-gal ($p<0.001$) (Figures 4.9 and 4.10). The arsenite-induced

senescent cells display altered morphological characteristics, i.e. larger cytoplasm and elongated appearance, in comparison to the non-senescent HUVECs in the control cell population (Figure 4.9). Arsenite induced SIPS in a concentration-dependent manner, with approximately 60% and 80% senescence induction for cells treated with 650 and 1,300 µg/L arsenite respectively. The percentage of SIPS in HUVECs treated with 1,300 µg/L arsenite was also seen to exceed the extent of SIPS seen as a result of t-BHP treatment (Figure 4.10).

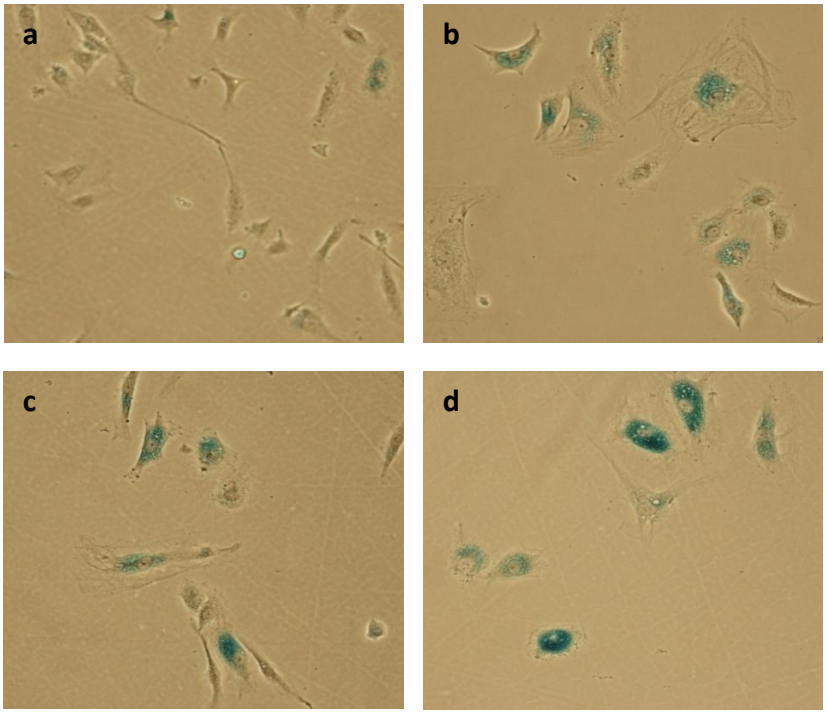

Figure 4.9 Induction of SIPS by arsenite. The images show HUVEC stained for SA-β-gal (blue) representing senescence after 3 days treatment with (a) no treatment, (b) 650 µg/l arsenite, (c) 1300 µg/l arsenite and (d) 50 µM t-BHP. The images were taken at x100 magnification.

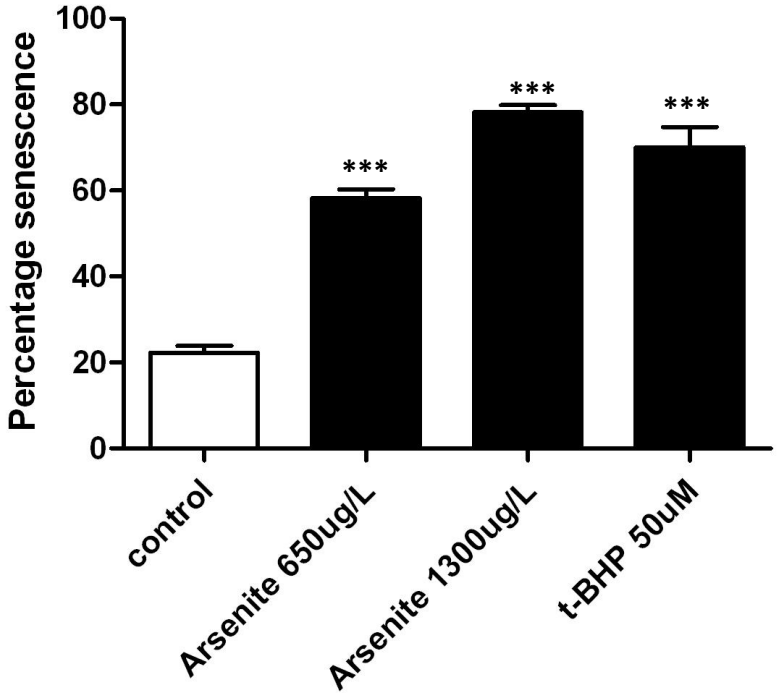

Figure 4.10 Arsenite induced SIPS of HUVEC cultures. The percentage of HUVEC having undergone senescence, stained positive for SA-β-gal, after 1 hour exposure to the stressors each day for 3 consecutive days. The values represent mean +SEM of n= 4. The data were analysed using one-way ANOVA with Dunnett post-test, using the untreated cells as the control (*** $p<0.001$ compared to the control; 0 μg/L).

4.4.3 Determination of arsenite induced ROS

4.4.3.1 Effect of arsenite on H_2O_2 generation in endothelial cells

The Amplex red assay was used to detect whether arsenite induced the generation of H_2O_2 in HUVECs treated with a range of sub-cytotoxic and cytotoxic concentrations, 1,000- 5,000 μg/L. To assess the responsiveness of the Amplex red assay, a range of H_2O_2 concetrations, 0, 20, 40, 60 and 80 μM respectively were investigated (Figure 4.11a). The flourescence response was approximately linear over this concentration range with a limit of detection in the low μM range. The standard curve also provided a reference against which the amount of H_2O_2 produced from the cells could be quantified.

The Bradford assay was employed after measuring H_2O_2 with the Amplex red assay, to measure the cellular protein levels, giving an estimation of cell mass, at the end of the 24 hour arsenite treatment. This was used to indicate whether arsenite induced cell death at any of the treatment concentrations used and could be used to normalise the data. A standard curve was made using known concentrations of BSA (Figure 4.11b), against which the amount of protein measured in the wells could be quantified.

The data represented in figure 4.11c show no significant differences in the raw estimates of H_2O_2 produced from any of the sodium arsenite treated cells in comparison to the untreated control cells, with the positive control menadione significantly increasing H_2O_2 production ($p<0.01$ compared to the control). However, there was a suggestion of a concentration-dependent decrease in the fluorescence seen with sodium arsenite treated cells; from the 1,196 AFU detected from untreated cells, to 869 AFU from cells treated with 1000 μg/L arsenite and approximately 700-730AFU from cells treated with 2,000-5,000 μg/L. This non-significant trend is probably due to the concentration-dependent decrease in cell mass observed with increasing sodium arsenite concentrations (Figure 4.11d) (at least $p<0.05$). However, normalising the mean fluorescence values detected from the cells against the protein concentration/ well values still showed decreased fluorescence detection from arsenite treated cells compared to the control cells (Figure 4.11e). Therefore, the results in figure 4.11 indicate that no increases in H_2O_2 generation were measured in HUVECs in response to arsenite.

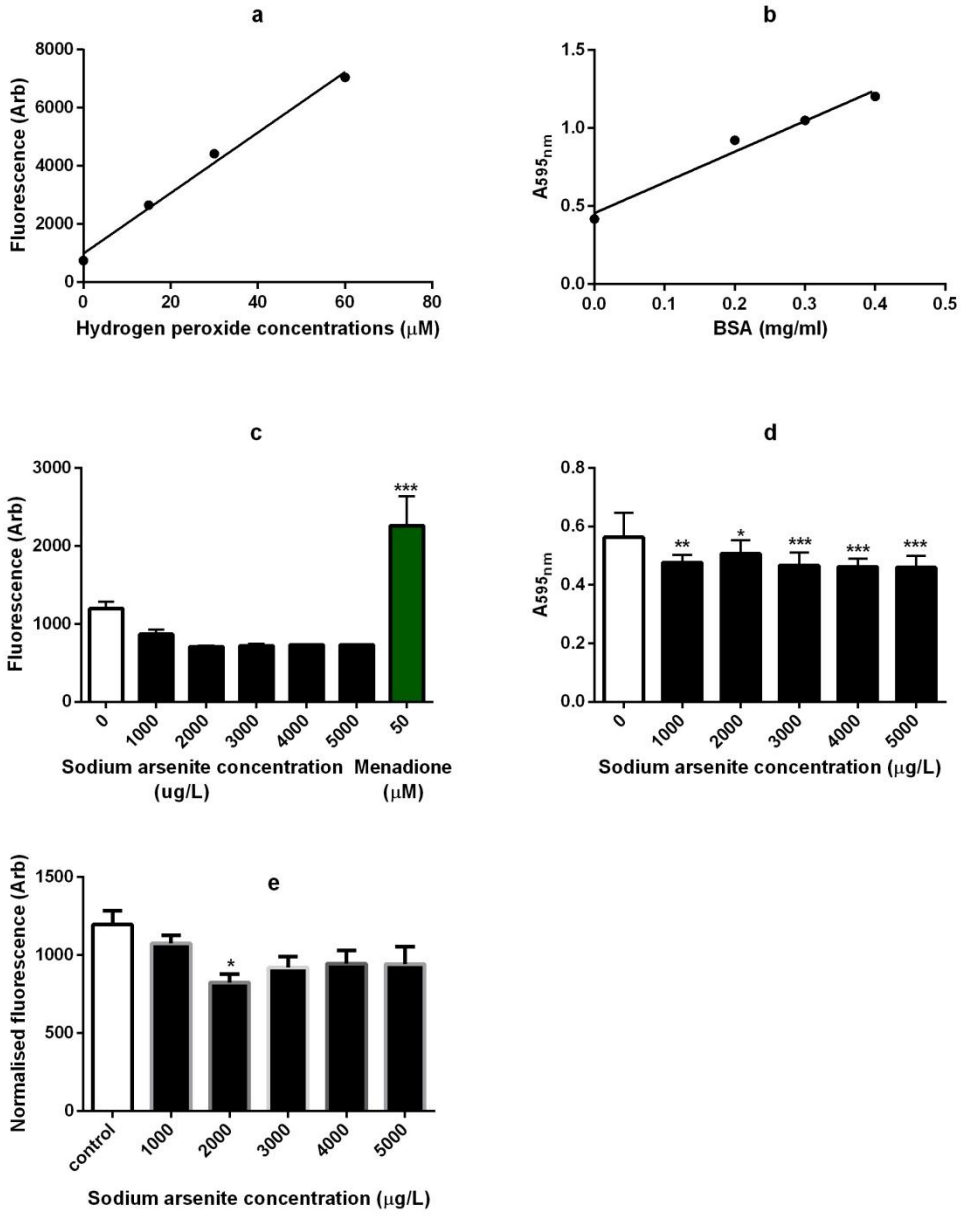

Figure 4.11 Effects of arsenite on H_2O_2 production in HUVEC cultures. H_2O_2; 0, 15, 30, 60, and 80 μM concentrations were used to create a standard curve using the Amplex red assay, the values represent means of n=3 (a) and BSA concentrations; 0, 0.1, 0.2, 0.3, 0.4, and 0.5 mg/ml were used to create a protein standard curve using the Bradford assay, values represent means of n=3 (b). After the exposing HUVECs to arsenite for 24 hours and 50 μM menadione for 1 hour, the Amplex red assay was used to measure the levels of H_2O_2 generated (c) after which the Bradford assay was applied to quantify the cellular proteins/well after the arsenite treatment to determine cytotoxicity (d). The fluorescence measured in (c) was normalised against the level of proteins/ well (d) to enable direct comparison between levels of H_2O_2 detected (e) which was plotted as a mean for visualisation. The values (c and d) represent mean +SEM n=5. Data were analysed using the one-way ANOVA with Dunnett post-test, using the untreated cells as the control (*p<0.05, **p<0.01, *** p<0.001 compared to the control; 0 μg/L).

4.4.3.2 Effect of arsenite on ROS production assessed using fluorescent probes

The widely studied HUVEC derived cell-line EA.hy 926 was used in the following experiments due to relative ease and reliability of culture compared with HUVECs. Induction of necrosis and apoptosis was firstly investigated using flow cytometry to define sub-cytotoxic concentrations of arsenite for subsequent experiments. The acute induction of apoptosis and necrosis was assessed after 1 hour and 4 hours treatment with arsenite at 10-fold increasing concentrations from 1-10,000 µg/L. Staurosporine (1 µM) was used as a positive control for apoptosis and 4 mM H_2O_2 as a positive control for necrosis. Cell death was measured using flow cytometry and the simultaneous staining with FITC-annexin V and PI (Figure 4.12).

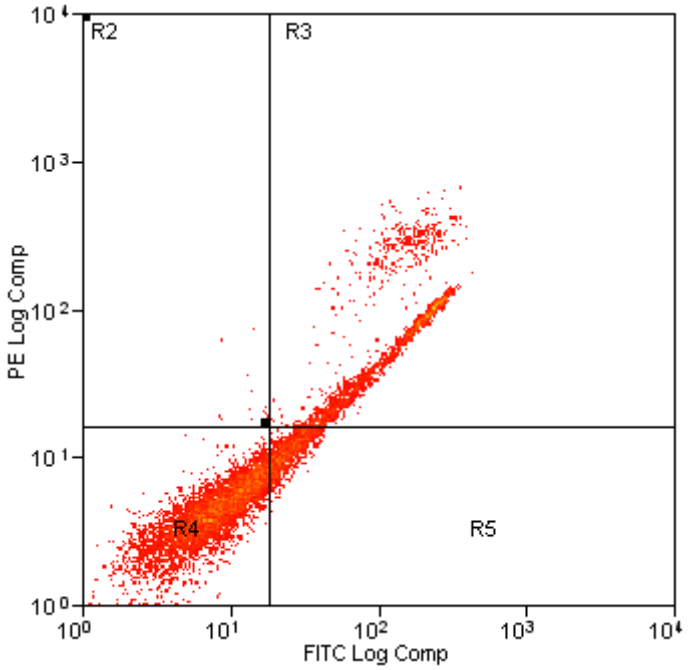

Figure 4.12 Annexin V-FITC and PI double staining of EA.hy 926 cells treated with 1 µM staurosporin for 1 hour, analysed using flow cytometry. R4 represents live cells, R5 represents early apoptosis, R3 represents late apoptosis and R2 represents necrotic cells.

As expected, after 1 hour treatment, none of the arsenite concentrations or 1 µM staurosporine resulted in any significant increases in either apoptosis or necrosis compared to the level detected in the control cells. EA.hy 926 cells treated with 4 mM H_2O_2 did however show a significant increase in both apoptosis and late apoptosis (also considered as necrosis) ($p<0.05$) after 1 hour treatment (Figure 4.13). Therefore, 1 hour exposure to arsenite did not induce cytotoxicity.

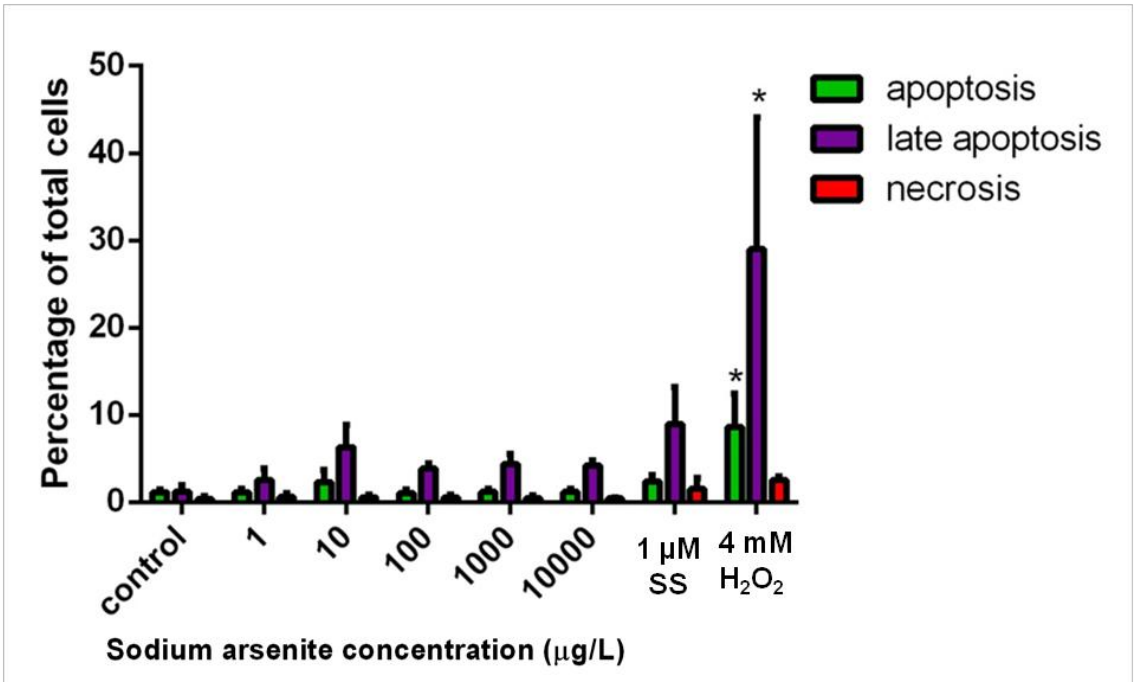

Figure 4.13 The effect of arsenite on apoptosis and necrosis in EA.hy 926 cultures (I). EA.hy 926 cells were treated with increasing arsenite concentrations and positive controls staurosporine (SS) and hydrogen peroxide (H_2O_2) for 1 hour and the induction of cell death measured. Annexin V and PI were simultaneously used with flow cytometry to determine the induction of apoptosis and necrosis respectively. The values represent means+SEM n=3. The data were analysed using one-way ANOVA with Dunnett post-test, using the untreated cells as the control (*$p<0.05$ compared to the untreated control cells).

The exposure of EA.hy 926 cells to arsenite for 4 hours also resulted in no increase in apoptosis or necrosis compared to the control, untreated cells (Figure 4.14). Although the percentage of late apoptotic cells detected at 10,000 µg/L appeared to increase this did not reach statistical significance (Figures 4.13 and 4.14 respectively). After 4 hours, 1 µM staurosporine induced a significant increase in apoptosis ($p<0.001$) and 4 mM H_2O_2 induced a significant increase in necrosis and late apoptosis ($p<0.001$) (Figure 4.14). In conclusion, arsenite at concentrations between 1 and 10,000 µg/L did not induce an increase in apoptosis or necrosis in EA.hy 926 cells after either 1 or 4 hours exposure.

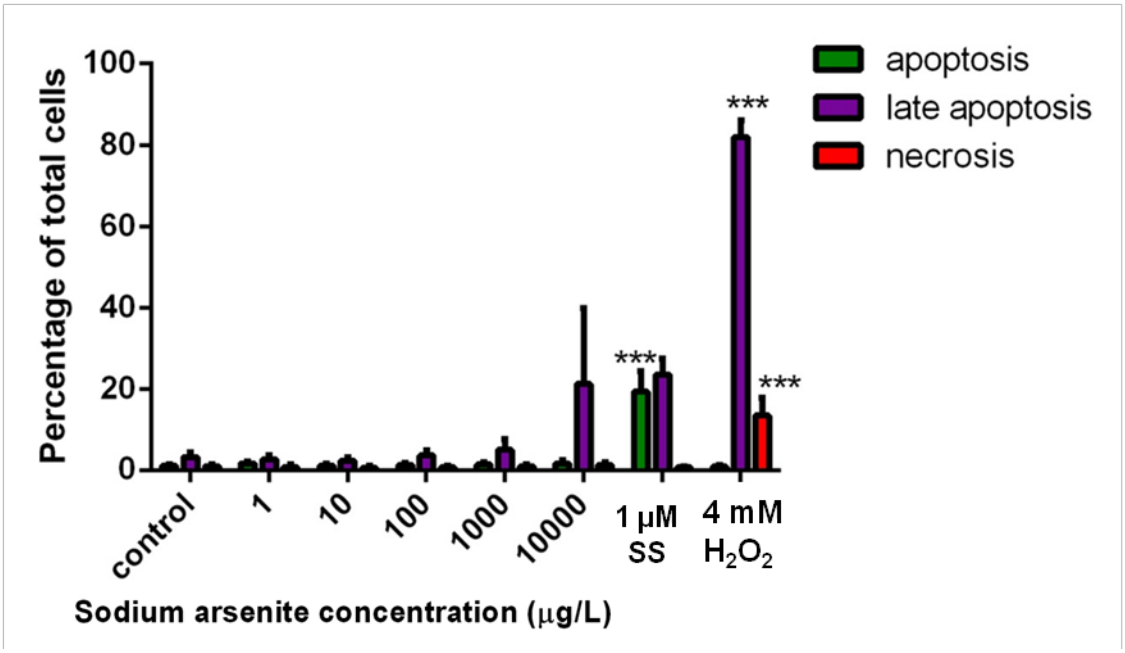

Figure 4.14 The effect of arsenite on apoptosis and necrosis in EA.hy 926 cultures (II). EA.hy 926 cells were treated with increasing arsenite concentrations and positive controls staurosporin (SS) and hydrogen peroxide (H_2O_2) for 4 hours and the induction of cell death measured. Annexin V and PI were simultaneously used with flow cytometry to determine the induction of apoptosis and necrosis respectively. The values represent means+SEM n=5. The data were analysed using one-way ANOVA with Dunnett post-test, using the untreated cells as the control (***$p<0.001$ compared to the untreated control cells).

4.4.3.3 Effect of arsenite on ROS measured using CM-H_2DCFDA

The effects of arsenite on the intracellular levels of ROS were also measured using flow cytometry with EA.hy 926 cell for the same treatment times as the cell death investigations. HUVECs were also assessed for ROS generation to ensure the data generated from EA.hy 926 cells were a true representation of endothelial cells.

The levels of intracellular ROS in EA.hy 926 cells exposed to 10-fold increasing arsenite concentration of 1 to 10,000 µg/L for 4 hours was measured using the fluorescent reporter CM-H_2DCFDA (Figure 4.15). A trend of increasing ROS levels was observed in a concentration-dependent manner, with 1,000 µg/L and 10,000 µg/L arsenite inducing a significant increase compared to the untreated control cells, with over 2-fold increase in ROS levels for both concentrations compared to the control ($p<0.05$). H_2O_2 (100 µM) was used as a positive control for ROS detection by CM-H_2DCFDA, showing a significant increase in ROS detected after 30 minutes of H_2O_2 exposure compared to the untreated control cells ($p<0.01$) (Figure 4.15).

Similarly, a concentration-dependent increase in ROS generation was seen for HUVECs in response to 4 hour treatment with arsenite (Figure 4.16). However, statistical significance for increased ROS generation was achieved for cells treated with lower arsenite concentration, that is at 100 µg/L ($P<0.0001$), than seen in EA.hy 926 cells. Arsenite induced higher levels of ROS in HUVECs compared to EA.hy 926 cells, with approximately 5-8 fold increases in ROS generation for 100-10,000 µg/L arsenite (Figure 4.16). Treating HUVECs with 1 mM H_2O_2 for 30 minutes as a positive control for ROS detection showed a significant increase in the level of ROS measured

compared to the untreated control cells ($p<0.001$). Thus, according to the ROS detecting fluorescent probe, CM-H_2DCFDA, assuming this probe faithfully reports ROS in cells, arsenite induces an increase in ROS generation in a concentration-dependent manner for both HUVECs and EA.hy 926 cells after 4 hour treatment.

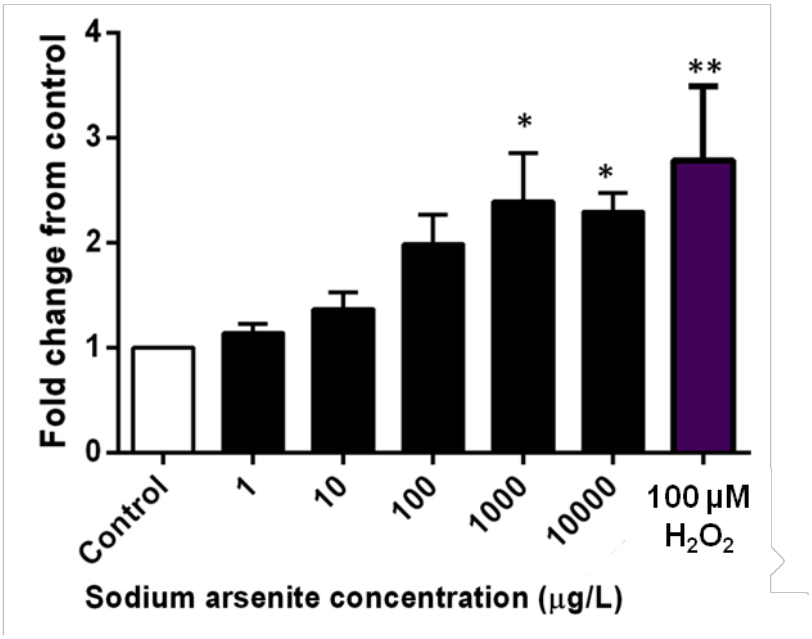

Figure 4.15 Effect of arsenite on CM-H_2DCFDA fluorescence in EA.hy 926 cultures. A range of arsenite concentrations was used to treat EA.hy 926 cells for 4 hours, with 100 µM hydrogen peroxide (H_2O_2) as a positive control for 30 minutes. CM-H_2DCFDA was used with flow cytometry to determine ROS generation. The values represent means+SEM n=7. The data were analysed using one-way ANOVA with Dunnett post-test, using the untreated cells as the control (*$p<0.05$ and **$p<0.01$ compared to the control; 0 µg/L).

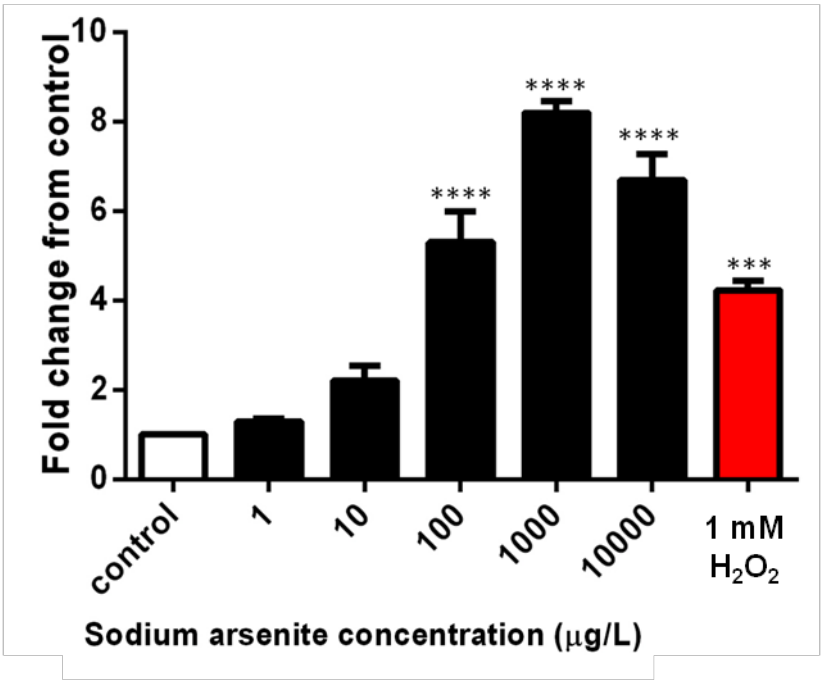

Figure 4.16 Effect of arsenite on CM-H_2DCFDA fluorescence in HUVECs. A range of arsenite concentrations was used to treat HUVECs for 4 hours, with 1 mM hydrogen peroxide (H_2O_2) as a positive control for 30 minutes. CM-H_2DCFDA was used with flow cytometry to determine ROS generation. The values represent means+SEM n=3. The data were analysed using one-way ANOVA with Dunnett post-test, using the untreated cells as the control (***$p<0.001$ and ****$p<0.0001$ compared to the control; 0 μg/L).

In an attempt to validate the findings from the experiments using CM-H_2DCFDA (Figures 4.15 and 4.16), and to determine the source of ROS generation within the cell, DHE and MitoSOX™ were used with both EA.hy 926 cells and HUVECs treated with arsenite to measure general and mitochondrial specific superoxide production respectively.

Exposing EA.hy 926 cells to an arsenite concentration range of 1-10,000 μg/L showed no significant effect on the mitochondrial generation of superoxide for either 1 or 4 hour treatment using MitoSOX™ (Figures 4.17 and 4.18 respectively). The treatment of EA.hy 926 cells with the positive control, 20 μM doxorubicin (DOX), for both the

experiments showed significant increases in mitochondrial superoxide compared to the untreated control cells ($p<0.001$) (Figures 4.17 and 4.18). Similarly, exposing HUVECs to the arsenite concentration range of 1-10,000 μg/L for 4 hours had no impact on MitoSOX™ fluorescence (Figure 4.19). The positive control, 1 hour treatment with 100 μM antimycin A, did show a significant increase in HUVEC MitoSOX™ fluorescence compared to the untreated control cells ($p<0.001$). Thus, arsenite does not appear to enhance mitochondrial ROS generation in either EA.hy 926 cells or HUVECs at concentrations of ≤10,000 μg/L for up to 4 hours exposure, suggesting any increased ROS might be from non-mitochondrial sources.

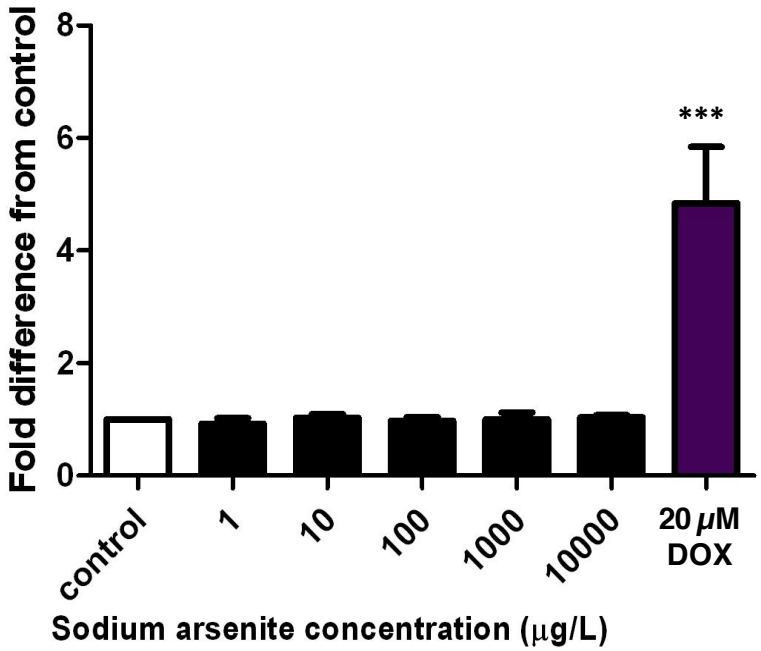

Figure 4.17 The effect of exposure to arsenite for 1 hour on mitochondrial superoxide generation in EA.hy 926 cells. EA.hy 926 cells were exposed to increasing arsenite concentrations and 20 μM doxorubicin (DOX) for 1 hour, mitochondrial superoxide was estimated using MitoSOX™ Red with flow cytometry. The values represent mean+SEM n=3. The data were analysed using one-way ANOVA with Dunnett post-test, using the untreated cells as the control (***$p<0.001$ compared to the control; 0 μg/L).

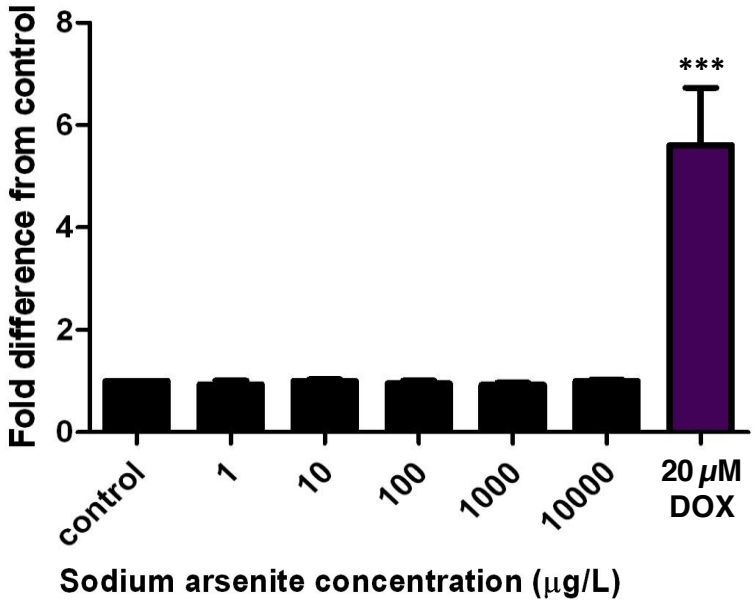

Figure 4.18 The effect of exposure to arsenite for 4 hours on mitochondrial superoxide generation in EA.hy 926 cells. EA.hy 926 cells were exposed to increasing arsenite concentrations and 20 μM doxorubicin (DOX) for 1 hour and mitochondrial superoxide was estimated using MitoSOX™ Red with flow cytometry. The values represent mean+SEM n=3. The data were analysed using one-way ANOVA with Dunnett post-test, using the untreated cells as the control (***$p<0.001$ compared to the control; 0 μg/L).

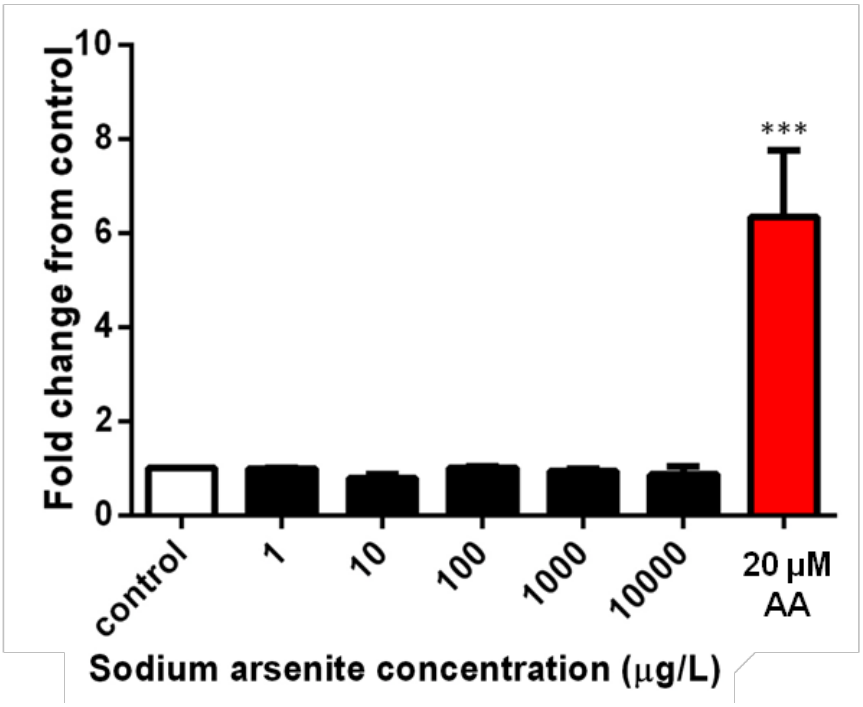

Figure 4.19 The effect of exposure to arsenite for 1 hour on mitochondrial superoxide generation in HUVECs. HUVECs were exposed to increasing arsenite concentrations and 100 µM antimycin A (AA) for 1 hour and mitochondrial superoxide was estimated using MitoSOX™ Red with flow cytometry. The values represent mean+SEM n=3. The data were analysed using one-way ANOVA with Dunnett post-test, using the untreated cells as the control (***$p<0.001$ compared to the control; 0 µg/L).

Further investigation into ROS generation in endothelial cells was undertaken using DHE as a reporter of cellular superoxide. The generation of cellular superoxide in EA.hy 926 cells was not altered by 1 or 4 hour arsenite exposure at concentrations of 1-10,000 µg/L (Figures 4.20 and 4.21). The exposure of the cells to 20 µM DOX as a positive control, for both 1 hour and 4 hours (Figures 4.20 and 4.21 respectively) gave a significant increase in superoxide compared to the control untreated cells ($p<0.05$).

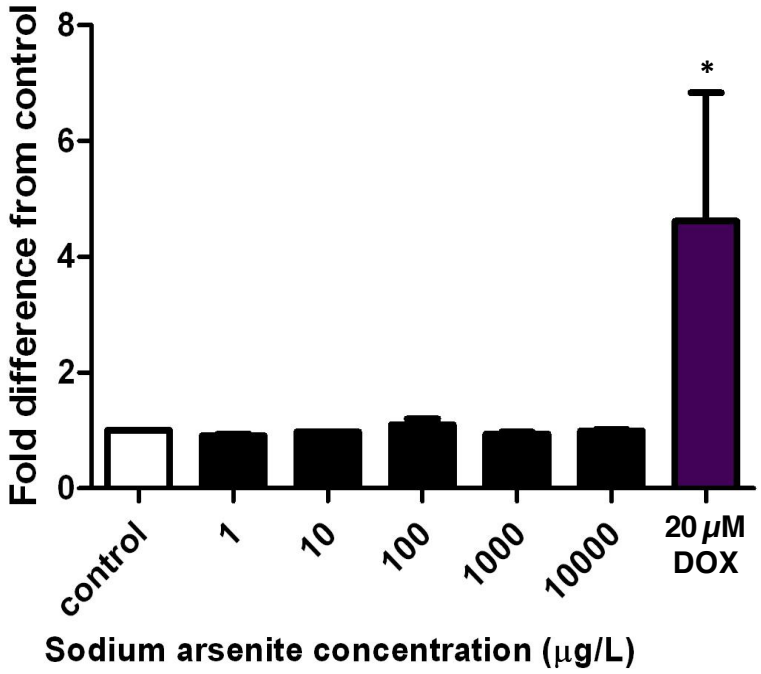

Figure 4.20 The effect of exposure to arsenite for 1 hour on superoxide generation in EA.hy 926 cells EA.hy 926 cells were exposed to increasing arsenite concentrations and 20 μM doxorubicin (DOX) for 1 hour and superoxide was estimated using DHE with flow cytometry. The values represent mean+SEM n=3. The data were analysed using one-way ANOVA with Dunnett post-test, using the untreated cells as the control (*$p<0.05$ compared to the control; 0 μg/L).

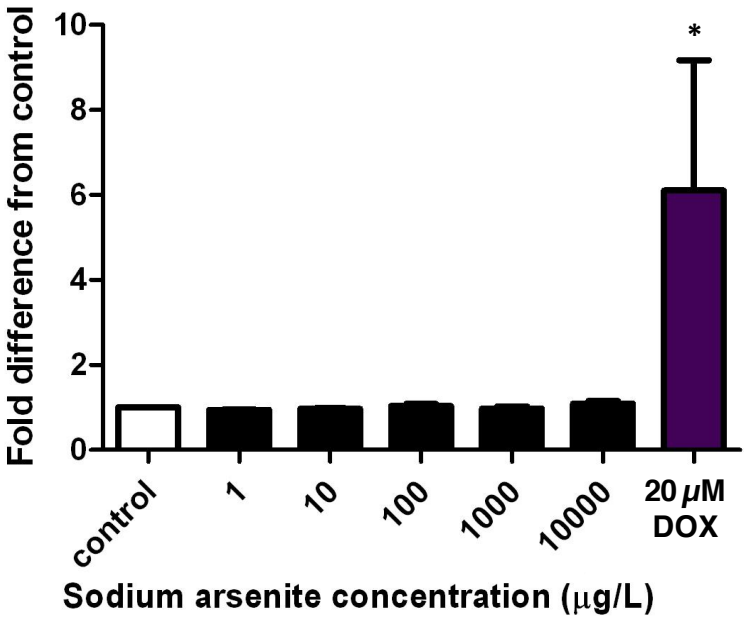

Figure 4.21 The effect of exposure to arsenite for 4 hours on superoxide generation in EA.hy 926 cells EA.hy 926 cells were exposed to increasing arsenite concentrations and 20 μM doxorubicin (DOX) for 1 hour and superoxide was estimated using DHE with flow cytometry. The values represent mean+SEM of n=3. The data were analysed using one-way ANOVA with Dunnett post-test, using the untreated cells as the control (*$p<0.05$ compared to the control; 0 μg/L).

Exposing HUVECS to arsenite concentrations of 1-10,000 μg/L for 4 hours (Figure 4.22) was consistent with the EA.hy 926 results (Figure 4.21), showing no increase in the levels of superoxide generated compared to the control, untreated cells using DHE. Treating HUVECS with the positive control of 25 μM menadione for 30 minutes showed a significant increase in ROS levels compared to the untreated control cells ($p<0.05$), confirming that arsenite does not induce detectable superoxide generation in cells after 4 hour exposure.

To assess whether increasing the treatment time of arsenite resulted in an enhanced superoxide level, HUVECs were treated with arsenite for 12 and 24 hours (Figures 4.23 and 4.24 respectively). There were no significant changes in the level of superoxide detected with DHE for either time point at concentrations ≤1,000 μg/L. At 10,000 μg/L arsenite treatment however, 12 hours exposure resulted in a significant increase in superoxide levels compared to the untreated control cells ($p<0.0001$). Therefore, at the highest, and cytotoxic concentration (Figures 4.2, 4.3 and 4.4), arsenite induced oxidative stress in HUVECS after 12 hour treatment. The 24 hour treatment of HUVECs with 10,000 μg/L arsenite also resulted in an increase in the level of superoxide measured, although the increase did not reach statistical significance. An increase in the level of superoxide measured for the positive control ($p<0.0001$), 1 hour treatment with 100 μM antimycin A, was observed in both the experiments.

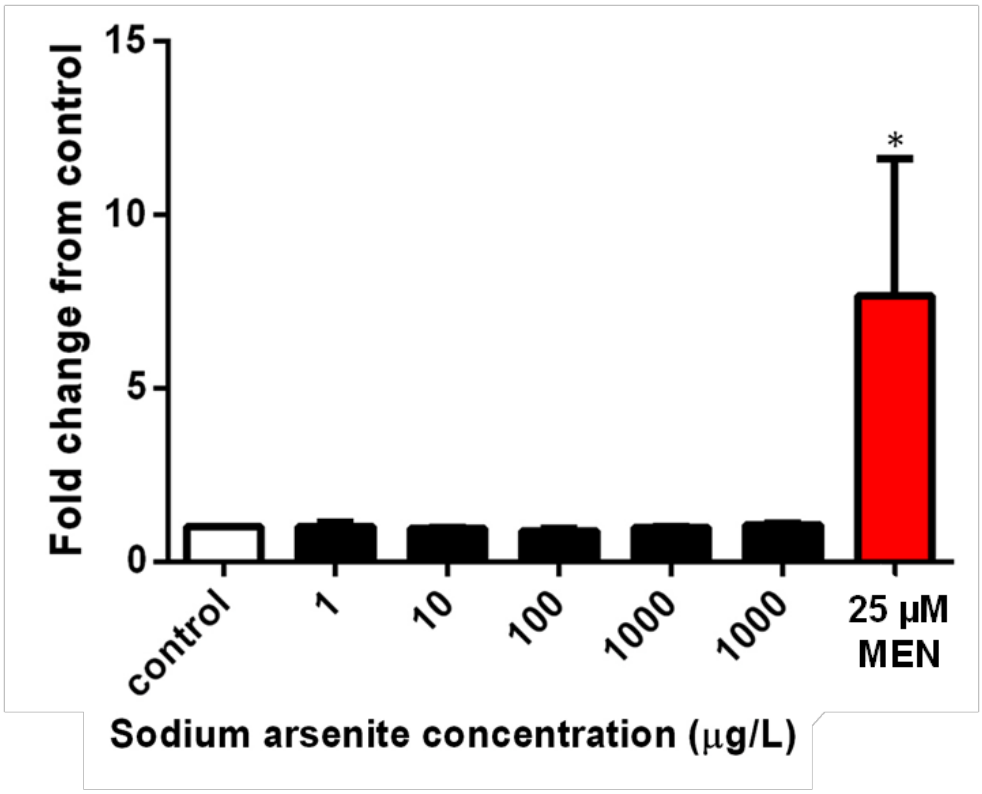

Figure 4.22 The effect of exposure to arsenite for 4 hours on superoxide generation in HUVECs. HUVECs were exposed to increasing arsenite concentrations and 25 µM menadione (MEN) for 30 minutes and superoxide was estimated using DHE with flow cytometry. The values represent mean+SEM of n=3. The data were analysed using one-way ANOVA with Dunnett post-test, using the untreated cells as the control (*$p<0.05$ compared to the control; 0 µg/L).

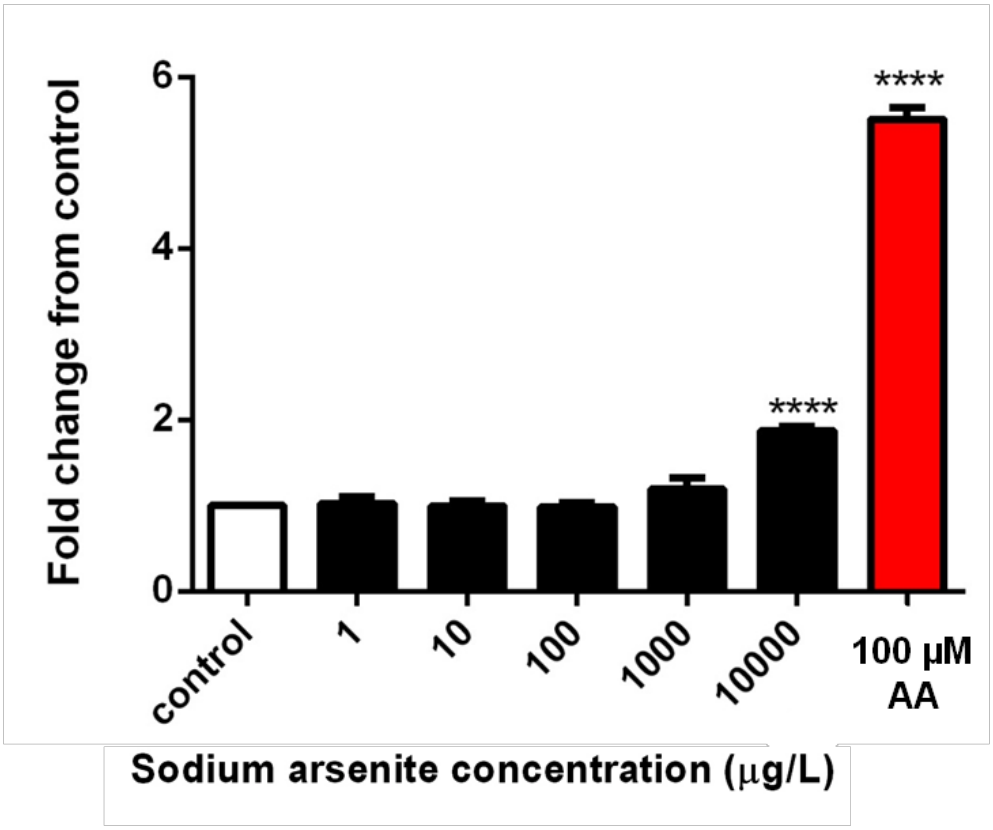

Figure 4.23 The effect of exposure to arsenite for 12 hours on superoxide generation in HUVECs. HUVECs were exposed to increasing arsenite concentrations and 100 µM antimycin A for 1 hour and superoxide was estimated using DHE with flow cytometry. The values represent mean+SEM of n=3. The data were analysed using one-way ANOVA with Dunnett post-test, using the untreated cells as the control (****$p<0.0001$ compared to the control; 0 µg/L).

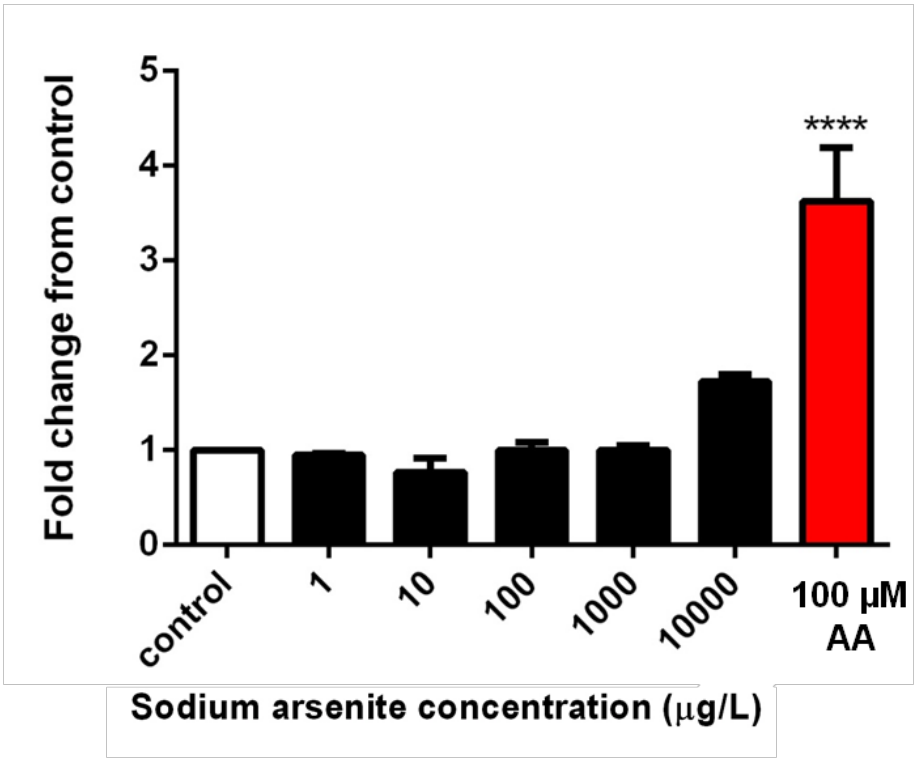

Figure 4.24 The effect of exposure to arsenite for 24 hours on superoxide generation in HUVECs. HUVECs were exposed to increasing arsenite concentrations and 100 µM antimycin A for 1 hour, superoxide was estimated using DHE with flow cytometry. The values represent mean+SEM of n=3. The data were analysed using one-way ANOVA with Dunnett post-test, using the untreated cells as the control (****$p<0.0001$ compared to the control; 0 µg/L).

4.5 Discussion

4.5.1 Establishing sub-cytotoxic arsenite concentrations for subsequent investigations

The focus of this thesis is to assess the mechanisms that lead to the onset of arsenite-mediated human endothelial cell dysfunction. In such investigations it is important to use precise concentration and treatment times, to ensure any effects observed might contribute to mechanistic information and are not effects mediated by cytotoxcity. Therefore, it is essential to first establish the appropriate sub-cytotoxic treatment conditions before carrying out these investigations.

Using the trypan blue exclusion assay, the sub-cytotoxic concentration established for arsenite over a 24 hour treatment time was ≤100 µg/L. However, since this method relies on the manual counting of cells, a lack of stringency and reproducibility in experimental repeats can occur, as shown by the increasing error bars with increasing arsenite concentration. Therefore in order to supplement the trypan blue exclusion data, a more quantitative method of measuring cell viability was employed, using the colorimetric CCK8 assay.

Based on the CCK8 assay, for investigations involving 24 hours treatment with arsenite, sub-cytotoxic concentrations were established at below 2,500 µg/L, with concentrations ≥5,000 µg/L inducing significant cell death. For an increased experimental treatment time of 5 days, the sub-cytotoxic concentrations of arsenite were identified below 200 µg/L, with concentrations ≥200 µg/L inducing significant cell death.

Comparing the results obtained from both these assays, a clear difference is observed for the concentration at which arsenite begins to induce cytotoxicity in HUVECs after 24 hours treatment, 1,000 µg/L with the trypan blue exclusion assay and 5000 µg/L with the CCK8 assay. This discrepancy may be due to the differences in the method of quantifying cell viability for both the assays, with the trypan blue exclusion assay being more subject to error due to the manual counting of cells. Thus, this may have resulted in an overestimation of the extent of arsenite induced cell death.

4.5.2 Stress induced premature senescence in arsenite treated HUVEC

The onset of senescence in endothelial cells results in cellular dysfunction, associated with a lack of NO generation, loss of antithrombogenic properties, and promotion of platelet aggregation (Goligorsky *et al*., 2009), hence promoting the atherosclerotic process. Epidemiological studies of humans chronically exposed to arsenic have found the prevalence of atherosclerosis (Zaldivar, 1980; Wang *et al*., 2002). We hypothesise that arsenite may induce senescence and this may therefore be one of the mechanisms by which arsenite initiates atherogenesis. There is however limited research carried out looking into the relationship between arsenic and senescence induction.

The results generated in this chapter show the novel finding of arsenite exposure leading to SIPS in HUVECs. This is also the first study to show arsenite inducing SIPS in any endothelial cell type and indicates the substantial impact arsenite may have on human endothelial cells. Since endothelial senescence is involved in the process of atherosclerosis (Vasile *et al*., 2001; Minamino *et al*., 2003; Hayashi *et al*., 2006),

arsenite-mediated SIPS can be seen as a potential mechanism by which arsenite causes accelerated atherosclerosis.

To gain a better understanding of the impact arsenite has on human endothelial cells, the intracellular changes that occur as a result of arsenite exposure, leading to premature endothelial senescence, need to be investigated. As outlined in section 1.4, many factors have been associated with the onset of premature endothelial senescence including oxidative stress (Furumoto *et al*., 1998, Kurz *et al*., 2004), NO (Vasa *et al*., 2000), inflammatory molecules (Breitschopf *et al*., 2001) and mitochondrial function (Schleicher *et al*., 2008). Since arsenic has been associated with the induction of oxidative stress in endothelial cells (see section 1.5.4), it is important to determine whether sub-cytotoxic arsenite concentrations induce oxidative stress in HUVECS, as a possible mechanism for SIPS.

4.5.3 Does arsenite induce ROS after short-term exposure?

Arsenic has been found to increase the generation of ROS in human and animal endothelial cells at both cytotoxic and sub-cytotoxic concentrations (see section 1.5.4). An arsenite concentration of 650 µg/L reportedly increased the generation of ROS in porcine aortic endothelial cells during 20 minutes exposure, measured using the homovanillic acid assay (Barchowsky *et al*., 1999), and after 1 hour exposure, measured using the superoxide-dependent lucigenin chemiluminescence method (Smith *et al*., 2001). Furthermore, an increase in ROS generation in HUVECs exposed to ≥650 µg/L arsenic has been detected after 2 hours using DHE with fluorescent microscopy (Sun *et al*. 2009) and 4 hours exposure using DCFH-DA with flow cytometry (Lii *et al*., 2011).

Shi *et al* (2010) also measured ROS using the fluorescent probe DCFH-DA with flow cytometry, however they found arsenic concentrations of 650 and 1300 µg/L to decrease ROS generation in HUVECs after 24 hours treatment, with concentrations of 2600-5200 µg/L causing an increase in ROS.

In this chapter, the effects of arsenite on acute ROS generation were assessed in both EA.hy 926 cells and HUVECs. Comparisons between the two cell types showed consistency in the levels of ROS measured, however inconsistencies were observed amongst the results obtained from the different ROS detection probes used.

The fluorescent probe DCF has been very widely recognised and used for *in vitro* investigations as a detector of oxidative stress (Cathcart *et al*., 1983; Kroll *et al*., 1998; Rothe *et al*., 1990; Duranteau *et al*., 1998; Aon *et al*., 2003). Thus, CM-H_2DCFDA was used to indicate the effects of arsenite on general cellular ROS generation. After 4 hours exposure to arsenite, both EA.hy 926 cell and HUVECs displayed a concentration-dependent increasing trend in DCF fluorescence, with EA.hy 926 cells showing significant increases with 1000 and 10,000 µg/L arsenite concentrations. HUVECs appeared more sensitive to arsenite with respect to DCF fluorescence, as significant increases were observed from a lower arsenite concentration of 100 µg/L.

The use of DCF based fluorescent probes for ROS detection, i.e. DCFH-DA, has recently been criticised for lack of specificity for measuring ROS. It has been suggested to react with many other species e.g. hydroxyl radicals, hypochlorous acid and reactive species formed from peroxynitrite decomposition (Kalyanaraman *et al*., 2012).

The processes of cell death, whether apoptosis or necrosis, has shown the involvement of increased cellular ROS from mitochondrial or non-mitochondrial sources as a late response to cellular stress (reviewed in Fiers *et al*., 1999), therefore it is important to distinguish whether the increase in cellular ROS observed after arsenite exposure is a primary response or a later stress response in a cell death pathway. Hence, the induction of both apoptosis and necrosis were measured in the EA.hy 926 cells in response to 1 and 4 hour arsenite treatment. For both the time-points, the cells did not display any significant increases in the induction of either apoptosis or necrosis, which may as a result of these time-points being too early to detect the induction of cell death. However, after 4 hours, there was a trend towards an increase in the level of late apoptosis observed for cells treated with 10,000 μg/L, although this did not reach statistical significance. This is reflective of the cell death measured using the CCK8 assay in HUVECs after 24 hours treatment with 5-10,000 μg/L, suggesting apoptosis as a possible mechanism of arsenite-induced cell death. This is supported by a study carried out by Shi *et al* (2010), in which increases in the induction of apoptosis in HUVECs after 24 hour treatment with ≥650 μg/L of arsenite were observed. Similarly, apoptosis was also observed in microvascular endothelial cells at 24 hours after treatment with ≥650 μg/L arsenite (Suriyo *et al*., 2012).

Furthermore, the fluorescent molecule DCF has been suggested to undergo rapid reaction with oxygen to generate superoxide, which can go on to produce further ROS, particularly H_2O_2. With H_2O_2 suggested to be involved in the process of DCF formation (Bonini *et al*., 2006), the increases in fluorescence seen by CM-H_2DCFDA in response to arsenite treated cells may be indicating increases in H_2O_2 that are not a consequence of arsenite exposure directly. Moreover, the release of cytochrome c from mitochondria

during apoptosis can lead to the oxidisation of DCFH to form DCF (Burkitt *et al*., 2001; Karlsson *et al*., 2010). This implies that, under certain conditions, CM-H_2DCFDA provides a measure of apoptosis rather than ROS generation.

Further investigations into establishing whether the increased fluorescent signals observed using CM-H_2DCFDA were a measure of arsenite mediated oxidative stress and/or other factors mentioned above would be required. In this project, DHE and MitoSOX™ were also used to detect ROS in both arsenite treated HUVECs and EA.hy 926 cells, as well as to indicate the possible source of potential ROS generation. Surprisingly, treating either cell type for up to 4 hours with arsenite (1-10,000 µg/L) revealed no increases in the generation of general or mitochondrial specific superoxide.

On the whole, the findings support studies suggesting that DCFH-DA probes may not be reliable for the measure of true ROS levels in cells alone and may give rise to false positives (Kalyanaraman *et al*., 2011). Furthermore, it was found through the exposure of HUVECs and EA.hy 926 cells to sub-cytotoxic concentrations of arsenite that increased oxidative stress does not appear to be the initial effect in arsenite-mediated cytotoxicity. However this is not consistent with previous research. Sun *et al* (2009) used DHE with fluorescent microscopy to measure the generation of superoxide in HUVECs after 2 hours exposure to ≤650 µg/L arsenite, observing an increase in superoxide generation. Furthermore, sub-cytotoxic arsenite exposure (650 µg/L for 20-60 minutes) of porcine aortic endothelial cells resulted in increased in ROS generation, measured using the homovanillic acid assay and superoxide-dependent lucigenin chemiluminescence method (Barchowsky *et al*., 1999; Smith *et al*,. 2001).

It is possible that the lack of superoxide measured from arsenite treated cells was a result of using DHE and MitoSOX™ to measure superoxide. The sub-cytotoxic treatments of EA.hy 926 cells and HUVECs may have generated low levels of ROS that were not detectable by the technique used. That is, this method is unsuitable for the detection of low levels of superoxide. Moreover, the use of DHE in superoxide detection has been criticised. DHE has been seen to react with superoxide to generate 2-OH-Et rather than ethidium (Zielonk and Kalyanaraman, 2010). Ethidium may also be generated by the hydroxylation of DHE by enzymes such as cytochrome P-450 (Kalyanaraman *et al*., 2011). Since the chemical structure of MitoSOX™ is similar to that of DHE, the same principle applies (Zielonka *et al*., 2008; Zielonka *et al*., 2010). Improved assays rely upon HPLC separation of DHE/MitoSOX™ products and specific detection of superoxide adducts such as 2-OH-Et (Laurindo *et al*., 2008). Therefore, the use of either DHE or MitoSOX™ with flow cytometry is not recommended to be exclusively relied on for the accurate measure of intracellular superoxide levels.

4.5.4 Summary

Arsenite was observed to display significant cell death in HUVECs at concentrations ≥2500 µg/L for 24 hour treatment and ≥200 µg/L for 5 days treatment. This identified the sub-cytotoxic concentrations of arsenite to use for investigating the mechanisms of arsenite mediated toxicity. At sub-cytotoxic conditions, arsenite was shown to induce premature senescence in HUVECs, a novel finding which sheds light on the potential mechanism by which arsenite may initiate the process of atherogenesis.

This chapter also suggests DCFH-DA based probes to have non-specificity for measuring intracellular ROS levels, indicating the possible measurement of early apoptotic events instead, such as cytochrome c release from mitochondria. Apoptosis may therefore be the mechanism by which arsenite induces cell death in HUVECs. Furthermore, contrary to the literature, sub-cytotoxic concentrations of arsenite did not increase ROS as determined using the Amplex red assay, DHE and MitoSOX™ with flow cytometry using either EA.hy 926 cells or HUVECs.

CHAPTER FIVE

Effects of Arsenite on DNA Damage

Chapter 5: Effects of Arsenite on DNA damage

5.1 Introduction

This chapter is focussed on determining the effects of arsenite on DNA damage in endothelial cells. Since endothelial dysfunction is one of the earliest events to occur in atherogenesis, identifying whether DNA damage is induced in response to arsenite treatment in endothelial cells can suggest a mechanism by which arsenite mediates endothelial dysfunction, instigating the process of atherosclerosis in exposed individuals.

5.1.1 DNA damage in atherosclerosis

It has become apparent in recent years that DNA damage plays an important role in the onset and progression of atherosclerosis (Oumouna-Benachour *et al*., 2007; Mercer *et al*., 2010). Despite not being extensively researched, this phenomenon has been supported by a number of *in vivo* and *in vitro* investigations (reviewed in Malik and Herbert, 2012). Studying patients with atherosclerosis has revealed increased levels of DNA damage, with patients displaying a high micronucleus index; a biomarker for determining genetic instability, which correlated with the extent of disease severity (Botto *et al*., 2001). Autopsies of humans with atherosclerosis has also displayed higher levels of bulky DNA adducts compared to autopsies of non-atherosclerotic humans (Binkova *et al*., 2002) Evidence for DNA damage has also been seen in cells involved in the formation of atherosclerotic plaques. Oxidative DNA damage was detected in human atherosclerotic plaques through the strong immunoreactivity response to the oxidative DNA damage marker 8-oxo-dG within the nucleus of smooth muscle cells, macrophages and endothelial cells (Martinet *et al*., 2002). Animal models for atherosclerosis have shown evidence of DNA damage, for example in the plaques of

atherosclerotic rabbits which display elevated levels of 8-oxo-dG (Martinet *et al*., 2001).

Research into atherosclerosis has also revealed the specific involvement of mtDNA damage. The mtDNA 4977 bp deletion, a common mitochondrial mutation seen in humans, is found at significantly higher incidence in patients with coronary artery disease and also observed in 21.7% of patients examined with atherosclerosis (Botto *et al*., 2005). Furthermore, carrying out investigations into the presence of mtDNA damage in human atherosclerotic specimens has shown a correlation between mtDNA damage and disease severity (Ballinger *et al*., 2002). Observations in mice have also suggested that mtDNA damage may cause atherosclerosis. Young apolipoprotein E (apoE) knock-out mice reveal the onset of mtDNA damage prior to the development of atherosclerosis pathology, thus implicating mtDNA damage as an early event in the pathogenesis of atherosclerosis rather than a result of the disease state (Ballinger *et al*., 2002).

5.2 Aims

The aim of this study was to determine whether nDNA damage and changes in the mitochondrial genome i.e. changes in mtDNA content and mtDNA damage, are seen as a result of arsenite exposure to HUVECs. This sheds light upon the possible mechanism by which arsenite brings about endothelial dysfunction to induce atherosclerosis.

5.3 Investigative methodology

All investigations were carried out on HUVECs, between passages 2-6, grown to approximately 80% confluence before being studied with the comet assay or qPCR techniques. The effect of arsenite treatment on HUVECs for 24 hour and 5 days, with the replacement of media containing arsenite each day, was observed.

5.3.1 Comet Assay

The comet assay or single-cell gel electrophoresis is a popular technique, widely used to measure DNA damage due to its simplicity, inexpensiveness, versatility and sensitivity. The alkaline comet assay developed by Singh *et al* (1988) was employed in this study, which involved the lysis of cells at pH 10 and electrophoresis at pH 13. The high salt content of the lysis buffer enabled the removal of the cellular components, leaving behind the nucleoid embedded in agarose gel. The DNA retained in the gel was able to migrate along the electrophoresis current revealing a tail of broken DNA stands, with the smallest fragments travelling furthest away from the intact DNA cluster, forming the comet-like appearance. The high alkali electrophoresis condition is suggested to aid the pronounced formation of the comet tail; assisting with the unwinding of the two DNA-strands. The comet tail represents both single- and double-stranded DNA damage (Collins, 2004; Collins *et al*., 2008). The percentage tail length, indicating the percentage of DNA present in the tail, was used as a measure for the extent of DNA damage within the samples.

5.3.2 Quantitative (real-time) polymerase chain reaction

Unlike conventional PCR assays which involve detection of the PCR amplicon at the end of the reaction, the qPCR method allows the detection to occur throughout the

exponential amplification period, where each cycle is undergoing doubling of the product, enabling the entire PCR reaction to be observed. The reaction was carried out using the SYBR green fluorescent dye, which binds to double-stranded DNA to give off a strong fluorescent signal. On the basis of the signal generated, the cycle threshold (Ct) value can be deduced for each reaction. The Ct value represents the amplification cycle at which the fluorescence of the amplicon exceeds that of the background fluorescence (Denman and McSweeney, 2005).

Direct quantification was used in this study where the Ct values generated were directly used against the standard curves of known concentrations for either mtDNA or nDNA (Figures 5.3 and 5.4 respectively), allowing quantification of the Ct values and extrapolation of the DNA concentration. Comparisons were made against the test sample and the reference sample to determine the differences in response to arsenite exposure. The fold-difference between the test and reference samples was calculated by first normalising each sample and then dividing the normalised test sample by the normalised reference sample:

$$(1)\ \text{Normalised target (test)} = \frac{\text{Arsenite treated sample}}{\text{Internal control sample}}$$

$$\text{Normalised target (reference)} = \frac{\text{Arsenite treated sample}}{\text{Internal control sample}}$$

$$(2)\ \text{Fold difference in target} = \frac{\text{Normalised test target}}{\text{Normalised reference target}}$$

In the case of mitochondrial content investigations, the test sample represents the mitochondrial genome and the reference represents the nuclear RPLPO gene (Table 3.13). In the mtDNA damage study the test sample represents a 972 bp area within the D-loop region of the mitochondrial genome and the reference sample represents a 55 bp area of the D-loop region (Table 3.14).

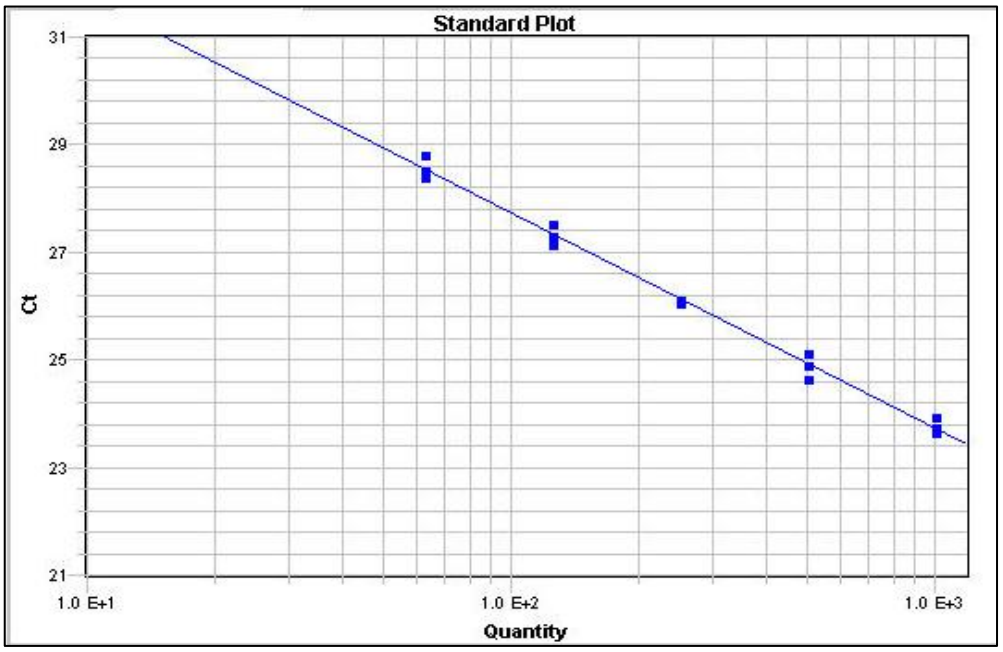

Figure 5.1 An example of the DNA standard curve used for determining the changes in mtDNA content, using the primers mt14260 and mt14841 which amplify the total mtDNA, in response to arsenite treatment. The standard curve shows the concentration range of mtDNA used to make the standard curve, with DNA concentration range made using a 2-fold dilution series 1000-62.5 pg. The standard curve for determining mtDNA damage uses the same DNA concentration range but using the primers AL4.F and AS1.R to amplify the D-loop region of the mitochondrial genome. Each blue square represents a technical replicate, with n=3 for each DNA concentration.

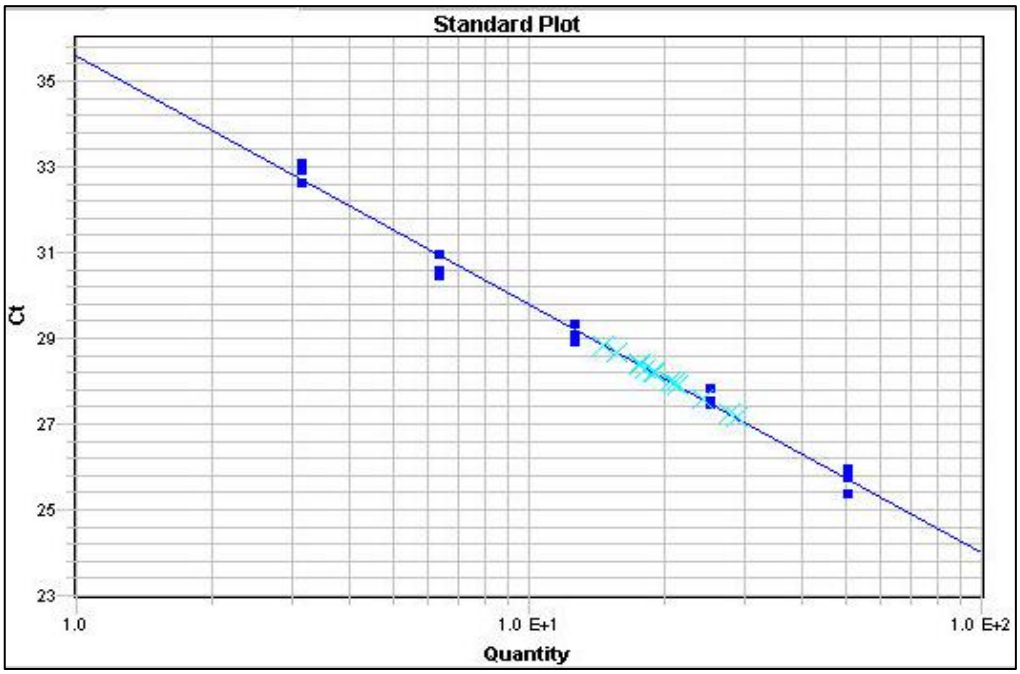

Figure 5.2 An example of the DNA standard curve used for determining the concentration of the reference nuclear gene *RPLO*, using the primers 36B4d and 36B4u, when measuring the mtDNA content in response to arsenite treatment. The standard curve shows the concentration range of nDNA used to make the standard curve, with DNA concentration range made using a 2-fold dilution series from 50-3.125 ng. Each blue square represents a technical replicate, with n=3 for each DNA concentration, the blue crosses represent the Ct values for the experimental DNA samples, with unknown DNA quantities that can be extrapolated from the standard curve.

5.4 Results

As shown in Chapter 4, the impact of continued exposure to arsenite in HUVECs results in cells undergoing stress-induced premature senescence (SIPS), a phenotype that could accelerate the onset of age-related diseases such as atherosclerosis in humans (Kunieda *et al*., 2006). To elucidate the mechanism by which arsenite-induced stress leads to this senescent phenotype, the effect of arsenite on DNA damage was studied. The effect of exposing HUVECs to sub-cytotoxic concentrations of arsenite and investigating the impact on nDNA and mtDNA would reveal whether DNA damaging effects of arsenite might be involved in the mechanism leading to the irreversible cell cycle arrest state seen in HUVECs.

5.4.1 Arsenite-induced DNA damage in HUVECs

The results obtained from employing the comet assay to investigate the effects of exposing HUVECs to sub-cytotoxic concentrations of arsenite for 24 hours are shown in figure 5.4. DNA damage was measured by the percentage of tail DNA, with 50 comets analysed per treated sample and two replicates of each treated sample per experiments. Arsenite induced a concentration-dependent increase in DNA damage, with the highest arsenite concentration; 1,000 μg/L, resulting in a statistically significant 3-fold increase in DNA damage ($p<0.01$ compared to the control). The damage seen represents the extent of single-stranded and double-stranded DNA damage present in the endothelial cell nucleus. Figure 5.3 shows an example of the comet results seen for each sample, illustrating the increasing tail length with increasing concentration of arsenite exposure.

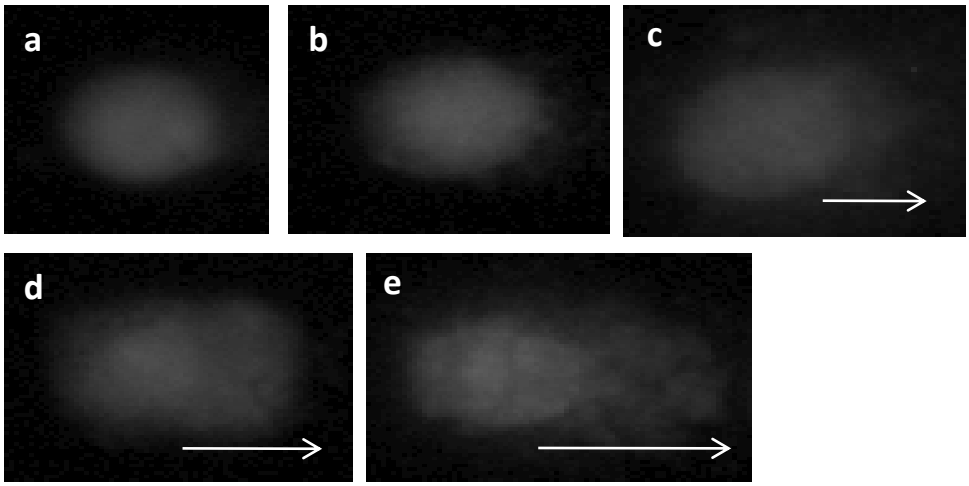

Figure 5.3 Fluorescence microphotography of propidium iodide stained HUVECS after the comet assay, analysing the effects of 24 hour arsenite exposure at the following concentrations; 0 (a) 1 (b), 10 (c), 100 (d) and 1,000 (e) µg/L. The images show an increase in comet tail length (highlighted by white arrows) reflecting a concentration-dependent increase in DNA damage as a result of arsenite exposure.

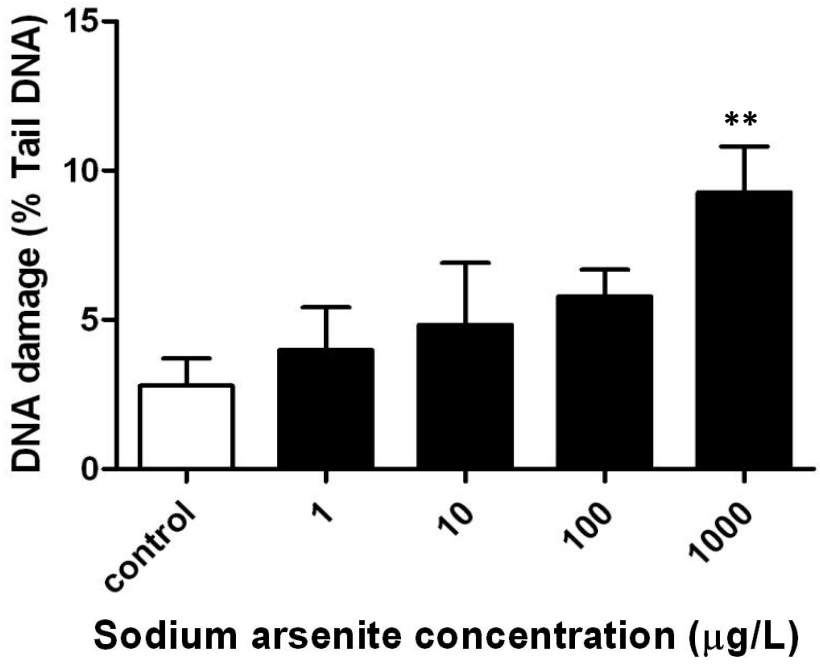

Figure 5.4 Nuclear DNA damage in HUVEC after 24 hour arsenite treatment detected using the comet assay. DNA damage is represented as the mean percentages of DNA present in the tail of the 'comets', n=4 +SEM. The data was analysed using one-way ANOVA with Dunnett post-test using the untreated cells as the control. (**$p<0.01$ compared to the control; 0 µg/L)

5.4.2 Impact of arsenite on mitochondrial DNA

In order to determine the effects of arsenite on mtDNA content and mtDNA damage, HUVECs were exposed to a range of non-cytotoxic concentrations of arsenite for 24 hours (Figures 5.5 and 5.7), and for 5 days (Figures 5.6 and 5.8). The concentrations used for each time-point were based on the cytotoxicity investigations carried out using the CCK8 assay for cell viability, described in chapter 4. Using non-cytotoxic concentrations ensured any effects seen were as a result of arsenite-mediated events and not the result of cell death. The highest two concentrations of arsenite used in figures 5.6 and 5.8; 200 and 400 µg/L, have been shown to be cytotoxic by significantly reducing cell viability (Figure 4.7), allowing a comparison between the effects of non-cytotoxic and cytotoxic concentrations of arsenite on the mitochondrial genome.

The mitochondrial genome is a very important aspect of cellular function and maintenance. The copies of mtDNA not only vary in different cell types, but alter in response to the energy demands of the cells (Niu *et al*., 2012). Investigating mtDNA content gives an indication of mitochondrial biogenesis, impairment of which has been associated with cardiovascular diseases (Ren *et al*., 2010; Karamanlidis *et al*., 2011).

Interestingly, qPCR investigations on HUVECs exposed to a range of non-cytotoxic concentrations of arsenite for 24 hours showed no statistically significant effect on the level of mtDNA content (Figure 5.5). However, one could argue for a trend towards increased mtDNA at higher arsenite concentrations. Consistent with this was the data from 5 days treatment of HUVECs with arsenite for both cytotoxic and non-cytotoxic concentrations, which also showed no significant differences in the fold difference of mtDNA content from the control cells (Figure 5.6). However, a concentration-

dependent increase in the fold-difference of mtDNA content again was seen for cells treated with the highest two arsenite concentrations. This observation is suggestive of an increase in the mtDNA content in response to increasing arsenite concentration.

Applying a sample size calculation with the mean fold change values for control cells against cells treated with 1,000 µg/L arsenite for 24 hours (Figure 5.5) and cells treated with 400 µg//L arsenite for 5 days (Figure 5.6) suggested a required sample size of n=11 and n=6 respectively to achieve significance (alpha error level of 5% and power of 0.80).

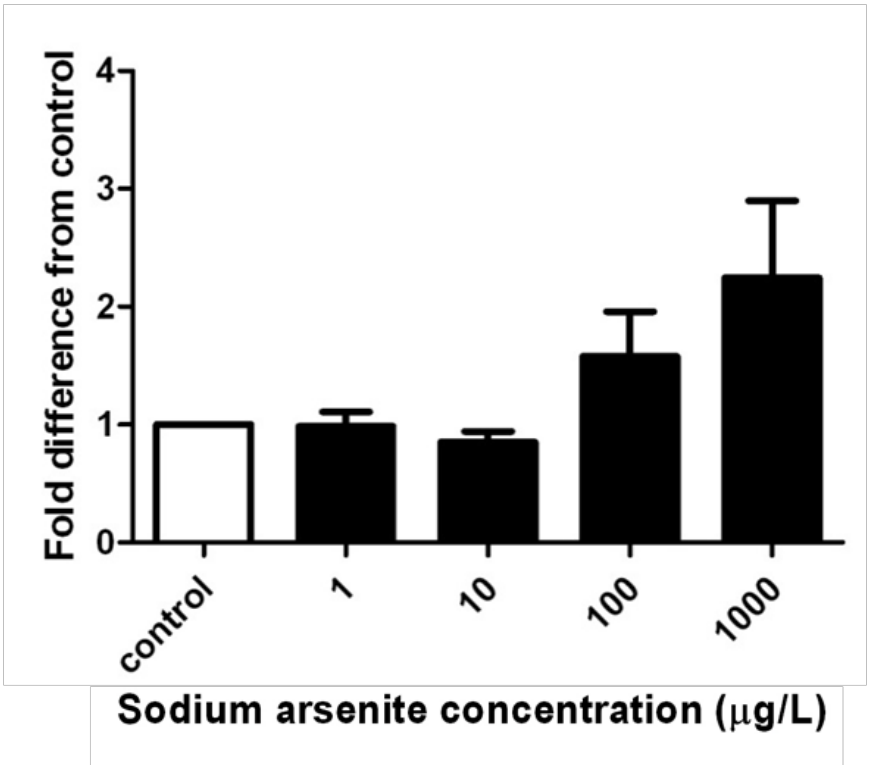

Figure 5.5 Mitochondrial DNA content in HUVEC treated with arsenite for 24 hours measured using qPCR. The values represent a mean of n=6 +SEM. The data were analysed using one-way ANOVA with Dunnett post-test, using the untreated cells as the control (No significant differences between the results were observed at $p<0.05$ when compared to the control; 0 µg/L).

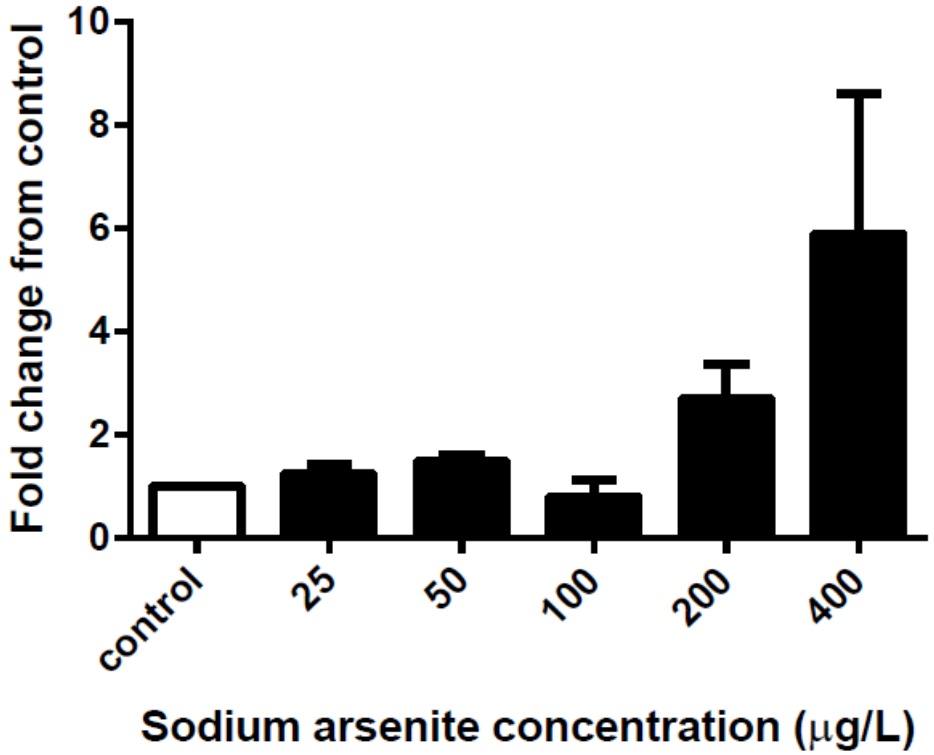

Figure 5.6 The graph represents the change in mitochondrial DNA content in HUVEC treated with arsenite for 5 days measured using qPCR. The values represent a mean of n=3 +SEM. The data were analysed using one-way ANOVA with Dunnett post-test, using the untreated cells as the control (No significant differences between the results were observed at $p<0.05$ when compared to the control; 0 μg/L).

Due to the highly oxidative environment of the mitochondria, mtDNA is more prone to oxidative DNA damage than nDNA, with mtDNA damage also suggested to be more persistent (Yakes and Van Houten, 1997). Since mtDNA encode many genes that are required for the production of ATP, damage to mtDNA can prove detrimental to the cell through a lack of ATP supply, as well as leading to mitochondrial and thus cellular dysfunction.

Using qPCR to assess mtDNA damage in HUVECs exposed to non-cytotoxic concentrations of arsenite showed no significant changes in the fold difference of DNA damage compared to the control cells. These findings were seen for both 24 hours and 5

days exposure time-points (Figures 5.7 and 5.8 respectively). HUVECs exposed to cytotoxic arsenite concentrations of 200 and 400 μg/L, for 5 days exposure, also show no significant changes in levels of mtDNA damage. For both time points there was a suggestion of a slight decrease in mtDNA damage with increases in concentrations of arsenite, although they did not reach statistical significance (Figures 5.7 and 5.8).

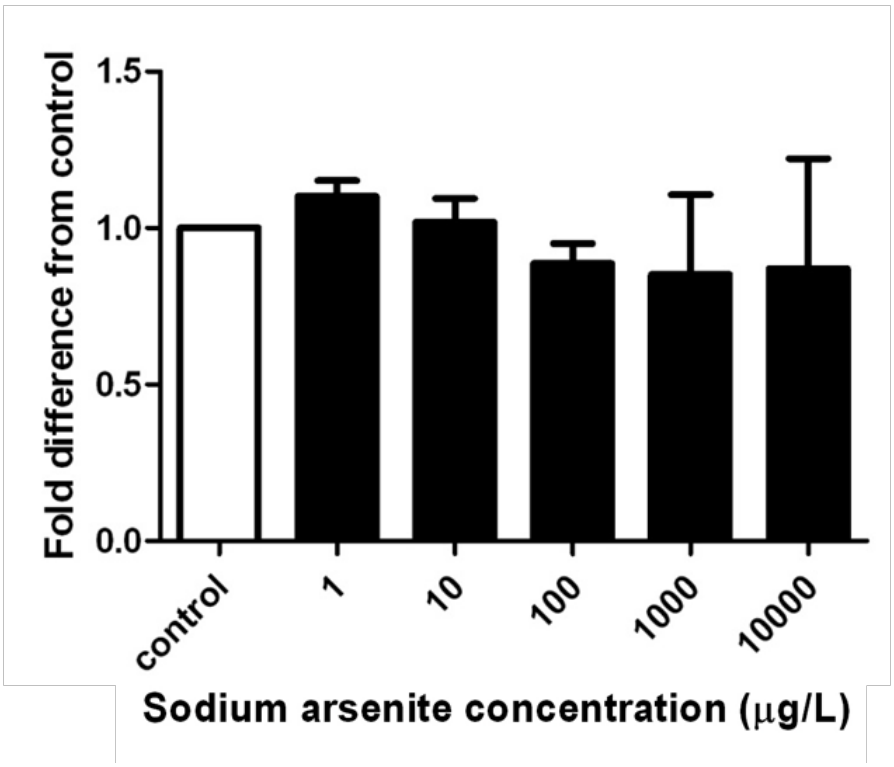

Figure 5.7 DNA damage levels at the D-loop region of the mitochondrial DNA. HUVECs were treated for 24 hours and mtDNA damage was measured using qPCR. The values represent the mean of n=4 +SEM. The data were analysed using one-way ANOVA with Dunnett post-test, using the untreated cells as the control. (No significant differences between the results were observed at $p<0.05$ when compared to the control; 0 μg/L)

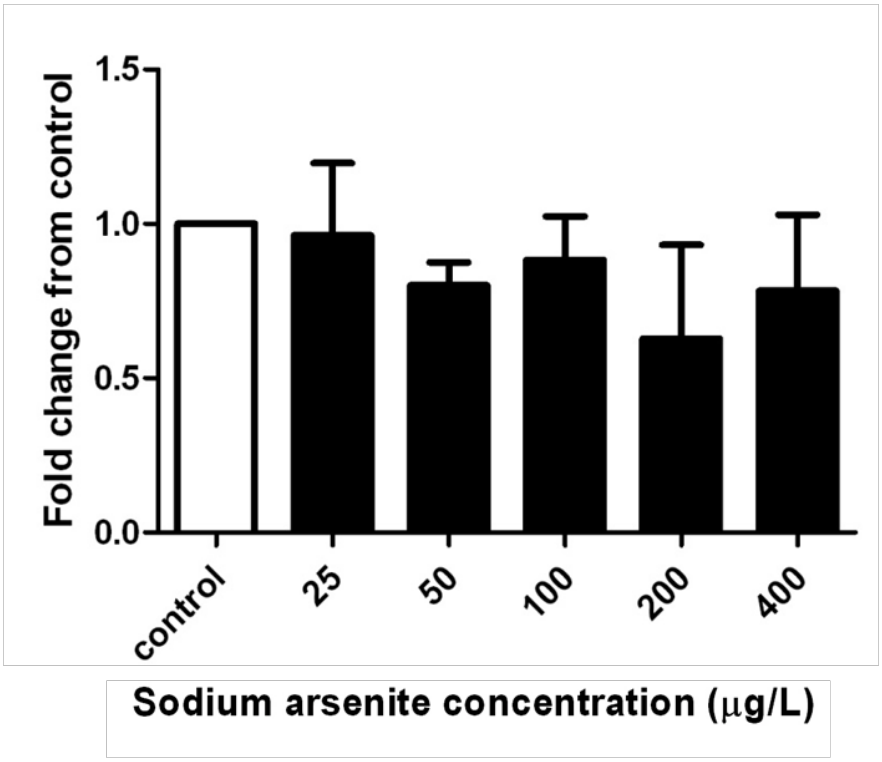

Figure 5.8 DNA damage levels at the D-loop region of the mitochondrial DNA. HUVECs were treated for 5 days and mtDNA damage was measured using qPCR. The values represent a mean of n=3 +SEM. The data were analysed using one-way ANOVA with Dunnett post-test, using the untreated cells as the control. (No significant differences between the results were observed at $p<0.05$ when compared to the control; 0 μg/L)

5.5 Discussion

5.5.1 Arsenite induced nuclear DNA damage

The induction of irreparable DNA damage results in the two fates; cell death or cellular senescence. The mechanism behind this decision is yet to be fully understood, however, the extent to which DNA damage is induced does play a role i.e. cells with lower levels of damage are reported to undergo senescence (Ben-Porath and Weinberg, 2005). DNA damage can result in damage to the repair machinery itself, in which case cells cannot undergo DNA damage repair (DDR) and consequently enter premature senescence (Duan *et al*., 2005). Furthermore, regions of the genome that have been identified as irreparable i.e. telomere tracts, presumably as a result of their function in avoiding the occurrence of chromosomal end fusion, result in the accumulation of DNA damage (Fumagalli *et al*., 2012). This therefore is associated with cellular ageing as a result of decreased telomere length, consequently the induction of replicative senescence.

Treating HUVECs with sub-cytotoxic concentrations of arsenite revealed a concentration-dependent increase in the level of nDNA damage measured. Due to the exposure of just 24 hours, this effect can be seen as one of the initial impacts of arsenite on the cells. As mentioned above, DNA damage can lead to the onset of stress-induced premature senescence, as well as initiate replicative senescence through damage at the telomere site (Ben-Porath and Weinberg, 2005; Fumagalli *et al*., 2012). Thus, DNA damage poses as an underlying mechanism through which arsenite induces premature senescence in endothelial cells. Moreover since these low concentrations of arsenite used to treat HUVECs exhibit low levels of DNA damage, the cells are likely to enter senescence rather than apoptosis (Ben-Porath and Weinberg, 2005).

Since these are novel findings in human endothelial cells, gaining an insight into the nature of the DNA damage would involve looking into similar *in vitro* investigations conducted on other endothelial cell types. Liu and Jan (2000) found an increase in the level of oxidative DNA damage in bovine aortic endothelial cells after 4 hours exposure to 650-26,000 μg/L arsenite, measured using the comet assay. This finding, together with the data outlined in previous literature on the increased generation of ROS from arsenic-exposed endothelial cells (Section 2.4.4), argue oxidative stress to be the cause of arsenite-mediated DNA damage observed in HUVECs.

Oxidative DNA damage is suggested to result in the onset of endothelial cellular senescence (Erusalimsky, 2009), with endothelial cellular senescence being associated with atherosclerosis (Burrig, 1991). Therefore, the occurrence of oxidative DNA damage forms a potential mechanism for the development of atherosclerosis in response to arsenite. This is supported by the elevated levels of oxidative DNA damage seen in human atherosclerotic plaques (Martinet *et al*., 2002) and the oxidat$ive DNA damage observed in endothelial cells exposed to the CVD risk factors; high glucose and angiotensin II (Mazza *et al*., 2003; Farhangkhoee *et al*., 2005; Quagliaro *et al*., 2005; Malik and Herbert, 2012).

5.5.2 Impact of arsenite on mitochondrial DNA

As previously mentioned, mitochondria are organelles rich in oxygen, therefore resulting in a constant background level of mitochondrial ROS, rendering mtDNA highly susceptible to oxidative damage. Therefore, any increase in oxidative stress in the mitochondria would result in a rise in the level of mtDNA damage. Investigating

endothelial mitochondrial ROS in response to arsenite showed no significant differences from the background ROS levels, which seems to be supported by results obtained from qPCR measurements of mtDNA content and mtDNA damage also displaying no significant differences from the control cells.

Mitochondria are organelles that play a vital role in the function and survival of cells therefore it is essential that they are able to maintain and preserve their functions under stressful conditions. Mitochondria have been seen to increase their mtDNA copy number as a feedback response under stressful conditions, to compensate for any mitochondrial damage and to maintain their normal function (Lee and Wei, 2000). Analysing the mitochondrial genome in aged, high passage, human cells showed an increase in the mtDNA copy number, suggesting the need for mitochondria to respond to accumulative stress seen in the process of senescence (Shmookler and Goldstein, 1983). This observation has been mirrored in ageing rats, which also displayed increased mtDNA copy number (Gadaleta *et al*., 1992).

Interestingly, when assessing mtDNA content, a concentration-dependent increase was suggested in response to arsenite concentrations after both 24 hours and 5 days exposure. Furthermore, a decrease in the level of mtDNA damage was also observed in arsenite exposed HUVECs at both time-points of exposure. These trends indicate a similar stress-induced compensatory mechanism occurring in the HUVEC mitochondria as mentioned above. Increased biogenesis of mitochondria in response to possible arsenite-induced mitochondrial damage would explain the increased copy number, and this would also account for the decreasing levels of mtDNA damage as a result of the newly synthesised mtDNA.

The stress-mediated compensatory increase in mitochondrial biogenesis seen in the literature, however, is suggested to be as a result of increased oxidative stress, as seen in aged rats (Gadaleta *et al*., 1992) and the lung and brain of aged humans (Lee *et al*., 1998; Barrientos *et al*., 1997). Furthermore, increased mitochondrial biogenesis has been seen as a stress-response to senescence. Human IMR90 fibroblasts with increased oncogenic *ras* expression, leading to increased cell growth and division, showed an increase in mtDNA copy number prior to the onset of senescence (Moiseeva *et al*., 2009). Senescent human lung fibroblasts also displayed an increase in mtDNA copy number, which was similarly noticed in non-senescent cells exposed to H_2O_2 (Lee *et al*., 2002). Moreover, increased mtDNA content was found to occur in the cardiovascular system of aged mice, seen through examining the senescent cardiac tissue (Schneider *et al*., 1995). Together, these studies suggest arsenite to potentially result in an increase in HUVEC mitochondrial biogenesis in response to the cellular stress associated with senescence, supporting the association between arsenite and SIPS seen previously (see section 4.4.2). However, the studies also imply a strong correlation between oxidative stress and increased mitochondrial biogenesis in senescent cells.

5.6 Summary

Investigations carried out in this chapter focus on the impact of arsenite on nDNA and mtDNA in HUVECs. Measuring the impact of sub-cytotoxic arsenite exposure for 24 hours on nDNA revealed the induction of DNA damage in a concentration-dependent manner. Investigations carried out into arsenite-mediated effects on the mitochondrial genome however displayed no statistical significant changes after both 24 hours and 5

days exposure, although interesting trends were observed. Arsenite influenced the mitochondrial genome through inducing increased mtDNA content and decreased levels of mtDNA damage in comparison to that of unexposed control cells. Since these trends were not significantly significant, mitochondria do not appear to be direct targets of arsenite.

The genotoxic effect of arsenite seen on nDNA provides a mechanism for arsenite-induced senescence in endothelial cells. The induction of senescence is further supported through the increased levels of mtDNA content observed, a trend that has also been linked to senescence by other research groups, as a compensatory feedback mechanism of the cell to enable a normal mitochondrial response to stress. Furthermore, literature based on the association between both nDNA and mtDNA alterations and senescence suggest this cellular outcome as a consequence of increased oxidative stress. This implies the possible involvement of oxidative stress in the arsenite-mediated changes seen in the nDNA and mitochondrial genome in HUVECs.

CHAPTER SIX

Effects of Arsenite on Mitochondrial Function

Chapter 6: Effects of Arsenite on Mitochondrial Function

6.1 Introduction

6.1.1 Effects of cellular oxidative stress on mitochondria

With mtDNA being in an environment of constant ROS generation, it is prone to oxidative damage. Thus mtDNA accumulate more oxidative damage than nDNA which persists for longer despite mtDNA damage repair mechanisms being in place (Richter *et al*., 1988). Increased oxidative mtDNA damage leading to mitochondrial dysfunction is seen with several diseases associated with ageing, i.e. neurological degeneration and CVD (Yakes & Van Houten, 1997). ROS induced mtDNA damage has been measured using qPCR in the SH-SY5Y neuroblastoma cell line showing a concentration-dependent increase of mtDNA damage by Rothfuss *et al* (2010). The regulatory D-Loop region of mtDNA was found to be the most vulnerable to oxidative damage, displaying greatly increased lesions in response to hydrogen peroxide (Rothfuss *et al*., 2010).

Interestingly, investigating the effects of defective mitochondria, with depleted mtDNA, in HeLa cells resulted in an increase in mitochondrial biogenesis (Miranda, 1999). The cells had increased intracellular oxidative stress in comparison to control cells with intact mitochondria, which caused enhanced expression of nuclear genes specific for mitochondrial biogenesis (Miranda, 1999). This can be seen as a protective cellular mechanism to restore normal mitochondrial function. Similarly, compensatory mechanisms of increased mitochondrial biogenesis are seen in response to stresses other than oxidative stress i.e. ageing. Samples of lung tissue from aged human individuals showed an increase in mtDNA copy number, seen as a feedback mechanism to compensate for the accumulated mtDNA damage and consequently the decline in respiratory function (Lee *et al*., 1998). Furthermore, human lung fibroblasts treated with

sub-lethal concentrations of hydrogen peroxide resulted in the induction of a senescence-like phenotype in the cells, with increased mitochondrial biogenesis and mtDNA copy number (Lee *et al*. 2000).

The accumulation of oxidative stress in mitochondria has also been shown to have an impact on mitochondrial bioenergetics. The effect of ROS on mitochondrial bioenergetics was observed through the exposure of the redox cycler dimethoxy-naphthoquinone (DMNQ) to endothelial cells, which results in the generation of intracellular superoxide and hydrogen peroxide. Increased ROS resulted in a significant decrease in the 'reserve capacity' of the mitochondria measured using the extracellular flux analyser (XF analyzer) (Dranka *et al*., 2010). The reserve capacity is a term used to describe the ability of the mitochondria to increase bioenergetic capacity to respond to increased energy demands from the cell, such as in instances of oxidative stress, in order to provide protection against damage and to maintain normal cellular function (Hill *et al*., 2009). Therefore, a decline in the reserve capacity in response to increased ROS suggests a mechanism by which ROS renders endothelial cells more susceptible to cellular damage and death. Furthermore, this effect was also observed in response to increased NO. NO acts as a modulator of mitochondrial function, with increased NO causing an inhibition of mitochondrial respiration in endothelial cells (Clementi *et al*., 1999). The addition of exogenous NO to endothelial cells resulted in a 4-fold decrease in the mitochondrial reserve capacity (Dranka *et al*., 2010).

6.1.2 Role of mitochondria in CVD

Research carried out on the mechanisms of CVD in mice (Dai *et al*., 2010) and human studies (Cizkova *et al*., 2008; Mayr *et al*., 2012) implicated the involvement of the

mitochondria, particularly in cases of atherosclerosis (Madamanchi and Runge, 2007). The involvement of mitochondrial dysfunction in the pathogenesis of atherosclerosis has been seen through the study of arterial samples from humans with atherosclerosis and in apoE knock-out mice that display early atherosclerosis (Ballinger *et al*., 2002). The results revealed a correlation between the amount of mtDNA damage present and the extent of atherosclerosis in all the samples, with young apoE knock-out mice displaying mtDNA damage prior to the onset of atherosclerosis, suggesting mtDNA as a contributor to the atherogenic process (Ballinger *et al*., 2002).

6.1.3 Endothelial cell mitochondria and atherosclerosis

Endothelial cells have been shown to rely mainly on glycolysis for their cellular energy requirements rather than mitochondrial oxidative phosporylation (Culic *et al*., 1997). However, this in no way should undermine the importance of mitochondria in the function of the endothelium. Along with the many roles that mitochondria play in the cell, being the main source of cellular ROS generation renders them highly important organelles in any cell type due to both the importance of ROS-based cellular signalling pathways, and the detrimental effects excessive ROS generation can have on the function of the cells (Section 1.5).

The importance of normal functioning mitochondria in endothelial cells can be seen through their contribution to the atherosclerotic process. Mitochondria play a role in endothelial dysfunction, one of the primary events seen in the pathogenesis of atherosclerosis (Anderson *et al*., 1995), through increased mitochondrial superoxide generation which depletes the NO availability (Cai and Harrison, 2000). Increased mitochondrial ROS has also been associated with the role of oxidised-LDL in

endothelial cell dysfunction during the pathogenesis of atherosclerosis. The exposure of endothelial cells to oxidised-LDLs results in the alteration of the intracellular redox balance through increasing mitochondrial ROS and RNS generation (Zmijewski *et al*., 2005), contributing to the damaging effects seen in atherogenesis. Furthermore, mitochondria are involved in the apoptosis of endothelial cells. Oxidised LDL disrupt the mitochondrial membrane potential, leading to the release of apoptotic factors that stimulate the process of apoptosis in endothelial cells (Walter *et al*., 1998), contributing to atherosclerosis.

Increased cellular ROS generation is seen as one of the main contributors to the onset of cellular senescence (Erusalimsky and Kurz, 2006). Endothelial senescence is found to contribute to atherogenesis, with senescent endothelial cells found in human atherosclerotic lesions (Minamino *et al*., 2003). This implies a potential role of mitochondria in the development of atherosclerosis as they are a major source of cellular ROS. Other than inflicting oxidative damage on telomeres (Henle *et al*., 1999), increased ROS can bring about senescence in endothelial cells through telomere-independent mechanisms, i.e. through mitochondrial damage. The significance of mitochondrial dysfunction and mitochondrial ROS in inducing endothelial cell senescence is seen through the study of prohibitin-1 (PHB1); a protein found in the inner membrane of mitochondria (Schleicher *et al*., 2008). These proteins play an important role in maintaining mitochondrial integrity (Steglich *et al*., 1999), the knockout of which in endothelial cells increased mitochondrial ROS through inhibition of complex I of the ETC, resulting in senescence (Schleicher *et al*., 2008).

6.1.4 Arsenic induced effects on mitochondria

As discussed in section 1.6.2, arsenite exposure has proven to have damaging effects on the mitochondria, through the induction of mtDNA mutation and reduction of mtDNA copy number observed in arsenite exposed A_L cells (Partridge *et al*., 2007). Other forms of arsenic have also proven to be detrimental to mitochondria. Arsenic trioxide exposure to myoblasts resulted in an increase in cellular ROS along with the release of cyt c from mitochondria and a decrease in the mitochondrial membrane potential, leading to apoptosis (Yen *et al*., 2012). Similar effects were also seen from the exposure of rat liver mitochondria to methylated forms of arsenic, MMA and DMA, which also induced apoptosis through a release of cyt c from the voltage-dependent anion channels of mitochondria and altering the mitochondrial membrane potential (Naranmandura *et al*., 2012). Together, these findings reveal an impact of arsenic on the mitochondria in many cell types, influencing the mitochondrial genome and inducing the mitochondrial intrinsic apoptotic pathway.

6.2 Aims

Mitochondria are very important cellular organelles, involved in vital cellular processes i.e. cell cycle, growth, signalling and apoptosis, the disruption of which has detrimental effects on the cell. This chapter will investigate the *in vitro* effects of arsenite on the mitochondrial function of endothelial cells and whether mitochondria play a significant role in arsenite-mediated toxicity. The investigations will include study of arsenite-mediated effects on mitochondrial function by investigating mitochondrial bioenergetics and ATP generation.

6.3 Investigative Methodology

6.3.1 Mitochondrial function

Mitochondrial function was investigated in early passage HUVECs, (passages 2-6) and EA.hy 926 cells, using the XF analyzer; the current gold standard platform for measuring cellular metabolism. Respiration was assessed through measurements of the cellular oxygen consumption (OC) in response to the sequential addition of known mitochondrial inhibitors. To investigate the effects of arsenite on mitochondrial respiration, oxygen consumption rate (OCR) was compared between arsenite exposed and non-exposed cells during mitochondrial inhibition. The compounds used have either stimulatory or inhibitory effects on the mitochondrial OCR. Based on these responses different parameters of mitochondrial respiration and function were deduced (see figure 6.1).

To accurately measure cellular bioenergetics using the XF analyzer, an important initial step was to ensure cells were grown to a confluent monolayer prior to OC measurements. This ruled out any variation in the results being a result of differences in the number of cells present per well. Therefore, cells were observed via microscopy to ensure confluence was reached before progressing with the experiment.

6.3.2 ATP generation

Despite mitochondria being the main source of ATP in cells, highly proliferative cells such as cancer cell lines rely on glycolysis for cellular energy conservation. This is known as the 'Warburg effect' (Warburg, 1956). The dependence of cells on glycolysis often results in the concealment of mitochondrial toxicity exhibited by a xenobiotic (Marroquin *et al*., 2007). This can be overcome by replacing the glucose in cell culture

media with galactose, forcing the cell to use mitochondrial oxidative phosphorylation for ATP production since unlike the conversion of glucose to pyruvate, the conversion of galactose to pyruvate does not involve ATP generation (Rossignol *et al*., 2004).

Most studies looking into the toxic effects of xenobiotics *in vitro* use cell lines over primary cells due to the limitations that are linked with primary cell culturing, i.e. more expensive, difficulties of cell isolation and limited cell survival in culture conditions. The process of adapting cells to grow under galactose conditions *in vitro*, requires cells to undergo a number of passages in galactose media, therefore HUVECs were not suitable for this purpose. Contrary to primary cells such as HUVECs, cell lines have an extended replicative life span whilst maintaining the cellular characteristics of their particular cell type, therefore initially EA.hy 926 cells were used in this experiment. However, EA.hy 926 cells did not show any signs of adaptation to the galactose media; in fact galactose resulted in cell death after just a few passages. After several unsuccessful attempts to adapt EA.hy 926 cells to galactose culture conditions, human hepatoma cell line; HepG2, was used following the protocol of Swiss and Will (2011). HepG2 cells are the current standard cell line to use in *in vitro* toxicology investigations as they are the most adaptable (Mersch-Sundermann *et al*., 2004).

6.3.2.1 HepG2 cell conditioning in Galactose containing media

Conditioning cells to use galactose instead of glucose forces the cell to rely on the mitochondria for its source of energy. This enables the identification of whether a compound affects a cell through specific mitochondrial targeting.

Cells were cultured in either high glucose or galactose containing media in T75 cm^3 flasks. In order to assess their conditioning, at every 2 passages cells were seeded into 96 well plates at 5,000 cells/ well and left over night to adhere. They were then treated with an antimycin A gradient of 300-2.3 nM in doubling dilutions in replicates of 3 wells/antimycin A concentration for 24 hours. ATP levels were then determined using the luciferase kit according to the manufacturer's instructions (see section 3.6). Conditioned galactose grown cells had significantly diminished ATP readings compared cells grown in high glucose containing media in response to antimycin A.

6.3.2.2 Measuring ATP levels in HepG2 cells

Conditioned HepG2 cells were seeded in two 96 well plates at 5,000 cells/ well, one with galactose grown cells and the other with high glucose grown cells, they were then incubated over night at 37°C and 5% CO_2. Each plate was treated with a range of arsenite concentrations and the antimycin A concentration gradient for 24 hours in a 37°C and 5% CO_2 incubator, the ATP determination kit was then applied and the ATP levels measured (see section 3.6).

6.4 Results

6.4.1 Assessing mitochondrial function

The mitochondrial respiratory chain was assessed through the sequential addition of the compounds; oligomycin, FCCP and antimycin A (Figure 6.1). Prior to the addition of the compound, the basal OCR was measured at 3 time points over a period of 20 minutes. The addition of oligomycin, a compound that targets the last complex of the respiratory chain; ATP synthase, reduced the OCR revealing the proportion of basal OC that is used to generate ATP. This was followed by the addition of FCCP, an 'uncoupler' or ionophore which disrupts the proton gradient across the inner mitochondrial membrane by increasing the permeability of the inner mitochondrial membrane to protons and electrons. Thus, FCCP stimulates the OCR of cells to their maximum potential. Lastly, the addition of antimycin A; an inhibitor of complex III in the respiratory chain, drastically reduces the OCR in mitochondria, revealing the remaining proportion of oxygen consumption that is used in the cell for non-mitochondrial work. Consequently, the mean value generated for antimycin A treatment needs to be subtracted from the mean values of all the basal, Oligomycin and FCCP measurements, to deduce the mitochondrial-specific parameters. One further parameter that is deducible from this response curve is the reserve capacity of the mitochondria. The reserve capacity is determined by calculating the difference between the maximum OCR and the basal OCR (Dranka *et al*., 2010). All the calculated parameters are schematically represented in figure 6.1.

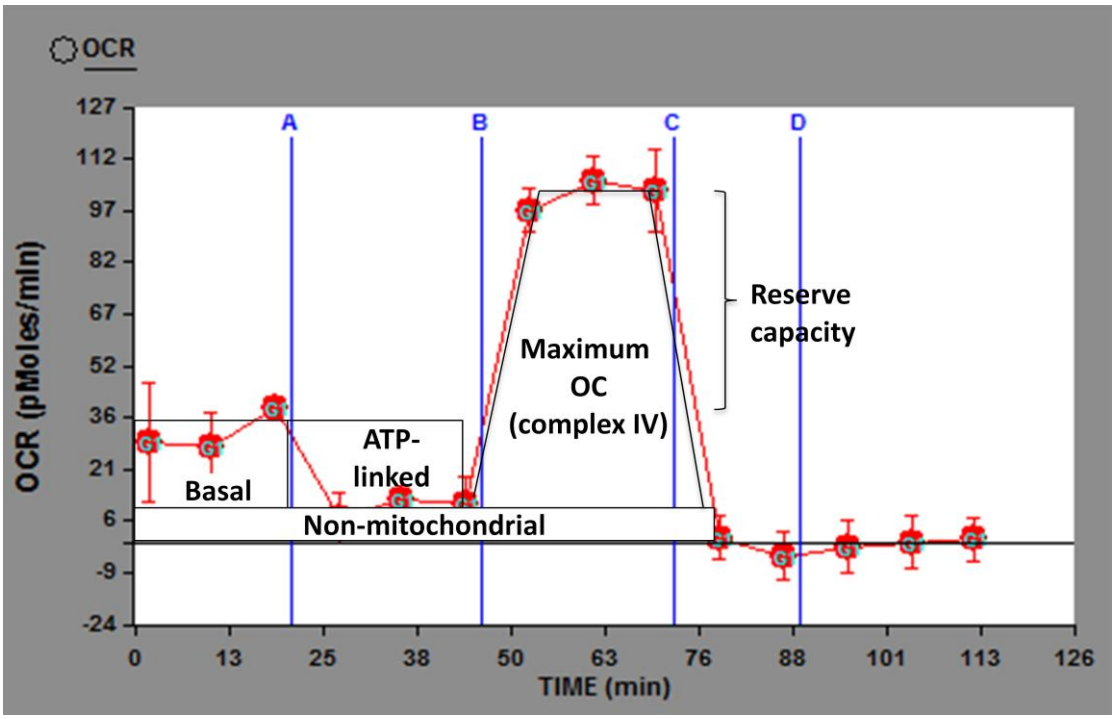

Figure 6.1 Measurement of the oxygen consumption rate (OCR) using the XF24 analyzer for HUVECs through a time course in response to the sequential addition of (A) 5 µM oligomycin, (B) 4 µM FCCP*, (C) 10 µM antimycin A and (D) culture media. The graph shows the parameters that can be deduced from the response curve; the basal, ATP-linked, maximum and non-mitochondrial oxygen consumption (OC) and the reserve capacity of the cells. The value shown are from a representative experiment with means of n=3 ±SEM. *Carbonyl cyanide 4-(trifluoromethoxy)phenylhydrazone.

Both HUVECs and EA.hy 92 cells were used to investigate the effect of arsenite on endothelial cell mitochondrial function. Both cell types were acutely exposed to sub-cytotoxic concentrations of arsenite for 1 hour and 4 hours prior to the measurement of OCR. With EA.hy 926 cells being immortalised HUVECs, similar outcomes for the mitochondrial function were expected in response to arsenite treatment with that of HUVECs, surprisingly however the cell types gave different outcomes.

Figure 6.2 and 6.6 show the effects of arsenite on the mitochondrial reserve capacity of endothelial cells after 1 and 4 hour exposure respectively. For HUVECs, 1 hour arsenite exposure induced a concentration-dependent decrease in the reserve capacity, with a

significant decrease ($p<0.01$) seen in cells exposed to the highest experimental arsenite concentration; 1,000 µg/L. The mitochondrial reserve capacity approached 50% of the control value at this concentration. However this trend was not observed in EA.hy 926 cells, which showed no significant differences to the untreated control cells due to wide variability in response (Figure 6.2). Exposing HUVECs to arsenite for 4 hours showed an initial significant increase ($p<0.05$) at 10 µg/L arsenite against the control, followed by a concentration dependent decrease, with the reserve capacity at 1,000 µg/L decreasing to approximately 75% of the control value. Again, no significant changes were seen in EA.hy 926 cells after 4 hour arsenite exposure (Figure 6.6).

Arsenite did not have a significant impact on the maximum OCR in either cell type after 1 hour exposure (Figure 6.3). The exposure of cells to arsenite for 4 hours resulted in a significant increase in the maximum OCR at 10 µg/L in HUVECs ($p<0.05$) followed by a concentration-dependent decrease with the subsequent arsenite concentrations, restoring the OCR back to basal level at 1,000 µg/L (Figure 6.7). EA.hy 926 showed no change in the maximum OCR from the basal level in control cells in response to 4 hour arsenite exposure (Figure 6.7).

Arsenite has no apparent significant effect on the ATP-linked OCR in HUVECs or EA.hy 926 cells compared to the control cells after 1 hour or 4 hours exposure. A significant decreases in the levels of OCR at 100 and 1,000 µg/L arsenite concentrations compared to the increased OCR at 10 µg/L was observed ($p<0.05$) (Figure 6.4). In response to the 1 hour arsenite exposure, OCR was not affected in EA.hy 926 cells (Figure 6.4). Both HUVECs and EA.hy 926 cells displayed a non-significant decrease in levels of ATP-linked OCRs in response to 4 hour arsenite treatment (Figure 6.8).

There was also no significant effect of arsenite seen on the non-mitochondrial OCR at either 1 or 4 hour treatment for HUVECs or EA.hy 926 cells (Figures 6.5 and 6.9). However, they both displayed a clear trend for increases in the OCR after 1 hour arsenite exposure (Figure 6.5). In the case of HUVECs, this affect appeared to be concentration-dependent and a 3-fold increase in non-mitochondrial OC was observed for 1,000 μg/L arsenite (Figure 6.5a).

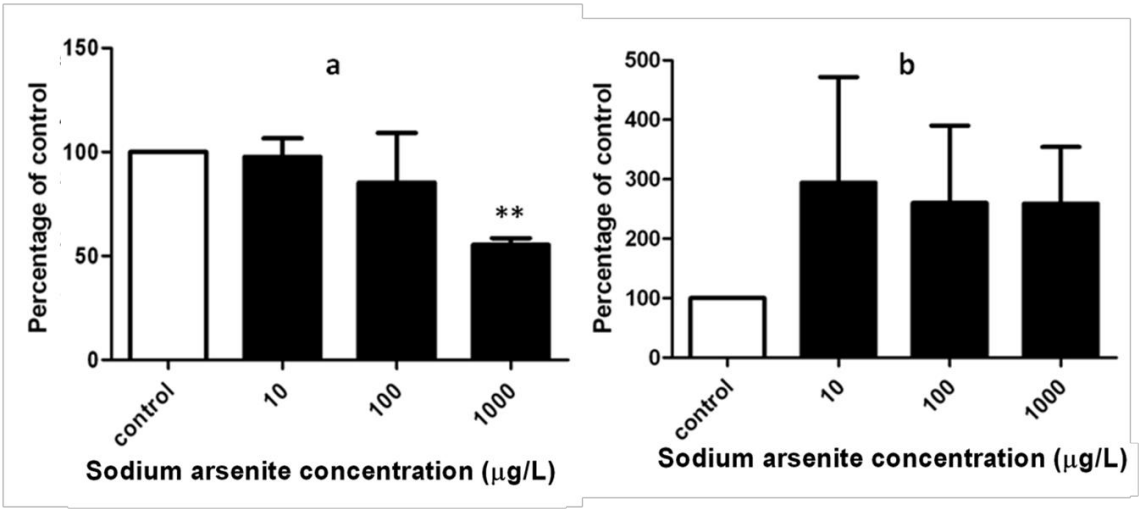

Figure 6.2 Percentage change in mitochondrial reserve capacity with increasing arsenite concentrations in (a) HUVEC and (b) EA.hy 926 cells treated for 1 hour. The values represent means and (a) n=3 +SEM and (b) n=6 +SEM. The data were analysed using one-way ANOVA with Tukey post-test (**$p<0.01$ compared to the control cells).

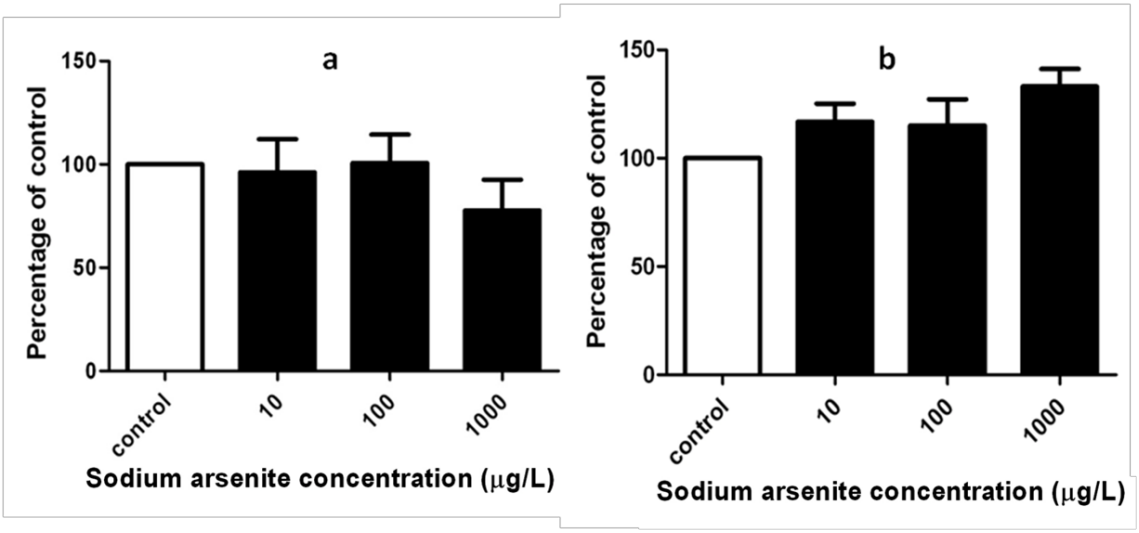

Figure 6.3 Percentage change in the maximum oxygen consumption of mitochondria with increasing concentrations of arsenite in (a) HUVEC and (b) EA.hy 926 cells treated for 1 hour. The values represent means and (a) n=3 +SEM and (b) n=6 +SEM. The data were analysed using one-way ANOVA with Tukey post-test, no significance was observed.

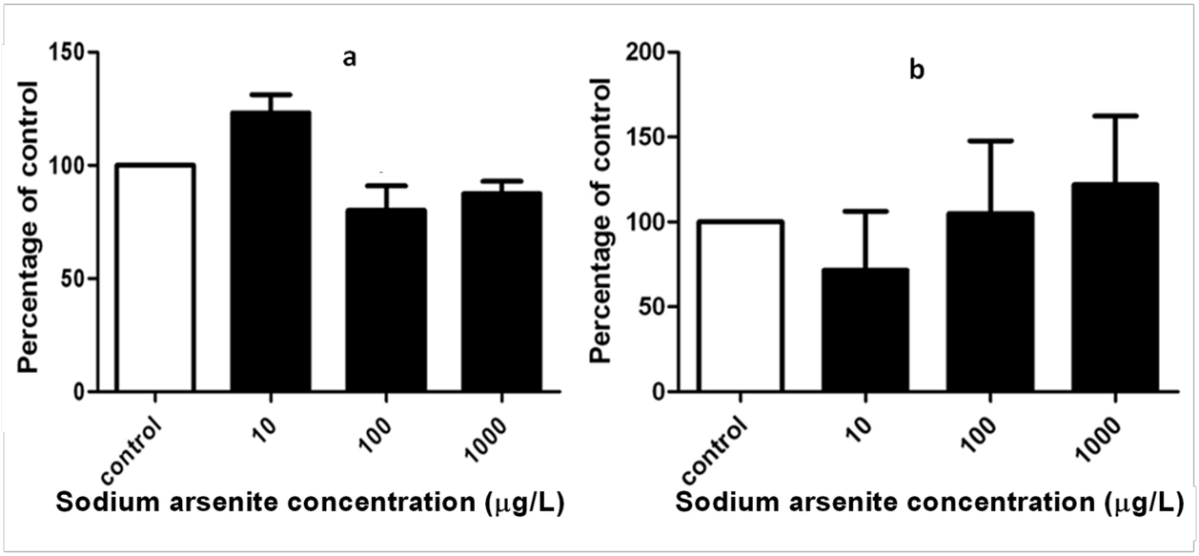

Figure 6.4 Percentage change in mitochondrial ATP-linked oxygen consumption in HUVEC treated for 1 hour with arsenite. The values represent (a) n=3 +SEM and (b) n=4 +SEM. The data were analysed using one-way ANOVA with Tukey post-test.

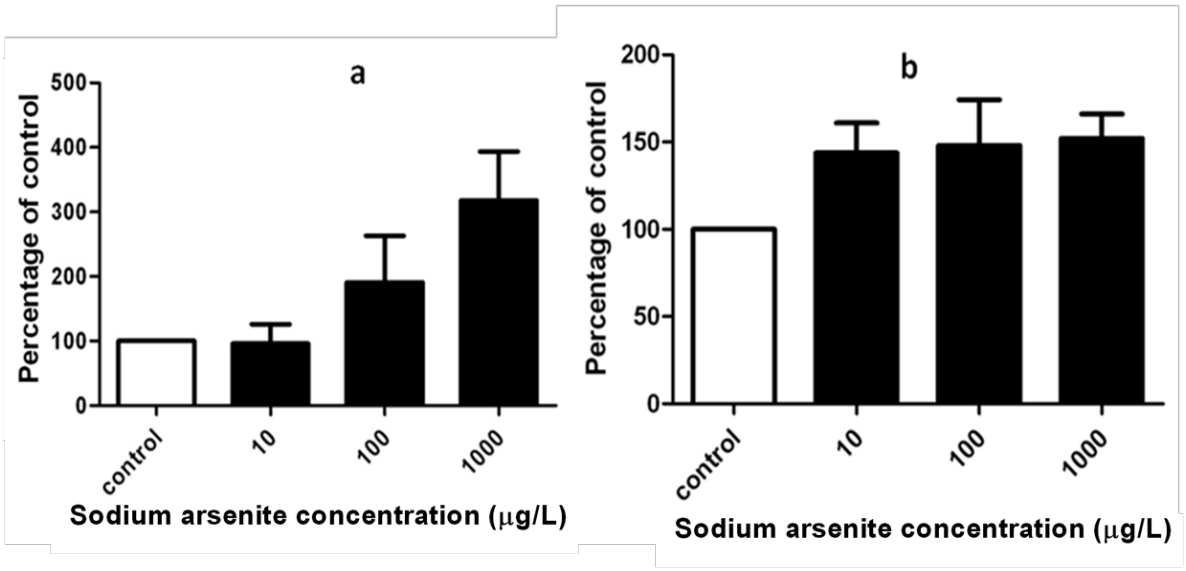

Figure 6.5 The percentage change in non-mitochondrial oxygen consumption in (a) HUVEC and (b) EA.hy 926 cells treated with arsenite for 1 hour. The values represent means and (a) n=3 +SEM and (b) n=6 +SEM. The data were analysed using one-way ANOVA with Tukey post-test, no significance was observed.

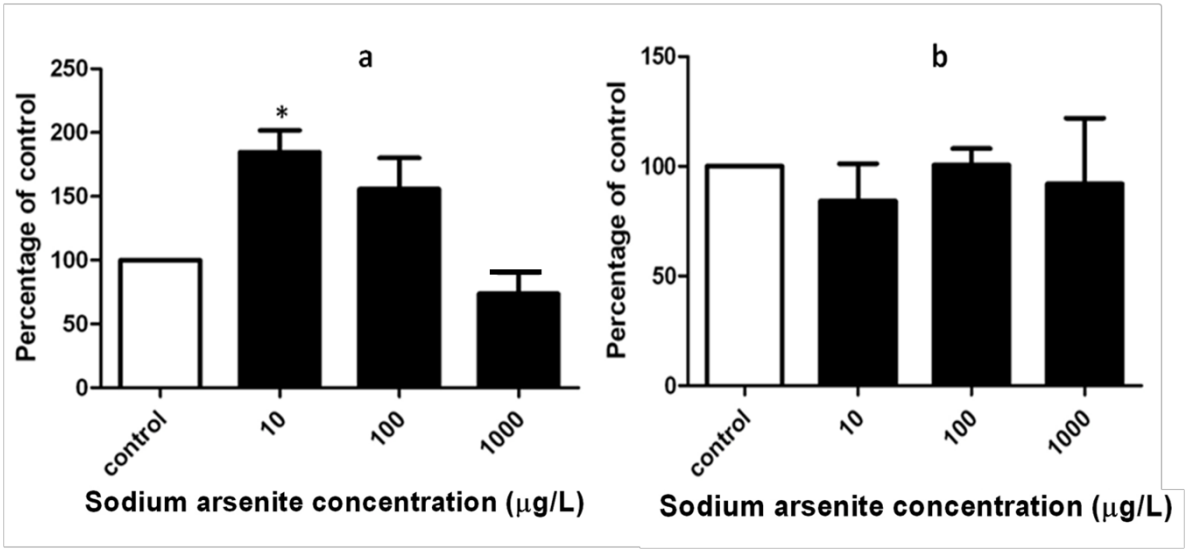

Figure 6.6 Percentage change in mitochondrial reserve capacity with increasing arsenite concentrations in (a) HUVEC and (b) EA.hy 926 cells treated for 4 hours. The values represent the means and (a) n=3 +SEM and (b) n=4 +SEM, the data were analysed using one-way ANOVA with the Tukey post-test (*$p<0.05$ compared to the untreated control cells).

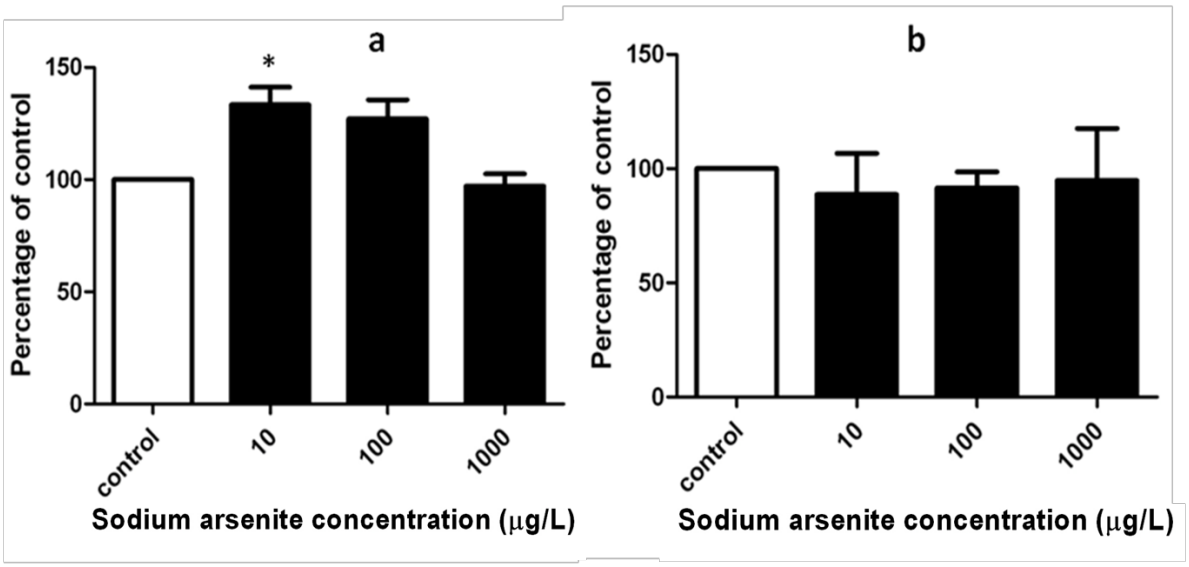

Figure 6.7 Percentage change in the maximum oxygen consumption of mitochondria with increasing concentrations of arsenite in (a) HUVEC and (b) EA.hy 926 cells treated for 4 hours. The values represent means and (a) n=3 +SEM and (b) n=4 +SEM. The data were analysed using one-way ANOVA with the Tukey post-test (*$p<0.05$ compared to the control; 0 μg/L).

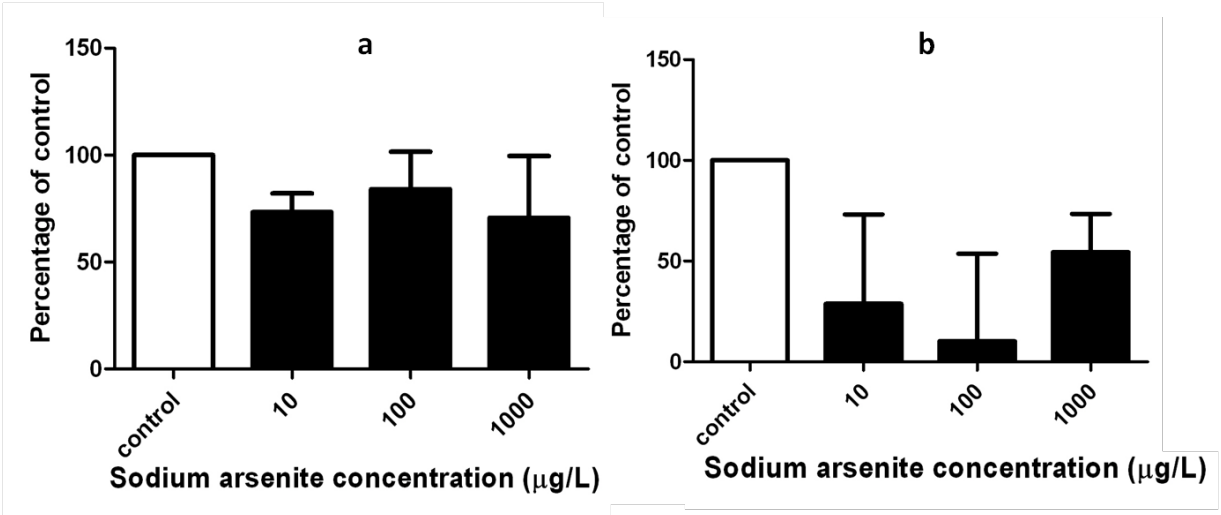

Figure 6.8 Percentage change in mitochondrial ATP-linked oxygen consumption in HUVEC treated for 4 hours with arsenite. The values represent mean and (a) n=3 +SEM and (b) n=4 +SEM. The data were analysed using one-way ANOVA with the Tukey post-test, no significance was observed.

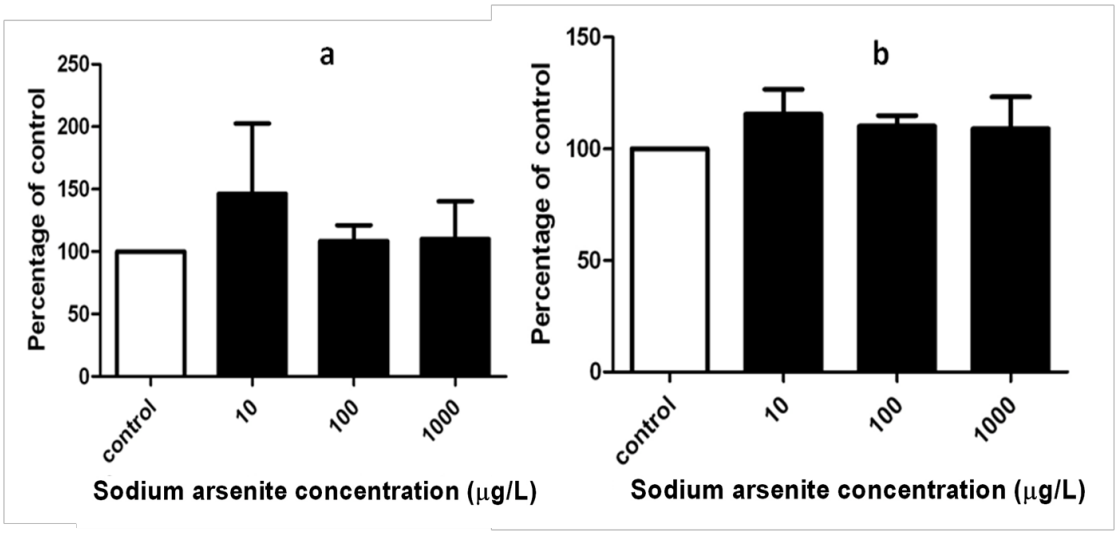

Figure 6.9 The percentage change in non-mitochondrial oxygen consumption in (a) HUVEC and (b) EA.hy 926 cells treated with arsenite for 4 hours. The values represent the means and (a) n=3 +SEM and (b) n=4 +SEM. The data were analysed using one-way ANOVA with the Tukey post-test, no significance was observed.

6.4.2 Determining mitochondrial toxicity

In order to assess whether arsenite directly targets mitochondria to elicit its toxicological effects in cells, HepG2 cells were forced to rely on their mitochondria as a source of energy by being cultured in glucose-free and galactose-containing media. To ensure the cells had fully adapted to using oxidative phosphorylation as their energy source rather than glycolysis, the cells were treated with the mitochondrial inhibitor antimycin A, at a 2-fold concentration range from 2.3 to 300 nM for 24 hours (Figure 6.10a and b) and ATP levels were compared between cells grown in galactose-containing media and glucose-containing media.

Antimycin A was toxic to HepG2 cells grown in either monosaccharide condition. In glucose-containing media, HepG2 cells responded to antimycin A treatment with a concentration-dependent loss of ATP for concentrations between 1 and 40 nM. Beyond 40 nM there were no apparent increases in ATP depletion and the maximum loss of

ATP was ~50% of control. HepG2 cells grown in galactose-containing media also showed an antimycin A concentration-dependent inhibition of ATP levels (Figure 10a) but the shape of the concentration-response curve was quite different to that of HepG2 cells grown in glucose-containing media, although this did not reach significance (Figure 6.10). At low antimycin A conditions, 2.3 and 4.6 nM, cells seemed slightly less sensitive to the toxic effects of antimycin A than the HepG2 cells grown in glucose-containing media (Figure 10a and b). However, the subsequent increased antimycin a concentrations revealed a remarkable inhibitory effect on the HepG2 cells, with a rapid loss of ATP in response, such that at 37 nM only ~5% control ATP remained.

A significant difference between the response to higher antimycin A concentrations; 37.5- 300 nM, was seen between the two experimental cell conditions ($p<0.001$), with these concentrations having apparent lethal effects on the HepG2 cells grown in galalctose-containing media. Thus, the cells successfully adapted to relying on their mitochondria for ATP production.

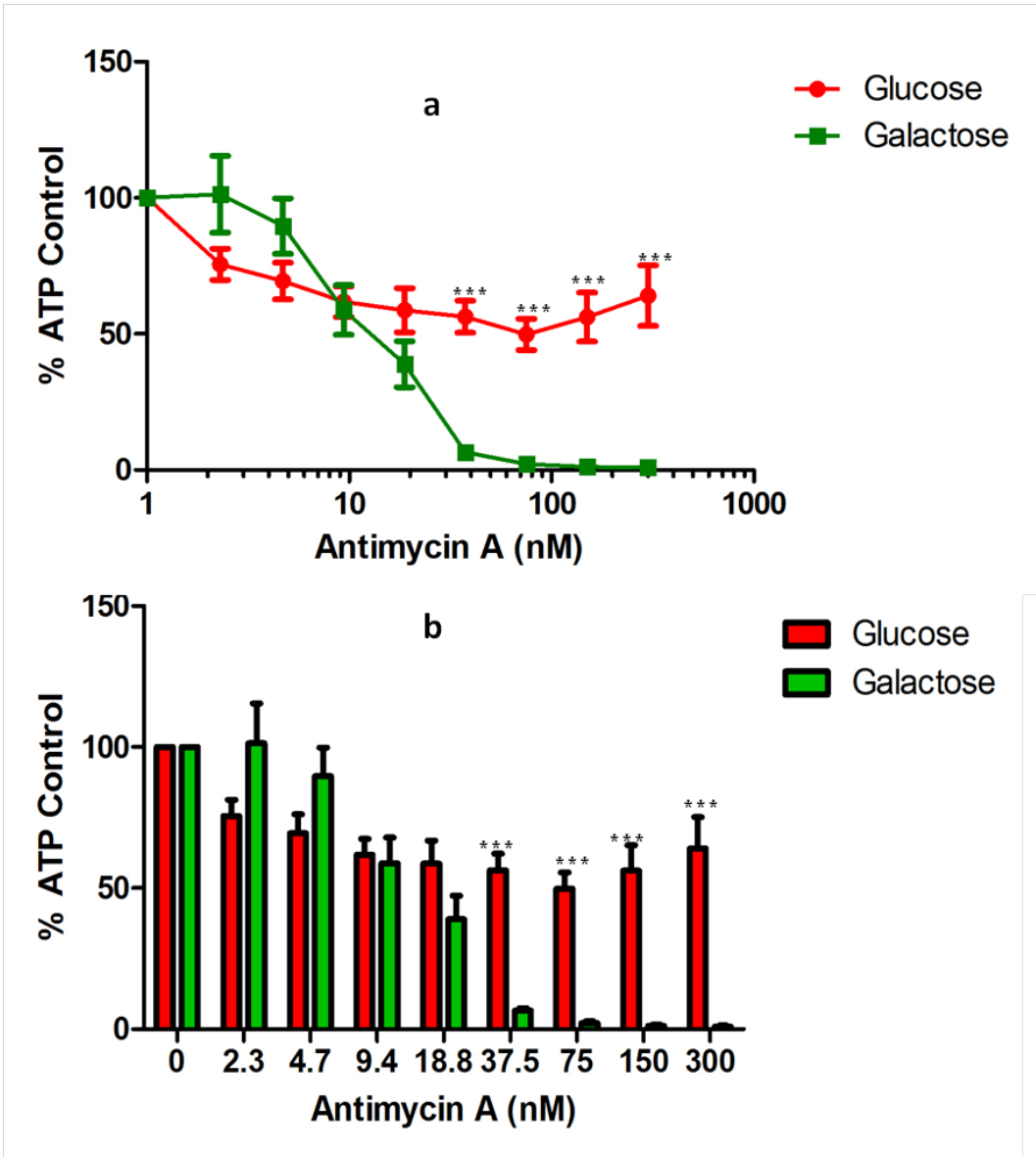

Figure 6.10 The response of HepG2 cells to a 24 hour treatment with a doubling concentration range of antimycin A; 2.3-300 nM. Cells were grown in media containing glucose (red) or galactose (green). The values represent means (n=5±SEM) and data is plotted in two ways to allow easy access to antimycin A concentrations. Data were analysed using 2-way ANOVA with the Bonferroni post-test which enabled a direct comparison between the effects of each antimycin A concentration on HepG2 cells grown in glucose-media and HepG2 cells grown in galactose-containing media (***$p<0.001$).

HepG2 cells of both experimental conditions were exposed to concentration ranges of arsenite. Figure 6.11a shows the response of the cells to an arsenite concentration gradient with 10-fold increases from 1-100,000 µg/L. No significant differences between the responses of the HepG2 cell types were seen over the whole range of concentrations. Interestingly an increase in ATP generation at 10,000 µg/L arsenite was observed in the response of both HepG2 cells in either sugar (Figure 6.11a). At 100,000 µg/L cells appeared to die in both glucose and galactose media (Figure 6.11a). Looking closer at this arsenite concentration range in a subsequent experiment between the ATP-generation peak at 10,000 µg/L and cell lethality at 100,000 µg/L was used to reveal whether this was a real effect.

Once again the responses of both cell types showed no significant differences (Figure 6.11b). Interestingly, an increase in ATP generation, ~2-fold compared to control, was observed at 5000 µg/L. The HepG2 cells responded to 10,000 µg/L arsenite with a further increase in ATP generation, ~3-fold increase compared to the control, yet neither of the increases were significantly different to the control. The lack of significance can be explained by the variability present in the data represented by the large error bars. The response seen of the HepG2 cells to increasing arsenite concentrations between 20,000 and 80,000 µg/L appeared to be a combination of cells producing increased levels of ATP compared to the control, i.e. 5000-10,000 µg/L, and a concentration-dependent increase in cytotoxicity and thus loss of cells, i.e. from 10,000-100,000 µg/L, (Figure 6.11b).

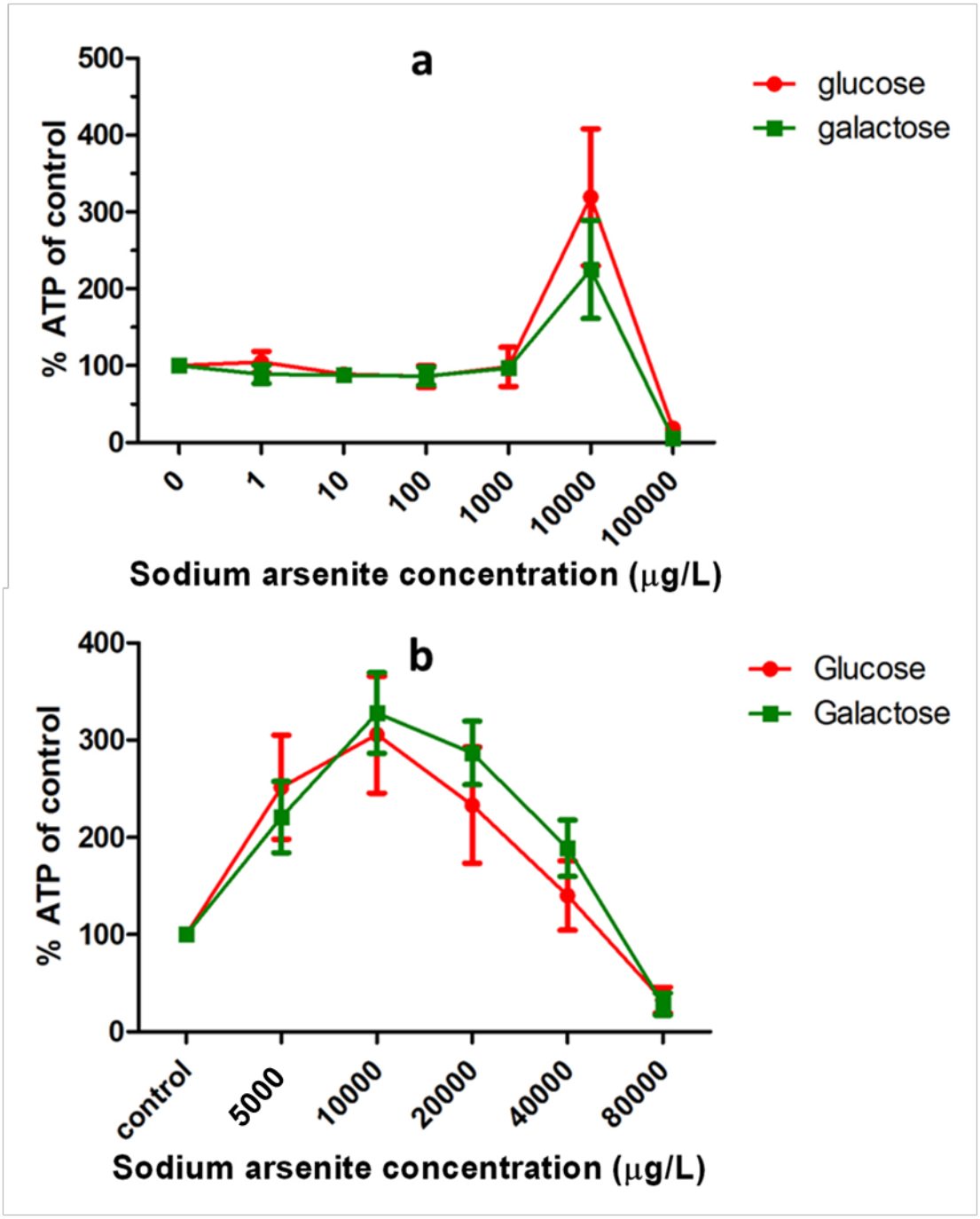

Figure 6.11 The response of HepG2 cells to a 24 hour treatment with arsenite in media containing glucose (red) or galactose (green). The values represent means (n=4±SEM). Data were analysed using 2-way ANOVA with the Bonferroni post-test which enabled a direct comparison between the effects of each arsenite concentration on HepG2 cells grown in glucose-media and HepG2 cells grown in galactose-containing media. No significant differences in the response of the cells to arsenite in the different conditions were seen.

6.5 Discussion

The aim of this chapter was to determine whether mitochondria were primary targets for arsenite-mediated toxicity. Previous work investigating the *in vitro* effects of arsenic on a number of cell types has shown arsenic-induced mitochondrial disruptions, leading on to cellular damage and apoptosis (Liu *et al*., 2005; Partridge *et al*., 2007; Naranmandura *et al*., 2012; Yen *et al*., 2012). Thus, mitochondria have been implicated as targets of arsenic. Furthermore, the effects of arsenite on mitochondrial function were assessed, looking into the impact of arsenite on the respiratory capacity of mitochondria and the ability of mitochondria to fulfil its role in providing cellular protection.

6.5.1 Are mitochondria direct targets of arsenite?

The toxicity of compounds that target the mitochondria are often masked when carrying out *in vitro* investigations due to the high glucose concentration in culture media; often 25 mM. This concentration of glucose is 5-fold higher than physiological concentrations and allows cells to use glycolysis to make sufficient ATP for cellular functions, including proliferation. Such a phenomenon has been seen in cancer cells, where the cells rely on glycolysis for cellular energy over oxidative phosphorylation, described as the Warburg effect (Warburg, 1956). This effect can be overcome by adapting cells to galactose-containing media instead, forcing them to rely on their mitochondria for ATP. However, not all cells are able to adapt well to utilising galactose instead of glucose and this approach may not give reproducible results. In this thesis, EA.hy 926 cells were investigated using this technique but found not to survive, the reason for which remains unclear. Therefore, HepG2 cells were used (Swiss and Will, 2011). HepG2 cells are human a hepatocellular carcinoma cell line that is used in toxicity studies due it being highly differentiated and retaining many of the genotypic features of normal liver cells

(Sassa *et al*., 1987; Gerets *et al*., 2012). These cells have been suggested as a useful means of assessing mitochondrial toxins *in vitro* (Swiss and Will, 2011).

The Warburg effect was clearly illustrated by comparing the ATP generation between HepG2 cells cultured in galactose media and normal glucose media in response to increasing concentrations of the mitochondrial toxin antimycin A. Antimycin A acts by disrupting the ETC, specifically binding to complex III, consequently preventing the transport of electrons between cytochrome b and c (Maguire *et al*., 1992). This causes a collapse of the protein gradient across the inner membrane and breakdown of the mitochondrial membrane potential (Campo *et al*., 1992). Abolishing the mitochondrial membrane potential results in the release of apoptotic factors such as cytochrome C, inducing apoptosis (Wolvetang *et al*., 1994). The significantly lower levels of ATP detected in galactose-adapted HepG2 cells reveal the extent to which mitochondrial toxicity is masked by cells grown in high glucose culture conditions.

Galactose-adapted HepG2 cells showed no difference in their response to arsenite when compared to HepG2 cells grown in high-glucose conditions. Thus, it is apparent that arsenite does not directly target the mitochondria, particularly not their respiratory capacity. Looking at these findings it can be concluded that arsenite-mediated mechanisms of toxicity do not rely on the mitochondria, rather any mitochondrial disturbances observed can be regarded as secondary effects of the initial arsenite-mediated cellular damage.

Despite there being limited literature available on the impact of arsenic on mitochondrial respiration, the results of this thesis are inconsistent with previous work.

Dwivedi *et al* (2011) looked into the chronic effects of arsenite on mitochondrial respiration in rats treated for 4 weeks. Examining their neuronal cells revealed diminished levels of ATP generation as a result of arsenite exposure when compared to non-exposed rat neuronal cells. However, examining brain slices of the rats also revealed a 5-fold increase in the levels of cyt c, providing strong support for apoptosis. Therefore, it is unclear whether the decreased levels of ATP are due to arsenite directly targeting the mitochondrial or as a result of cellular damage leading to apoptosis. Investigating the effects of arsenic trioxide does however suggest the mitochondria as direct targets. The exposure of arsenic trioxide has been shown to decrease ATP generation in the mitochondria by inhibiting complex IV of the ETC in T47D breast cancer cells (Sun *et al*., 2011). The difference between the effects on ATP generation in response to arsenite as observed in this thesis and that of arsenic trioxide (Sun *et al*., 2011) can be explained by the different cell types used in both these investigations. Furthermore, Hornhardt *et al* (2006) have shown these forms of arsenic to have very different cytotoxic outcomes on exposure, and are therefore regarded as mediating their effects by targeting distinct cellular pathways.

6.5.2 Impact of arsenite on the mitochondrial function

6.5.2.1 Stimulatory effects of arsenite

Assessing the effects of arsenite on the mitochondrial function of endothelial cells using the XF analyzer revealed the stimulatory effects arsenite has on mitochondrial function at low concentrations. After 4 hours exposure to 10 µg/L arsenite, HUVECs displayed a significant increase in the maximum OCR, followed by a reduction with increasing arsenite concentrations; 100 and 1,000 µg/L. This pattern was also seen in the effects of 4 hour arsenite exposure on the mitochondrial reserve capacity in HUVECs, with a

significant increase in reserve capacity at 10 µg/L followed by a concentration-dependent reduction with higher arsenite concentrations. This supports the notion of arsenite having a stimulatory effect on cellular processes at low concentrations, as seen in the increase in cell viability noted at low arsenite concentrations (see chapter 4). Thus arsenite significantly enhances the function of endothelial mitochondria at low concentrations; 10 µg/L, albeit after short-term exposure *in vitro*.

The significant increase in the reserve capacity can be regarded as a protective mechanism of the mitochondria to the initial, potentially harmful effects arsenite has on the cells. Endothelial mitochondrial reserve capacity has been hypothesised to play an important role in providing protection against oxidative stress (Dranka *et al*., 2010), suggesting an acute increase in ROS to be the possible immediate effects of arsenite exposure in HUVECs, resulting in a compensatory stress response which may include increasing antioxidant protection. Such a protective response to stress, to prevent stress-induced damage, is known as 'stress-response hormesis' (Gems and Partridge, 2008). A similar 'stress-response hormesis' effect involving the mitochondria has been seen previously when investigating the effects of statins, a medication prescribed for cardiovascular disease, on mitochondrial biogenesis (Bouitbir *et al*., 2012). Statins are found to provide protection against cardiovascular-morbidity in patients, however also causing skeletal muscle injury (Echaniz-Laguna *et al*., 2010; Bouitbir *et al*., 2012). Investigating the effects of statins on both humans and rats found the statins to lead to transcriptional activation of mitochondrial biogenesis genes in the myocardium along with antioxidants through ROS signalling mechanisms, with the myocardium showing low ROS levels. Whereas the skeletal muscle showed low antioxidant activity and deactivation of mitochondrial biogenesis gene expression, with high levels of oxidative

stress (Bouitbir *et al*., 2012). Thus, this study carried out by Bouitbir *et al* (2012) demonstrates the ability of the cardiovascular system to respond to ROS by stimulating a protective stress response, providing support for the possible involvement of 'stress-mediated hormesis' as a protective response by endothelial cells to arsenite exposure.

6.5.2.2 Inhibitory effects of arsenite

Even the acute exposure of 1 hour to non-cytotoxic concentrations of 1,000 µg/L arsenite resulted in a significant decline in the mitochondrial reserve capacity in HUVECs. A similar decline in reserve capacity was seen by Dranka *et al* (2010) when investigating the effects of low levels NO and ROS-generating redox-cycling agent 2,3-dimethoxy-1,4-napthoquinone (DMNQ) exposure on endothelial cells. Both treatments resulted in a decline in the reserve capacity of mitochondria, rendering the cells more vulnerable to oxidative damage. Therefore the reserve capacity is hypothesised to protect cells against oxidative stress (Dranka *et al*., 2010). Furthermore, despite the significant increase in the reserve capacity seen after 4 hours exposure to 10 µg/L arsenite, this increase was significantly reduced when compared to the reserve capacity measured at 1,000 µg/L arsenite exposure in HUVECs. Thus, higher levels of arsenite appear to overcome the stimulation of the mitochondrial reserve capacity at lower concentrations.

By inducing a decline in the reserve capacity, HUVECs are less able to meet the increased energy demands on the cells due to arsenite-mediated stress. Reducing this ability of endothelial mitochondria to provide protection against cellular damage could lead to the onset of endothelial dysfunction. Furthermore, with the important role of mitochondria in cellular signalling and processes i.e. cell cycle control, cellular

development, metabolism and apoptosis (see section 1.6.1), defects in the mitochondria could prove detrimental to the cell. Collectively, the decline in the reserve capacity either through inducing mitochondrial dysfunction or bringing about damage to the cell, i.e. oxidative damage, would lead to endothelial dysfunction, revealing a potential mechanism by which arsenite initiates the pathogenesis of atherosclerosis.

6.5.3 Effects of arsenite on non-mitochondrial oxygen consumption

The XF analyzer enables the analysis of oxygen consumption by the cell that is used for non-mitochondrial processes. HUVECs showed a concentration-dependent increasing trend in the non-mitochondrial OCR after 1 hour arsenite exposure compared to the non-exposed cells, with EA.hy 926 cells also displaying a trend towards increased OCR in cells treated with arsenite at all concentrations. Together with the significant increase in the reserve capacity, which potentially implicates an acute increase in cellular oxidative stress (Dranka *et al*., 2010), the increase in non-mitochondrial OCR may be due to an acute increase in ROS production from non-mitochondrial sources.

Research carried out by several groups has shown arsenic to increase ROS generation via the activation of NADPH oxidases in many cell types (Lynn *et al*., 2000; Lemarie *et al*., 2008; Wang *et al*., 2008), including endothelial cells (Barchowsky *et al*., 1999; Edwards *et al*., 2013). NADPH oxidase are suggested to be the major source for ROS generation in endothelial cells (Frey *et al*., 2009), which are activated by a number of stimuli i.e. cytokines, growth factors, hypoxia and stress (Griendling *et al*., 2000). Phagocyte NADPH oxidases comprise of the membrane bound cytochrome b_{558} complex that consists of catalytic subunit $gp91^{phox}$ (Nox2) and a regulatory subunit $p22^{phox}$, as well as cytosolic subunits; $p40^{phox}$, $p47^{phox}$, $p67^{phox}$ and the GTPase Rac

(DeLeo *et al*., 1998). In endothelial cells, the $gp91^{phox}$ human homologs Nox_1, Nox_2, Nox_4 and Nox_5 have been identified with Nox_2 being critical for endothelial NADPH oxidase (Jones *et al*., 1996; BelAiba *et al*., 2007; Frey et al., 2009). Smith *et al* (2000) have shown porcine endothelial cell to express the two NADPH oxidase regulatory proteins $p67^{phox}$ and Rac1, however contrary to phagocytes, $p67^{phox}$ was expressed in the membrane of the endothelial cells as opposed to the cytosol.

In macrophages, the activation of NADPH oxidase by arsenic was suggested to occur through the stimulation of the p38-mitogen activated protein kinase (MAPK) pathway (Lemarie *et al*., 2008), a pathway stimulated by environmental stress and proinflammatory factors (Obata *et al*., 2000). Lemarie *et al* (2008) found arsenic-induced stimulation of this pathway to lead to the phosphorylation and membrane bound translocation of the NADPH oxidase subunit $p47^{phox}$, and increased translocation of Rac1 and $p67^{phox}$, resulting in an increase in ROS. This therefore forms a possible mechanism by which arsenic may bring about NADPH oxidase activation in endothelial cells, resulting in the increase in the usage of oxygen to generate ROS, which would explain the increase in non-mitochondrial oxygen consumption observed.

When carrying out these investigations to assess the effects of arsenite on mitochondrial function, there were many discrepancies between the mitochondrial responses to compounds between HUVECs and EA.hy 926 cells. It has therefore become apparent that the EA.hy 926 cells derived from primary HUVECS do not retain all their characteristics. This raises the question of whether using EA.hy 926 cells is an appropriate model to employ *in vitro*, particularly when assessing endothelial

mitochondrial function. Moreover, the importance of using primary cells in *in vitro* investigations is thus highlighted.

6.5.3 Summary

Studying the effects of arsenite on mitochondria strongly suggests that arsenite is not a direct mitochondrial toxicant, indicating that mitochondria are not the primary cellular targets. The exposure of arsenite to HUVECs for 1 hour suggests a potential increase in the generation of non-mitochondrial ROS, which could lead to subsequent damaging effects in the cell, i.e. including the decrease in the mitochondrial reserve capacity observed after 1 hour arsenite exposure. This suggests the occurrence of mitochondrial dysfunction as an early, rather than primary, cellular response in arsenite-mediated cytotoxicity.

Furthermore, the significant boost in the HUVEC mitochondrial reserve capacity and maximum OC capacity in response to 4 hour exposure to a low-arsenite concentration implies a protective/ adaptive response to the early damaging effects of arsenite seen at 1 hour exposure that is a 'stress-mediated hormesis' effect. Conclusively, despite mitochondria not being primary targets, they are still affected by arsenite, and possibly undergo dysfunction. This could lead to the onset of endothelial dysfunction providing a potential mechanism for the arsenite-induced initiation of atherosclerosis.

CHAPTER SEVEN

Transcriptomics

Chapter 7: Transcriptomics

7.1 Introduction

Preceding chapters in this thesis described the *in vitro* effect of inorganic arsenite on HUVEC ageing, production of ROS, DNA damage and mitochondrial function. The original hypothesis proposed arsenite to be a mitochondrial toxin, which caused an increase in the generation of mitochondrial ROS as an initial response, leading to further toxic effects. However, investigations carried out in chapters 5 and 6 have suggested that arsenite has limited direct effects on mitochondria. Arsenite did not induce mtDNA damage. With mtDNA being highly susceptible to damage in response to stress-induced mitochondrial ROS, if arsenite directly targeted the mitochondria an increase in mtDNA damage would have been likely. Further support for this was obtained from assessing mitochondrial function. Although a decrease in the mitochondrial reserve capacity was observed due to arsenite, no direct disruptions to the ETC or oxidative phosphorylation process and no alterations in ATP generation were measured. Therefore, as there is no strong evidence to suggest mitochondria being the primary target of arsenite, the original hypothesis can be rejected. In order to generate an alternative hypothesis on the mechanism of action for arsenite on endothelial cell function and ageing, and to build upon the positive observations made, this chapter focuses on the genome-wide effects of arsenite exposure.

Microarray-based transcription profiling was employed to analyse the mRNA changes in HUVECs *in vitro* in response to arsenite exposure. Microarray is a powerful tool used to examine the unique pattern of gene expression changes in cells and tissues. In the context of toxicology it has been used to generate a molecular signature for specific toxins (Gatzidou *et al*., 2007). This is useful when conducting mechanistic studies as

well as identifying appropriate biomarkers for toxicity investigations (Waters and Yauk, 2007). The use of microarray for *in vitro* studies is useful for such investigations, giving an indication of the cellular targets of a toxin without having to conduct lengthy and expensive *in vivo* studies (van Hummelen and Sasaki, 2010; Zimmer *et al*., 2008).

Looking at the changes in mRNA through microarray allows the comparison of transcriptional profiles derived from treated against control samples, enabling the identification of the early toxicological responses, subtle gene expression changes and potential molecular pathways affected. This is an important aspect of *in vitro* toxicogenomics as it reveals information about the immediate toxicant-mediated response to the cell. In most cases, the initial response identified is that of expression changes in genes involved in cellular protection. The effects in gene expression seen later with continued exposure or with a higher toxicant concentration may be as a result of the irreversible damage to the cells rather than a direct toxicant response (Zhou *et al*., 2007; Zhou *et al*., 2009).

7.2 Aims

The aim of this study was to observe the transcriptional profiles of HUVECs that were exposed to inorganic arsenite, in comparison to untreated control HUVECs. This was done to suggest the immediate gene targets and molecular pathways implicated in arsenite mediated endothelial toxicity.

7.3 Investigative Methodology

Six biological repeats of HUVECs of early passage (2 to 4), were either treated with 1,000 µg/L arsenite for 24 hours or left untreated (n=6) before undergoing mRNA extraction (as described in section 3.10). The dosage of arsenite was determined based on the cell viability test carried out using the CCK8 assay (see section 4.4.1). Exposing HUVECs to 1,000 µg/L arsenite for 24 hours did not induce significant cell death. This was important as the aim of this study was to investigate the immediate effects of arsenite exposure, without having induced substantial cellular damage.

The Illumina Whole-Genome Gene Expression BeadChip Human HT-12 v4 used for the transcriptomic investigations (see section 3.10) and consists of 12 sample arrays, comprising more than 47,000 probes (Illumina®). Each probe represents a specific sequence used to make a 50-mer oligonucleotide, which is attached to a 29-mer address sequence that binds to a bead (Figure 7.1). The beads sit in microwells on the arrays and the address sequences enable the location of the bead to be mapped along the BeadChip. Each bead represents one probe, with hundreds of thousands of copies of that specific probe oligonucleotide bound. There are on average 30 beads that represent the same probe, randomly placed on the beadchip with 99.98% of each bead type being present in each of the 12 arrays. The 50-mer sequence of each probe binds to biotin labelled cRNA by direct hybridisation. The hybridised BeadChip is exposed to steptavidin-Cy3; a fluorescent cyanine dye bound protein with a high affinity for biotin. The Cy3 yellow/green fluorescing molecules are detected by the microarray laser detection system.

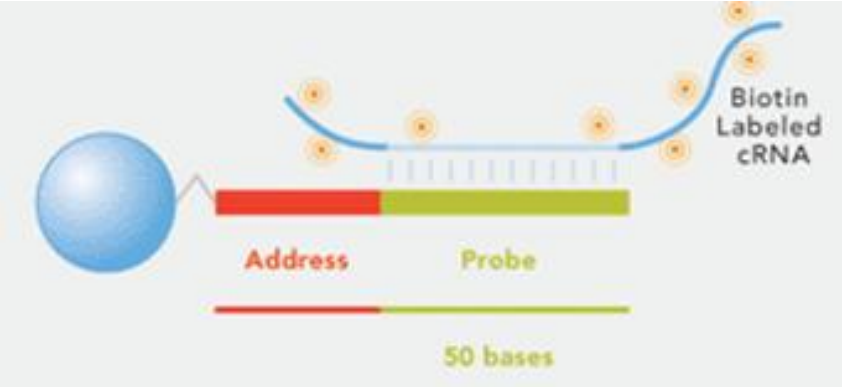

Figure 7.1 An overview of the direct hybridisation assay showing a bead attached to a probe with an address sequence. The probe is hybridised to a biotin labelled cRNA synthesised from the extracted RNA sample (Image taken from Illumina, 2011).

7.4 Results

7.4.1 Generating Transcriptional Profiles

The raw data from the microarray were visualised and analysed using the GenomeStudio Software and entered into Array Track™ for normalisation and analysis. The raw data were normalised to ensure any systematic variation that may interfere with the identification of real gene expression changes was eliminated from the datasets; this was done using the quantile normalisation method. The quantile normalisation method (explained in Bolstad *et al*., 2003) has been seen as the most favourable in comparison to other methods with respect to its speed and the level of bias and variability measured (Bolstad *et al*., 2003). Principal component analysis (PCA) was then carried out on the data set prior to further analysis into gene expression changes.

PCA is a mathematical means of reducing the dimensionality of a dataset that consists of many inter-related variables, while retaining as much of the variation as possible (Jolliffe, 2002). This is done by implementing new sets of variables; i.e. principal

components (PCs), which recognise and form relationships between the key variables in the dataset. In this way, the same level of variability is retained with only a few PC variables, as was present in the many original variables (Jolliffe, 2002). PCs are orthogonal, linear combinations of the original variables, with the first few PCs retaining most the variation of the dataset (Raychaudhuri *et al*., 2000; Jolliffe, 2002). Using PCA enables a simplified visualisation of complex data, such as that generated by microarray investigations, enabling outlier identification and pattern recognition to observe differences within datasets.

Carrying out PCA on the six biological repeats of each experimental condition; i.e. untreated controls and samples treated with 1,000 μg/L arsenite for 24 hours, showed clear differential gene expression patterns for the two experimental conditions, both of which formed distinct clusters. PCA also revealed an outlier amongst the biological repeats for the arsenite treated samples, which was thus excluded from further analysis (Figure 7.2). There was no obvious reason for this sample to be so different from the other test samples. The corrected microarray data were subjected to two filters in order to identify genes that significantly differed in expression; false discovery rate (FDR) of 0.05 and a fold change (FC) cut off of >1.5. This gave a total significant gene list of 2084 genes of which 989 genes were up-regulated and 1095 genes were down-regulated.

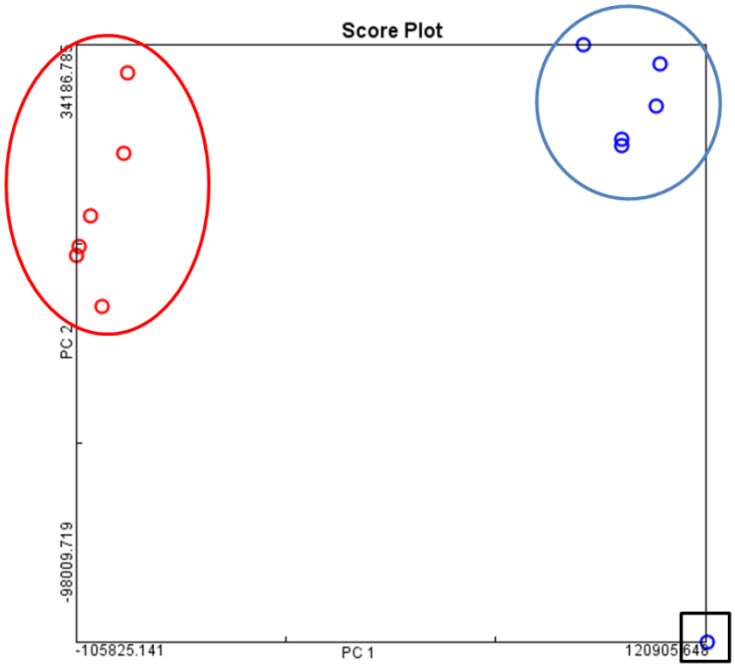

Figure 7.2 PCA of all transcription profiles showing two main clusters; control data highlighted in red and the arsenite treated data highlighted in blue. The black square represents an outlier amongst the arsenite treated data.

7.4.2 Gene expression analysis

7.4.2.1 Arsenite induced differential gene expression

The acquired significant gene list (FDR=0.05 and FC>1.5) with corresponding gene expression fold changes was uploaded to the Ingenuity pathway analysis (IPA) software (Ingenuity® Systems). Gene lists of the ten most significantly up and down-regulated genes in response to the arsenite treatment were identified (Table 7.1 and 7.2 respectively). The ten most significantly up-regulated genes listed in table 7.1 were comprised mainly of the metallothioneins (MTs), with six of the ten genes being MTs. The metallothionein 1X (MT1X) protein coding gene was the most up-regulated with a 15.2 fold increase in expression, followed by metallothionein 1G (MT1G) and metallothionein 1H (MT1H) with a fold change increase of 10.3 and 9.7 respectively.

This indicates the functional importance of metallothioneins in the cellular toxicological response to arsenite exposure.

Symbol	Entrez Gene Name	Fold Change
MT1X	metallothionein 1X	15.2
MT1G	metallothionein 1G	10.3
MT1H	metallothionein 1H	9.7
RASD1	RAS, dexamethasone-induced 1	7.0
MT1M	metallothionein 1M	6.3
MT1F	metallothionein 1F	6.1
GDF15	growth differentiation factor 15	5.2
MT1E	metallothionein 1E	5.1
SLC7A11	solute carrier family 7 (anionic amino acid transporter light chain, xc- system), member 11	5.1

Table 7.1 The 10 most significantly up-regulated genes in response to 24 hour, 1000 µg/L arsenite treatment. The gene list was generated using IPA (FDR=0.05 and FC>1.5).

The most down-regulated gene was regulator of G-protein signalling 4 (RGS4) the expression of which was down-regulated by 8.7 fold (Table 7.2). A significant down-regulation was also observed in the GPCR binding chemokine (C-C motif) ligands 14 and 15 (CCL14 and CCL15 respectively). The expression of CCL14 was found to be decreased by 5.5 fold and the expression of CCL15 by 5.3 fold in response to arsenite exposure.

Symbol	Entrez Gene Name	Fold Change
RGS4	regulator of G-protein signaling 4	-8.7
PLAT	plasminogen activator, tissue	-6.3
CCL14	chemokine (C-C motif) ligand 14	-5.5
EFEMP1	EGF containing fibulin-like extracellular matrix protein 1	-5.5
CCL15	chemokine (C-C motif) ligand 15	-5.3
FAM107A	family with sequence similarity 107, member A	-5.0
CDCA7	cell division cycle associated 7	-4.9
NR2F1	nuclear receptor subfamily 2, group F, member 1	-4.7
KLF2	Kruppel-like factor 2 (lung)	-4.7
CLDN11	claudin 11	-4.7

Table 7.2 The 10 most significantly down-regulated genes in response to 24 hour 1000 μg/L arsenite treatment, gene list obtained using IPA (FDR=0.05 and FC>1.5).

IPA enabled the identification of functional pathways affected by arsenite exposure through the differential transcriptional effects on gene expression. Study of these pathways enables the identification of possible mechanisms leading to arsenite toxicity. With the proposed role of arsenite on oxidative stress, as suggested by other research groups (see section 1.5), the consequence of arsenite on the expression of antioxidant genes was studied (Table 7.3). Interestingly, of the three antioxidant genes affected, two were significantly up-regulated; NAD(P)H dehydrogenase, quinone 1 (NQO1) displayed a 2.3 fold increase and superoxide dismutase 1 (SOD1) a 1.6 fold increase in expression. Interestingly, the gene for the mitochondrial specific antioxidant, superoxide dismutase 2 (SOD2), was down-regulated by 1.7 fold.

7.4.2.2 Arsenite induced gene expression changes in cellular pathways

Research carried out in chapter 4 revealed the effects of arsenite on cell viability and premature senescence. Investigating the impact of arsenite on the genes involved in these pathways would therefore help elucidate the underlying mechanisms leading to these cellular phenotypes. Tables 7.4 and 7.5 list the genes differentially expressed in the IPA pathways termed 'vascular endothelial cell viability' and 'vascular endothelial cell proliferation' respectively. DNA damage-inducible transcript 3 (DDIT3) was the most significantly up-regulated gene in the 'vascular endothelial cell viability' pathway with a 2.3 fold increase in expression and the most down-regulated was the heat shock 70kDa protein (HSPA5) gene which had a 2.9 fold decrease in expression (Table 7.4). Arsenite affected many more genes involved in the 'vascular endothelial cell proliferation pathway', with the up-regulation of seven genes and down-regulation of fifteen genes. The most up-regulated being interleukin 8 (IL8) with a 2.9 fold increase

in gene expression and the most down-regulated being the gene for angiopoietin 2 (ANGPT2) with a 3.1 fold decrease in expression (Table 7.5).

Symbol	Entrez Gene Name	Fold Change
NQO1	NAD(P)H dehydrogenase, quinone 1	2.3
SOD1	Superoxide dismutase 1, soluble	1.6
SOD2	Superoxide dismutase 2, mitochondrial	-1.7

Table 7.3 Transcriptional changes for antioxidant genes observed in response to 24 hour 1000 µg/L arsenite treatment identified using IPA (FDR=0.05 and FC>1.5).

Symbol	Entrez Gene Name	Fold Change
DDIT3	DNA-damage-inducible transcript 3	2.3
LPAR2	lysophosphatidic acid receptor 2	2.0
DAB2	disabled homolog 2, mitogen-responsive phosphoprotein (Drosophila)	1.6
NDP	Norrie disease (pseudoglioma)	-1.6
HSPA5	heat shock 70kDa protein 5 (glucose-regulated protein, 78kDa)	-2.9

Table 7.4 Transcriptional changes for genes involved in vascular endothelial cell viability in response to 24 hour 1000 µg/L arsenite treatment, identified using IPA (FDR=0.05 and FC>1.5).

Symbol	Entrez Gene Name	Fold Change
IL8	interleukin 8	2.9
CDKN1A	cyclin-dependent kinase inhibitor 1A (p21, Cip1)	2.7
MDK	midkine (neurite growth-promoting factor 2)	2.5
LPAR2	lysophosphatidic acid receptor 2	2.0
HIF1A	hypoxia inducible factor 1, alpha subunit (basic helix-loop-helix transcription factor)	1.9
DAB2	disabled homolog 2, mitogen-responsive phosphoprotein (Drosophila)	1.6
PTPN1	protein tyrosine phosphatase, non-receptor type 1	1.6
KDR	kinase insert domain receptor (a type III receptor tyrosine kinase)	-1.6
RGS5	regulator of G-protein signaling 5	-1.6
NDP	Norrie disease (pseudoglioma)	-1.6
ANG	angiogenin, ribonuclease, RNase A family, 5	-1.7
COL18A1	collagen, type XVIII, alpha 1	-1.7
SKP2	S-phase kinase-associated protein 2, E3 ubiquitin protein ligase	-1.8
SEMA6B	sema domain, transmembrane domain (TM), and cytoplasmic domain, (semaphorin) 6B	-1.8
KLK3	kallikrein-related peptidase 3	-1.9
FABP4	fatty acid binding protein 4, adipocyte	-1.9
TNFRSF6B	tumor necrosis factor receptor superfamily, member 6b, decoy	-2.3
NRP1	neuropilin 1	-2.3
ENG	endoglin	-2.4
THBS1	thrombospondin 1	-2.6

Table 7.5 continued

DKK1	**dickkopf 1 homolog (Xenopus laevis)**	**-3.0**
ANGPT2	angiopoietin 2	-3.1

Table 7.5 Transcriptional changes for genes involved in vascular endothelial cell proliferation in response to 24 hour 1000 μg/L arsenite treatment, identified using IPA (FDR=0.05 and FC>1.5).

7.4.3 Molecular pathway analysis

Carrying out molecular pathway analysis is important to begin to understand how individual gene expression changes combine to contribute to the pathophysiology of diseases and toxic mechanisms. Through IPA, genes were arranged into networks that were made up of specific pathways related to biological functions and diseases (Table 7.6). The networks were organised in order of significance through a scoring system. The scores were derived using the Fisher exact test, which reflected that the assignment of genes to groups was not due to chance alone. The networks were ranked in order of score, with the highest score representing the network that contains the most statistical significant interconnected genes (Nakou *et al*., 2010).

The fifteen most significant networks identified were listed in table 7.6. The diseases most significantly associated with arsenite exposure were cancer and CVD, in close agreement with epidemiological evidence in human studies (see section 1.2). The biological processes most frequently listed were the ones involved in cell viability, genome maintenance i.e. DNA damage repair and recombination processes, and the cell cycle; the interactions between the genes involved in these biological processes are illustrated in a gene-signalling map (Figure 7.3). The map illustrates an overall down-regulation (green) of these processes through high number of genes that have decreased

expression in response to arsenite. Interestingly, a large proportion of gene expression changes showed a connection to histone H3, an important component of the nucleosome which packages DNA in eukaryotic cells. Since epigenetic modifications at the histone N-terminal tails are crucial for modulating gene expression (Zhou *et al*., 2008), altering these modifications poses as a potential mechanism by which arsenite brings about its differential gene expression effects.

The effects of gene expression changes on signalling pathways involved in specific biological functions such as response to 'cellular stress and injury' (Figure 7.4), 'cellular growth, proliferation and development' (Figure 7.5) and 'toxicological response' (Figure 7.6) were also determined using IPA, giving a detailed account of the number of genes up and down-regulated for all the pathways affected within each biological network. The pathways involved in the response network for 'cellular stress and injury' and 'toxicity response' were examined to further understand the mechanisms underlying arsenite induced cytotoxicity in endothelial cells.

The pathways with the highest number of genes affected for both of these networks are those involved in the cellular response to stress. The 'cellular stress and injury' network shows the p38 MAP kinase (MAPK) signalling pathway to have the highest number of genes affected, with ~65% of the affected genes being up-regulated (Figure 7.4). Similarly for the 'toxicological response' network, the NF-E2 related factor-2 (NRF2)-mediated oxidative stress response pathway appears to have the highest number of genes affected, with ~72% of these up-regulated (Figure 7.6). Since the MAPK signalling pathway is involved in managing cellular stresses such as inflammation, DNA damage and oxidative stress, together with the NRF2-mediated oxidative stress

response pathway, the overall up-regulation of these pathways gives an insight into the impact arsenite has on the cell. Additionally, the overall down-regulation of some of the DNA damage response pathways (Figure 7.4) and the cell cycle DNA damage checkpoint regulation pathways (Figure 7.6) imply the induction of DNA damage as a toxic response of arsenite.

The pathways involved in the 'cell growth, proliferation and development' networks (Figure 7.5) were used to give an insight into the mechanisms of arsenite-induced premature senescence, which was observed in chapter 4. The mammalian target of rapamycin (mTOR) signalling and the P13K/AKT (serine-threonine kinase) signalling pathways were both found to be largely up-regulated, while the insulin-like growth factor (IGF-1) signalling pathway showed an overall down-regulated in response to arsenite.

ID	Genes in Network	Score	Top Functions
1	ABL2,ADNP,ARID1A,CCNE2,CDKN1A,EXO1,FH,HOXA5,IMPDH2,KIAA0101,LDHA,LTBP2,MKI67,MKI67IP,MTHFD2,MXI1,MYCN,NCL,PRPF19,RB1CC1,RNF144B,RRM1,RRM2,RRM2B,SIVA1,SLC29A1,SNORD3A,SNRPG,SPHK2,STMN1,SYNM,TIP60,TP53INP1,USP11,ZBTB17	31	Cancer, Reproductive System Disease, Nucleic Acid Metabolism
2	AADAC,ATP2A2,CTSB,DAB2,DHRS3,DUSP3,DVL3,FBXL13,FILIP1L,FSH,GK,GOT1,HBP1,LAMB3,Lh,LRRFIP2,MCOLN1,MGEA5,MSMO1,MT1X,MYCT1,PDLIM3,PMAIP1,POP5,PFIA4,PPIH,PPRC1,RAB5C,RGS5,SIGIRR,TFPI2,TK1,TM6SF1,TUBA1A,UBR4	29	Cancer, Reproductive System Disease, Carbohydrate Metabolism
3	ASNS,ATF3,ATF4,C1QBP,C20orf111,CDCA5,CTH,DDIT3,EGR1,ERK,GADD45B,GARS,GDF15,Hdac,HLX,IFRD1,KDM5B,KLF6,MAP2K1/2,MIR155HG,MKNK2,MT1E,MT1F,MT1H,NDRG1,NDRG4,PAQR3,PCK2,PHF15,PSPH,RGS4,SCD,SPTSSA,STC2,TRIB3	27	Digestive System Development and Function, Endocrine System Development and Function, Organ Morphology
4	ADD3,ADRB2,ASF1B,BTG3,CD24,Ctbp,CXCR7,ERMAP,Histone h3,Histone h4,HOXA9,JMJD1C,KIF4A,KIFC1,LPP,MBNL1,MT1G,MTUS1,NCAPD2,NCAPG,OSGIN1,PALLD,PPP2R2B,PRC1,RACGAP1,RPS6KA3,RUNX1T1,SBF1,SLC30A1,SMC4,SPTA1,TM4SF18,TUFT1,TYMS,UBB	27	DNA Replication, Recombination, and Repair, Cellular Assembly and Organization, Cell Cycle
5	ABCA1,ARHGAP28,CXCL16,ECE1,ERAP2,FABP4,GNL3L,HDL,IL1,IL33,IRAK1,IRAK2,KSR2,LDB2,LDL,MICU1,MLKL,NFkB (complex),NOP14,NOS3,OPTN,PELI1,PELI2,PLIN2,RIOK3,RIPK2,RNF11,RUSC2,SCARB1,ST3GAL1,TAX1BP1,TJP2,TNFSF18,TRIM8,WDR34	25	Cardiovascular Disease, Organismal Injury and Abnormalities, Lipid Metabolism
6	Actin,FBL,GBP1,GBP4,HERC5,HIP1R,ICMT,IFI6,IFI27,IFITM1,IL7R,IRF9,KIAA0430,MAP1B,MICAL1,NFE2L3,NME1,NOP56,NOP58,PA2G4,PABPN1,PDXP,PECAM1,Rb,RIOK1,SEMA3A,STK38,TCR,USP18	25	RNA Post-Transcriptional Modification, Post-Translational Modification, Protein Folding
7	APH1B,CALD1,CAPRIN1,CDH11,COL13A1,COL4A1,COL4A5,Creb,DCHS1,DHCR7,EMP1,estrogen receptor,FABP5,FASN,HMGCR,HNRPDL,HSP90AA1,HSPA1A/HSPA1B,IFI35,IgG,JAG1,JUP,KRT15,KRT19,LDLR,NR5A2,NT5E,PCDH7,PCDH10,PCDH19,PSEN1,PTPRF,Secretase gamma,TACSTD2,TNPO1	25	Cancer, Lipid Metabolism, Small Molecule Biochemistry
8	ACVR1,ADAMTS1,BDNF,BMP4,CYR61,DKK1,DLL3,Eotaxin,ERK1/2,GATA2,HEY1,IGF2R,IL1RL1,ITGA5,ITGB3,KDR,LIMS1,LRP5,NEU1,NOTCH4,Notch,NR2F2,NRP1,PFKFB4,PROCR,PTGER4,PTPRE,RAB4B,S1PR1,SFRP1,SMAD1/5,SMOOTH MUSCLE ACTIN,SULF2,TIMP2,TSPYL2	24	Cardiovascular System Development and Function, Organismal Development, Cellular Development

Table 7.6 continued

ID	Genes in Network	Score	Top Functions
9	Proteasome,ADRM1,AURKB,BIRC5,BNIP3,C1QTNF5,CCNG2,CDC42EP3,CDCA8,CYLD,DYNLL1,FBXO32,Fcer1,FOXO3,GMNN,H6PD,IER3,IKBKG,LMNB2,MAP1LC3B,MCM3,MCM4,MCM5,MCM6,MCM7,mir	24	Cancer, Cell Cycle, DNA Replication, Recombination, and Repair
10	AKAP12,ATP6V0C,CHKA,CTPS1,Cyclin E,DLEU1,E2F2,E2f,FAM53C,FHL2,Gamma tubulin,HIF1A,HINFP,HIST1H2BJ/HIST1H2BK,HIST1H4A,HTATIP2,KIF15,MCM10,NASP,NOX4,NUDCD2,NUSAP1,OIP5,PLK4,POLA1,Ppp2c,PTTG1,RUVBL1,SESN2,SKA2,TPX2,TTK,TUBB2A,TUBG1,Vegf	24	Cell Cycle, DNA Replication, Recombination, and Repair, Infectious Disease
11	APC(complex),Cbp/p300,CCNA1,CCNF,CDC20,CDC25B,CDK1,CDT1,CKS1B,CSNK2A1,Cyclin A,Cyclin B,FBXO5,FEN1,FOXM1,FST,GTSE1,HSPB1,HSPB8,IGFBP3,IGFBP4,IGFBP6,ITPR1,LYVE1,MAD2L1,MAD2L1BP,N-cor,P38MAPK,PBK,RANBP1,RND3,SKP2,TRIB1,UBE2C,ULK1	22	Cancer, Cell Cycle, Reproductive System Disease
12	ABCE1,ADORA2A,Akt,ANGPT2,Calcineurin protein(s),Cg,DUSP6,EDNRB,ENG,FOXC2,GABBR2,HTRA1,ITGA6,ITGB4,KITLG,KLHL21,LYAR,Mapk,MDK,Mek,mir-21,NDP,OSBPL8,PDGFBB,PIK3CG,PIK3IP1,PLAT,PPAT,PUS7,PYCARD,RGS2,SPRY1,TPM1,VEGFC,ZYX	22	Cardiovascular System Development and Function, Cellular Movement, Organismal Development
13	AMD1,ANPEP,BCR(complex),caspase,CNA2,CD3,CEL,CHTF18,CLIP1,CXCR4,DNMT1,FTH1,GADD45A,GBP2 (includes EG:14468),GRN,Igm,IKK (complex),JUND,KLF9,LIG1,LPXN,MRAS,MSRB2,PARP1,PARP2,PCNA,PINK1,PLK2,Rap1,RIN1,SAT1,SERPINB2,TFDP1,TFRC,USP1	22	DNA Replication, Recombination, and Repair, Cancer, Cell Cycle
14	14-3-ANG,ASB9,ASGR1,CASP6,Caspase3/7,CDC25A,CKB,CTGF,DNAJB1,DPP3,DUSP16,HCLS1,HMGB2,Hsp27,Hsp70,Hsp90,HSPA8,Jnk,KLF2,MAP1LC3A,MAP3K3,MAP3K5,NADPH oxidase,NQO1,NRG1,PARD6A,PIM1,SPHK1,SQSTM1,TP53BP2,TRA2B,TRIAP1,UCHL1,YWHAH	20	Cell Death and Survival, Protein Synthesis, Cardiovascular System Development and Function
15	Actin,AKAP8L,ANTXR1,APOL3,ASCC2,CAP2,CD34,CD46,COL18A1,DDX58,DHX9,GEMIN4,IFN Beta,IL12(complex),Immunoglobulin,INSIG1,Interferon alpha,KLF11,MAFF,PNP,Rac,RAD51AP1,RELB,RNA polymerase II,SOD2,SPOCK1,TBC1D10A,TICAM1,TNFRSF1B,TRIM25,TRIOBP,TRIP4,TXNRD1,TYMP,WDR36	20	Organ Morphology, Cell Signaling, Small Molecule Biochemistry

Table 7.6 The 15 most significant networks determined using IPA for biological functions affected by 24 hours treatment with 1000 µg/L arsenite (FDR=0.05 and FC>1.5).

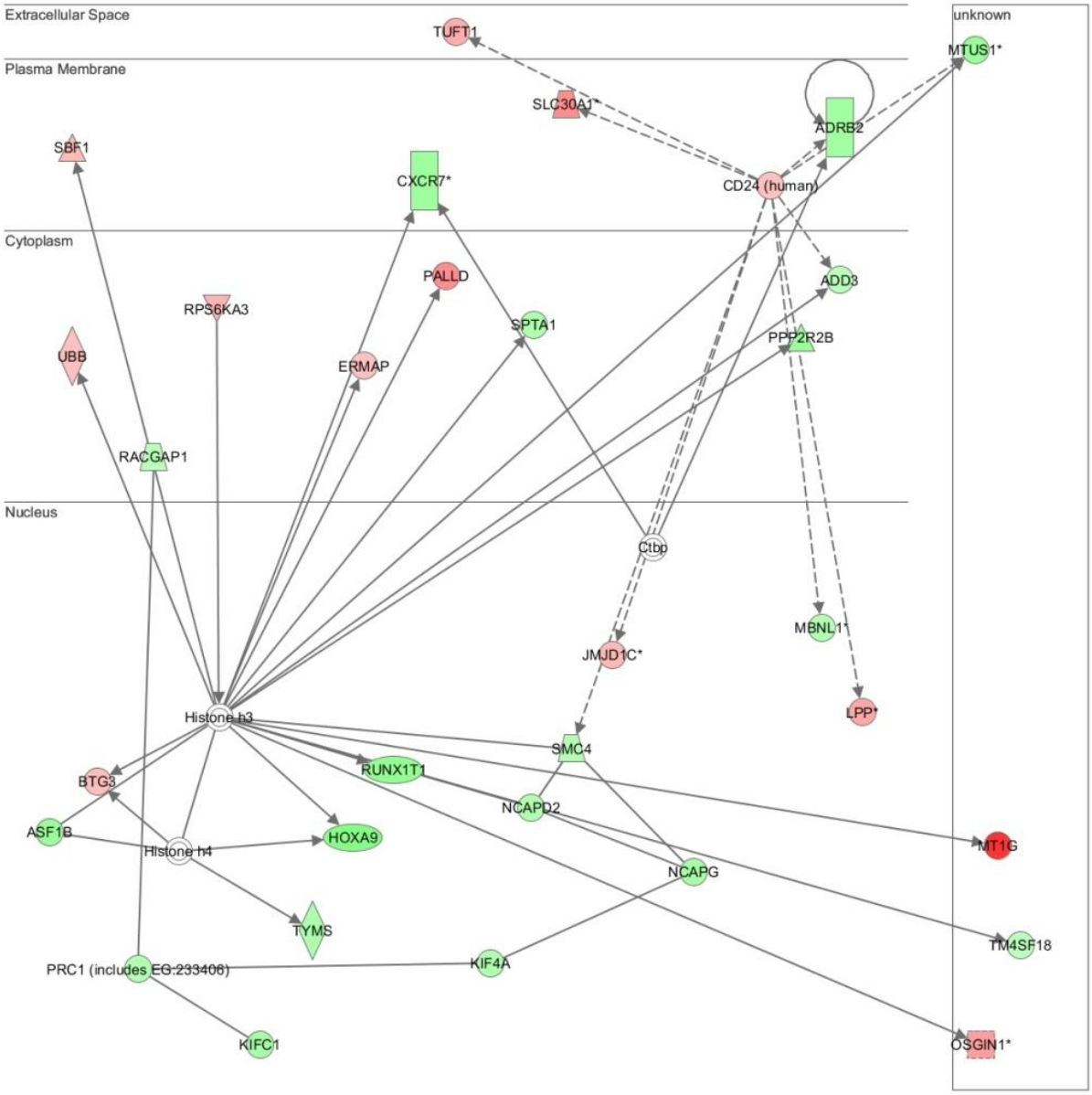

Figure 7.3 Gene-signalling map showing direct (unbroken lines) and indirect (broken lines) relationships between genes involved in DNA replication, recombination and repair and cellular assembly, organisation and cycle. Genes illustrated in green represents down-regulation and red represents up-regulation of gene expression.

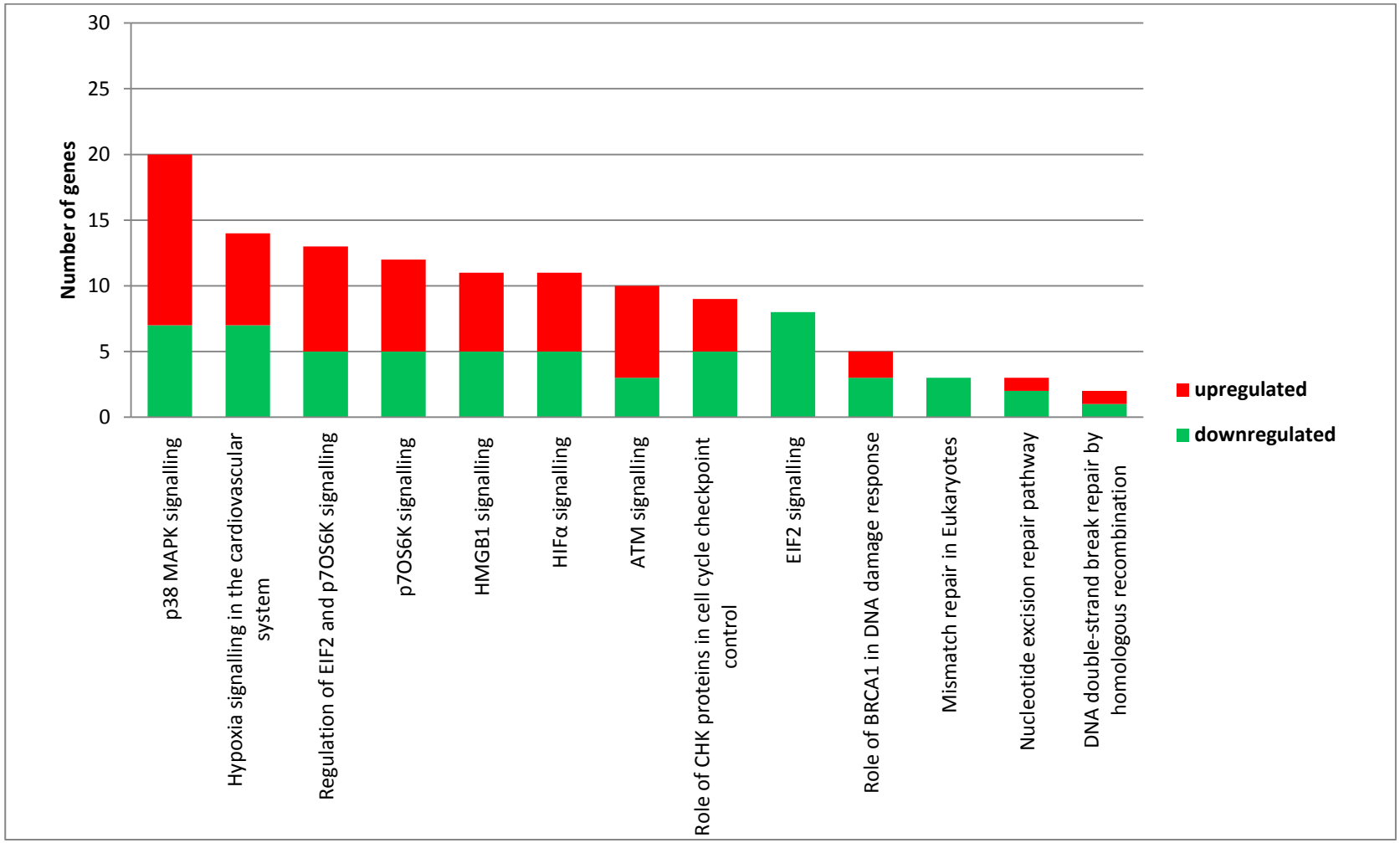

Figure 7.4 Gene expression changes in several pathways involved in the 'cellular stress and injury' response. HUVECs were treated for 24 hour with 1000 µg/L arsenite and gene-expression was analysed by microarray (FDR=0.05 and FC>1.5). The functional categorisation of genes and pathways was performed in IPA.

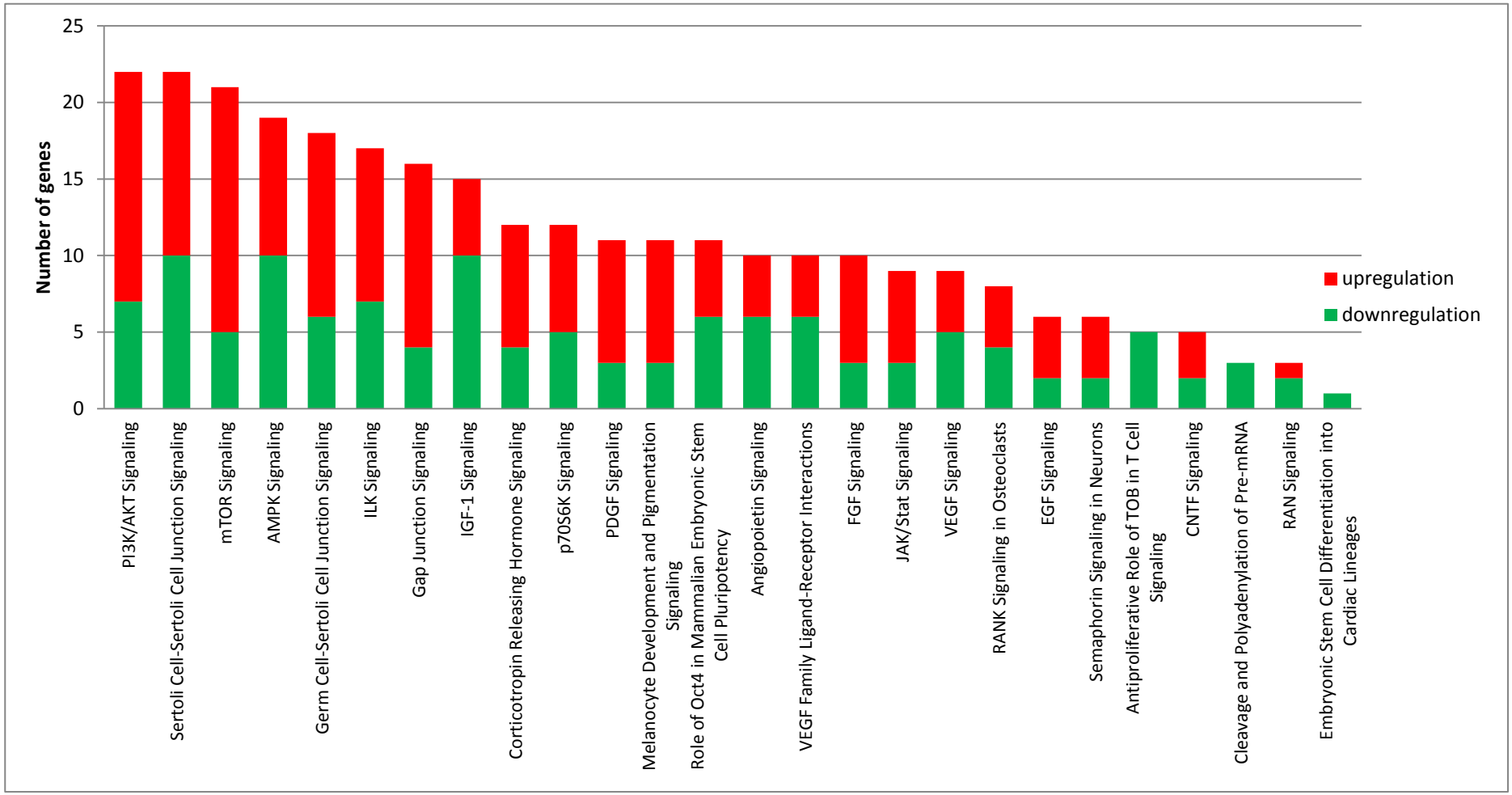

Figure 7.5 Gene expression changes in several pathways involved in the 'cellular growth, proliferation and development' response. HUVECs were treated for 24 hour with 1000 µg/L arsenite and gene-expression was analysed by microarray (FDR=0.05 and FC>1.5). The functional categorisation of genes and pathways was performed in IPA.

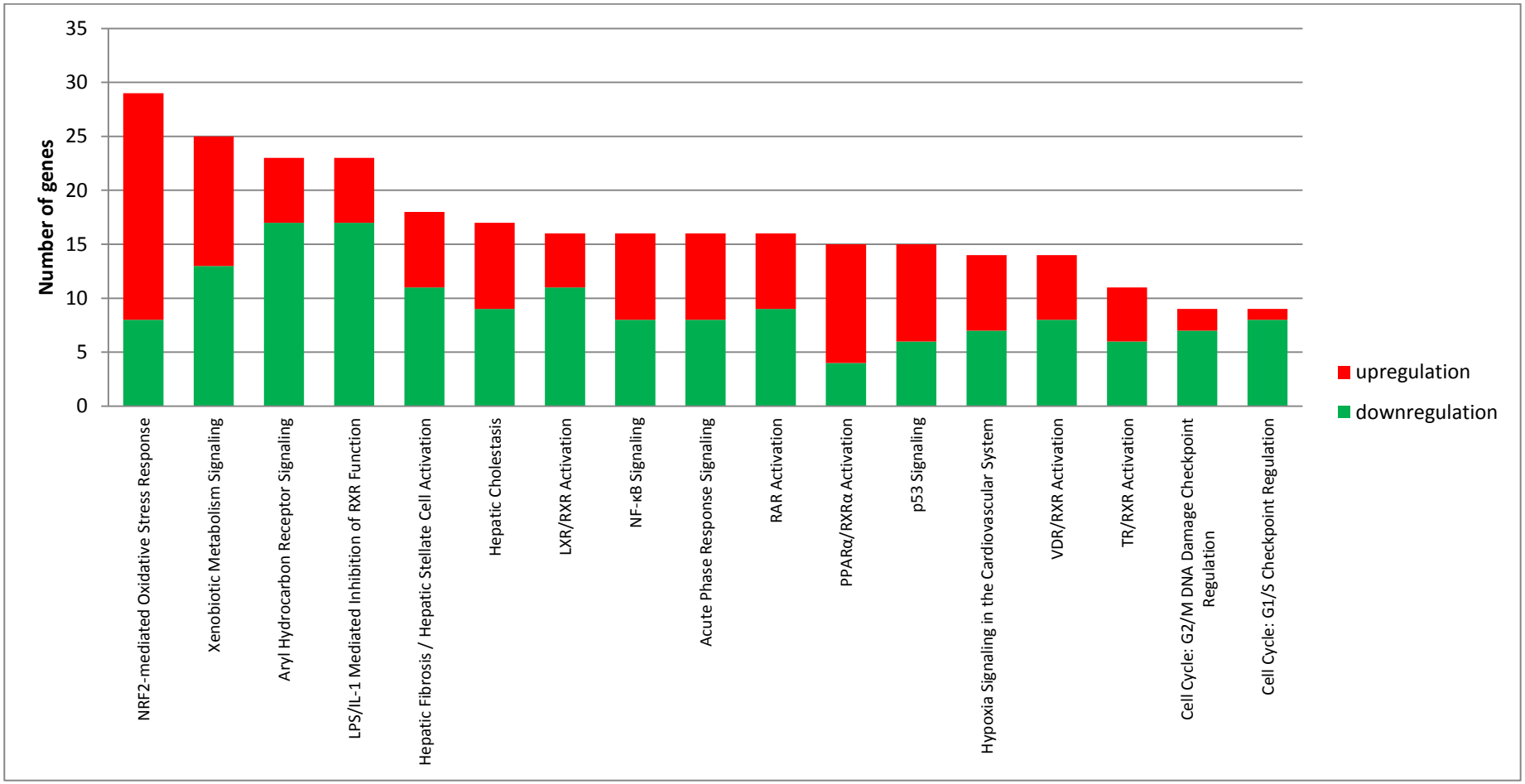

Figure 7.6 Gene expression changes in several pathways involved in the 'toxicological response'. HUVECs were treated for 24 hour with 1000 µg/L arsenite and gene-expression was analysed by microarray (FDR=0.05 and FC>1.5). The functional categorisation of genes and pathways was performed in IPA.

7.5 Discussion

The results presented in this chapter focussed on the effects of a non-lethal concentration of arsenite on HUVECs in order to suggest early targets/ pathways by which arsenite promotes endothelial cell dysfunction which may subsequently lead to CVD development and/or progression. Using the IPA platform for the analysis of the transcriptional expression profile data, the impact of arsenite on the expression of specific genes as well as the analysis of pathway responses was possible. These results are discussed further in sections 7.5.1 and 7.5.2.

The original hypothesis for this thesis suggested arsenite to induce oxidative stress in endothelial cells, by targeting mitochondria, resulting in intracellular oxidative damage and the onset of premature senescence. The proposed role for mitochondria as primary targets of arsenite can now be rejected after observing the results in chapter 6. In this chapter studying the genes and pathways most affected in response to arsenite *in vitro* has enabled the generation of a new hypothesis, which indicates arsenite-mediated toxicity to occur via non-mitochondrial oxidative stress, resulting in the onset of stress-induced premature senescence (SIPS) in endothelial cells.

7.5.1 Gene expression analysis

7.5.1.1 Metallothionein gene family up-regulation

Of the up-regulated genes, the most striking up-regulation of the MTs can be rationalised in terms of the toxic nature of arsenite and the functions of MTs in cells. MTs have been shown to maintain metal ion homeostasis in cells as well as carrying out metal detoxification (Sutherland *et al*., 2010). MTs are proteins containing several

cysteine residues with two thiol-rich metal binding domains (Babula *et al*., 2012). They have a high affinity for binding to the monovalent and divalent periodic table group 11 and 12 metals respectively, particularly Zn^{2+}. Therefore, MTs are predominantly found in cells as Zn-MT species (Sutherland and Stillman, 2011). Despite arsenite (As^{3+}) being suggested to bind to MTs with a slower rate than the group 11 and 12 metals (Ngu and Stillman, 2006), the extent of up-regulation of MT genes in table 7.1 suggests the MT gene-family to be substantially involved in the responsiveness of HUVECs to arsenite exposure at least *in vitro*. As the known mechanisms of arsenite detoxification in the human body involve thiol-based proteins (DeMel *et al*., 2004), the significant increase in expression of cysteine-rich MTs as an immediate response, suggests their possible involvement in arsenite metabolism (Ngu *et al*., 2008). Ngu e*t al* (2008) found that with the two-domain structure of MTs, they can bind to As^{3+} at a faster rate than they previously reported (Ngu and Stillman, 2006). With the ability of binding six As^{3+} ions per MT protein, MTs prove efficient scavengers of As^{3+}, thus supporting the up-regulation of MTs as an initial response to arsenite exposure.

Furthermore, MTs also have an important role in cellular protection against oxidative damage, particularly when bound to Zn. MTs are found in the cytosol and within cellular organelles but predominately in mitochondria (Sutherland and Stillman, 2011), which is believed to be the main source of ROS generation in many cell types. ROS such as H_2O_2 bind to the Zn-MT complexes resulting in the release of Zn^{2+}, which goes on to initiate further MT expression (Zhang *et al*., 2003). Therefore, the increased generation of ROS leads to an increased expression of MTs as an oxidative stress response. Despite MTs being recognised as antioxidants, the exact mechanism through which they bring about their protective effects is still unknown (Babula *et al*., 2012),

however *in vitro* investigations have shown the level of MTs to increase in response to H_2O_2 (Kling and Olsson, 2000) and a role for MTs as hydroxyl radical scavengers has been described (Thornalley and Vasak, 1985). Together, these findings allude to arsenite inducing oxidative stress in endothelial cells as a mechanism of toxicity, which would be counteracted by the antioxidant properties of MTs that are expressed as a result of Zn^{2+} displacement by ROS.

Moreover, section 7.5.1.2 discusses the effects of arsenite on cellular pathways and gene expression changes that indicate an increase in oxidative stress. Despite the lack of evidence for direct increases in ROS by arsenite in chapter 4, this further supports the ROS-mediated increase in MT expression.

7.5.1.2 Effect of arsenite on oxidative stress and inflammation

HUVECs treated with arsenite showed a significant up-regulation in the expression of cytoplasmic antioxidants NQO1 and SOD1, indicating an increase in ROS generation as an arsenite response. The increase in the antioxidant gene expression may be as a result of the NRF2- mediated oxidative stress response pathway which is also shown to be partly up-regulated. Activation of the transcription factor NRF2 in response to arsenite has been seen previously in a number of cell types, e.g. bladder urothelial cells (Wang *et al*., 2007), keratinocytes (Pi *et al*., 2003), and placental choriocarcinoma cells (Massrieh *et al*., 2006). Arsenite has also been shown to evoke a NRF2 signalling pathway-mediated antioxidant response in the human bladder urothelium cell line (UROtsa cells). Interestingly, 4 hour exposure to 2,600 μg/L arsenite resulted in the increase in the NRF2 half-life from 9 minutes to 19 minutes, furthermore, 16 hours

exposure to 1,300 µg/L arsenite revealed an increase in the expression of antioxidants NQO1 and HO-1 (Wang *et al*., 2008).

The activation of NRF2 occurs as a result of an increase in electrophiles, oxidative stress or inflammation (Osburn and Kensler, 2008), which in turn regulates the gene expression of antioxidants, maintaining the cellular redox balance (Hybertson *et al*., 2011). Since the gene expression of NQO1 and SOD1 are induced by NRF2 (Venugopal and Jaiswal, 1996; Dreger *et al*., 2009), the increase in this cellular protective pathway supports the apparent increase in arsenite mediated cellular ROS. An increase in ROS generation was not observed in this thesis either through detection of superoxide (total cellular and mitochondrial) or H_2O_2. This may be due to the redox balance being rapidly restored by the antioxidant activity or the inherent lack of sensitivity of the ROS reporters used.

Oxidative stress can lead to endothelial dysfunction, one of the primary events in the pathogenesis of atherosclerosis (Victor *et al*., 2009). It can also lead to an increase in inflammation through the increased secretion of interleukin 8 (IL8), such an increase (~3-fold) was seen in this study. IL8 is a proinflammatory chemokine which is present at very low levels under normal circumstances, but in response to stress its secretion rapidly increases (Hoffman *et al*., 2002). IL8 goes on to bring about an inflammatory response by activating and causing accumulation of neutrophils (Baggiolini and Clark-Lewis, 1992). This observation is supported by the overall up-regulation of the p38 MAPK signalling pathway, which responds to stress and inflammatory stimuli and has been found to be activated in inflammatory diseases (Herlaar and Brown, 1999).

Furthermore, the increase in expression of the lysophosphatidic acid receptor 2 (LPAR2) also indicates a cellular inflammatory response to arsenite. LPAR2 is a GPCR that binds to lysophosphatidic acid (LPA), a signalling molecule that has been associated with endothelial dysfunction, LDL uptake and monocyte recruitment and adhesion (Lin *et al*., 2010), thus an up-regulation in LPAR2 can lead to an increase in LPA binding. Of the many LPA binding receptors, a study carried out on LPAR1/LPAR2 double knock-out mice showed the specific involvement of these receptors in the pathogenesis of atherosclerosis (Panchatcharam *et al*., 2008). The regulation of such inflammatory diseases involves transcription factors such as NRF2 which, as well as oxidative stress, also control inflammatory gene expression (Liu *et al*. 2010). Therefore the increase seen in the NRF2-mediated response pathway further supports the possible increase in oxidative stress and inflammation in response to arsenite, as a mechanism of atherosclerosis development.

7.5.1.3 Arsenite mediated effects on GPCR signalling

Of the top ten down-regulated genes, the expression of the regulator of G-protein signalling 4 (RGS4) was the most significantly affected in response to arsenite. This is an interesting outcome, given the importance of RGS4 in the cardiovascular system. G-proteins are important signal transducers coupled to specific receptors; GPCRs. These receptors play a vital role in our physiological response to external and internal stimuli, therefore enabling communication between intracellular and extracellular environments (Rosenbaum *et al*., 2009). The binding of ligands to GPCRs activates the G-proteins that go on to bind effector proteins and cause a cascade of downstream effects (Rosenbaum *et al*., 2009).

In the cardiovascular system, GPCRs are involved in the regulation of many processes such as contractility of the heart, the heart rate and vascular tone (Tang and Insel, 2004). GPCRs are substantially involved in the stimulation of vasoconstriction, i.e. angiotensin II AT_1, endothelin-1 ET_A receptors, α_1 and α_2-adrenoceptors (Maguire and Davenport, 2005), and vasodilation through G-protein signalling in endothelial i.e. muscarinic M_1 and M_3 receptors, and vascular muscle cells i.e. β-adrenoceptors (Hendriks-Balk *et al*., 2008). Consequently, abnormal levels of GPCR signalling have been linked to the development of cardiovascular complications.

RGS proteins have the important role of assisting the deactivation of G-proteins to prevent the over stimulation of effector proteins (Gu *et al*., 2009). RGS are crucial in cardiovascular homeostasis (Heximer, 2012) and RGS4 has been suggested to have a protective role in CVD. This has been specifically seen in hypertrophic mouse models where over-expression of RGS4 prevented cellular growth and myofilament organisation in neonatal cardiac myocytes (Tamirisa *et al*., 1999), preventing the onset of a hypertrophic phenotype mouse hearts in response to pressure overload by transverse aortic constriction (Rogers *et al*. 1999). The increase in RGS4 expression was also seen in the failing left ventricular myocardium of human hearts as a potential protective mechanism (Mittmann *et al*., 2002).

Therefore, the down regulation of RGS4 expression observed here in endothelial cells suggests that arsenite exposure renders cells (i.e. cardiac myocytes) more sensitive to G-protein mediated damage through the over stimulation of effector proteins. With the onset of endothelial dysfunction seen in experimentally-induced myocardial hypertrophy (MacCarthy *et al*., 2000; MacCarthy *et al*., 2001) and the important role the

endothelium plays in cardiac myocyte function, particularly through the production of NO (Tirziu and Simons, 2008), arsenite-mediated effects on endothelial cells also may be indirectly involved in the pathophysiology of hypertrophy.

The link of arsenite with hypertrophy is further supported by a study carried out on mice that showed chronic consumption of arsenite contaminated drinking water gave rise to hypertrophy and hypertension (Sanchez-Soria *et al*., 2012). Signs of left ventricular hypertrophy have also been detected in individuals from Bangladesh that were exposed to arsenic. This was assessed using electrocardiography, which also showed signs of ischemic heart disease amongst other cardiovascular abnormalities (Ahmad *et al*., 2006).

Two members of the chemokine family are also significantly down-regulated in response to arsenite; CCL14 and CCL15. Since chemokines function as ligands for GPCRs, this is surprising and inconsistent in comparison with the cardiovascular outcomes potentially associated with the down-regulation of RGS4. The levels of chemokines are generally up-regulated in cardiovascular dysfunction (Tarzami, 2011); a predictable outcome given the function of chemokines in leukocyte activation. Chemokines can be seen to contribute to atherogenesis as atherosclerotic plaques involve the accumulation of leukocytes and lipids at the innermost layer of the blood vessel wall. However, chemokines have also been suggested to have inhibitory roles in atherogenesis, depending on the receptors they target (reviewed in Wan and Murphy, 2012). Thus, the down-regulation of CCL14 and CCL15 in response to arsenite may suggest these specific chemokines as having inhibitory role in the process of

atherogenesis, therefore down-regulation in their expression would decrease the inhibitory signals for atherogenesis.

7.5.1.4 Transcriptional response indicating changes in to cell viability

Observing the transcriptional changes for specific genes i.e. DNA-damage-inducible transcript 3 (DDIT3) and heat shock 70kDa protein 5 (HSPA5) revealed the involvement of the endoplasmic reticulum (ER) in arsenite induced apoptosis. The ER has an important role in protein folding and protein secretion, malfunctions in which trigger the unfolded protein response (UPR) to restore normal ER function (Scull and Tabas, 2011). The significant down regulation of HSPA5, which is involved in the accurate folding of proteins (Lee, 2005), may lead to ER stress.

DDIT3 is involved in the UPR to ER stress in endothelial cells, observed as a result of atherosclerosis-promoting factors such as modified LDL (Civelek *et al*., 2009). Therefore it can be hypothesised that the transcriptional change in DDIT3 plays a role via ER stress in arsenite mediated atherosclerosis.

Arsenite seems to trigger an apoptotic response through the down-regulation of HSPA5 which has anti-apoptotic properties (Lee, 2005) and the up-regulation of DDIT3 which is proapoptotic (Scull and Tabas, 2011). Endothelial cells having undergone apoptosis are associated with atherosclerosis progression as they have shown to manifest procoagulant activity; inducing thrombogenesis, (Bombeli *et al*., 1997) and becoming proadhesive to the binding of platelets, further contributing to the thrombotic pathology (Bombeli *et al*., 1999). The up-regulation of hypoxia-inducible factor-1α (HIF1A) indicates apoptotic responses. Lida *et al* (2002) investigated the effects of transfecting

the HIF1A gene into endothelial cells, with apoptosis as one of the cellular outcomes, along with a decrease in the expression of the anti-apoptotic gene, BCL2. The implicated role of arsenite in inducing endothelial cell apoptosis would hence contribute in the progression of atherosclerosis.

The study carried out by Lida *et al* (2002) also saw cellular senescence, reduced cell proliferation, cycle arrest and an increase in the expression of CDKN1A (also known as P21) in the HIF1A transfected endothelial cells. CDKN1A is shown to be up-regulated in SIPS in endothelial cells (Oh *et al*., 2001) and in other cell types (Li, 2009). Thus the up-regulation in CDKN1A seen here indicates is consistent with the onset of SIPS in response to arsenite, supporting the findings in chapter 4. Although not studied to date, arsenite could contribute to cardiovascular complications, particularly atherosclerosis through the induction of SIPS. Aged endothelial cells can result in the onset of endothelial dysfunction as a result of impaired NO production (Erusalimsky, 2009) and senescent endothelial cells have been observed in atherosclerotic plaques of humans (Burrig, 1991). Since endothelial dysfunction is seen to be one of the earliest events in the occurrence of atherosclerosis, arsenite mediated SIPS could be a possible initiator of arsenite induced atherosclerosis, although this requires further investigation.

7.5.1.5 Role of arsenite in epigenetic modifications

The gene signalling map showed a visual representation of the interactions between the genes involved in DNA replication, recombination and repair and cellular assembly, organisation and cycle, with the effects of arsenite on their expression. A large proportion of the differentially expressed genes, interestingly, revealed a link back to histone H3. Literature published on the mechanisms by which arsenite brings about

gene expression changes has found epigenetic alterations as one of the proposed mechanisms. Changes to the DNA methylation status of the genome has been seen to occur in arsenite induced carcinogenesis, with hypomethylation resulting in over-expression of certain genes (Marsit *et al*., 2006) and hypermethylation leading to gene silencing (Reichard *et al*., 2007).

In addition to altering the methylation status of DNA, arsenite has also been seen to affect the methylation patterns of histone N-terminal tails, specifically at histone H3 (Zhou *et al*., 2008). The 'histone code' hypothesis predicts that each histone tail has a specific post-translational modification; these modifications together or individually control the transcriptionally active or inactive state of gene expression (Jenuwein and Allis, 2001). Arsenite has been found to affect the extent of methylation at the tails of histone H3 in human lung carcinoma A549 cells, resulting in an increase in dimethylation at the tail H3K9 and a decrease in trimethylation at H2K27, both of which would result in gene silencing. Moreover, increased trimethylation at H3K4 was also observed, which would result in transcriptional activation (Zhou *et al*., 2008). These observations suggesting histone H3 as a specific target of arsenite, giving an insight into the role of epigenetics in the mechanism by which arsenite brings about the gene expression changes observed in the HUVECs.

7.5.2 Pathway analysis

IPA gives an accurate overview of the up-to-date cellular pathways and gene-signalling networks affected by disease and exposure to toxins *in vivo* and *in vitro*. This proved interesting for arsenite, with the data also revealing the possible mechanisms involved

in bringing about the cytotoxic effects of arsenite in endothelial cells. The fifteen most significantly affected gene networks by arsenite treatment were deduced, which gave information on the cellular functions that would be affected as a result of the transcriptional changes and the potential impact they would have on disease development, should the work on a single cell type *in vitro* translate to *in vivo*.

Despite the limitations of extrapolating data generated from the artificial environment of *in vitro* to *in vivo* situations, *in vitro* studies can still prove very informative, with a high level of accuracy for this translation. This is shown in the pathway analysis of the transcriptomics data. Of the 15 most significantly affected networks identified after arsenite exposure, cancer networks were the most affected. Furthermore, an overall up-regulation of the PI3K/AKT signalling pathway was observed. The PI3K/AKT signalling pathway has the important role of modulating the cell cycle, cellular survival and cellular growth pathways (Fresno Vara *et al*., 2004), therefore, alterations in this signalling pathway have been associated with human cancers. Increases in the PI3K gene has been found in cervical and ovarian cancer (Shayesteh *et al*., 1999; Ma *et al*., 2000) and increases in the expression of the AKT gene has been associated with cancers such as ovarian and breast cancer (Bellacosa *et al*., 1995). Since arsenite has been identified as a group 1 carcinogen (IARC, 2012), with cancer being the most prevalent disease group linked to arsenic exposure in humans, these finding are very consistent with *in vivo* investigations, potentially shedding light onto the pathways involved in cancer development and progression by arsenite in humans.

Interestingly, the effects of arsenite exposure on gene networks leading to CVD were almost as high scoring as those for cancer induction, highlighting the importance of

carrying out investigations into the mechanisms behind arsenite-induced CVD development.

7.5.2.1 DNA damage and Cell cycle

Arsenite affected vital cellular functions including DNA replication, DNA repair and the cell cycle. Disruptions to these functions further support the observation on induction of SIPS in endothelial cells by arsenite. As discussed above this is a possible mechanism involved in the pathophysiology of cardiovascular diseases, particularly atherosclerosis (see chapter 4). Pathways which are specifically involved in controlling and monitoring the cell cycle were transcriptionally altered by arsenite exposure. The checkpoint kinase (CHK) mediated cell cycle control plays a crucial role in the cell cycle response to DNA damage (Zhou and Elledge, 2000). CHK proteins are phosphorylated and activated by ataxia telangiectasia mutated (ATM) kinases on DNA damage detection to go on to bring about DNA damage repair, chromatin remodelling, cell cycle arrest and apoptosis (Bartek and Lukas, 2003). Alterations in the ATM signalling and the CHK mediated cell cycle checkpoint control pathway render cells prone to apoptosis and premature senescence; these events are proposed to lead to the onset of cardiovascular diseases such as atherosclerosis (Golubnitschaja, 2006).

The considerable up-regulation seen in the mTOR signalling pathway is additional support for the onset of premature senescence. Dysfunction of the cell cycle can result in the cell having different fates; mTOR is required to send the cell into the senescence state (Schug, 2010), thus the up-regulation of mTOR strongly supports the finding of SIPS induction (see section 4.4.2).

Furthermore, insulin-like growth factor-1 (IGF-1) which functions as a stimulator of cellular proliferation, important for the cell cycle progression from the G1/S phase (Mairet-Coello *et al*., 2009), was shown to be down-regulated by arsenite. The down-regulation of IGF-1 signalling has been associated with CVD, specifically with the destabilisation of atherosclerotic plaques (von der Thusen *et al*., 2011).

The pathways involved in DNA damage repair were also broadly affected. The mismatch, DSB and NER repair pathways were down-regulated in response to arsenite. This supports and possibly explains the persistence of increased DNA damage observed in chapter 4 after 24 hours of treatment with 1,000 µg/L arsenite.

7.5.2.2 Impact of arsenite on the mitochondrial dysfunction pathway

Further support for rejecting the original hypothesis, which implicated an essential role of mitochondria in eliciting arsenite-induced toxicity in endothelial cells, comes from the lack of effect arsenite had on the expression of genes relevant to the mitochondria and mitochondrial function. The 'mitochondrial dysfunction pathway' showed no significant change in response to arsenite exposure, and was not implicated in any of the most affected networks observed. It can therefore be confirmed that mitochondria are not direct targets of arsenite, effects seen on the mitochondrial function, i.e. a decrease in the mitochondrial reserve capacity (Chapter 6), may be an adverse effect of arsenite-induced cellular stress.

7.5.3 Limitations of data

There are obvious limitations to this work that need to be taken into consideration when interpreting the data. HUVECs were used to carry out this investigation as they are a widely used model for human endothelial cells. Additionally, being primary cells they represent a good model for *in vitro* investigations of ageing/ senescence. However, the use of HUVECs will have discrepancies to the responses seen in endothelial cells from other blood vessels, therefore the data cannot be broadly extrapolated to the general response of all human endothelial cells to arsenite. It would thus be worth replicating this investigation in coronary endothelial cells. Furthermore, cell culture is an artificial model setting which will not account for some effects seen *in vivo*.

The relatively acute dosage of arsenite used in this investigation is not comparable to the chronic exposure of arsenite to individuals through contaminated drinking water; therefore certain effects i.e. the accumulative effects of arsenite on the transcription profile may not be seen in the endothelial cell model. The use of IPA to analyse the data also has its limitations of being reliant on published literature for genes and pathways and their current associations to functional processes and diseases to form response pathways and networks. Lastly, the application of filters to the gene lists analysed through IPA would have resulted in some data being disregarded, i.e. subtle gene expression changes, which would therefore be excluded from the analysis.

Transcriptomics analysis was undertaken late in this project due to the lack of mitochondrial effects observed. Therefore, validation of gene expression changes observed with arsenite were not performed, e.g. by qPCR. This presents a limitation for firm conclusion to be drawn and is an area for future work.

7.5.4 Summary

Observing the transcriptional changes in HUVECs in response to the sub-cytotoxic arsenite treatment (1,000 μg/L for 24 hours) has potentially given an insight into the initial arsenite-mediated cellular responses and possible mechanisms involved in bringing about arsenite-induced cardiovascular toxicity. Significant alterations in gene expression and signalling pathways indicated an initial increase in cellular ROS, which may be short-lived due to the immediate increase in antioxidants and oxidative stress response pathways. Increases in DNA damage and cell cycle dysfunction were also implicated. These cellular responses result in further inhibition of cellular function and could be underlying initiators of endothelial dysfunction in vascular disease. Aberrations specifically linked to the pathogenesis of CVD i.e. atherosclerosis in particular, included the up-regulation of inflammatory responses, modified GPCR signalling and the transcriptional changes associated with SIPS.

CHAPTER EIGHT

General Discussion and Future Work

Chapter 8: General discussion and future work

To gain an insight into the possible mechanisms by which arsenite exposure of humans results in the development and/or progression of CVD, particularly atherosclerosis, the *in vitro* effects of arsenite exposure on human vascular endothelial cells were investigated. The primary aim of this thesis was to determine whether arsenite resulted in the onset of endothelial senescence. Having established the onset of stress-induced premature senescence (SIPS) in HUVECs through arsenite exposure, the underlying mechanisms for this were investigated.

8.1 Effects of arsenite on mitochondria

Previous studies have suggested arsenic to induce its toxic effects on mitochondria. Arsenic exposure has been suggested to induce mtDNA damage and a decline in mtDNA copy number in A_L cells (Partridge *et al*., 2007), as well as a decrease in mitochondrial membrane potential and release of cyt c in myoblasts (Yen *et al*., 2012) and rat liver mitochondria (Naranmandura *et al*., 2012), with implications for apoptosis. In the initial hypothesis for this thesis, mitochondria were thought to be the initial targets of arsenite, resulting in an increased generation of mitochondrial ROS through which arsenite mediated its effects on ageing and cell death in endothelial cells. However, the investigations carried out to study this reveal contradictory results.

Since mitochondria are the major sources of ROS generation in cells (Lesnefsky *et al*., 2001; Wallace, 2000), disruption to the mitochondria could result in a marked increase in mitochondrial ROS generation, however no changes in the levels of mitochondrial superoxide were observed using MitoSox™ with flow cytometry. Despite the limitations of using MitoSox™ to measure superoxide (Zielonka *et al*., 2010), studies

assessing mtDNA content and damage support the lack of mitochondrial ROS generated. Since mtDNA is vulnerable to oxidative damage (Yakes and Van Houten, 1997), the lack of any significant mtDNA damage or alterations in mitochondrial DNA content suggest no increases in the levels of mitochondrial ROS. This is in accordance with the literature which suggests arsenic may increase intracellular ROS generation through NADPH oxidase (Barchowsky *et al*., 1999; Smith *et al*., 2000; Smith *et al*., 2001).

Further support for mitochondria not being primary targets of arsenite comes from the effects on oxidative phosphorylation, examined in HepG2 cells. HepG2 cells, a human hepatocyte cell line, have been defined as the current gold standard for *in vitro* toxicology investigations of mitochondrial toxicity (Swiss and Will, 2011) as they are easily adaptable *in vitro* (Mersch-Sundermann *et al*., 2004).

Arsenite treated HepG2 cells adapted to galactose-containing culture media, forcing cells to rely on mitochondrial oxidative phosphorylation for ATP synthesis, showed no differences in ATP generation and cell viability when compared to arsenite treated HepG2 cells grown in glucose-containing culture media, which mainly rely on glycolysis. Adapting cells to using galactose over glucose is a way of determining whether a xenobiotic causes mitochondrial toxicity on a cell by overcoming the Warburg effect (Warburg, 1956; Marroquin *et al*., 2007). Thus, the lack of difference, shown for the first time in this thesis, between the effect of arsenite on ATP generation in glucose-grown and galactose-grown HepG2 cells after 24 hour arsenite treatment strongly suggests that arsenite does not act as a direct mitochondrial toxicant.

However, mitochondria were still affected by arsenite, not as primary targets but as a downstream effect of cellular stress. This is indicated through the analysis of the mitochondrial reserve capacity. Mitochondrial reserve capacity is a phenomenon suggested to play an important role in the ability of mitochondria to combat stressful cellular situations (Dranka *et al*., 2010), allowing cells to respond and repair damage. Arsenite brought about a significant decrease in the reserve capacity of HUVECs after the acute exposure of 1 hour to the sub-cytotoxic concentration of 1000 μg/L. With the reserve capacity being suggested as a response to cellular stress (Dranka *et al*., 2010) rather than a direct consequence of mitochondrial damage, the decline observed may be a result of stress induced mitochondrial dysfunction i.e. through signalling via non-mitochondrial ROS to dampen the reserve capacity.

The concept of mitochondrial dysfunction occurring as a later event in arsenite-mediated cellular stress is also supported through the trend towards increased mtDNA copy number observed in HUVECs. Sub-cytotoxic treatments of HUVECs for both 24 hours and 5 days revealed increases in mtDNA copy number in a concentration-dependent manner, although not reaching statistical significance. Increases in mtDNA copy number have been viewed as a stress-induced compensatory mechanism to increase mitochondrial biogenesis in response to mitochondrial damage and dysfunction (Ahuja *et al*., 2013). This indicates the possibility of the toxicity of arsenite in endothelial cells leading to mitochondrial dysfunction, although further study is required, which has been shown to be involved in the pathogenesis and progression of atherosclerosis (reviewed in Madamanchi and Runge, 2007).

Further support for mitochondria not being direct targets of arsenite comes from the transcriptomics analysis of HUVECs exposed to sub-cytotoxic arsenite conditions; 1000 µg/L treatment for 24 hours. Arsenite had no effect on the expression of genes relevant to mitochondria and mitochondrial function, as well as there being no change to the 'mitochondrial dysfunction pathway' in response to arsenite. Thus, from the investigations conducted in this thesis, arsenite does not appear to directly target mitochondria, although it may bring about mitochondrial dysfunction as a downstream consequence of other cellular effects.

8.2 EA.hy 926 cells as a model for HUVECs

The use of primary cells for *in vitro* investigations has the obvious advantage over cell lines for being more physiologically relevant and therefore generating data that would provide a better representation of the effects observed *in vivo* (Chen, 2010). However, there are many disadvantages associated with primary cells which result in many investigators conducting research on cell lines. These limitations include the limited lifespan of primary cells which makes carrying out long term experiments difficult, the loss of the specialised tissue function with successive passages (CAAT, 1990) and the potential difficulties of growing primary cells in artificial culture conditions. For these reasons, in this thesis the EA.hy 926 cell line, formed by fusing HUVECs with the permanent human cell line A549 derived from a human lung carcinoma (Edgell *et al*., 1983), was used along with primary HUVECs.

EA.hy 926 cells are widely used *in vitro* when conducting investigations into human endothelial cells. When comparing the results obtained in this thesis on EA.hy 926 cells

and HUVECs, similarities as well as differences were observed. Detecting ROS generation in EA.hy 926 cells and HUVECs in response to arsenite exposure using the fluorescent probes CM-H_2DCFDA, DHE and MitoSOX™ with flow cytometry gave similar results. In both cell types, a concentration-dependent increase in DCF fluorescence was observed after 4 hours arsenite treatment, with no effect seen with DHE or MitoSOX™.

However, when conducting investigations into the impact of arsenite on mitochondrial function, using the XF analyzer, there were many inconsistences observed. The exposure of HUVECs to 1000 µg/L arsenite for 1 hour displayed a decrease in the mitochondrial reserve capacity, however no change was observed in EA.hy 926 cells under the same treatment conditions. Furthermore, 4 hour exposure of 10 µg/L arsenite to HUVECs resulted in a statistically significant increase in the mitochondrial reserve capacity and maximum oxygen consumption, whereas EA.hy 926 cells displayed no changes compared to the control. Therefore, from the observations in this thesis, it appears that EA.hy 926 cells may not be a good model to use for determining some of the physiological effects, e.g. mitochondrial function, of human endothelial cells *in vitro*.

8.3 Oxidative stress and arsenite

A concentration-dependent increase in supposed intracellular ROS levels was observed only when using the fluorescent probe CM-H_2DCFDA with flow cytometry in HUVECs and EA.hy 926 cells after 4 hours sub-cytotoxic arsenite treatment. However, the use of this probe in ROS investigations has been criticised for lacking specificity for ROS and

for being more of an indicator of the levels of cytochrome c in the cytoplasm (Kalyanaraman *et al*., 2012). Therefore CM-H_2DCFDA can be seen to measure the intrinsic pathway of apoptosis through the mitochondrial release of cyt c. Since arsenite induced significant levels of cell death at concentrations ≥5000 µg/L after 24 hours exposure, the significant increase in DCF fluorescence in HUVECs and EA.hy 926 cells with 10, 000 µg/L arsenite is likely to be an indication of arsenite-induced apoptosis through the intrinsic pathway.

Measuring cellular and mitochondrial superoxide levels using DHE or MitoSox respectively, showed no induction of oxidative stress in either HUVECS or EA.hy 926 cells in response to sub-cytotoxic treatments with arsenite. This would indicate that arsenite does not induce cellular oxidative stress, however, other investigations carried out in this thesis provide strong evidence for the occurrence of oxidative stress as an early cellular response to arsenite. Furthermore, previous studies have suggested arsenite induces oxidative stress in endothelial cells (Barchowsky *et al*., 1999; Smith *et al*., 2001; Sun *et al*., 2009; Shi *et al*., 2010). Therefore, it may be possible that these probes used lack the required sensitivity to measure the low levels of ROS which may have been generated.

Transcriptomics analysis to assess the gene expression changes in HUVECs after sub-cytotoxic arsenite exposure for 24 hours, indicated the onset of oxidative stress. The most up-regulated genes in response to arsenite exposure were from the metallothionein (MT) family. MTs have been suggested to assist in metal detoxification, by chelating metal ions and aiding their removal from the body (Sears, 2013), as seen in the rapid transport of cadmium ions from the blood to the kidney for excretion when bound to

MTs (Sigel *et al*., 2009). Therefore, the significant up-regulation of MTs suggests a role for them in arsenite detoxification by chelating arsenite ions and assisting in their excretion. Other than metal detoxification, MTs have been associated with combating oxidative stress. MTs are thiol rich and due to their cysteine residues, MTs have been found to scavenge free radicals such as superoxide and hydroxyl radicals, and to remove hydrogen peroxide (Thornalley and Vasak, 1985; Sato and Bremner, 1993; Chubatsu and Meneghini, 1993) and protect against oxidative damage *in vivo* (Yang *et al*., 1994; Iszard *et al*., 1995; Sato *et al*., 1995). Therefore, the increased expression of MTs in response to arsenite may be as cellular protective response to oxidative stress.

Arsenite was found to significantly up-regulate the expression of the cytoplasmic antioxidants NQO1 and SOD1, suggesting an increase in ROS from a cytoplasmic source rather than mitochondrial, supporting previous literature which indicates arsenic-induced superoxide generation from NADPH oxidase (Barchowsky *et al*., 1999; Smith *et al*., 2000; Smith *et al*., 2001). The NRF2-mediated oxidative stress response pathway was also up-regulated in response to arsenite. Since the activation of the transcription factor NRF2 occurs in response to oxidative stress (Osburn and Kensler, 2008), to regulate cellular antioxidant levels and maintain the cellular redox balance (Hybertson *et al*., 2011), this provides further support for oxidative stress conditions evoked in HUVECs by arsenite exposure. Moreover, NRF2 is able to modulate the expression of both NQO1 and SOD1 (Venugopal and Jaiswal, 1996), therefore this may be the mechanism through which these antioxidants were up-regulated.

Other support for arsenite-induced oxidative stress comes from the study of mitochondrial function in HUVEC mitochondria. The increase in the reserve capacity in response to the acute exposure to 10 μg/L arsenite suggests a protective response to oxidative stress, as the reserve capacity has been suggested to provide protection against oxidative damage (Dranka *et al*., 2010). Moreover, the observed trend for increase in the rate of non-mitochondrial oxygen consumption with arsenite treatment could be as a result of the increased use of oxygen in the cytoplasm to generate ROS. Lastly, the trend for an increase in mtDNA copy number seen in response to sub-cytotoxic arsenite treatment, suggests an increase in mitochondrial biogenesis; this has also been observed in many other cell types in response to cellular oxidative stress (Gadaleta *et al*., 1992; Barrientos *et al*., 1997; Lee *et al*., 1998; Lee *et al*., 2002).

Taken together, these results imply the induction of oxidative stress as an acute and possibly initial effect of arsenite in HUVECs, followed by a rapid increase in the cellular antioxidant mechanisms, i.e. up-regulation of metallothioneins, NFR2-mediated oxidative stress pathway and cytoplasmic antioxidants, restoring the cellular redox balance. Along with the criticisms of the ROS detection probes used to measure oxidative stress, the rapid antioxidant response, seen after 24 hours arsenite exposure, may be a potential reason for the lack of detection of ROS. However, the acute increase in ROS may still have detrimental effects on the cell, such as being a possible cause for the nDNA damage observed and potentially contributing to the onset of stress-induced premature senescence (SIPS).

8.4 Comparison of *in vitro* and *in vivo* microarray-based transcriptomics analysis

The transcriptomics data generated in this thesis was based on the *in vitro* analysis of arsenite sub-cytotoxicity in HUVECs. In comparison to *in vivo* investigations, the use of *in vitro* assays has clear limitations. The gene-expression analysis of toxicity using an *in vivo* model gives a complete representation of the effects the toxin has on the whole organism, taking into account the multiple complex interactions that occur between cells and tissues (Hartung and Daston, 2009). Since, this is not possible when conducting *in vitro* investigations, the gene-expression profile generated does not necessarily comply with the *in vivo* profile.

However, the use of *in vitro*-based transcriptomics has many advantages which has made it a widely used platform in toxicity investigations. *In vitro* platforms enable high throughput toxicity screening, with investigations being more cost effective and less time consuming (van Hummelen and Sasaki, 2010). Moreover, *in vitro* and *in vivo* investigations have often been found to generate similar gene-exporession profiles (Boess *et al*., 2007; Zimmer *et al*., 2008). Therefore, using *in vitro* transcriptomics is seen as a valid platform to give an indication of the gene-expression profile of a toxin and to indicate potential *in vivo* toxicity targets (Zimmer *et al*., 2008).

8.5 Mechanisms of arsenite-induced senescence

Cellular senescence, discovered in fibroblasts by Hayflick and colleagues (Hayflick, 1965), describes a cellular state in which cells are viable but have undergone permanent cell cycle arrest. The first hypothesis for why cells undergo senescence was as an anti-cancer mechanism, accounting for why cellular senescence is beneficial (Campisi and d'Adda di Fagagna, 2007), however the second hypothesis shed light on the detrimental

effects of senescence, i.e. *in vitro* senescence being a representation of the deterioration of *in vivo* cellular repair and tissue regeneration capacity with age (Campisi and d'Adda di Fagagna, 2007). Senescence cells are also suggested to secrete factors that can affect neighbouring cells, senescence-associated secretory phenotype (SASP), such factors include pro-inflammatory cytokines which may contribute to the onset of inflammatory diseases (Orjalo *et al*., 2009; Wang and Bennett, 2012). Thus, senescence is associated with promoting ageing (Hornsby, 2002), and has been implicated in many age-related and inflammatory human diseases i.e. atherosclerosis (Ross *et al*., 1984; Burrig, 1991; Bennett *et al*., 1995; Gorenne *et al*., 2006).

This thesis has been the first to show the induction of SIPS in HUVECs in response to arsenite exposure. Further support for the onset of senescence was provided by transcriptomics analysis of arsenite treated HUVECs, revealing the up-regulation of the CDK1A (P21) gene, the up-regulation of which has been associated with SIPS (Frippiat *et al*., 2000; Matthaei *et al*., 2012). Nevertheless, further investigations into the induction of senescence by arsenite are warranted in order to validate the results in this thesis (see section 8.6.5).

Investigating the mechanisms by which endothelial cells undergo premature senescence in response to arsenite revealed the possible involvement of mitochondrial damage. The sub-cytotoxic treatment of HUVECs with arsenite revealed a concentration-dependent increase in mtDNA copy number, although this data did not reach statistical significance, it suggests an increase in mitochondrial biogenesis as a possible compensatory response to arsenite-induced mitochondrial damage. Increased mitochondrial biogenesis has been observed in aged rats as well as aged humans

(Barrientos *et al*., 1997; Lee *et al*., 1998; Gadaleta *et al*., 1992), identifying a link between mitochondrial damage and the process of ageing. Furthermore, increased mtDNA copy number has been found in senescent human fibroblasts (Moiseeva *et al*., 2009; Lee *et al*., 2002), with the increase in mtDNA copy number being associated with mitochondrial dysfunction (Passos *et al*. 2007). Therefore, the non-significant trend for increased mtDNA copy number observed in HUVECs suggests that arsenite induces mitochondrial dysfunction which may be involved in the onset of SIPS.

The apparent onset of mitochondrial dysfunction with increasing arsenite concentrations would explain the concentration-dependent decrease in the mitochondrial reserve capacity also observed in response to arsenite in HUVECs. This suggests a mechanism for the premature senescence induced by arsenite (Figure 8.1). Since the reserve capacity is suggested to enable the mitochondria to provide protection against cellular oxidative damage (Dranka *et al*., 2010), the decline in this reserve capacity and thus the protective role of mitochondria would result in non-reversible intracellular damage leading to SIPS. Such non-reversible damage could be a result of the increased oxidative stress suggested with arsenite exposure, leading to damage such as the concentration-dependent increase in nDNA damage observed in HUVECs.

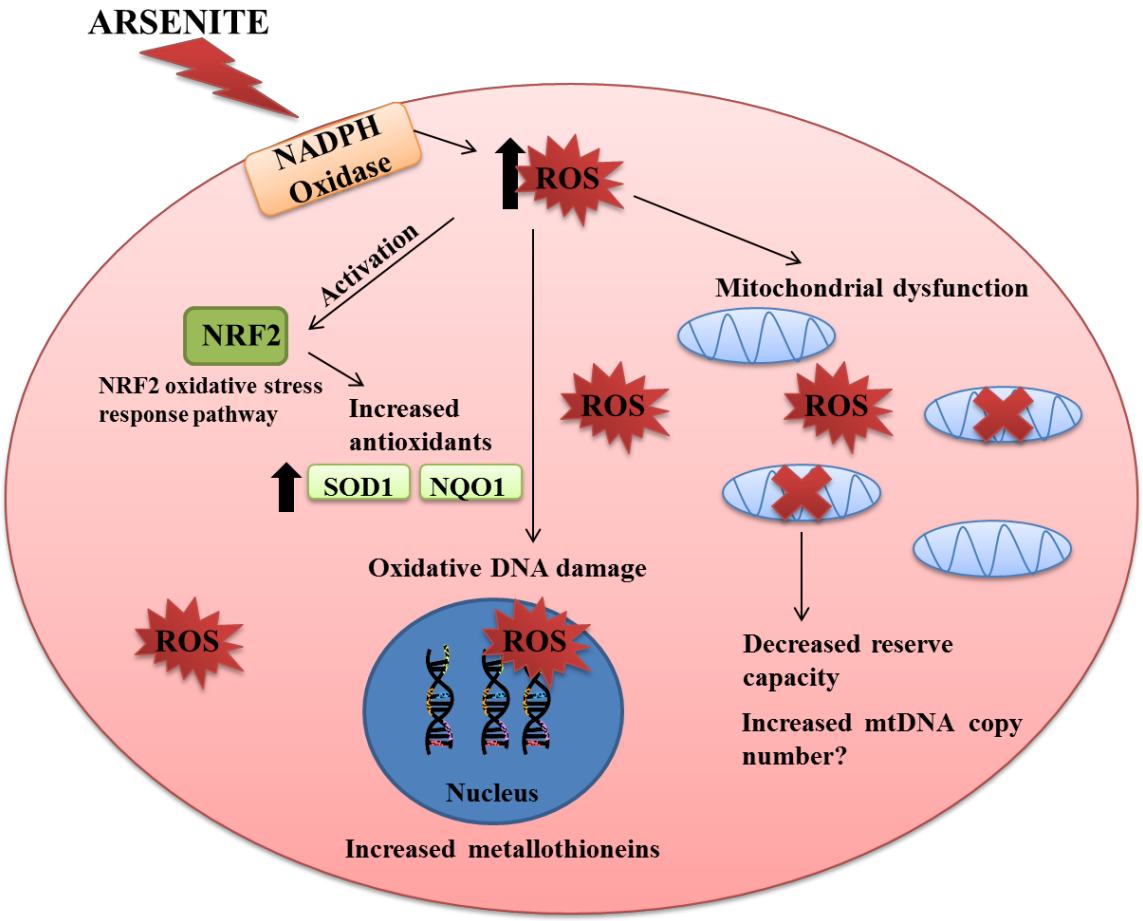

Figure 8.1 The proposed mechanism for SIPS in HUVECs as a result of arsenite exposure. Arsenite has been suggested to induce oxidative stress through the generation of ROS via NADPH oxidase. Increased oxidative stress would lead to intracellular oxidative damage such as irreversible damage to nDNA. Mitochondrial dysfunction has been implicated in response to arsenite through decreased mitochondrial reserve capacity and potential increase in mtDNA copy number suggesting a mitochondrial damage-induced compensatory increase in mitochondrial biogenesis. Mitochondrial dysfunction results in an inability of the mitochondria to protect the cell from oxidative damage, leading to SIPS (Barchowsky *et al*., 1999; Smith *et al*., 2000; Smith *et al*., 2001; Passos *et al*., 2007).

8.6 Future work

The hypothesis presented in pictorial form in figure 8.1 requires further investigation. Some of the possible avenues for future work are described below.

8.6.1 Determining arsenite-induced ROS generation

So far, from data presented in this thesis, there is only indirect evidence for ROS generation by arsenite in human endothelial cells. It is important to fully explore ROS production in further studies. The fluorescent probes used in this thesis to detect ROS have been criticised for their lack of specificity to ROS (Kalyanaraman *et al*., 2012), therefore giving a false account of the extent of oxidative stress induced by arsenite. Since the literature indicates arsenic to target endothelial cells and induce ROS through NADPH oxidase (Barchowsky *et al*,. 1999; Smith *et al*., 2000; Smith *et al*., 2001), the best way to approach the investigation of whether arsenite is inducing oxidative stress in endothelial cells would be to measure intracellular superoxide levels. The use of high performance liquid chromatography (HPLC) with DHE has been suggested to be a more accurate measure for superoxide (Zhao *et al*., 2005). Laurindo *et al* (2008) have developed a method of specifically detecting the generation of superoxide from NADPH oxidase with DHE-HPLC, this approach would clarify the production of superoxide by arsenite.

The use of the single cell gel electrophoresis/ comet assay revealed a concentration-dependent increase in nDNA damage in response to arsenite. Co-treating HUVECs with arsenite and an antioxidant, e.g. N-acetyl cysteine (NAC), would confirm whether the nDNA damage measured was as a result of oxidative stress. This would further support whether arsenite induced ROS and shed more light on whether the ROS was of a non-

mitochondrial source. In addition, incorporation of a DNA repair enzyme step into the comet assay, e.g. hOGG1 (Smith *et al*., 2006), would highlight the induction of oxidative lesions within the DNA and further define a role for oxidative stress in arsenite toxicity.

8.6.2 Determining the effects of arsenite on endothelial mitochondria

The qPCR based investigations carried out on mtDNA indicated a trend of increasing mtDNA copy number, suggesting an increase in mitochondrial biogenesis in response to mitochondrial dysfunction. However, since the increases observed in mtDNA copy number were not statistically significant, further repeats of this experiment would be required to confirm whether this trend was a significant effect of arsenite on HUVEC mitochondria.

Along with the qPCR data, measuring the membrane potential of HUVEC mitochondria would provide additional support to whether arsenite induces mitochondrial dysfunction (Brand and Nicholls, 2011). This can be done by using a fluorescent probe such as tetramethylrhodamine methyl ester (TMRM). Due to the lipophilic and cationic properties of TMRM, this probe is able to pass through the mitochondrial membranes and accumulate within the mitochondria of the cells. Changes in fluorescence intensity for the probes reflect changes in the mitochondrial membrane potential. The loss of the mitochondrial membrane potential results in TMRM leaking out of the mitochondria, therefore a diminished fluorescent intensity is observed in mitochondrial dysfunction where the membrane potential is disrupted (Joshi and Bakowska, 2011).

To further investigate the impact of arsenite on endothelial mitochondria, the effects of arsenite on rho (ρ) endothelial cells, e.g. HUVECs lacking mtDNA, could be compared

to cells with intact mitochondria. This would give an indication of how the importance of the mitochondria in arsenite-mediated toxicity.

8.6.3 Determining whether arsenite induces apoptosis

The induction of apoptosis was implied through the use of the CM-H_2DCFDA probe, which has been suggested to directly or indirectly undergo oxidation with cyt c (Kalyanaraman 2012), indicating the early stage of apoptosis. Cell death was observed at 24 hours following exposure to ≥5000 µg/L. To confirm whether the increase in DCF fluorescence was an indication of apoptosis, the release of cyt c from HUVEC mitochondria could be measured in cells. This could be done using a technique such as that described by Campos *et al* (2006) which involves measuring cyt c using digitonin with flow cytometry. Temporal changes in cyt c release with DCF fluorescence would be informative.

8.6.4 Validation of gene expression changes

In this thesis, through the use of microarray-based transcription profiling, many gene expression changes were observed that have proved highly insightful in suggesting mechanisms for the effects of arsenite, e.g. the up-regulation of the MTs, antioxidants SOD1 and NQO1, and the NRF2 oxidative stress response pathway, and the down regulation of the regulator of G-protein signalling 4 gene (RGS4) and the genes involved in DNA damage repair (DDR). Therefore to validate the changes in expression of these genes, it would be important to use qPCR to confirm differential expression in HUVECs in response to arsenite treatment.

8.6.5 Further investigating the onset of senescence

To further validate the onset of premature senescence of endothelial cells in response to arsenite, the accumulation of DNA damage can be measured, using the extent of histone H2A.X phosphorylation (γ-H2A.X) as a biomarker of senescence induction. Phosphorylation of H2A.X has been suggested to assist with DNA damage foci formation (von Zglinicki *et al*., 2005). With the accumulation of DNA damage being found to contribute to senescence (Chen *et al*., 2007), immunohistochemistry has been used to detect the extent of γ-H2A.X *in vivo* (von Zglinicki *et al*., 2005). Thus, this technique can be employed to assess the *in vivo* effects of arsenite on senescence, by examining tissue samples from the blood vessels of an animal model, e.g. mice, exposed to arsenite contaminated drinking water. The use of γ-H2A.X with immunohistochemistry has also been used for the *in vitro* determination of senescence (Wang *et al*., 2009), therefore, this technique may also be used with arsenite exposed HUVECs to validate the onset of SIPS observed in this thesis with SA-β-gal staining.

APPENDICES

Appendix 1

The CD attached contains the raw microarray data file named ‘Appendix 1’.

Appendix 2

The CD attached contains the normalized and significant (FDR of 0.05 and FC >1.5) microarray data used for the analysis carried out in this thesis. File named ‘Appendix 2’.

References

ABERNATHY, C.O., THOMAS, D.J. and CALDERON, R.L., 2003. Health effects and risk assessment of arsenic. *The Journal of nutrition*, **133**(5 Suppl 1), pp. 1536S-8S.

AHMAD, S.A., KHATUN, F., SAYED, M.H., KHAN, M.H., AZIZ, R., HOSSAIN, M.Z. and FARUQUEE, M.H., 2006. Electrocardiographic abnormalities among arsenic-exposed persons through groundwater in Bangladesh. *Journal of health, population, and nutrition*, **24**(2), pp. 221-227.

AHUJA, P., WANAGAT, J., WANG, Z., WANG, Y., LIEM, D.A., PING, P., ANTOSHECHKIN, I.A., MARGULIES, K.B. and MACLELLAN, W.R., 2013. Divergent mitochondrial biogenesis responses in human cardiomyopathy. *Circulation*, **127**(19), pp. 1957-1967.

ALBORES, A., KOROPATNICK, J., CHERIAN, M.G. and ZELAZOWSKI, A.J., 1992. Arsenic induces and enhances rat hepatic metallothionein production in vivo. *Chemico-biological interactions*, **85**(2-3), pp. 127-140.

ANDERSON, T.J., GERHARD, M.D., MEREDITH, I.T., CHARBONNEAU, F., DELAGRANGE, D., CREAGER, M.A., SELWYN, A.P. and GANZ, P., 1995. Systemic nature of endothelial dysfunction in atherosclerosis. *The American Journal of Cardiology*, **75**(6), pp. 71B-74B.

AON, M.A., CORTASSA, S., MARBAN, E. and O'ROURKE, B., 2003. Synchronized whole cell oscillations in mitochondrial metabolism triggered by a local release of reactive oxygen species in cardiac myocytes. *The Journal of biological chemistry*, **278**(45), pp. 44735-44744.

ATTARDI, G. and SCHATZ, G., 1988. Biogenesis of mitochondria. *Annual Review of Cell Biology*, **4**, pp. 289-333.

AVIV, H., KHAN, M.Y., SKURNICK, J., OKUDA, K., KIMURA, M., GARDNER, J., PRIOLO, L. and AVIV, A., 2001. Age dependent aneuploidy and telomere length of the human vascular endothelium. *Atherosclerosis*, **159**(2), pp. 281-287.

BABIOR, B.M., 2004. NADPH oxidase. *Current opinion in immunology*, **16**(1), pp. 42-47.

BABULA, P., MASARIK, M., ADAM, V., ECKSCHLAGER, T., STIBOROVA, M., TRNKOVA, L., SKUTKOVA, H., PROVAZNIK, I., HUBALEK, J. and KIZEK, R., 2012. Mammalian metallothioneins: properties and functions. *Metallomics : integrated biometal science*, **4**(8), pp. 739-750.

BAGGIOLINI, M. and CLARK-LEWIS, I., 1992. Interleukin-8, a chemotactic and inflammatory cytokine. *FEBS letters*, **307**(1), pp. 97-101.

BALAKUMAR, P. and KAUR, J., 2009. Arsenic exposure and cardiovascular disorders: an overview. *Cardiovascular toxicology*, **9**(4), pp. 169-176.

BALLINGER, S.W., PATTERSON, C., KNIGHT-LOZANO, C.A., BUROW, D.L., CONKLIN, C.A., HU, Z., REUF, J., HORAIST, C., LEBOVITZ, R., HUNTER, G.C., MCINTYRE, K. and RUNGE, M.S., 2002. Mitochondrial integrity and function in atherogenesis. *Circulation*, **106**(5), pp. 544-549.

BASSON, M., 2008. Cardiovascular disease. *Nature*, **451**(7181), pp. 903-957.

BARCHOWSKY, A., DUDEK, E.J., TREADWELL, M.D. and WETTERHAHN, K.E., 1996. Arsenic induces oxidant stress and NF-kappa B activation in cultured aortic endothelial cells. *Free radical biology & medicine,* **21**(6), pp. 783-790.

BARCHOWSKY, A., KLEI, L.R., DUDEK, E.J., SWARTZ, H.M. and JAMES, P.E., 1999. Stimulation of reactive oxygen, but not reactive nitrogen species, in vascular endothelial cells exposed to low levels of arsenite. *Free radical biology & medicine,* **27**(11-12), pp. 1405-1412.

BARRIENTOS, A., CASADEMONT, J., CARDELLACH, F., ESTIVILL, X., URBANO-MARQUEZ, A. and NUNES, V., 1997. Reduced steady-state levels of mitochondrial RNA and increased mitochondrial DNA amount in human brain with aging. *Brain research.Molecular brain research,* **52**(2), pp. 284-289.

BARTEK, J. and LUKAS, J., 2003. Chk1 and Chk2 kinases in checkpoint control and cancer. *Cancer cell,* **3**(5), pp. 421-429.

BATES, M.N., SMITH, A.H. and HOPENHAYN-RICH, C., 1992. Arsenic ingestion and internal cancers: a review. *American Journal of Epidemiology,* **135**(5), pp. 462-476.

BELAIBA, R.S., DJORDJEVIC, T., PETRY, A., DIEMER, K., BONELLO, S., BANFI, B., HESS, J., POGREBNIAK, A., BICKEL, C. and GORLACH, A., 2007. NOX5 variants are functionally active in endothelial cells. *Free radical biology & medicine,* **42**(4), pp. 446-459.

BELLACOSA, A., KUMAR, C.C., DI CRISTOFANO, A. and TESTA, J.R., 2005. Activation of AKT kinases in cancer: implications for therapeutic targeting. *Advances in Cancer Research,* **94**, pp. 29-86.

BENNETT, M.R., EVAN, G.I. and SCHWARTZ, S.M., 1995. Apoptosis of human vascular smooth muscle cells derived from normal vessels and coronary atherosclerotic plaques. *The Journal of clinical investigation,* **95**(5), pp. 2266-2274.

BENNETT, M.R., MACDONALD, K., CHAN, S.W., BOYLE, J.J. and WEISSBERG, P.L., 1998. Cooperative interactions between RB and p53 regulate cell proliferation, cell senescence, and apoptosis in human vascular smooth muscle cells from atherosclerotic plaques. *Circulation research,* **82**(6), pp. 704-712.

BEN-PORATH, I. and WEINBERG, R.A., 2005. The signals and pathways activating cellular senescence. *The international journal of biochemistry & cell biology,* **37**(5), pp. 961-976.

BHATNAGAR, A., 1994. Biochemical mechanism of irreversible cell injury caused by free radical-initiated reactions. *Molecular and cellular biochemistry,* **137**(1), pp. 9-16.

BHATTACHARJEE, H., ROSEN, B.P. and MUKHOPADHYAY, R., 2009. Aquaglyceroporins and metalloid transport: implications in human diseases. *Handbook of Experimental Pharmacology,* **(190):309-25. doi**(190), pp. 309-325.

BINKOVA, B., SMERHOVSKY, Z., STREJC, P., BOUBELIK, O., STAVKOVA, Z., CHVATALOVA, I. and SRAM, R.J., 2002. DNA-adducts and atherosclerosis: a study of accidental and sudden death males in the Czech Republic. *Mutation research,* **501**(1-2), pp. 115-128.

BOEKEMA, E.J. and BRAUN, H.P., 2007. Supramolecular structure of the mitochondrial oxidative phosphorylation system. *The Journal of biological chemistry,* **282**(1), pp. 1-4.

BOESS, F., DURR, E., SCHAUB, N., HAIKER, M., ALBERTINI, S. and SUTER, L., 2007. An in vitro study on 5-HT6 receptor antagonist induced hepatotoxicity based on biochemical assays and

toxicogenomics. *Toxicology in vitro : an international journal published in association with BIBRA*, **21**(7), pp. 1276-1286.

BOLSTAD, B.M., IRIZARRY, R.A., ASTRAND, M. and SPEED, T.P., 2003. A comparison of normalization methods for high density oligonucleotide array data based on variance and bias. *Bioinformatics (Oxford, England)*, **19**(2), pp. 185-193.

BOMBELI, T., KARSAN, A., TAIT, J.F. and HARLAN, J.M., 1997. Apoptotic vascular endothelial cells become procoagulant. *Blood*, **89**(7), pp. 2429-2442.

BOMBELI, T., SCHWARTZ, B.R. and HARLAN, J.M., 1999. Endothelial cells undergoing apoptosis become proadhesive for nonactivated platelets. *Blood*, **93**(11), pp. 3831-3838.

BONINI, M.G., ROTA, C., TOMASI, A. and MASON, R.P., 2006. The oxidation of 2',7'-dichlorofluorescin to reactive oxygen species: a self-fulfilling prophesy? *Free radical biology & medicine*, **40**(6), pp. 968-975.

BOTTO, N., BERTI, S., MANFREDI, S., AL-JABRI, A., FEDERICI, C., CLERICO, A., CIOFINI, E., BIAGINI, A. and ANDREASSI, M.G., 2005. Detection of mtDNA with 4977 bp deletion in blood cells and atherosclerotic lesions of patients with coronary artery disease. *Mutation research*, **570**(1), pp. 81-88.

BOTTO, N., RIZZA, A., COLOMBO, M.G., MAZZONE, A.M., MANFREDI, S., MASETTI, S., CLERICO, A., BIAGINI, A. and ANDREASSI, M.G., 2001. Evidence for DNA damage in patients with coronary artery disease. *Mutation research*, **493**(1-2), pp. 23-30.

BOUITBIR, J., CHARLES, A.L., ECHANIZ-LAGUNA, A., KINDO, M., DAUSSIN, F., AUWERX, J., PIQUARD, F., GENY, B. and ZOLL, J., 2012. Opposite effects of statins on mitochondria of cardiac and skeletal muscles: a 'mitohormesis' mechanism involving reactive oxygen species and PGC-1. *European heart journal*, **33**(11), pp. 1397-1407.

BRADFORD, M.M., 1976. A rapid and sensitive method for the quantitation of microgram quantities of protein utilizing the principle of protein-dye binding. *Analytical Biochemistry*, **72**, pp. 248-254.

BRADLAW, J. and FLINT, O., 1990. Technical Report No. 4: Cell culture systems04and in vitro toxicity testing. [online]. CAAT, Baltimore. [viewed 16/07/2013]. Available from: http://caat.jhsph.edu/publications/tech_reports/4.html

BRAND, M.D. and NICHOLLS, D.G., 2011. Assessing mitochondrial dysfunction in cells. *The Biochemical journal*, **435**(2), pp. 297-312.

BREITSCHOPF, K., ZEIHER, A.M. and DIMMELER, S., 2001. Pro-atherogenic factors induce telomerase inactivation in endothelial cells through an Akt-dependent mechanism. *FEBS letters*, **493**(1), pp. 21-25.

BROUILETTE, S., SINGH, R.K., THOMPSON, J.R., GOODALL, A.H. and SAMANI, N.J., 2003. White cell telomere length and risk of premature myocardial infarction. *Arteriosclerosis, Thrombosis, and Vascular Biology*, **23**(5), pp. 842-846.

BROUILETTE, S.W., MOORE, J.S., MCMAHON, A.D., THOMPSON, J.R., FORD, I., SHEPHERD, J., PACKARD, C.J., SAMANI, N.J. and WEST OF SCOTLAND CORONARY PREVENTION STUDY GROUP, 2007. Telomere length, risk of coronary heart disease, and statin treatment in the West of Scotland Primary Prevention Study: a nested case-control study. *Lancet*, **369**(9556), pp. 107-114.

BURKITT, M.J. and WARDMAN, P., 2001. Cytochrome C is a potent catalyst of dichlorofluorescin oxidation: implications for the role of reactive oxygen species in apoptosis. *Biochemical and biophysical research communications*, **282**(1), pp. 329-333.

BURRIG, K.F., 1991. The endothelium of advanced arteriosclerotic plaques in humans. *Arteriosclerosis and Thrombosis : A Journal of Vascular Biology / American Heart Association*, **11**(6), pp. 1678-1689.

BUTTKE, T.M. and SANDSTROM, P.A., 1994. Oxidative stress as a mediator of apoptosis. *Immunology today*, **15**(1), pp. 7-10.

CADENAS, E. and DAVIES, K.J., 2000. Mitochondrial free radical generation, oxidative stress, and aging. *Free radical biology & medicine*, **29**(3-4), pp. 222-230.

CAI, H. and HARRISON, D.G., 2000. Endothelial dysfunction in cardiovascular diseases: the role of oxidant stress. *Circulation research*, **87**(10), pp. 840-844.

CAMPISI, J. and D'ADDA DI FAGAGNA, F., 2007. Cellular senescence: when bad things happen to good cells. *Nature reviews.Molecular cell biology*, **8**(9), pp. 729-740.

CAMPO, M.L., KINNALLY, K.W. and TEDESCHI, H., 1992. The effect of antimycin A on mouse liver inner mitochondrial membrane channel activity. *The Journal of biological chemistry*, **267**(12), pp. 8123-8127.

CAMPOS, C.B., PAIM, B.A., COSSO, R.G., CASTILHO, R.F., ROTTENBERG, H. and VERCESI, A.E., 2006. Method for monitoring of mitochondrial cytochrome c release during cell death: Immunodetection of cytochrome c by flow cytometry after selective permeabilization of the plasma membrane. *Cytometry.Part A : the journal of the International Society for Analytical Cytology*, **69**(6), pp. 515-523.

CAPELL, B.C., COLLINS, F.S. and NABEL, E.G., 2007. Mechanisms of cardiovascular disease in accelerated aging syndromes. *Circulation research*, **101**(1), pp. 13-26.

CAPLAN, B.A. and SCHWARTZ, C.J., 1973. Increased endothelial cell turnover in areas of in vivo Evans Blue uptake in the pig aorta. *Atherosclerosis*, **17**(3), pp. 401-417.

CATHCART, R., SCHWIERS, E. and AMES, B.N., 1983. Detection of picomole levels of hydroperoxides using a fluorescent dichlorofluorescein assay. *Analytical Biochemistry*, **134**(1), pp. 111-116.

CHANCE, B., SIES, H. and BOVERIS, A., 1979. Hydroperoxide metabolism in mammalian organs. *Physiological Reviews*, **59**(3), pp. 527-605.

CHANG, B.D., SWIFT, M.E., SHEN, M., FANG, J., BROUDE, E.V. and RONINSON, I.B., 2002. Molecular determinants of terminal growth arrest induced in tumor cells by a chemotherapeutic agent. *Proceedings of the National Academy of Sciences of the United States of America*, **99**(1), pp. 389-394.

CHANG, E. and HARLEY, C.B., 1995. Telomere length and replicative aging in human vascular tissues. *Proceedings of the National Academy of Sciences of the United States of America*, **92**(24), pp. 11190-11194.

CHAO, J.I., HSU, S.H. and TSOU, T.C., 2006. Depletion of securin increases arsenite-induced chromosome instability and apoptosis via a p53-independent pathway. *Toxicological sciences : an official journal of the Society of Toxicology*, **90**(1), pp. 73-86.

CHEN, C.J., HSUEH, Y.M., LAI, M.S., SHYU, M.P., CHEN, S.Y., WU, M.M., KUO, T.L. and TAI, T.Y., 1995. Increased prevalence of hypertension and long-term arsenic exposure. *Hypertension,* **25**(1), pp. 53-60.

CHEN, C.J., KUO, T.L. and WU, M.M., 1988. Arsenic and cancers. *Lancet,* **1**(8582), pp. 414-415.

CHEN, J., HALES, C.N. and OZANNE, S.E., 2007. DNA damage, cellular senescence and organismal ageing: causal or correlative? Nucleic acids research, 35(22), pp. 7417-7428.

CHEN, J.H., HALES, C.N. and OZANNE, S.E., 2007. DNA damage, cellular senescence and organismal ageing: causal or correlative? *Nucleic acids research,* **35**(22), pp. 7417-7428.

CHEN, Q., FISCHER, A., REAGAN, J.D., YAN, L.J. and AMES, B.N., 1995. Oxidative DNA damage and senescence of human diploid fibroblast cells. *Proceedings of the National Academy of Sciences of the United States of America,* **92**(10), pp. 4337-4341.

CHEN, Q.M., BARTHOLOMEW, J.C., CAMPISI, J., ACOSTA, M., REAGAN, J.D. and AMES, B.N., 1998. Molecular analysis of H2O2-induced senescent-like growth arrest in normal human fibroblasts: p53 and Rb control G1 arrest but not cell replication. *The Biochemical journal,* **332 (Pt 1)**(Pt 1), pp. 43-50.

CHEN, T., 2010. A practical guide to assay development and high-throughput screening in drug discovery. Boca Raton: CRC Press.

CHEN, Y. and AHSAN, H., 2004. Cancer burden from arsenic in drinking water in Bangladesh. *American Journal of Public Health,* **94**(5), pp. 741-744.

CHEN, Y., HAKIM, M.E., PARVEZ, F., ISLAM, T., RAHMAN, A.M. and AHSAN, H., 2006. Arsenic exposure from drinking-water and carotid artery intima-medial thickness in healthy young adults in Bangladesh. *Journal of health, population, and nutrition,* **24**(2), pp. 253-257.

CHENG, H., QIU, L., ZHANG, H., CHENG, M., LI, W., ZHAO, X., LIU, K., LEI, L. and MA, J., 2011. Arsenic trioxide promotes senescence and regulates the balance of adipogenic and osteogenic differentiation in human mesenchymal stem cells. *Acta biochimica et biophysica Sinica,* **43**(3), pp. 204-209.

CHUBATSU, L.S. and MENEGHINI, R., 1993. Metallothionein protects DNA from oxidative damage. *The Biochemical journal,* **291 (Pt 1)**(Pt 1), pp. 193-198.

CIVELEK, M., MANDUCHI, E., RILEY, R.J., STOECKERT, C.J.,JR and DAVIES, P.F., 2009. Chronic endoplasmic reticulum stress activates unfolded protein response in arterial endothelium in regions of susceptibility to atherosclerosis. *Circulation research,* **105**(5), pp. 453-461.

CIZKOVA, A., STRANECKY, V., MAYR, J.A., TESAROVA, M., HAVLICKOVA, V., PAUL, J., IVANEK, R., KUSS, A.W., HANSIKOVA, H., KAPLANOVA, V., VRBACKY, M., HARTMANNOVA, H., NOSKOVA, L., HONZIK, T., DRAHOTA, Z., MAGNER, M., HEJZLAROVA, K., SPERL, W., ZEMAN, J., HOUSTEK, J. and KMOCH, S., 2008. TMEM70 mutations cause isolated ATP synthase deficiency and neonatal mitochondrial encephalocardiomyopathy. *Nature genetics,* **40**(11), pp. 1288-1290.

CLEMENTI, E., BROWN, G.C., FOXWELL, N. and MONCADA, S., 1999. On the mechanism by which vascular endothelial cells regulate their oxygen consumption. *Proceedings of the National Academy of Sciences of the United States of America,* **96**(4), pp. 1559-1562.

COLLINS, A.R., 2004. The comet assay for DNA damage and repair: principles, applications, and limitations. *Molecular biotechnology,* **26**(3), pp. 249-261.

COLLINS, A.R., OSCOZ, A.A., BRUNBORG, G., GAIVAO, I., GIOVANNELLI, L., KRUSZEWSKI, M., SMITH, C.C. and STETINA, R., 2008. The comet assay: topical issues. *Mutagenesis,* **23**(3), pp. 143-151.

COMPTON, S.J. and JONES, C.G., 1985. Mechanism of dye response and interference in the Bradford protein assay. *Analytical Biochemistry,* **151**(2), pp. 369-374.

CULIC, O., GRUWEL, M.L. and SCHRADER, J., 1997. Energy turnover of vascular endothelial cells. *The American Journal of Physiology,* **273**(1 Pt 1), pp. C205-13.

D'ADDA DI FAGAGNA, F., REAPER, P.M., CLAY-FARRACE, L., FIEGLER, H., CARR, P., VON ZGLINICKI, T., SARETZKI, G., CARTER, N.P. and JACKSON, S.P., 2003. A DNA damage checkpoint response in telomere-initiated senescence. *Nature,* **426**(6963), pp. 194-198.

DAI, D.F., CHEN, T., WANAGAT, J., LAFLAMME, M., MARCINEK, D.J., EMOND, M.J., NGO, C.P., PROLLA, T.A. and RABINOVITCH, P.S., 2010. Age-dependent cardiomyopathy in mitochondrial mutator mice is attenuated by overexpression of catalase targeted to mitochondria. *Aging cell,* **9**(4), pp. 536-544.

DAVIDSON, S.M. and DUCHEN, M.R., 2007. Endothelial mitochondria: contributing to vascular function and disease. *Circulation research,* **100**(8), pp. 1128-1141.

DAVIGNON, J. and GANZ, P., 2004. Role of endothelial dysfunction in atherosclerosis. *Circulation,* **109**(23 Suppl 1), pp. III27-32.

DE LANGE, T., 2005. Shelterin: the protein complex that shapes and safeguards human telomeres. *Genes & development,* **19**(18), pp. 2100-2110.

DEBUSK, F.L., 1972. The Hutchinson-Gilford progeria syndrome. Report of 4 cases and review of the literature. *The Journal of pediatrics,* **80**(4), pp. 697-724.

DELEO, F.R., RENEE, J., MCCORMICK, S., NAKAMURA, M., APICELLA, M., WEISS, J.P. and NAUSEEF, W.M., 1998. Neutrophils exposed to bacterial lipopolysaccharide upregulate NADPH oxidase assembly. *The Journal of clinical investigation,* **101**(2), pp. 455-463.

DEMEL, S., SHI, J., MARTIN, P., ROSEN, B.P. and EDWARDS, B.F., 2004. Arginine 60 in the ArsC arsenate reductase of E. coli plasmid R773 determines the chemical nature of the bound As(III) product. *Protein science : a publication of the Protein Society,* **13**(9), pp. 2330-2340.

DENMAN, S.E. and MCSWEENEY, C.S., 2005. Quantitative (real-time) PCR. In: H.P.S. MAKKAR and C.S. MCSWEENEY, eds. Methods in gut microbial ecology for ruminants. Dordrecht: Springer, pp. 105-115.

DESJARDINS, F. and BALLIGAND, J.L., 2006. Nitric oxide-dependent endothelial function and cardiovascular disease. *Acta Clinica Belgica,* **61**(6), pp. 326-334.

DEVASAGAYAM, T.P., TILAK, J.C., BOLOOR, K.K., SANE, K.S., GHASKADBI, S.S. and LELE, R.D., 2004. Free radicals and antioxidants in human health: current status and future prospects. *The Journal of the Association of Physicians of India,* **52**, pp. 794-804.

DIMRI, G.P., LEE, X., BASILE, G., ACOSTA, M., SCOTT, G., ROSKELLEY, C., MEDRANO, E.E., LINSKENS, M., RUBELJ, I. and PEREIRA-SMITH, O., 1995. A biomarker that identifies senescent human cells in culture and in aging skin in vivo. *Proceedings of the National Academy of Sciences of the United States of America*, **92**(20), pp. 9363-9367.

DRANKA, B.P., HILL, B.G. and DARLEY-USMAR, V.M., 2010. Mitochondrial reserve capacity in endothelial cells: The impact of nitric oxide and reactive oxygen species. *Free radical biology & medicine*, **48**(7), pp. 905-914.

DREGER, H., WESTPHAL, K., WELLER, A., BAUMANN, G., STANGL, V., MEINERS, S. and STANGL, K., 2009. Nrf2-dependent upregulation of antioxidative enzymes: a novel pathway for proteasome inhibitor-mediated cardioprotection. *Cardiovascular research*, **83**(2), pp. 354-361.

DUAN, J., DUAN, J., ZHANG, Z. and TONG, T., 2005. Irreversible cellular senescence induced by prolonged exposure to H2O2 involves DNA-damage-and-repair genes and telomere shortening. *The international journal of biochemistry & cell biology*, **37**(7), pp. 1407-1420.

DUMONT, P., ROYER, V., PASCAL, T., DIERICK, J.F., CHAINIAUX, F., FRIPPIAT, C., DE MAGALHAES, J.P., ELIAERS, F., REMACLE, J. and TOUSSAINT, O., 2001. Growth kinetics rather than stress accelerate telomere shortening in cultures of human diploid fibroblasts in oxidative stress-induced premature senescence. *FEBS letters*, **502**(3), pp. 109-112.

DURANTEAU, J., CHANDEL, N.S., KULISZ, A., SHAO, Z. and SCHUMACKER, P.T., 1998. Intracellular signaling by reactive oxygen species during hypoxia in cardiomyocytes. *The Journal of biological chemistry*, **273**(19), pp. 11619-11624.

DWIVEDI, N., MEHTA, A., YADAV, A., BINUKUMAR, B.K., GILL, K.D. and FLORA, S.J., 2011. MiADMSA reverses impaired mitochondrial energy metabolism and neuronal apoptotic cell death after arsenic exposure in rats. *Toxicology and applied pharmacology*, **256**(3), pp. 241-248.

ECHANIZ-LAGUNA, A., MOHR, M. and TRANCHANT, C., 2010. Neuromuscular symptoms and elevated creatine kinase after statin withdrawal. *The New England journal of medicine*, **362**(6), pp. 564-565.

EDGELL, C.J., MCDONALD, C.C. and GRAHAM, J.B., 1983. Permanent cell line expressing human factor VIII-related antigen established by hybridization. *Proceedings of the National Academy of Sciences of the United States of America*, **80**(12), pp. 3734-3737.

EDWARDS, D.H., LI, Y., ELLINSWORTH, D.C. and GRIFFITH, T.M., 2013. The effect of inorganic arsenic on endothelium-dependent relaxation: role of NADPH oxidase and hydrogen peroxide. *Toxicology*, **306**, pp. 50-58.

ERUSALIMSKY, J.D., 2009. Vascular endothelial senescence: from mechanisms to pathophysiology. *Journal of applied physiology (Bethesda, Md.: 1985)*, **106**(1), pp. 326-332.

ERUSALIMSKY, J.D. and KURZ, D.J., 2006. Endothelial cell senescence. *Handbook of Experimental Pharmacology*, **(176 Pt 2)**(176 Pt 2), pp. 213-248.

FALK, E., 2006. Pathogenesis of atherosclerosis. *Journal of the American College of Cardiology*, **47**(8 Suppl), pp. C7-12.

FARAGHER, R.G. and KIPLING, D., 1998. How might replicative senescence contribute to human ageing? *BioEssays : news and reviews in molecular, cellular and developmental biology*, **20**(12), pp. 985-991.

FARHANGKHOEE, H., KHAN, Z.A., BARBIN, Y. and CHAKRABARTI, S., 2005. Glucose-induced up-regulation of CD36 mediates oxidative stress and microvascular endothelial cell dysfunction. *Diabetologia*, **48**(7), pp. 1401-1410.

FIERS, W., BEYAERT, R., DECLERCQ, W. and VANDENABEELE, P., 1999. More than one way to die: apoptosis, necrosis and reactive oxygen damage. *Oncogene*, **18**(54), pp. 7719-7730.

FRANK, S., GAUME, B., BERGMANN-LEITNER, E.S., LEITNER, W.W., ROBERT, E.G., CATEZ, F., SMITH, C.L. and YOULE, R.J., 2001. The role of dynamin-related protein 1, a mediator of mitochondrial fission, in apoptosis. *Developmental cell*, **1**(4), pp. 515-525.

FRESNO VARA, J.A., CASADO, E., DE CASTRO, J., CEJAS, P., BELDA-INIESTA, C. and GONZALEZ-BARON, M., 2004. PI3K/Akt signalling pathway and cancer. *Cancer treatment reviews*, **30**(2), pp. 193-204.

FREY, R.S., USHIO-FUKAI, M. and MALIK, A.B., 2009. NADPH oxidase-dependent signaling in endothelial cells: role in physiology and pathophysiology. *Antioxidants & redox signaling*, **11**(4), pp. 791-810.

FRIPPIAT, C., CHEN, Q.M., REMACLE, J. and TOUSSAINT, O., 2000. Cell cycle regulation in H(2)O(2)-induced premature senescence of human diploid fibroblasts and regulatory control exerted by the papilloma virus E6 and E7 proteins. *Experimental gerontology*, **35**(6-7), pp. 733-745.

FRIPPIAT, C., CHEN, Q.M., ZDANOV, S., MAGALHAES, J.P., REMACLE, J. and TOUSSAINT, O., 2001. Subcytotoxic H2O2 stress triggers a release of transforming growth factor-beta 1, which induces biomarkers of cellular senescence of human diploid fibroblasts. *The Journal of biological chemistry*, **276**(4), pp. 2531-2537.

FUMAGALLI, M., ROSSIELLO, F., CLERICI, M., BAROZZI, S., CITTARO, D., KAPLUNOV, J.M., BUCCI, G., DOBREVA, M., MATTI, V., BEAUSEJOUR, C.M., HERBIG, U., LONGHESE, M.P. and D'ADDA DI FAGAGNA, F., 2012. Telomeric DNA damage is irreparable and causes persistent DNA-damage-response activation. *Nature cell biology*, **14**(4), pp. 355-365.

FURUMOTO, K., INOUE, E., NAGAO, N., HIYAMA, E. and MIWA, N., 1998. Age-dependent telomere shortening is slowed down by enrichment of intracellular vitamin C via suppression of oxidative stress. *Life Sciences*, **63**(11), pp. 935-948.

GADALETA, M.N., RAINALDI, G., LEZZA, A.M., MILELLA, F., FRACASSO, F. and CANTATORE, P., 1992. Mitochondrial DNA copy number and mitochondrial DNA deletion in adult and senescent rats. *Mutation research*, **275**(3-6), pp. 181-193.

GARELICK, H., JONES, H., DYBOWSKA, A. and VALSAMI-JONES, E., 2008. Arsenic pollution sources. *Reviews of environmental contamination and toxicology*, **197**, pp. 17-60.

GATZIDOU, E.T., ZIRA, A.N. and THEOCHARIS, S.E., 2007. Toxicogenomics: a pivotal piece in the puzzle of toxicological research. *Journal of applied toxicology : JAT*, **27**(4), pp. 302-309.

GERETS, H.H., TILMANT, K., GERIN, B., CHANTEUX, H., DEPELCHIN, B.O., DHALLUIN, S. and ATIENZAR, F.A., 2012. Characterization of primary human hepatocytes, HepG2 cells, and HepaRG cells

at the mRNA level and CYP activity in response to inducers and their predictivity for the detection of human hepatotoxins. *Cell biology and toxicology*, **28**(2), pp. 69-87.

GIVAN, A.L., 2004. Flow cytometry: an introduction. *Methods in molecular biology (Clifton, N.J.)*, **263**, pp. 1-32.

GOLIGORSKY, M.S., CHEN, J. and PATSCHAN, S., 2009. Stress-induced premature senescence of endothelial cells: a perilous state between recovery and point of no return. *Current opinion in hematology*, **16**(3), pp. 215-219.

GOLUBNITSCHAJA, O., 2007. Cell cycle checkpoints: the role and evaluation for early diagnosis of senescence, cardiovascular, cancer, and neurodegenerative diseases. *Amino acids*, **32**(3), pp. 359-371.

GORENNE, I., KAVURMA, M., SCOTT, S. and BENNETT, M., 2006. Vascular smooth muscle cell senescence in atherosclerosis. *Cardiovascular research*, **72**(1), pp. 9-17.

GRIENDLING, K.K., MINIERI, C.A., OLLERENSHAW, J.D. and ALEXANDER, R.W., 1994. Angiotensin II stimulates NADH and NADPH oxidase activity in cultured vascular smooth muscle cells. *Circulation research*, **74**(6), pp. 1141-1148.

GRIENDLING, K.K., SORESCU, D. and USHIO-FUKAI, M., 2000. NAD(P)H oxidase: role in cardiovascular biology and disease. *Circulation research*, **86**(5), pp. 494-501.

GU, S., CIFELLI, C., WANG, S. and HEXIMER, S.P., 2009. RGS proteins: identifying new GAPs in the understanding of blood pressure regulation and cardiovascular function. *Clinical science (London, England : 1979)*, **116**(5), pp. 391-399.

HARMAN, D., 1972. The biologic clock: the mitochondria? *Journal of the American Geriatrics Society*, **20**(4), pp. 145-147.

HARMAN, D., 1956. Aging: a theory based on free radical and radiation chemistry. *Journal of gerontology*, **11**(3), pp. 298-300.

HARTUNG, T. and DASTON, G., 2009. Are in vitro tests suitable for regulatory use? *Toxicological sciences : an official journal of the Society of Toxicology*, **111**(2), pp. 233-237.

HAYASHI, T., MATSUI-HIRAI, H., MIYAZAKI-AKITA, A., FUKATSU, A., FUNAMI, J., DING, Q.F., KAMALANATHAN, S., HATTORI, Y., IGNARRO, L.J. and IGUCHI, A., 2006. Endothelial cellular senescence is inhibited by nitric oxide: implications in atherosclerosis associated with menopause and diabetes. *Proceedings of the National Academy of Sciences of the United States of America*, **103**(45), pp. 17018-17023.

HAYFLICK, L., 1965. The Limited in Vitro Lifetime of Human Diploid Cell Strains. *Experimental cell research*, **37**, pp. 614-636.

HAYFLICK, L. and MOORHEAD, P.S., 1961. The serial cultivation of human diploid cell strains. *Experimental cell research*, **25**, pp. 585-621.

HEI, T.K. and FILIPIC, M., 2004. Role of oxidative damage in the genotoxicity of arsenic. *Free radical biology & medicine*, **37**(5), pp. 574-581.

HEI, T.K., LIU, S.X. and WALDREN, C., 1998. Mutagenicity of arsenic in mammalian cells: role of reactive oxygen species. *Proceedings of the National Academy of Sciences of the United States of America*, **95**(14), pp. 8103-8107.

HEINZEL, B., JOHN, M., KLATT, P., BOHME, E. and MAYER, B., 1992. Ca2+/calmodulin-dependent formation of hydrogen peroxide by brain nitric oxide synthase. *The Biochemical journal*, **281 (Pt 3)**(Pt 3), pp. 627-630.

HENDRIKS-BALK, M.C., PETERS, S.L., MICHEL, M.C. and ALEWIJNSE, A.E., 2008. Regulation of G protein-coupled receptor signalling: focus on the cardiovascular system and regulator of G protein signalling proteins. *European journal of pharmacology*, **585**(2-3), pp. 278-291.

HENLE, E.S., HAN, Z., TANG, N., RAI, P., LUO, Y. and LINN, S., 1999. Sequence-specific DNA cleavage by Fe2+-mediated fenton reactions has possible biological implications. *The Journal of biological chemistry*, **274**(2), pp. 962-971.

HERLAAR, E. and BROWN, Z., 1999. p38 MAPK signalling cascades in inflammatory disease. *Molecular medicine today*, **5**(10), pp. 439-447.

HEXIMER, S.P., 2012. Intracellular regulation of heterotrimeric G-protein signaling in normal and diseased tissues of the cardiovascular system. Drug discovery today: disease models, 9(3), pp. e91-e96.

HILL, B.G., DRANKA, B.P., ZOU, L., CHATHAM, J.C. and DARLEY-USMAR, V.M., 2009. Importance of the bioenergetic reserve capacity in response to cardiomyocyte stress induced by 4-hydroxynonenal. *The Biochemical journal*, **424**(1), pp. 99-107.

HOFFMANN, E., DITTRICH-BREIHOLZ, O., HOLTMANN, H. and KRACHT, M., 2002. Multiple control of interleukin-8 gene expression. *Journal of leukocyte biology*, **72**(5), pp. 847-855.

HOLMGREN, A., 1985. Thioredoxin. *Annual Review of Biochemistry*, **54**, pp. 237-271.

HORNHARDT, S., GOMOLKA, M., WALSH, L. and JUNG, T., 2006. Comparative investigations of sodium arsenite, arsenic trioxide and cadmium sulphate in combination with gamma-radiation on apoptosis, micronuclei induction and DNA damage in a human lymphoblastoid cell line. *Mutation research*, **600**(1-2), pp. 165-176.

HORNSBY, P.J., 2002. Cellular senescence and tissue aging in vivo. *The journals of gerontology.Series A, Biological sciences and medical sciences*, **57**(7), pp. B251-6.

HUANG, H. and MANTON, K.G., 2004. The role of oxidative damage in mitochondria during aging: a review. *Frontiers in bioscience : a journal and virtual library*, **9**, pp. 1100-1117.

HUANG, S., LEE, L., HANSON, N.B., LENAERTS, C., HOEHN, H., POOT, M., RUBIN, C.D., CHEN, D.F., YANG, C.C., JUCH, H., DORN, T., SPIEGEL, R., ORAL, E.A., ABID, M., BATTISTI, C., LUCCI-CORDISCO, E., NERI, G., STEED, E.H., KIDD, A., ISLEY, W., SHOWALTER, D., VITTONE, J.L., KONSTANTINOW, A., RING, J., MEYER, P., WENGER, S.L., VON HERBAY, A., WOLLINA, U., SCHUELKE, M., HUIZENGA, C.R., LEISTRITZ, D.F., MARTIN, G.M., MIAN, I.S. and OSHIMA, J., 2006. The spectrum of WRN mutations in Werner syndrome patients. *Human mutation*, **27**(6), pp. 558-567.

HYBERTSON, B.M., GAO, B., BOSE, S.K. and MCCORD, J.M., 2011. Oxidative stress in health and disease: the therapeutic potential of Nrf2 activation. *Molecular aspects of medicine*, **32**(4-6), pp. 234-246.

IARC WORKING GROUP ON THE EVALUATION OF CARCINOGENIC RISKS TO HUMANS, 2012. Arsenic, metals, fibres, and dusts. *IARC monographs on the evaluation of carcinogenic risks to humans / World Health Organization, International Agency for Research on Cancer,* **100**(Pt C), pp. 11-465.

IBRAHIM, S.F. and VAN DEN ENGH, G., 2007. Flow cytometry and cell sorting. *Advances in Biochemical Engineering/Biotechnology,* **106**, pp. 19-39.

IBSEN, K.H., 1961. The Crabtree effect: a review. *Cancer research,* **21**, pp. 829-841.

IGNARRO, L.J., BUGA, G.M., WOOD, K.S., BYRNS, R.E. and CHAUDHURI, G., 1987. Endothelium-derived relaxing factor produced and released from artery and vein is nitric oxide. *Proceedings of the National Academy of Sciences of the United States of America,* **84**(24), pp. 9265-9269.

IIDA, T., MINE, S., FUJIMOTO, H., SUZUKI, K., MINAMI, Y. and TANAKA, Y., 2002. Hypoxia-inducible factor-1alpha induces cell cycle arrest of endothelial cells. *Genes to cells : devoted to molecular & cellular mechanisms,* **7**(2), pp. 143-149.

ILLUMINA, 2011. Array-based gene expression analysis: expression profiling products tailored for a variety of genetic research applications. [online]. Illumina Inc., San Diego. [viewed 04/07/2013]. Available from: http://res.illumina.com/documents/products/datasheets/datasheet_gene_exp_analysis.pdf

ISZARD, M.B., LIU, J. and KLAASSEN, C.D., 1995. Effect of several metallothionein inducers on oxidative stress defense mechanisms in rats. *Toxicology,* **104**(1-3), pp. 25-33.

JENUWEIN, T. and ALLIS, C.D., 2001. Translating the histone code. *Science (New York, N.Y.),* **293**(5532), pp. 1074-1080.

JONES, C.G., HARE, J.D. and COMPTON, S.J., 1989. Measuring plant protein with the Bradford assay. Journal of chemical ecology, 15(3), pp. 979-992.

JONES, S.A., O'DONNELL, V.B., WOOD, J.D., BROUGHTON, J.P., HUGHES, E.J. and JONES, O.T., 1996. Expression of phagocyte NADPH oxidase components in human endothelial cells. *The American Journal of Physiology,* **271**(4 Pt 2), pp. H1626-34.

JOSHI, D.C. and BAKOWSKA, J.C., 2011. Determination of mitochondrial membrane potential and reactive oxygen species in live rat cortical neurons. *Journal of visualized experiments : JoVE,* **(51). pii: 2704. doi**(51), pp. 10.3791/2704.

KALYANARAMAN, B., DARLEY-USMAR, V., DAVIES, K.J., DENNERY, P.A., FORMAN, H.J., GRISHAM, M.B., MANN, G.E., MOORE, K., ROBERTS, L.J.,2ND and ISCHIROPOULOS, H., 2012. Measuring reactive oxygen and nitrogen species with fluorescent probes: challenges and limitations. *Free radical biology & medicine,* **52**(1), pp. 1-6.

KARAMANLIDIS, G., BAUTISTA-HERNANDEZ, V., FYNN-THOMPSON, F., DEL NIDO, P. and TIAN, R., 2011. Impaired mitochondrial biogenesis precedes heart failure in right ventricular hypertrophy in congenital heart disease. *Circulation.Heart failure,* **4**(6), pp. 707-713.

KARLSSON, M., KURZ, T., BRUNK, U.T., NILSSON, S.E. and FRENNESSON, C.I., 2010. What does the commonly used DCF test for oxidative stress really show? *The Biochemical journal,* **428**(2), pp. 183-190.

KEDDERIS, G.L., ELMORE, A.R., CRECELIUS, E.A., YAGER, J.W. and GOLDSWORTHY, T.L., 2006. Kinetics of arsenic methylation by freshly isolated B6C3F1 mouse hepatocytes. *Chemico-biological interactions*, **161**(2), pp. 139-145.

KHANSARI, N., SHAKIBA, Y. and MAHMOUDI, M., 2009. Chronic inflammation and oxidative stress as a major cause of age-related diseases and cancer. *Recent patents on inflammation & allergy drug discovery*, **3**(1), pp. 73-80.

KILL, I.R., FARAGHER, R.G., LAWRENCE, K. and SHALL, S., 1994. The expression of proliferation-dependent antigens during the lifespan of normal and progeroid human fibroblasts in culture. *Journal of cell science*, **107 (Pt 2)**(Pt 2), pp. 571-579.

KLING, P.G. and OLSSON, P., 2000. Involvement of differential metallothionein expression in free radical sensitivity of RTG-2 and CHSE-214 cells. *Free radical biology & medicine*, **28**(11), pp. 1628-1637.

KODAMA, R., KATO, M., FURUTA, S., UENO, S., ZHANG, Y., MATSUNO, K., YABE-NISHIMURA, C., TANAKA, E. and KAMATA, T., 2013. ROS-generating oxidases Nox1 and Nox4 contribute to oncogenic Ras-induced premature senescence. *Genes to cells : devoted to molecular & cellular mechanisms*, **18**(1), pp. 32-41.

KOJO, S., 2004. Vitamin C: basic metabolism and its function as an index of oxidative stress. *Current medicinal chemistry*, **11**(8), pp. 1041-1064.

KONDO, T., HIROSE, M. and KAGEYAMA, K., 2009. Roles of oxidative stress and redox regulation in atherosclerosis. *Journal of Atherosclerosis and Thrombosis*, **16**(5), pp. 532-538.

KROLL, S.L. and CZYZYK-KRZESKA, M.F., 1998. Role of H2O2 and heme-containing O2 sensors in hypoxic regulation of tyrosine hydroxylase gene expression. *The American Journal of Physiology*, **274**(1 Pt 1), pp. C167-74.

KUBOTA, R., KUNITO, T., AGUSA, T., FUJIHARA, J., MONIRITH, I., IWATA, H., SUBRAMANIAN, A., TANA, T.S. and TANABE, S., 2006. Urinary 8-hydroxy-2'-deoxyguanosine in inhabitants chronically exposed to arsenic in groundwater in Cambodia. *Journal of environmental monitoring : JEM*, **8**(2), pp. 293-299.

KUILMAN, T., MICHALOGLOU, C., MOOI, W.J. and PEEPER, D.S., 2010. The essence of senescence. *Genes & development*, **24**(22), pp. 2463-2479.

KUMAGAI, Y. and PI, J., 2004. Molecular basis for arsenic-induced alteration in nitric oxide production and oxidative stress: implication of endothelial dysfunction. *Toxicology and applied pharmacology*, **198**(3), pp. 450-457.

KUNIEDA, T., MINAMINO, T., NISHI, J., TATENO, K., OYAMA, T., KATSUNO, T., MIYAUCHI, H., ORIMO, M., OKADA, S., TAKAMURA, M., NAGAI, T., KANEKO, S. and KOMURO, I., 2006. Angiotensin II induces premature senescence of vascular smooth muscle cells and accelerates the development of atherosclerosis via a p21-dependent pathway. *Circulation*, **114**(9), pp. 953-960.

KURZ, D.J., DECARY, S., HONG, Y. and ERUSALIMSKY, J.D., 2000. Senescence-associated (beta)-galactosidase reflects an increase in lysosomal mass during replicative ageing of human endothelial cells. *Journal of cell science*, **113 (Pt 20)**(Pt 20), pp. 3613-3622.

KURZ, D.J., DECARY, S., HONG, Y., TRIVIER, E., AKHMEDOV, A. and ERUSALIMSKY, J.D., 2004. Chronic oxidative stress compromises telomere integrity and accelerates the onset of senescence in human endothelial cells. *Journal of cell science*, **117**(Pt 11), pp. 2417-2426.

LANDMESSER, U., HORNIG, B. and DREXLER, H., 2004. Endothelial function: a critical determinant in atherosclerosis? *Circulation*, **109**(21 Suppl 1), pp. II27-33.

LAURINDO, F.R., FERNANDES, D.C. and SANTOS, C.X., 2008. Assessment of superoxide production and NADPH oxidase activity by HPLC analysis of dihydroethidium oxidation products. *Methods in enzymology*, **441**, pp. 237-260.

LEE, A.S., 2005. The ER chaperone and signaling regulator GRP78/BiP as a monitor of endoplasmic reticulum stress. *Methods (San Diego, Calif.)*, **35**(4), pp. 373-381.

LEE, B.Y., HAN, J.A., IM, J.S., MORRONE, A., JOHUNG, K., GOODWIN, E.C., KLEIJER, W.J., DIMAIO, D. and HWANG, E.S., 2006. Senescence-associated beta-galactosidase is lysosomal beta-galactosidase. *Aging cell*, **5**(2), pp. 187-195.

LEE, H.C., LU, C.Y., FAHN, H.J. and WEI, Y.H., 1998. Aging- and smoking-associated alteration in the relative content of mitochondrial DNA in human lung. *FEBS letters*, **441**(2), pp. 292-296.

LEE, H.C., YIN, P.H., CHI, C.W. and WEI, Y.H., 2002. Increase in mitochondrial mass in human fibroblasts under oxidative stress and during replicative cell senescence. *Journal of Biomedical Science*, **9**(6 Pt 1), pp. 517-526.

LEE, M.Y., JUNG, B.I., CHUNG, S.M., BAE, O.N., LEE, J.Y., PARK, J.D., YANG, J.S., LEE, H. and CHUNG, J.H., 2003. Arsenic-induced dysfunction in relaxation of blood vessels. *Environmental health perspectives*, **111**(4), pp. 513-517.

LEMARIE, A., BOURDONNAY, E., MORZADEC, C., FARDEL, O. and VERNHET, L., 2008. Inorganic arsenic activates reduced NADPH oxidase in human primary macrophages through a Rho kinase/p38 kinase pathway. *Journal of immunology (Baltimore, Md.: 1950)*, **180**(9), pp. 6010-6017.

LESNEFSKY, E.J., MOGHADDAS, S., TANDLER, B., KERNER, J. and HOPPEL, C.L., 2001. Mitochondrial dysfunction in cardiac disease: ischemia--reperfusion, aging, and heart failure. *Journal of Molecular and Cellular Cardiology*, **33**(6), pp. 1065-1089.

LI, D., MORIMOTO, K., TAKESHITA, T. and LU, Y., 2001. Arsenic induces DNA damage via reactive oxygen species in human cells. *Environmental health and preventive medicine*, **6**(1), pp. 27-32.

LI, G., LUNA, C., QIU, J., EPSTEIN, D.L. and GONZALEZ, P., 2009. Alterations in microRNA expression in stress-induced cellular senescence. *Mechanisms of ageing and development*, **130**(11-12), pp. 731-741.

LIAO, K.H., GUSTAFSON, D.L., FOX, M.H., CHUBB, L.S., REARDON, K.F. and YANG, R.S., 2001. A biologically based model of growth and senescence of Syrian hamster embryo (SHE) cells after exposure to arsenic. *Environmental health perspectives*, **109**(12), pp. 1207-1213.

LIBBY, P. and AIKAWA, M., 2002. Stabilization of atherosclerotic plaques: new mechanisms and clinical targets. *Nature medicine*, **8**(11), pp. 1257-1262.

LII, C.K., LIN, A.H., LEE, S.L., CHEN, H.W. and WANG, T.S., 2011. Oxidative modifications of proteins by sodium arsenite in human umbilical vein endothelial cells. *Environmental toxicology*, **26**(5), pp. 459-471.

LIN, M.E., HERR, D.R. and CHUN, J., 2010. Lysophosphatidic acid (LPA) receptors: signaling properties and disease relevance. *Prostaglandins & other lipid mediators*, **91**(3-4), pp. 130-138.

LIOCHEV, S.I. and FRIDOVICH, I., 2002. The Haber-Weiss cycle -- 70 years later: an alternative view. *Redox report : communications in free radical research*, **7**(1), pp. 55-7; author reply 59-60.

LIU, F. and JAN, K.Y., 2000. DNA damage in arsenite- and cadmium-treated bovine aortic endothelial cells. *Free radical biology & medicine*, **28**(1), pp. 55-63.

LIU, Q., ZHANG, H., SMEESTER, L., ZOU, F., KESIC, M., JASPERS, I., PI, J. and FRY, R.C., 2010. The NRF2-mediated oxidative stress response pathway is associated with tumor cell resistance to arsenic trioxide across the NCI-60 panel. *BMC medical genomics*, **3**, pp. 37-8794-3-37.

LIU, S.X., DAVIDSON, M.M., TANG, X., WALKER, W.F., ATHAR, M., IVANOV, V. and HEI, T.K., 2005. Mitochondrial damage mediates genotoxicity of arsenic in mammalian cells. *Cancer research*, **65**(8), pp. 3236-3242.

LUCHTRATH, H., 1983. The consequences of chronic arsenic poisoning among Moselle wine growers. Pathoanatomical investigations of post-mortem examinations performed between 1960 and 1977. *Journal of cancer research and clinical oncology*, **105**(2), pp. 173-182.

LUONG, J.H.T., Majid, E. and Male, K.B., 2007. Analytical tools for monitoring arsenic in the environment. The open analytical chemistry journal, 1, pp. 7-14.

LYNN, S., GURR, J.R., LAI, H.T. and JAN, K.Y., 2000. NADH oxidase activation is involved in arsenite-induced oxidative DNA damage in human vascular smooth muscle cells. *Circulation research*, **86**(5), pp. 514-519.

MA, Y.Y., WEI, S.J., LIN, Y.C., LUNG, J.C., CHANG, T.C., WHANG-PENG, J., LIU, J.M., YANG, D.M., YANG, W.K. and SHEN, C.Y., 2000. PIK3CA as an oncogene in cervical cancer. *Oncogene*, **19**(23), pp. 2739-2744.

MACCARTHY, P.A., GRIEVE, D.J., LI, J.M., DUNSTER, C., KELLY, F.J. and SHAH, A.M., 2001. Impaired endothelial regulation of ventricular relaxation in cardiac hypertrophy: role of reactive oxygen species and NADPH oxidase. *Circulation*, **104**(24), pp. 2967-2974.

MACCARTHY, P.A. and SHAH, A.M., 2000. Impaired endothelium-dependent regulation of ventricular relaxation in pressure-overload cardiac hypertrophy. *Circulation*, **101**(15), pp. 1854-1860.

MADAMANCHI, N.R. and RUNGE, M.S., 2007. Mitochondrial dysfunction in atherosclerosis. *Circulation research*, **100**(4), pp. 460-473.

MAGUIRE, J.J. and DAVENPORT, A.P., 2005. Regulation of vascular reactivity by established and emerging GPCRs. *Trends in pharmacological sciences*, **26**(9), pp. 448-454.

MAGUIRE, J.J., KAGAN, V.E. and PACKER, L., 1992. Electron transport between cytochrome c and alpha tocopherol. *Biochemical and biophysical research communications*, **188**(1), pp. 190-197.

MAIER, J.A., STATUTO, M. and RAGNOTTI, G., 1993. Senescence stimulates U937-endothelial cell interactions. *Experimental cell research*, **208**(1), pp. 270-274.

MAIRET-COELLO, G., TURY, A. and DICICCO-BLOOM, E., 2009. Insulin-like growth factor-1 promotes G(1)/S cell cycle progression through bidirectional regulation of cyclins and cyclin-dependent kinase inhibitors via the phosphatidylinositol 3-kinase/Akt pathway in developing rat cerebral cortex. *The Journal of neuroscience : the official journal of the Society for Neuroscience*, **29**(3), pp. 775-788.

MALIK, Q. and HERBERT, K.E., 2012. Oxidative and non-oxidative DNA damage and cardiovascular disease. *Free radical research*, **46**(4), pp. 554-564.

MARROQUIN, L.D., HYNES, J., DYKENS, J.A., JAMIESON, J.D. and WILL, Y., 2007. Circumventing the Crabtree effect: replacing media glucose with galactose increases susceptibility of HepG2 cells to mitochondrial toxicants. *Toxicological sciences : an official journal of the Society of Toxicology*, **97**(2), pp. 539-547.

MARSIT, C.J., KARAGAS, M.R., DANAEE, H., LIU, M., ANDREW, A., SCHNED, A., NELSON, H.H. and KELSEY, K.T., 2006. Carcinogen exposure and gene promoter hypermethylation in bladder cancer. *Carcinogenesis*, **27**(1), pp. 112-116.

MARTINET, W., KNAAPEN, M.W., DE MEYER, G.R., HERMAN, A.G. and KOCKX, M.M., 2002. Elevated levels of oxidative DNA damage and DNA repair enzymes in human atherosclerotic plaques. *Circulation*, **106**(8), pp. 927-932.

MARTINET, W., KNAAPEN, M.W., DE MEYER, G.R., HERMAN, A.G. and KOCKX, M.M., 2001. Oxidative DNA damage and repair in experimental atherosclerosis are reversed by dietary lipid lowering. *Circulation research*, **88**(7), pp. 733-739.

MARTIN-PARDILLOS, A., SOSA, C. and SORRIBAS, V., 2013. Arsenic increases Pi-mediated vascular calcification and induces premature senescence in vascular smooth muscle cells. *Toxicological sciences : an official journal of the Society of Toxicology*, **131**(2), pp. 641-653.

MASSRIEH, W., DERJUGA, A. and BLANK, V., 2006. Induction of endogenous Nrf2/small maf heterodimers by arsenic-mediated stress in placental choriocarcinoma cells. *Antioxidants & redox signaling*, **8**(1-2), pp. 53-59.

MATES, J.M., PEREZ-GOMEZ, C. and NUNEZ DE CASTRO, I., 1999. Antioxidant enzymes and human diseases. *Clinical biochemistry*, **32**(8), pp. 595-603.

MATSUSHITA, H., CHANG, E., GLASSFORD, A.J., COOKE, J.P., CHIU, C.P. and TSAO, P.S., 2001. eNOS activity is reduced in senescent human endothelial cells: Preservation by hTERT immortalization. *Circulation research*, **89**(9), pp. 793-798.

MATTHAEI, M., MENG, H., MEEKER, A.K., EBERHART, C.G. and JUN, A.S., 2012. Endothelial Cdkn1a (p21) overexpression and accelerated senescence in a mouse model of Fuchs endothelial corneal dystrophy. *Investigative ophthalmology & visual science*, **53**(10), pp. 6718-6727.

MAYR, J.A., HAACK, T.B., GRAF, E., ZIMMERMANN, F.A., WIELAND, T., HABERBERGER, B., SUPERTI-FURGA, A., KIRSCHNER, J., STEINMANN, B., BAUMGARTNER, M.R., MORONI, I., LAMANTEA, E., ZEVIANI, M., RODENBURG, R.J., SMEITINK, J., STROM, T.M., MEITINGER, T., SPERL, W. and PROKISCH, H., 2012. Lack of the mitochondrial protein acylglycerol kinase causes Sengers syndrome. *American Journal of Human Genetics*, **90**(2), pp. 314-320.

MAZZA, F., GOODMAN, A., LOMBARDO, G., VANELLA, A. and ABRAHAM, N.G., 2003. Heme oxygenase-1 gene expression attenuates angiotensin II-mediated DNA damage in endothelial cells. *Experimental biology and medicine (Maywood, N.J.),* **228**(5), pp. 576-583.

MCBRIDE, H.M., NEUSPIEL, M. and WASIAK, S., 2006. Mitochondria: more than just a powerhouse. *Current biology : CB,* **16**(14), pp. R551-60.

MCCORD, J.M. and FRIDOVICH, I., 1969. Superoxide dismutase. An enzymic function for erythrocuprein (hemocuprein). *The Journal of biological chemistry,* **244**(22), pp. 6049-6055.

MECOCCI, P., FANO, G., FULLE, S., MACGARVEY, U., SHINOBU, L., POLIDORI, M.C., CHERUBINI, A., VECCHIET, J., SENIN, U. and BEAL, M.F., 1999. Age-dependent increases in oxidative damage to DNA, lipids, and proteins in human skeletal muscle. *Free radical biology & medicine,* **26**(3-4), pp. 303-308.

MERCER, J.R., CHENG, K.K., FIGG, N., GORENNE, I., MAHMOUDI, M., GRIFFIN, J., VIDAL-PUIG, A., LOGAN, A., MURPHY, M.P. and BENNETT, M., 2010. DNA damage links mitochondrial dysfunction to atherosclerosis and the metabolic syndrome. *Circulation research,* **107**(8), pp. 1021-1031.

MERSCH-SUNDERMANN, V., KNASMULLER, S., WU, X.J., DARROUDI, F. and KASSIE, F., 2004. Use of a human-derived liver cell line for the detection of cytoprotective, antigenotoxic and cogenotoxic agents. *Toxicology,* **198**(1-3), pp. 329-340.

MILLER, D.M., BUETTNER, G.R. and AUST, S.D., 1990. Transition metals as catalysts of "autoxidation" reactions. *Free radical biology & medicine,* **8**(1), pp. 95-108.

MINAMINO, T., MIYAUCHI, H., YOSHIDA, T. and KOMURO, I., 2003. Endothelial cell senescence in human atherosclerosis: role of telomeres in endothelial dysfunction. *Journal of cardiology,* **41**(1), pp. 39-40.

MIRANDA, S., FONCEA, R., GUERRERO, J. and LEIGHTON, F., 1999. Oxidative stress and upregulation of mitochondrial biogenesis genes in mitochondrial DNA-depleted HeLa cells. *Biochemical and biophysical research communications,* **258**(1), pp. 44-49.

MITTAL, C.K. and MURAD, F., 1977. Activation of guanylate cyclase by superoxide dismutase and hydroxyl radical: a physiological regulator of guanosine 3',5'-monophosphate formation. *Proceedings of the National Academy of Sciences of the United States of America,* **74**(10), pp. 4360-4364.

MITTMANN, C., CHUNG, C.H., HOPPNER, G., MICHALEK, C., NOSE, M., SCHULER, C., SCHUH, A., ESCHENHAGEN, T., WEIL, J., PIESKE, B., HIRT, S. and WIELAND, T., 2002. Expression of ten RGS proteins in human myocardium: functional characterization of an upregulation of RGS4 in heart failure. *Cardiovascular research,* **55**(4), pp. 778-786.

MOISEEVA, O., BOURDEAU, V., ROUX, A., DESCHENES-SIMARD, X. and FERBEYRE, G., 2009. Mitochondrial dysfunction contributes to oncogene-induced senescence. *Molecular and cellular biology,* **29**(16), pp. 4495-4507.

MOSSE, P.R., CAMPBELL, G.R., WANG, Z.L. and CAMPBELL, J.H., 1985. Smooth muscle phenotypic expression in human carotid arteries. I. Comparison of cells from diffuse intimal thickenings adjacent to atheromatous plaques with those of the media. *Laboratory investigation; a journal of technical methods and pathology,* **53**(5), pp. 556-562.

MUSCARI, C., GIACCARI, A., GIORDANO, E., CLO, C., GUARNIERI, C. and CALDARERA, C.M., 1996. Role of reactive oxygen species in cardiovascular aging. *Molecular and cellular biochemistry*, **160-161**, pp. 159-166.

NAJJAR, S.S., SCUTERI, A. and LAKATTA, E.G., 2005. Arterial aging: is it an immutable cardiovascular risk factor? *Hypertension*, **46**(3), pp. 454-462.

NAKADA, K., INOUE, K. and HAYASHI, J., 2001. Interaction theory of mammalian mitochondria. *Biochemical and biophysical research communications*, **288**(4), pp. 743-746.

NAKOU, M., BERTSIAS, G., STAGAKIS, I., CENTOLA, M., TASSIULAS, I., HATZIAPOSTOLOU, M., KRITIKOS, I., GOULIELMOS, G., BOUMPAS, D.T. and ILIOPOULOS, D., 2010. Gene network analysis of bone marrow mononuclear cells reveals activation of multiple kinase pathways in human systemic lupus erythematosus. *PloS one*, **5**(10), pp. e13351.

NARANMANDURA, H., CHEN, X., TANAKA, M., WANG, W.W., REHMAN, K., XU, S., CHEN, Z., CHEN, S.Q. and SUZUKI, N., 2012. Release of apoptotic cytochrome C from mitochondria by dimethylarsinous acid occurs through interaction with voltage-dependent anion channel in vitro. *Toxicological sciences : an official journal of the Society of Toxicology*, **128**(1), pp. 137-146.

NGU, T.T., EASTON, A. and STILLMAN, M.J., 2008. Kinetic analysis of arsenic-metalation of human metallothionein: significance of the two-domain structure. *Journal of the American Chemical Society*, **130**(50), pp. 17016-17028.

NGU, T.T. and STILLMAN, M.J., 2006. Arsenic binding to human metallothionein. *Journal of the American Chemical Society*, **128**(38), pp. 12473-12483.

NIU, R., YOSHIDA, M. and LING, F., 2012. Increases in mitochondrial DNA content and 4977-bp deletion upon ATM/Chk2 checkpoint activation in HeLa cells. *PloS one*, **7**(7), pp. e40572.

NORDENSON, I. and BECKMAN, L., 1991. Is the genotoxic effect of arsenic mediated by oxygen free radicals? *Human heredity*, **41**(1), pp. 71-73.

NOWAK, R., SIWICKI, J.K., CHECHLINSKA, M. and MARKOWICZ, S., 2002. Telomere shortening and atherosclerosis. *Lancet*, **359**(9310), pp. 976; author reply 976-7.

NUNTHARATANAPONG, N., CHEN, K., SINHASENI, P. and KEANEY, J.F.,JR, 2005. EGF receptor-dependent JNK activation is involved in arsenite-induced p21Cip1/Waf1 upregulation and endothelial apoptosis. *American journal of physiology.Heart and circulatory physiology*, **289**(1), pp. H99-H107.

OBATA, T., BROWN, G.E. and YAFFE, M.B., 2000. MAP kinase pathways activated by stress: the p38 MAPK pathway. *Critical Care Medicine*, **28**(4 Suppl), pp. N67-77.

OESEBURG, H., DE BOER, R.A., VAN GILST, W.H. and VAN DER HARST, P., 2010. Telomere biology in healthy aging and disease. *Pflugers Archiv : European journal of physiology*, **459**(2), pp. 259-268.

OGAMI, M., IKURA, Y., OHSAWA, M., MATSUO, T., KAYO, S., YOSHIMI, N., HAI, E., SHIRAI, N., EHARA, S., KOMATSU, R., NARUKO, T. and UEDA, M., 2004. Telomere shortening in human coronary artery diseases. *Arteriosclerosis, Thrombosis, and Vascular Biology*, **24**(3), pp. 546-550.

OH, C.W., BUMP, E.A., KIM, J.S., JANIGRO, D. and MAYBERG, M.R., 2001. Induction of a senescence-like phenotype in bovine aortic endothelial cells by ionizing radiation. *Radiation research,* **156**(3), pp. 232-240.

ORJALO, A.V., BHAUMIK, D., GENGLER, B.K., SCOTT, G.K. and CAMPISI, J., 2009. Cell surface-bound IL-1alpha is an upstream regulator of the senescence-associated IL-6/IL-8 cytokine network. *Proceedings of the National Academy of Sciences of the United States of America,* **106**(40), pp. 17031-17036.

ORMEROD, M.G., SUN, X.M., BROWN, D., SNOWDEN, R.T. and COHEN, G.M., 1993. Quantification of apoptosis and necrosis by flow cytometry. *Acta Oncologica (Stockholm, Sweden),* **32**(4), pp. 417-424.

OSBURN, W.O. and KENSLER, T.W., 2008. Nrf2 signaling: an adaptive response pathway for protection against environmental toxic insults. *Mutation research,* **659**(1-2), pp. 31-39.

OUMOUNA-BENACHOUR, K., HANS, C.P., SUZUKI, Y., NAURA, A., DATTA, R., BELMADANI, S., FALLON, K., WOODS, C. and BOULARES, A.H., 2007. Poly(ADP-ribose) polymerase inhibition reduces atherosclerotic plaque size and promotes factors of plaque stability in apolipoprotein E-deficient mice: effects on macrophage recruitment, nuclear factor-kappaB nuclear translocation, and foam cell death. *Circulation,* **115**(18), pp. 2442-2450.

PACKARD, R.R. and LIBBY, P., 2008. Inflammation in atherosclerosis: from vascular biology to biomarker discovery and risk prediction. *Clinical chemistry,* **54**(1), pp. 24-38.

PANCHATCHARAM, M., MIRIYALA, S., YANG, F., ROJAS, M., END, C., VALLANT, C., DONG, A., LYNCH, K., CHUN, J., MORRIS, A.J. and SMYTH, S.S., 2008. Lysophosphatidic acid receptors 1 and 2 play roles in regulation of vascular injury responses but not blood pressure. *Circulation research,* **103**(6), pp. 662-670.

PARTRIDGE, M.A., HUANG, S.X., HERNANDEZ-ROSA, E., DAVIDSON, M.M. and HEI, T.K., 2007. Arsenic induced mitochondrial DNA damage and altered mitochondrial oxidative function: implications for genotoxic mechanisms in mammalian cells. *Cancer research,* **67**(11), pp. 5239-5247.

PASSOS, J.F., SARETZKI, G., AHMED, S., NELSON, G., RICHTER, T., PETERS, H., WAPPLER, I., BIRKET, M.J., HAROLD, G., SCHAEUBLE, K., BIRCH-MACHIN, M.A., KIRKWOOD, T.B. and VON ZGLINICKI, T., 2007. Mitochondrial dysfunction accounts for the stochastic heterogeneity in telomere-dependent senescence. *PLoS biology,* **5**(5), pp. e110.

PASSOS, J.F., SARETZKI, G. and VON ZGLINICKI, T., 2007. DNA damage in telomeres and mitochondria during cellular senescence: is there a connection? *Nucleic acids research,* **35**(22), pp. 7505-7513.

PESHAVARIYA, H.M., DUSTING, G.J. and SELEMIDIS, S., 2007. Analysis of dihydroethidium fluorescence for the detection of intracellular and extracellular superoxide produced by NADPH oxidase. *Free radical research,* **41**(6), pp. 699-712.

PFAFFL, M.W., 2001. A new mathematical model for relative quantification in real-time RT-PCR. *Nucleic acids research,* **29**(9), pp. e45.

PI, J., QU, W., REECE, J.M., KUMAGAI, Y. and WAALKES, M.P., 2003. Transcription factor Nrf2 activation by inorganic arsenic in cultured keratinocytes: involvement of hydrogen peroxide. *Experimental cell research,* **290**(2), pp. 234-245.

PUCK, T.T., WUTHIER, P., JONES, C. and KAO, F.T., 1971. Genetics of somatic mammalian cells: lethal antigens as genetic markers for study of human linkage groups. *Proceedings of the National Academy of Sciences of the United States of America,* **68**(12), pp. 3102-3106.

QUAGLIARO, L., PICONI, L., ASSALONI, R., DA ROS, R., MAIER, A., ZUODAR, G. and CERIELLO, A., 2005. Intermittent high glucose enhances ICAM-1, VCAM-1 and E-selectin expression in human umbilical vein endothelial cells in culture: the distinct role of protein kinase C and mitochondrial superoxide production. *Atherosclerosis,* **183**(2), pp. 259-267.

RAMIREZ, R.D., MORALES, C.P., HERBERT, B.S., ROHDE, J.M., PASSONS, C., SHAY, J.W. and WRIGHT, W.E., 2001. Putative telomere-independent mechanisms of replicative aging reflect inadequate growth conditions. *Genes & development,* **15**(4), pp. 398-403.

RAYCHAUDHURI, S., STUART, J.M. and ALTMAN, R.B., 2000. Principal components analysis to summarize microarray experiments: application to sporulation time series. *Pacific Symposium on Biocomputing.Pacific Symposium on Biocomputing,* , pp. 455-466.

REICHARD, J.F., SCHNEKENBURGER, M. and PUGA, A., 2007. Long term low-dose arsenic exposure induces loss of DNA methylation. *Biochemical and biophysical research communications,* **352**(1), pp. 188-192.

REN, J., PULAKAT, L., WHALEY-CONNELL, A. and SOWERS, J.R., 2010. Mitochondrial biogenesis in the metabolic syndrome and cardiovascular disease. *Journal of Molecular Medicine (Berlin, Germany),* **88**(10), pp. 993-1001.

RICHTER, C., PARK, J.W. and AMES, B.N., 1988. Normal oxidative damage to mitochondrial and nuclear DNA is extensive. *Proceedings of the National Academy of Sciences of the United States of America,* **85**(17), pp. 6465-6467.

ROBLES, S.J. and ADAMI, G.R., 1998. Agents that cause DNA double strand breaks lead to p16INK4a enrichment and the premature senescence of normal fibroblasts. *Oncogene,* **16**(9), pp. 1113-1123.

ROSENBAUM, D.M., RASMUSSEN, S.G. and KOBILKA, B.K., 2009. The structure and function of G-protein-coupled receptors. *Nature,* **459**(7245), pp. 356-363.

ROSENKRANZ, A.R., SCHMALDIENST, S., STUHLMEIER, K.M., CHEN, W., KNAPP, W. and ZLABINGER, G.J., 1992. A microplate assay for the detection of oxidative products using 2',7'-dichlorofluorescin-diacetate. *Journal of immunological methods,* **156**(1), pp. 39-45.

ROSS, M.F., KELSO, G.F., BLAIKIE, F.H., JAMES, A.M., COCHEME, H.M., FILIPOVSKA, A., DA ROS, T., HURD, T.R., SMITH, R.A. and MURPHY, M.P., 2005. Lipophilic triphenylphosphonium cations as tools in mitochondrial bioenergetics and free radical biology. *Biochemistry.Biokhimiia,* **70**(2), pp. 222-230.

ROSS, R., WIGHT, T.N., STRANDNESS, E. and THIELE, B., 1984. Human atherosclerosis. I. Cell constitution and characteristics of advanced lesions of the superficial femoral artery. *The American journal of pathology,* **114**(1), pp. 79-93.

ROSSIGNOL, R., GILKERSON, R., AGGELER, R., YAMAGATA, K., REMINGTON, S.J. and CAPALDI, R.A., 2004. Energy substrate modulates mitochondrial structure and oxidative capacity in cancer cells. *Cancer research,* **64**(3), pp. 985-993.

ROTH, S. and DROGE, W., 1987. Regulation of T-cell activation and T-cell growth factor (TCGF) production by hydrogen peroxide. *Cellular immunology,* **108**(2), pp. 417-424.

ROTHE, G. and VALET, G., 1990. Flow cytometric analysis of respiratory burst activity in phagocytes with hydroethidine and 2',7'-dichlorofluorescin. *Journal of leukocyte biology,* **47**(5), pp. 440-448.

ROTHFUSS, O., GASSER, T. and PATENGE, N., 2010. Analysis of differential DNA damage in the mitochondrial genome employing a semi-long run real-time PCR approach. *Nucleic acids research,* **38**(4), pp. e24.

SAMANI, N.J., BOULTBY, R., BUTLER, R., THOMPSON, J.R. and GOODALL, A.H., 2001. Telomere shortening in atherosclerosis. *Lancet,* **358**(9280), pp. 472-473.

SAMANI, N.J. and VAN DER HARST, P., 2008. Biological ageing and cardiovascular disease. *Heart (British Cardiac Society),* **94**(5), pp. 537-539.

SANCHEZ-SORIA, P., BROKA, D., MONKS, S.L. and CAMENISCH, T.D., 2012. Chronic low-level arsenite exposure through drinking water increases blood pressure and promotes concentric left ventricular hypertrophy in female mice. *Toxicologic pathology,* **40**(3), pp. 504-512.

SANZ, A. and STEFANATOS, R.K., 2008. The mitochondrial free radical theory of aging: a critical view. *Current aging science,* **1**(1), pp. 10-21.

SASSA, S., SUGITA, O., GALBRAITH, R.A. and KAPPAS, A., 1987. Drug metabolism by the human hepatoma cell, Hep G2. *Biochemical and biophysical research communications,* **143**(1), pp. 52-57.

SATO, I., MORITA, I., KAJI, K., IKEDA, M., NAGAO, M. and MUROTA, S., 1993. Reduction of nitric oxide producing activity associated with in vitro aging in cultured human umbilical vein endothelial cell. *Biochemical and biophysical research communications,* **195**(2), pp. 1070-1076.

SATO, M. and BREMNER, I., 1993. Oxygen free radicals and metallothionein. *Free radical biology & medicine,* **14**(3), pp. 325-337.

SATO, M., SASAKI, M. and HOJO, H., 1995. Antioxidative roles of metallothionein and manganese superoxide dismutase induced by tumor necrosis factor-alpha and interleukin-6. *Archives of Biochemistry and Biophysics,* **316**(2), pp. 738-744.

SAVOIA, C. and SCHIFFRIN, E.L., 2007. Vascular inflammation in hypertension and diabetes: molecular mechanisms and therapeutic interventions. *Clinical science (London, England : 1979),* **112**(7), pp. 375-384.

SCHLEICHER, M., SHEPHERD, B.R., SUAREZ, Y., FERNANDEZ-HERNANDO, C., YU, J., PAN, Y., ACEVEDO, L.M., SHADEL, G.S. and SESSA, W.C., 2008. Prohibitin-1 maintains the angiogenic capacity of endothelial cells by regulating mitochondrial function and senescence. *The Journal of cell biology,* **180**(1), pp. 101-112.

SCHNEIDER, S., WILLIS, P.E. and PARKHOUSE, W.S., 1995. The effects of age and physical activity on cardiac mitochondrial DNA template availability. AGE, 18(4), pp. 151-157.

SCHRECK, R., RIEBER, P. and BAEUERLE, P.A., 1991. Reactive oxygen intermediates as apparently widely used messengers in the activation of the NF-kappa B transcription factor and HIV-1. *The EMBO journal,* **10**(8), pp. 2247-2258.

SCHUG, T.T., 2010. mTOR favors senescence over quiescence in p53-arrested cells. *Aging*, **2**(6), pp. 327-328.

SCULL, C.M. and TABAS, I., 2011. Mechanisms of ER stress-induced apoptosis in atherosclerosis. *Arteriosclerosis, Thrombosis, and Vascular Biology*, **31**(12), pp. 2792-2797.

SEARS, M.E., 2013. Chelation: Harnessing and enhancing heavy metal detoxification – a review. The scientific world journal, 2013(219840), 13 pages, doi:10.1155/2013/219840.

SHAYESTEH, L., LU, Y., KUO, W.L., BALDOCCHI, R., GODFREY, T., COLLINS, C., PINKEL, D., POWELL, B., MILLS, G.B. and GRAY, J.W., 1999. PIK3CA is implicated as an oncogene in ovarian cancer. *Nature genetics*, **21**(1), pp. 99-102.

SHI, Y., WEI, Y., QU, S., WANG, Y., LI, Y. and LI, R., 2010. Arsenic induces apoptosis of human umbilical vein endothelial cells through mitochondrial pathways. *Cardiovascular toxicology*, **10**(3), pp. 153-160.

SHIMIZU, M., HOCHADEL, J.F., FULMER, B.A. and WAALKES, M.P., 1998. Effect of glutathione depletion and metallothionein gene expression on arsenic-induced cytotoxicity and c-myc expression in vitro. *Toxicological sciences : an official journal of the Society of Toxicology*, **45**(2), pp. 204-211.

SHIRASU, K., DIXON, R.A. and LAMB, C., 1996. Signal transduction in plant immunity. *Current opinion in immunology*, **8**(1), pp. 3-7.

SHMOOKLER REIS, R.J. and GOLDSTEIN, S., 1983. Mitochondrial DNA in mortal and immortal human cells. Genome number, integrity, and methylation. *The Journal of biological chemistry*, **258**(15), pp. 9078-9085.

SIEGEL-AXEL, D., DAUB, K., SEIZER, P., LINDEMANN, S. and GAWAZ, M., 2008. Platelet lipoprotein interplay: trigger of foam cell formation and driver of atherosclerosis. *Cardiovascular research*, **78**(1), pp. 8-17.

SIGEL, A., SIGEL, H. and SIGEL, R.K.O., 2009. Metal ions in life sciences (vol. 5): Metallothioneins and related chelators. Cambridge: Royal Society of Chemistry.

SINGH, N.P., MCCOY, M.T., TICE, R.R. and SCHNEIDER, E.L., 1988. A simple technique for quantitation of low levels of DNA damage in individual cells. *Experimental cell research*, **175**(1), pp. 184-191.

SMITH, A.H., HOPENHAYN-RICH, C., BATES, M.N., GOEDEN, H.M., HERTZ-PICCIOTTO, I., DUGGAN, H.M., WOOD, R., KOSNETT, M.J. and SMITH, M.T., 1992. Cancer risks from arsenic in drinking water. *Environmental health perspectives*, **97**, pp. 259-267.

SMITH, A.H., LINGAS, E.O. and RAHMAN, M., 2000. Contamination of drinking-water by arsenic in Bangladesh: a public health emergency. *Bulletin of the World Health Organization*, **78**(9), pp. 1093-1103.

SMITH, A.H., LOPIPERO, P.A., BATES, M.N. and STEINMAUS, C.M., 2002. Public health. Arsenic epidemiology and drinking water standards. *Science (New York, N.Y.)*, **296**(5576), pp. 2145-2146.

SMITH, C.C., O'DONOVAN, M.R. and MARTIN, E.A., 2006. hOGG1 recognizes oxidative damage using the comet assay with greater specificity than FPG or ENDOIII. *Mutagenesis*, **21**(3), pp. 185-190.

SMITH, K.R., KLEI, L.R. and BARCHOWSKY, A., 2001. Arsenite stimulates plasma membrane NADPH oxidase in vascular endothelial cells. *American journal of physiology.Lung cellular and molecular physiology*, **280**(3), pp. L442-9.

STEGLICH, G., NEUPERT, W. and LANGER, T., 1999. Prohibitins regulate membrane protein degradation by the m-AAA protease in mitochondria. *Molecular and cellular biology*, **19**(5), pp. 3435-3442.

STORZ, G., TARTAGLIA, L.A. and AMES, B.N., 1990. Transcriptional regulator of oxidative stress-inducible genes: direct activation by oxidation. *Science (New York, N.Y.)*, **248**(4952), pp. 189-194.

STROBER, W., 2001. Trypan blue exclusion test of cell viability. *Current protocols in immunology / edited by John E.Coligan ...[et al.]*, **Appendix 3**, pp. Appendix 3B.

SUN, R.C., BOARD, P.G. and BLACKBURN, A.C., 2011. Targeting metabolism with arsenic trioxide and dichloroacetate in breast cancer cells. *Molecular cancer*, **10**, pp. 142-4598-10-142.

SUN, X., PI, J., LIU, W., HUDSON, L.G., LIU, K.J. and FENG, C., 2009. Induction of heme oxygenase 1 by arsenite inhibits cytokine-induced monocyte adhesion to human endothelial cells. *Toxicology and applied pharmacology*, **236**(2), pp. 202-209.

SUNDARESAN, M., YU, Z.X., FERRANS, V.J., IRANI, K. and FINKEL, T., 1995. Requirement for generation of H2O2 for platelet-derived growth factor signal transduction. *Science (New York, N.Y.)*, **270**(5234), pp. 296-299.

SUTHERLAND, D.E. and STILLMAN, M.J., 2011. The "magic numbers" of metallothionein. *Metallomics: integrated biometal science*, **3**(5), pp. 444-463.

SUTHERLAND, D.E., WILLANS, M.J. and STILLMAN, M.J., 2010. Supermetalation of the beta domain of human metallothionein 1a. *Biochemistry*, **49**(17), pp. 3593-3601.

SUZUKI, Y., SAKURABA, H. and OSHIMA, A., 1995. β-galactosidase deficiency (β-galactosidosis): GM1 gangliosidosis and Morquio B disease. In: C.R. Scriver, A.L. BEAUDET and W.S. SLY, eds. The metabolic and molecular bases of inherited disease. 7th ed. New York: McGraw-Hill, pp. 2801-2810.

SWISS, R. and WILL, Y., 2011. Assessment of mitochondrial toxicity in HepG2 cells cultured in high-glucose- or galactose-containing media. *Current protocols in toxicology / editorial board, Mahin D.Maines (editor-in-chief) ...[et al.]*, **Chapter 2**, pp. Unit2.20.

TAMIRISA, P., BLUMER, K.J. and MUSLIN, A.J., 1999. RGS4 inhibits G-protein signaling in cardiomyocytes. *Circulation*, **99**(3), pp. 441-447.

TANG, C.M. and INSEL, P.A., 2004. GPCR expression in the heart; "new" receptors in myocytes and fibroblasts. *Trends in cardiovascular medicine*, **14**(3), pp. 94-99.

TARZAMI, S.T., 2011. Chemokines and inflammation in heart disease: adaptive or maladaptive? *International journal of clinical and experimental medicine*, **4**(1), pp. 74-80.

THORNALLEY, P.J. and VASAK, M., 1985. Possible role for metallothionein in protection against radiation-induced oxidative stress. Kinetics and mechanism of its reaction with superoxide and hydroxyl radicals. *Biochimica et biophysica acta*, **827**(1), pp. 36-44.

TIRZIU, D. and SIMONS, M., 2008. Endothelium-driven myocardial growth or nitric oxide at the crossroads. *Trends in cardiovascular medicine,* **18**(8), pp. 299-305.

TSENG, C.H., 2002. An overview on peripheral vascular disease in blackfoot disease-hyperendemic villages in Taiwan. *Angiology,* **53**(5), pp. 529-537.

TSENG, C.H., CHONG, C.K., CHEN, C.J. and TAI, T.Y., 1996. Dose-response relationship between peripheral vascular disease and ingested inorganic arsenic among residents in blackfoot disease endemic villages in Taiwan. *Atherosclerosis,* **120**(1-2), pp. 125-133.

TSENG, C.H., CHONG, C.K., TSENG, C.P., HSUEH, Y.M., CHIOU, H.Y., TSENG, C.C. and CHEN, C.J., 2003. Long-term arsenic exposure and ischemic heart disease in arseniasis-hyperendemic villages in Taiwan. *Toxicology letters,* **137**(1-2), pp. 15-21.

TSENG, W.P., CHU, H.M., HOW, S.W., FONG, J.M., LIN, C.S. and YEH, S., 1968. Prevalence of skin cancer in an endemic area of chronic arsenicism in Taiwan. *Journal of the National Cancer Institute,* **40**(3), pp. 453-463.

TSOU, T.C., YEH, S.C., TSAI, E.M., TSAI, F.Y., CHAO, H.R. and CHANG, L.W., 2005. Arsenite enhances tumor necrosis factor-alpha-induced expression of vascular cell adhesion molecule-1. *Toxicology and applied pharmacology,* **209**(1), pp. 10-18.

TSOU, T.C., YEH, S.C., TSAI, F.Y. and CHANG, L.W., 2004. The protective role of intracellular GSH status in the arsenite-induced vascular endothelial dysfunction. *Chemical research in toxicology,* **17**(2), pp. 208-217.

UPPU, R.M., NOSSAMAN, B.D., GRECO, A.J., FOKIN, A., MURTHY, S.N., FONSECA, V.A. and KADOWITZ, P.J., 2007. Cardiovascular effects of peroxynitrite. *Clinical and experimental pharmacology & physiology,* **34**(9), pp. 933-937.

VALKO, M., LEIBFRITZ, D., MONCOL, J., CRONIN, M.T., MAZUR, M. and TELSER, J., 2007. Free radicals and antioxidants in normal physiological functions and human disease. *The international journal of biochemistry & cell biology,* **39**(1), pp. 44-84.

VALKO, M., RHODES, C.J., MONCOL, J., IZAKOVIC, M. and MAZUR, M., 2006. Free radicals, metals and antioxidants in oxidative stress-induced cancer. *Chemico-biological interactions,* **160**(1), pp. 1-40.

VAN DER HARST, P., VAN DER STEEGE, G., DE BOER, R.A., VOORS, A.A., HALL, A.S., MULDER, M.J., VAN GILST, W.H., VAN VELDHUISEN, D.J. and MERIT-HF STUDY GROUP, 2007. Telomere length of circulating leukocytes is decreased in patients with chronic heart failure. *Journal of the American College of Cardiology,* **49**(13), pp. 1459-1464.

VAN HUMMELEN, P. and SASAKI, J., 2010. State-of-the-art genomics approaches in toxicology. *Mutation research,* **705**(3), pp. 165-171.

VASA, M., BREITSCHOPF, K., ZEIHER, A.M. and DIMMELER, S., 2000. Nitric oxide activates telomerase and delays endothelial cell senescence. *Circulation research,* **87**(7), pp. 540-542.

VASILE, E., TOMITA, Y., BROWN, L.F., KOCHER, O. and DVORAK, H.F., 2001. Differential expression of thymosin beta-10 by early passage and senescent vascular endothelium is modulated by VPF/VEGF: evidence for senescent endothelial cells in vivo at sites of atherosclerosis. *FASEB journal : official publication of the Federation of American Societies for Experimental Biology,* **15**(2), pp. 458-466.

VENUGOPAL, R. and JAISWAL, A.K., 1996. Nrf1 and Nrf2 positively and c-Fos and Fra1 negatively regulate the human antioxidant response element-mediated expression of NAD(P)H:quinone oxidoreductase1 gene. *Proceedings of the National Academy of Sciences of the United States of America,* **93**(25), pp. 14960-14965.

VERMES, I., HAANEN, C., STEFFENS-NAKKEN, H. and REUTELINGSPERGER, C., 1995. A novel assay for apoptosis. Flow cytometric detection of phosphatidylserine expression on early apoptotic cells using fluorescein labelled Annexin V. *Journal of immunological methods,* **184**(1), pp. 39-51.

VICTOR, V.M., ROCHA, M., SOLA, E., BANULS, C., GARCIA-MALPARTIDA, K. and HERNANDEZ-MIJARES, A., 2009. Oxidative stress, endothelial dysfunction and atherosclerosis. *Current pharmaceutical design,* **15**(26), pp. 2988-3002.

VON DER THUSEN, J.H., BORENSZTAJN, K.S., MOIMAS, S., VAN HEININGEN, S., TEELING, P., VAN BERKEL, T.J. and BIESSEN, E.A., 2011. IGF-1 has plaque-stabilizing effects in atherosclerosis by altering vascular smooth muscle cell phenotype. *The American journal of pathology,* **178**(2), pp. 924-934.

VON ZGLINICKI, T., PILGER, R. and SITTE, N., 2000. Accumulation of single-strand breaks is the major cause of telomere shortening in human fibroblasts. *Free radical biology & medicine,* **28**(1), pp. 64-74.

VON ZGLINICKI, T., SARETZKI, G., LADHOFF, J., D'ADDA DI FAGAGNA, F. and JACKSON, S.P., 2005. Human cell senescence as a DNA damage response. *Mechanisms of ageing and development,* **126**(1), pp. 111-117.

WALLACE, D.C., 2000. Mitochondrial defects in cardiomyopathy and neuromuscular disease. *American Heart Journal,* **139**(2 Pt 3), pp. S70-85.

WALTER, D.H., HAENDELER, J., GALLE, J., ZEIHER, A.M. and DIMMELER, S., 1998. Cyclosporin A inhibits apoptosis of human endothelial cells by preventing release of cytochrome C from mitochondria. *Circulation,* **98**(12), pp. 1153-1157.

WAN, W. and MURPHY, P.M., 2013. Regulation of atherogenesis by chemokines and chemokine receptors. *Archivum Immunologiae et Therapiae Experimentalis,* **61**(1), pp. 1-14.

WANG, C., JURK, D., MADDICK, M., NELSON, G., MARTIN-RUIZ, C. and VON ZGLINICKI, T., 2009. DNA damage response and cellular senescence in tissues of aging mice. *Aging cell,* **8**(3), pp. 311-323.

WANG, C.H., JENG, J.S., YIP, P.K., CHEN, C.L., HSU, L.I., HSUEH, Y.M., CHIOU, H.Y., WU, M.M. and CHEN, C.J., 2002. Biological gradient between long-term arsenic exposure and carotid atherosclerosis. *Circulation,* **105**(15), pp. 1804-1809.

WANG, J., LI, L., CANG, H., SHI, G. and YI, J., 2008. NADPH oxidase-derived reactive oxygen species are responsible for the high susceptibility to arsenic cytotoxicity in acute promyelocytic leukemia cells. *Leukemia research,* **32**(3), pp. 429-436.

WANG, J.C. and BENNETT, M., 2012. Aging and atherosclerosis: mechanisms, functional consequences, and potential therapeutics for cellular senescence. *Circulation research,* **111**(2), pp. 245-259.

WANG, X.J., SUN, Z., CHEN, W., EBLIN, K.E., GANDOLFI, J.A. and ZHANG, D.D., 2007. Nrf2 protects human bladder urothelial cells from arsenite and monomethylarsonous acid toxicity. *Toxicology and applied pharmacology,* **225**(2), pp. 206-213.

WANG, X.J., SUN, Z., CHEN, W., LI, Y., VILLENEUVE, N.F. and ZHANG, D.D., 2008. Activation of Nrf2 by arsenite and monomethylarsonous acid is independent of Keap1-C151: enhanced Keap1-Cul3 interaction. *Toxicology and applied pharmacology*, **230**(3), pp. 383-389.

WARBURG, O., 1956. On the origin of cancer cells. *Science (New York, N.Y.)*, **123**(3191), pp. 309-314.

WATERS, M. and YAUK, C., 2007. Consensus recommendations to promote and advance predictive systems toxicology and toxicogenomics. *Environmental and molecular mutagenesis*, **48**(5), pp. 400-403.

WHO, 2001. Arsenic and arsenic compounds (Environmental health criteria 224). 2nd ed. Geneva: World Health Organization.

WOLVETANG, E.J., JOHNSON, K.L., KRAUER, K., RALPH, S.J. and LINNANE, A.W., 1994. Mitochondrial respiratory chain inhibitors induce apoptosis. *FEBS letters*, **339**(1-2), pp. 40-44.

WONG, R.H., KUO, C.Y., HSU, M.L., WANG, T.Y., CHANG, P.I., WU, T.H. and HUANG, S., 2005. Increased levels of 8-hydroxy-2 -deoxyguanosine attributable to carcinogenic metal exposure among schoolchildren. *Environmental health perspectives*, **113**(10), pp. 1386-1390.

WOOD, Z.A., SCHRODER, E., ROBIN HARRIS, J. and POOLE, L.B., 2003. Structure, mechanism and regulation of peroxiredoxins. *Trends in biochemical sciences*, **28**(1), pp. 32-40.

WRIGHT, W.E., PIATYSZEK, M.A., RAINEY, W.E., BYRD, W. and SHAY, J.W., 1996. Telomerase activity in human germline and embryonic tissues and cells. *Developmental genetics*, **18**(2), pp. 173-179.

WYSOCKI, R. and TAMAS, M.J., 2010. How Saccharomyces cerevisiae copes with toxic metals and metalloids. *FEMS microbiology reviews*, **34**(6), pp. 925-951.

YAKES, F.M. and VAN HOUTEN, B., 1997. Mitochondrial DNA damage is more extensive and persists longer than nuclear DNA damage in human cells following oxidative stress. *Proceedings of the National Academy of Sciences of the United States of America*, **94**(2), pp. 514-519.

YANCY, S.L., SHELDEN, E.A., GILMONT, R.R. and WELSH, M.J., 2005. Sodium arsenite exposure alters cell migration, focal adhesion localization and decreases tyrosine phosphorylation of focal adhesion kinase in H9C2 myoblasts. *Toxicological sciences : an official journal of the Society of Toxicology*, **84**(2), pp. 278-286.

YANG, C.L., DU, X.H., ZHAO, J.H., CHEN, W. and HAN, Y.X., 1994. Zinc-induced metallothionein synthesis could protect from gentamicin nephrotoxicity in suspended proximal tubules of rats. *Renal failure*, **16**(1), pp. 61-69.

YEN, Y.P., TSAI, K.S., CHEN, Y.W., HUANG, C.F., YANG, R.S. and LIU, S.H., 2012. Arsenic induces apoptosis in myoblasts through a reactive oxygen species-induced endoplasmic reticulum stress and mitochondrial dysfunction pathway. *Archives of Toxicology*, **86**(6), pp. 923-933.

YOKOI, T., FUKUO, K., YASUDA, O., HOTTA, M., MIYAZAKI, J., TAKEMURA, Y., KAWAMOTO, H., ICHIJO, H. and OGIHARA, T., 2006. Apoptosis signal-regulating kinase 1 mediates cellular senescence induced by high glucose in endothelial cells. *Diabetes*, **55**(6), pp. 1660-1665.

YUAN, C., ZHANG, S.X., POLISSAR, N.L., ECHELARD, D., ORTIZ, G., DAVIS, J.W., ELLINGTON, E., FERGUSON, M.S. and HATSUKAMI, T.S., 2002. Identification of fibrous cap rupture with magnetic resonance imaging is highly associated with recent transient ischemic attack or stroke. *Circulation*, **105**(2), pp. 181-185.

ZALDIVAR, R., 1980. A morbid condition involving cardio-vascular, broncho-pulmonary, digestive and neural lesions in children and young adults after dietary arsenic exposure. *Zentralblatt fur Bakteriologie.1.Abt.Originale B, Hygiene, Krankenhaushygiene, Betriebshygiene, praventive Medizin,* **170**(1-2), pp. 44-56.

ZALDIVAR, R., PRUNES, L. and GHAI, G.L., 1981. Arsenic dose in patients with cutaneous carcinomata and hepatic hemangio-endothelioma after environmental and occupational exposure. *Archives of Toxicology,* **47**(2), pp. 145-154.

ZHANG, B., GEORGIEV, O., HAGMANN, M., GUNES, C., CRAMER, M., FALLER, P., VASAK, M. and SCHAFFNER, W., 2003. Activity of metal-responsive transcription factor 1 by toxic heavy metals and H2O2 in vitro is modulated by metallothionein. *Molecular and cellular biology,* **23**(23), pp. 8471-8485.

ZHAO, H., JOSEPH, J., FALES, H.M., SOKOLOSKI, E.A., LEVINE, R.L., VASQUEZ-VIVAR, J. and KALYANARAMAN, B., 2005. Detection and characterization of the product of hydroethidine and intracellular superoxide by HPLC and limitations of fluorescence. *Proceedings of the National Academy of Sciences of the United States of America,* **102**(16), pp. 5727-5732.

ZHOU, B.B. and ELLEDGE, S.J., 2000. The DNA damage response: putting checkpoints in perspective. *Nature,* **408**(6811), pp. 433-439.

ZHOU, T., CHOU, J., WATKINS, P.B. and KAUFMANN, W.K., 2009. Toxicogenomics: transcription profiling for toxicology assessment. *EXS,* **99**, pp. 325-366.

ZHOU, T., CHOU, J., ZHOU, Y., SIMPSON, D.A., CAO, F., BUSHEL, P.R., PAULES, R.S. and KAUFMANN, W.K., 2007. Ataxia telangiectasia-mutated dependent DNA damage checkpoint functions regulate gene expression in human fibroblasts. *Molecular cancer research : MCR,* **5**(8), pp. 813-822.

ZHOU, X., SUN, H., ELLEN, T.P., CHEN, H. and COSTA, M., 2008. Arsenite alters global histone H3 methylation. *Carcinogenesis,* **29**(9), pp. 1831-1836.

ZHUO, Y., LUO, H. and ZHANG, K., 2012. Leber hereditary optic neuropathy and oxidative stress. *Proceedings of the National Academy of Sciences of the United States of America,* **109**(49), pp. 19882-19883.

ZIELONKA, J. and KALYANARAMAN, B., 2010. Hydroethidine- and MitoSOX-derived red fluorescence is not a reliable indicator of intracellular superoxide formation: another inconvenient truth. *Free radical biology & medicine,* **48**(8), pp. 983-1001.

ZIELONKA, J., SRINIVASAN, S., HARDY, M., OUARI, O., LOPEZ, M., VASQUEZ-VIVAR, J., AVADHANI, N.G. and KALYANARAMAN, B., 2008. Cytochrome c-mediated oxidation of hydroethidine and mito-hydroethidine in mitochondria: identification of homo- and heterodimers. *Free radical biology & medicine,* **44**(5), pp. 835-846.

ZIMMERER, J.M., LESINSKI, G.B., RUPPERT, A.S., RADMACHER, M.D., NOBLE, C., KENDRA, K., WALKER, M.J. and CARSON, W.E.,3RD, 2008. Gene expression profiling reveals similarities between the in vitro and in vivo responses of immune effector cells to IFN-alpha. *Clinical cancer research : an official journal of the American Association for Cancer Research,* **14**(18), pp. 5900-5906.

ZMIJEWSKI, J.W., MOELLERING, D.R., LE GOFFE, C., LANDAR, A., RAMACHANDRAN, A. and DARLEY-USMAR, V.M., 2005. Oxidized LDL induces mitochondrially associated reactive oxygen/nitrogen species formation in endothelial cells. *American journal of physiology.Heart and circulatory physiology,* **289**(2), pp. H852-61.